

Calculation of ampacity ratings of power cable systems by the use of thermal quadrupoles under consideration of soil properties

Balzer, Constantin

(2020)

DOI (TUpprints): <https://doi.org/10.25534/tuprints-00017220>

License:



CC-BY-SA 4.0 International - Creative Commons, Attribution Share-alike

Publication type: Ph.D. Thesis

Division: 18 Department of Electrical Engineering and Information Technology

Original source: <https://tuprints.ulb.tu-darmstadt.de/17220>



TECHNISCHE
UNIVERSITÄT
DARMSTADT

Calculation of ampacity ratings of power cable systems by the use of thermal quadrupoles under consideration of soil properties

vom Fachbereich 18
Elektrotechnik und Informationstechnik
der Technischen Universität Darmstadt

zur Erlangung der Würde eines Doktor-Ingenieurs (Dr.-Ing.)

genehmigte

Dissertation

Constantin Balzer, M. Sc.
geboren am 19.04.1988 in Heppenheim

Referent: Prof. Dr.-Ing. Volker Hinrichsen

Korreferent: Prof. Dr. Ingo Sass

Tag der Einreichung: 29. Juli 2020

Tag der mündlichen Prüfung: 16. November 2020

Darmstadt 2020

Balzer, Constantin : Calculation of ampacity ratings of power cable systems by the use of thermal quadrupoles under consideration of soil specific properties of the bedding
Darmstadt, Technische Universität Darmstadt

Jahr der Veröffentlichung der Dissertation auf TUpprints: 2020

URN: urn:nbn:de:tuda-tuprints-172203

Tag der mündlichen Prüfung: 16. November 2020

Veröffentlicht unter CC BY-SA 4.0 International
<https://creativecommons.org/licenses/>

Vorwort

Die vorliegende Dissertation entstand während meiner Zeit als Mitarbeiter am Fachgebiet Hochspannungstechnik der Technischen Universität Darmstadt. Daher gilt mein besonderer Dank zunächst Herrn Prof. Dr.-Ing. Volker Hinrichsen – für das Vertrauen bei der Einstellung, die sehr gute Zusammenarbeit während meiner Anstellung und vor allem die zahlreichen Anregungen zu dieser Arbeit, die maßgeblich zum Gelingen derselben beigetragen haben.

Ebenso bedanke ich mich bei Herrn Prof. Dr. Ingo Sass für die Offenheit, die eine interdisziplinäre Zusammenarbeit erst ermöglicht hat, sowie die Übernahme des Korreferats und die damit einhergehenden fachlichen Diskussionen.

Meinen Kollegen am Fachgebiet danke ich für die vielfältigen fachlichen Diskussionen sowie die angenehme Atmosphäre am Lehrstuhl. Dies gilt vor allem für meine Bürokollegen Herrn Dr.-Ing. Mohammad H. Nazemi, Herrn Henning Janssen sowie Herrn Martin Hallas. Auch den Mitarbeitern der Werkstatt sowie Herrn Dr.-Ing. Thomas Wietoska sei herzlich gedankt für die Unterstützung des Betriebs des Kabeltestfeldes sowie Frau Cornelia Richter Steinmetz und Ulla Brunner bei der Lösung von administrativen Fragen. Und schließlich gilt mein besonderer Dank meinen Kollegen am Fachgebiet für Angewandte Geothermie – Herrn Dr.-Ing. Johannes Stegner, Herrn Christoph Drefke sowie Herrn Markus Schedel, die mir geholfen haben, mich in die Thematik der Bodenphysik einzuarbeiten. Ohne die vertrauensvolle Zusammenarbeit über die Fachgrenzen hinweg hätte diese Arbeit nicht entstehen können.

Und natürlich danke ich vor allem meiner Familie: Meinen Eltern und meiner Schwester, die mich immer bedingungslos unterstützt haben und ohne deren Hilfe all dies nicht möglich gewesen wäre. Und schließlich danke ich meiner Frau und meinen beiden Kindern – schlicht und ergreifend für ihr Dasein.

Summary

Summary	i
List of symbols	iv
List of abbreviations	xv
Abstract	xvi
Kurzfassung	xvii
1 Motivation and scope of this work	1
1.1 Motivation	1
1.2 Structure	5
2 Components and Configurations of Single Core Cables	7
2.1 Conductor	7
2.2 Inner and outer semicon layer	8
2.3 Insulation	8
2.4 Screen	8
2.5 Armouring	9
2.6 Outer jacket	9
2.7 Laying Configurations	9
3 Present standards	10
3.1 IEC 60287	10
3.2 IEC 60853	13
3.3 DIN VDE 0276	18
3.4 Conclusion and assessment of the present standards	19
4 Theoretical fundamentals	21
4.1 Fundamental equations	21
4.1.1 Fundamental equations of electrodynamics	21
4.1.2 Fundamental equations of heat conduction	23
4.1.3 Fundamental equations of coupled heat and mass diffusion within soils	24
4.1.3.1 Mass transfer in soils	24
4.1.3.2 Heat transfer in soils	27
4.2 Boundary and initial conditions	30
4.3 Simplifications of the derived partial differential equations	32
4.3.1 Adoption to dependencies in time	32
4.3.2 Adoption to the geometry	33
4.4 Solution strategies	36
4.4.1 Separation of variables	36
4.4.2 Solution of ordinary, linear differential equations	37
4.4.3 Green's functions	38
5 Solutions to relevant geometries	42
5.1 Calculation of cable losses	42
5.1.1 Calculation of the conductor losses	42
5.1.2 Dielectric losses inside the insulation	45

5.1.3	Losses inside the screen	45
5.2	Calculation of heat conduction inside cable elements	46
5.2.1	Stationary conditions	46
5.2.2	Periodic conditions	48
5.2.3	Transient conditions	51
5.3	Calculation of heat conduction inside the homogenous bedding	54
5.3.1	Stationary conditions	54
5.3.2	Periodic conditions	57
5.3.3	Transient conditions	59
6	The use of thermal quadropoles	61
6.1	The definition of input and output variables	61
6.2	Introduction to quadrupoles	62
6.3	The use of the frequency domain	64
6.4	Calculation of thermal quadrupoles	66
6.4.1	Conductor	68
6.4.2	Insulation	71
6.4.3	Screen or armour	73
6.4.4	Outer jacket	73
6.4.5	Soil	74
6.4.6	Reference temperature	75
6.5	Complete equivalent circuit for one cable	75
6.6	Total equivalent circuit for a group of cables	76
6.7	Comparison of quadrupoles and the Van Wormer representation	77
7	Possibilities of a refined thermal model of the bedding	79
7.1	Introduction	79
7.1.1	Water retention characteristic	80
7.1.2	Hydraulic conductivity	81
7.1.3	Thermal conductivity	81
7.1.4	The drying-out of soils	85
7.2	Implementation of soil drying-out into ampacity calculations by the two-zone model	87
7.2.1	Present adoption of the two-zone models to specific soils	88
7.2.2	Shortcomings of the two-zone model	89
7.3	Results in stationary conditions	92
7.3.1	Influence of the maximum temperature	93
7.3.2	Influence of the ambient water content	95
7.3.3	Influence of the hydraulic conductivity	101
7.3.4	Influence of the soil types	103
7.4	Results under stationary periodic conditions	105
7.5	Results under transient conditions	106
8	Resumé and outlook	109
8.1	Resumé	109
8.2	Outlook	111
	Appendix	113

A1	Additional information to relevant fundamental systems	113
A1.1	$u(x) = 0$ and $v(x) = 0$	113
A1.2	$u(x) = c(x)$ and $v(x) = 0$	114
A1.3	$u(x) = 0$ and $v(x) = -\beta^2$	115
A1.4	$u(x) = 0$ and $v(x) = +\beta^2$	116
A1.5	$u(x) = x^{-1}$ and $v(x) = \beta^2 \cdot n^2 \cdot x^{-2}$	117
A1.6	$u(x) = x^{-1}$ and $v(x) = n^2 \cdot x^{-2} - \beta^2$	118
A2	Van Genuchten parameters from E-DIN 4220	119
A3	Estimation of bulk density from E-DIN 4220	120
A4	Derivation of the diffusion coefficients	121
A4.1	Diffusion coefficients of water	121
A5	On the temperature dependency of the retention curve and hydraulic conductivity	124
A6	Diffusion coefficients as a function of the hydraulic height	125
Bibliography		126

List of symbols

Symbol	Signification	Unit
\vec{A}	Magnetic vector Potential	$\frac{\text{V} \cdot \text{s}}{\text{m}}$
A_c	Nominal conductor cross section	mm^2
$[A]$	Chain matrix of a quadrupole	-
$a_{n,n}$	Components of the chain matrix of a quadrupole	-
\vec{B}	Magnetic flux density	$\frac{\text{V} \cdot \text{s}}{\text{m}^2}$
C'	Electric capacitance per unit length of a single cable	$\frac{\text{A} \cdot \text{s}}{\text{V} \cdot \text{m}} = \frac{\text{F}}{\text{m}}$
$C'_{\text{th,con}}$	Heat capacitance per unit length of the cable conductor	$\frac{\text{J}}{\text{K} \cdot \text{m}}$
C_{tot}	Total volumetric heat capacity of the soil	$\frac{\text{J}}{\text{K} \cdot \text{m}^3}$
c_n	Functions subsuming terms in the heat and mass transfer equations	-
c_p	Specific heat capacity at constant pressure	$\frac{\text{J}}{\text{kg} \cdot \text{K}}$
$c_{p,c}$	Specific heat capacity of the conductor material at constant pressure	
$c_{p,w}$	Specific heat capacity of liquid water at constant pressure	
$c_{p,s}$	Specific heat capacity at constant pressure of the solid fraction of the soil	
\vec{D}	Displacement field	$\frac{\text{A} \cdot \text{s}}{\text{m}^2}$
$D(T)$	Diffusion coefficient of water vapor in air as a function of temperature	$\frac{\text{m}^2}{\text{s}}$
$D_{h_{\text{hy}}}$	Diffusion coefficient of mass due to gradients of the pressure head	$\frac{\text{m}}{\text{s}}$
$D_{l,h_{\text{hy}}}$	Diffusion coefficient of liquid water due to gradients of the pressure head	$\frac{\text{m}}{\text{s}}$
$D_{l,T}$	Diffusion coefficient of liquid water due to gradients of temperature (with the volumetric water content as state variable)	$\frac{\text{m}^2}{\text{K} \cdot \text{s}}$
D_{l,θ_l}	Diffusion coefficient of liquid water due to gradients of the volumetric water content	$\frac{\text{m}^2}{\text{s}}$

D_{v,θ_l}^*	Diffusion coefficient of water vapor due to gradients of the volumetric water content before the application of correction factors $F(\theta_l)$ and G	$\frac{m^2}{s}$
D_{v,θ_l}	Diffusion coefficient of water vapor due to gradients of the volumetric water content	
$D'_{v,h_{hy}}$	Diffusion coefficient of water vapor due to gradients of the pressure head before the application of correction factors $F(\theta_l)$ and G	$\frac{m}{s}$
$D_{v,h_{hy}}$	Diffusion coefficient of water vapor due to gradients of the pressure head	
$D'_{v,T}$	Diffusion coefficient of water vapor due to gradients of temperature (with the hydraulic height as state variable) before the application of correction factors $F(\theta_l)$ and G	$\frac{m}{K \cdot s}$
$D_{v,T}$	Diffusion coefficient of water vapour due to gradients of temperature	
$D_{v,T}^*$	Diffusion coefficient of water vapor due to gradients of temperature (with the volumetric water content as state variable) before the application of correction factors $F(\theta_l)$ and G	$\frac{m^2}{K \cdot s}$
$D_{v,T}^{**}$	Diffusion coefficient of water vapor due to gradients of temperature (with the volumetric water content as state variable)	
$d, d_{m,n}$	Distance between the centers of two adjacent cables or the cables with indexes m and n	m
$d\dot{Q}'_1$	Supplementary flux source of a thermal quadrupole due to a volumetric heat generation	$\frac{W}{m}$
dT_{crit}	Critical temperature rise above the reference temperature, at which drying out is assumed in the two-zone model: $dT_{\text{crit}} = T_{\text{crit}} - T_{\text{ref}}$	$^{\circ}\text{C}$ or K
$dT_{\text{max,e}}$	Difference between the temperature at the outer surface of the jacket at maximum conductor temperature and the reference temperature: $dT_{\text{max,e}} = T_{\text{max,e}} - T_{\text{ref}}$	
dT_i	the effect of the step function of amplitude Y_i at the moment of the highest conductor temperature	
dT_1	Supplementary temperature source of a thermal quadrupole due to a volumetric heat generation	
\vec{E}	Electric field strength	$\frac{V}{m}$
$\vec{e}_r, \vec{e}_\varphi$	Directional vectors in cylindrical coordinates	-

$\vec{e}_\eta, \vec{e}_\Psi$	Directional vector in bipolar-cylindrical coordinates	
$Ei(x)$	Exponential integral function of x	
$F(\theta_l)$	Correction factor of vapor diffusion as a function of the volumetric water content	-
$F_{1D,=}, F_{2D,=}, F_{3D,=}$	Fundamental solution of the stationary heat equation in one, two and three dimensions	
$F_{2D,\sim}, F_{2D,\tau}$	Fundamental solution of the two dimensional heat equation for periodic and transient dependency of time	
f	Frequency	Hz
$f_1(x), f_2(x)$	Fundamental system of a second degree PDE of the variable x	
$f_a(x), f_b(x)$	Functions of one variable resulting from a separation of variables	
$f_p(x)$	Particular solution of an ODE of the variable x	
$f_h(x)$	Solution of a homogenous ODE of the variable x	
G	Correction factor of vapor diffusion	-
$G(t)$	Green's function with respect to time	
$G_{3D,=}(\vec{r}, \vec{r}')$, $G_{1D,=}(\vec{r}, \vec{r}')$	Green's function for the stationary heat equation in three and one dimensions	
$G_{1D,\sim}(\vec{r}, \vec{r}', \omega_{th})$, $G_{1D,\tau}(\vec{r}, \vec{r}', t, \tau)$	Green's function for one dimension for periodic and transient dependency of time	
g	Gravitational acceleration, $g = 9.81 \frac{\text{m}}{\text{s}^2}$	$\frac{\text{m}}{\text{s}^2}$
g	Volumetric heat generation	
g_{di}	Volumetric heat generation by dielectric losses	$\frac{\text{W}}{\text{m}^3}$
g_{scr}	Volumetric heat generation by screen losses	
H	Enthalpy density	$\frac{\text{J}}{\text{m}^3}$
\vec{H}	Magnetic field strength	$\frac{\text{A}}{\text{m}}$
$[H]$	H matrix of a quadrupole	-
$[H]^*$	H matrix of a quadrupole regarding heat flux densities	-
H_{tot}	Total enthalpy density inside a soil	$\frac{\text{J}}{\text{m}^3}$
$H_n^{(1)}, H_n^{(2)}$	Hankel function of first and second kind of order n	-
h	Specific enthalpy	$\frac{\text{J}}{\text{kg}}$

h_h	Hydraulic head	m
h_{hy}	Pressure head	
$h_{n,n}$	Components of the H matrix of a quadrupole	
$h_{n,n}^*$	Components of the H matrix of a quadrupole regarding heat flux densities	
h_{rel}	Relative humidity	
h_{rob}	Convection coefficient	$\frac{W}{m^2 \cdot K}$
I_i	Average current in the i-th hour before the peak temperature	
I_{max}	Maximum current during one load cycle	
I_{jns}	Current into the insulation	
I_r	Resistive component of the current into the insulation	
$I_{max,60287,hom}$	Maximum conductor current for stationary load by neglecting dielectric losses and a homogenous bedding according to IEC 60287	A
$I_{max,60287}$	Maximum conductor current for stationary load by neglecting dielectric losses according to IEC 60287	
$I_{max,60853,hom}$	Maximum conductor current for periodic load by neglecting dielectric losses and a homogenous bedding according to IEC 60853	
$I_{max,60287}$	Maximum conductor current for stationary load by neglecting dielectric losses according to IEC 60287	
I_{sc}	Induced screen current	
$I_m(x)$	Modified Bessel function of first kind of order m of x	-
\vec{J}	Current density	$\frac{A}{m^2}$
$J_m(x)$	Bessel function of first kind of order m of x	-
\vec{J}_s	Surface current density	$\frac{A}{m}$
K	Permeability of a soil	m^2
$K_m(x)$	Modified Bessel function of second kind of order m of x	-
k	Hydraulic conductivity	$\frac{m}{s}$
k_0	Hydraulic conductivity as assumed by E-DIN 4220	
k_{IEC}	Ratio of the temperature drop across the bedding to the total temperature drop between conductor and ground surface as defined by IEC 60853	-

k_s	Factor taking into account the conductor geometry to calculate the skin-effect factor according to IEC 60287	-
k_{sat}	Hydraulic conductivity of soil in saturated state	$\frac{\text{m}}{\text{s}}$
k	Separation constant from the quasistationary magnetic equation	$\frac{1}{\text{m}}$
L	Specific heat of vaporization of water	$\frac{\text{J}}{\text{kg}}$
l	Length of an arbitrary path from the soil surface to the cable outer jacket, strictly perpendicularly to the isotherms	m
l_{crit}	Length of an arbitrary path from the soil surface to the beginning of the dried region, strictly perpendicular to the isotherms	
M	Molar mass of water	$\frac{\text{kg}}{\text{mol}}$
M_{IEC}	Rating factor due to a cyclic variation of load current from IEC 60853	-
m	Mass	kg
\vec{m}_l	Mass flux density of liquid water	$\frac{\text{kg}}{\text{m}^2 \cdot \text{s}}$
\vec{m}	Total mass flux density	
\vec{m}_v	Mass flux density of water vapour	
m_{VDE}	Load factor as defined by DIN VDE 0276	-
n	Number of conductors in one cable	
n_{Gen}	Fitting parameter of the Van Genuchten Model	
$\vec{n}_i:$	Normal vector on the boundary i	
$\vec{n}_{1,2}$	Normal vector on the boundary from area 1 to area 2	
$P'_{\text{cab}}(T_{\max})$:	Total Joule losses per cable and unit length at maximum operating temperature	
P'_{con}	Total conductor losses per unit length	$\frac{\text{W}}{\text{m}}$
P'_{ins}	Total dielectric losses per unit length	
P'_{screen}	Total screen losses per unit length	
P	Arbitrary state variable	-
$P_i(\vec{r})$	Initial value distribution for the arbitrary state variable P	
p	Pressure	
p_{hy}	Hydraulic pressure	$\frac{\text{kg}}{\text{s}^2 \cdot \text{m}} = \text{Pa}$
p_v	Partial pressure of vapor	

p_v^{sat}	Saturation pressure of water vapor	$\frac{\text{kg}}{\text{s}^2 \cdot \text{m}} = \text{Pa}$
p_{Wor}	Van Wormer parameter	-
Q'	Instantaneous heat per unit length, released by a line source	$\frac{\text{J}}{\text{m}}$
$\dot{Q}, \dot{Q}', \dot{Q}''$	Heat flux, heat flux per unit length and heat flux density, injected by a point, line or surface source	$\frac{\text{W}}{\text{W}}, \frac{\text{W}}{\text{m}}, \frac{\text{W}}{\text{m}^2}$
Q_{eq}	Phasor of the equivalent flux source per unit length of a thermal Norton source	$\frac{\text{W}}{\text{m}}$
$Q_i(t)$	Time dependent total heat flux as input variable	W
$\underline{\dot{Q}_1}, \underline{\dot{Q}_2}$	Phasors of the total heat fluxes into a thermal quadrupole	
$\underline{\dot{Q}'_1}, \underline{\dot{Q}'_2}$	Phasors of the total heat fluxes per unit length into a thermal quadrupole	$\frac{\text{W}}{\text{m}}$
\vec{q}	Heat flux density	$\frac{\text{W}}{\text{m}^2}$
\vec{q}_{adv} :	Heat flux density due to advection	
\vec{q}_{con}	Heat flux density exclusively due to conduction	
$\vec{q}_i:$	Heat flux density on the inner boundary	-
$\vec{q}_{\text{lat}}:$	Heat flux density due to the transport of latent heat	$\frac{\text{W}}{\text{m}^2}$
R	Universal gas constant	$\frac{\text{kg} \cdot \text{m}^2}{\text{s}^2 \cdot \text{mol} \cdot \text{K}}$
$R'_{\text{con,DC}}$	Electric DC-resistance per unit length of the conductor	$\frac{\text{V}}{\text{A} \cdot \text{m}} = \frac{\Omega}{\text{m}}$
$R'_{\text{con},\sim(T_{\text{max}})}$	Electric AC-resistance per unit length of the conductor at maximum conductor temperature	
$R_{\text{th,iso}}$	Thermal resistance of the insulation to a heat flux per unit length	$\frac{\text{K} \cdot \text{m}}{\text{W}}$
$R_{\text{th,jac}}$	Thermal resistance of the outer jacket to a heat flux per unit length	
$R_{\text{th,e}}$	Thermal resistance of the surrounding bedding to a heat flux per unit length	
r, r'	Radial coordinate in cylindrical coordinates	-
\vec{r}, \vec{r}'	Position vector	
r_{con}	Radius of the cable conductor	
\vec{r}_i	Position vector of the boundary i	
r_i	Radius of the inner boundary of a hollow cylinder geometry	m

$r_{i,ins}, r_{o,ins}$	Inner and outer radius of the insulation	m
$r_{i,jac}, r_{o,jac}$	Inner and outer radius of the outer jacket	
$r_{i,sc}, r_{o,sc}$	Inner and outer radius of the screen	
r_o	Radius of the outer boundary of a (hollow) cylinder geometry	
S_{eff}	Saturation	
S_1, S_2	Factors of the Green's function in equation (4.144)	-
s_a	Ambient saturation	
s_{cr}	Critical saturation	
$s_{\mathcal{F}S_{\mathcal{L}}}$	Variable of the Fourier -Transformation	
$s_{\mathcal{L}}$	Variable of the Laplace -Transformation	
T	Temperature	$^{\circ}\text{C}$ or K
T_{crit}	Critical temperature rise at which soil drying-out appears according to the two-zone model	
T_h	Temperature due to the homogenous equation	
$T_o(t)$	Time dependent temperature as output variable	
T_p	Temperature due to the non-homogenous equation	
$\underline{T}_1, \underline{T}_2$	Temperature phasors at thermal quadrupoles	
T_i	Initial temperature distribution	
T_{\max}	Maximum conductor temperature	
$T_{\max,e}$	Maximum temperature inside the bedding at maximum conductor temperature	
T_e	Temperature at the inner boundary of the bedding (equals the surface of the outer jacket)	
T_o	Temperature on the outer boundary	
T_{ref}	Reference temperature to which the temperature rise of a cable system is calculated. [VDE0276-620] proposes $T_{\text{ref}} = 20 \text{ }^{\circ}\text{C}$	
t	Time	
$\tan \delta$	Dissipation factor	
U	Total inner energy	
U_m	Highest voltage for equipment	
$u(x)$	Arbitrary, one-dimensional function	m^3
V	Volume	

\vec{v}	Darcy velocity	$\frac{\text{m}}{\text{s}}$
$v(x)$	Arbitrary, one-dimensional function	-
w_w	Specific weight of water	$\frac{\text{kg}}{\text{s}^2 \cdot \text{m}^2} = \frac{\text{N}}{\text{m}^3}$
x_s^2	Skin effect variable as defined by equation (5.20)	-
x_{IEC}^2	Skin effect variable as defined by IEC 60287	-
$Y_{c,1}, Y_{c,2}$	Cross admittances of the π – equivalent circuit of a quadrupole	$\frac{\text{W}}{\text{K} \cdot \text{m}}$
Y_i	Factor proportional to the current dependent losses in the i -th hour before the highest temperature (used in IEC 60853)	-
\underline{Y}	Longitudinal admittance of the π – equivalent circuit of a quadrupole	$\frac{\text{W}}{\text{K} \cdot \text{m}}$
$Y_m(x)$	Bessel function of second kind of order m	-
$[Y]$	Admittance matrix of a quadrupole	-
$y_{n,n}$	Components of the admittance matrix of a thermal quadrupole	-
y_p	Proximity-effect factor	-
y_s	Skin-effect factor	-
y_0	Laying depth of a cable	m
Z_c	Cross impedances of the T – equivalent circuit of a quadrupole	-
Z_{eq}	Equivalent thermal impedance of a thermal Norton source	$\frac{\text{K} \cdot \text{m}}{\text{W}}$
$Z_{l,1}, Z_{l,2}$	Longitudinal impedances of the T – equivalent circuit of a quadrupole	$\frac{\text{W}}{\text{K} \cdot \text{m}}$
$Z_{\text{th,soil}}$	Thermal impedance of the soil	-
z	Variable of space in the direction of gravitational force	m
z_{ref}	Reference height in the direction of gravitational force	m
$[Z]$	Impedance matrix of a quadrupole	-
$Z_{n,n}$	Components of the impedance matrix of a thermal quadrupole	-
$\Gamma(x)$	Gamma function of x	-
$\theta(t)$	Transient temperature rise of conductor above the ambient temperature at time t after the application of a unity step function of the nominal stationary current acc. to IEC 60283	$^{\circ}\text{C}$

$\theta(\infty)$	Conductor steady state temperature rise above ambient due to $P'_{\text{cable}}(T_{\max})$ only (i.e. disregarding dielectric losses) used in IEC 60853	°C
$\theta_c(t)$	Transient temperature rise of conductor above the outer surface of a cable at time t after the application of a unity step function of the nominal stationary current in IEC 60853	-
θ_{crit}	Critical volumetric water content	-
$\theta_e(t)$	Transient temperature rise of the outer surface of a cable at time t after the application of a unity step function of the nominal stationary current in IEC 60853	°C
θ_{fresh}	Volumetric water content in a fresh state	-
θ_l	Volumetric water content as a fraction of the pore space volume	-
θ_m	Maximum conductor current for a daily load cycle whose peak current is the sustained rated current used in IEC 60853	-
$\theta_R(i)$	Conductor temperature rise above ambient at time i hours due to the application of a step function of load current equal to the sustained rated current used in IEC 60853	°C
θ_v	Volumetric content of the condensed water vapour as a fraction of the pore space volume	-
α	Thermal diffusivity	$\frac{\text{m}^2}{\text{s}}$
α_{Gen}	Fitting parameter of the Van Genuchten Model $[\alpha_{\text{Gen}}] = \text{m}^{-1}$ for h_{hy} in m	$\frac{1}{\text{m}}$
α_{IEC}	Ratio between the actual and steady state temperature rise inside to the cable according to IEC 60853	-
β	Constant arising from the separation of variables	$\frac{1}{\text{m}}$
$\delta(x)$	Dirac delta distribution of x	$\frac{1}{[x]}$
ϵ	Permittivity	$\frac{\text{A} \cdot \text{s}}{\text{V} \cdot \text{m}}$
ϵ''	Imaginary part of the permittivity	-
ϵ_r	Relative permittivity	-
ϵ_{soil}	Porosity as fraction of the total volume	-
ϵ_0	Permittivity of vacuum, $\epsilon_0 = 8,854 \cdot 10^{-12}$	$\frac{\text{A} \cdot \text{s}}{\text{V} \cdot \text{m}}$
κ	Electric conductivity	$\frac{\text{A}}{\text{V} \cdot \text{m}}$

η	Variable of space in bipolar-cylindrical coordinates	-
η_D	Ratio of the diffusion coefficient $D_{v,T}$ to $D_{l,\theta}$ at full saturation of the soil	$\frac{1}{K}$
λ	Thermal conductivity. For heat and mass diffusion, this describes the apparent thermal conductivity (see equation (4.56))	$\frac{W}{m \cdot K}$
λ'	Actual thermal conductivity for heat and mass transfer mechanisms	$\frac{W}{m \cdot K}$
λ_{dry}	Thermal conductivity of soil in the dry region, assuming a two-zone model	$\frac{W}{m \cdot K}$
λ_{wet}	Thermal conductivity of soil in the region that has not been dried-out assuming a two-zone model	
λ_{IEC}	Ratio of the losses between screen and conductor losses as defined by IEC 60287	-
μ	Magnetic permeability	$\frac{V \cdot s}{A \cdot m}$
μ_0	Magnetic permeability of vacuum, $\mu_0 = 4\pi \cdot 10^{-7}$	
μ_r	Relative magnetic permeability	
μ_{IEC}	Loss load factor as defined by IEC 60853	
μ_w	Dynamic viscosity of water	$\frac{kg}{m \cdot s} = Pa \cdot s$
ξ_n	Eigenvalues	
$\vec{\xi}_n$	Eigenvectors	
ρ	Density	
ρ_b	Bulk density of soil	
ρ_c	Density of the conductor material	$\frac{kg}{m^3}$
ρ_w	Density of water	
ρ_s	Density of the solid content of the soil	
σ	Surface charge	$\frac{As}{m^2}$
$\sigma(T)$	Surface tension of water	$\frac{kg}{s^2} = \frac{N}{m}$
ς	Degree of freedom	
τ	Parameter of tortuosity in the Van Genuchten Model	
ϕ	Phase angle of a phasor	rad
φ	Angular coordinate in cylindrical coordinates	-

$\chi_{\text{clay}}, \chi_{\text{Sand}}$	Fraction of mass of the corresponding particle sizes	
ψ	Variable of space in bipolar-cylindrical coordinates	
ω	Angular frequency	
ω_{el}	Angular frequency for quasistationary electromagnetic processes, in this work, ω_{el} equals the grid frequency	rad s
ω_{th}	Angular frequency for thermal processes regarding cable losses	
$\omega_{\text{th},2}$	Angular frequency for thermal processes regarding the oscillation of soil surface temperature	

Functions and Operators

$\mathcal{L}\{f(x)\}(s_L)$	Laplace transformation of $f(x)$
div	Divergence of a scalar field
grad	Gradient of a scalar field
rot	Rotation of a vector field
$L\left(\frac{d}{dt}\right)$	Differential operator
Δ	Laplace Operator
$\vec{\Delta}$	Vector Laplace Operator
$\Re\{\underline{x}\}$	Real part of a complex variable \underline{x}
$\Im\{\underline{x}\}$	Imaginary part of a complex variable \underline{x}

List of abbreviations

Abbreviation	Signification
AC	Alternating current
HD-PE	High Density Polyethylene
XLPE	Cross-linked Polyethylene
PVC	Polyvinylchloride
ODE	Ordinary differential equation
PDE	Partial differential equation

Abstract

The so-called ampacity rating, i.e. the maximum admissible conductor current due to thermal restrictions, represents the major constraint for the power transmission by cable systems. In order to determine this rating, two methodologies can be employed: On the one hand side, the calculation on the basis of analytical expressions allows a fast computation “with pen and paper”. Yet, complex configurations or non-linear material properties of the bedding can only be approximated. In contrast to this, numerical simulations can implement any sort of configurations or material properties, but on the expense of a high demand in computing capacity.

However, the requirements on the operation of power grids are changing: The load patterns become more and more fluctuating due to power injection from dispersed generation. Also, enhanced measurement and control techniques in combination with incentive regulation encourage system operators to make the best use of their existing infrastructure and investments. Against this background, the need for a calculation method that combines both advantages of the aforementioned methods, i.e. the rapidity of analytical calculations with the universal possibilities of numerical simulations, is rising. Only with such methods, real time capable ampacity ratings can be included into an intelligent system operation, providing flexible thermal limits adopted to the actual properties of the load flow and bedding materials.

As the hitherto existing methods for such real time capable algorithms rely on analytical approximations that entail restrictions to their application, the presented work aims at deriving an exact analytical method. In order to do so, solutions for all elements of cable systems have been brought together or derived by the author himself. Furthermore, it is shown that with the help of thermal quadrupoles, the separated solutions can be subsumed into one single network for the total cable system. Moreover, for elements that cannot be calculated analytically, such as the thermal coupling of multiple cables inside a non-homogenous bedding, numerically calculated spectra can be incorporated into the network of thermal quadrupoles. All dependencies in time, i.e. stationary, periodic and transient, can be calculated with the help of the methodology.

Furthermore, an enhanced determination of cable ampacity ratings cannot be performed without reviewing the heat and mass transfer mechanisms inside the bedding. With the help of numerical simulations that have been validated through laboratory experiments, the factors of influence on the soil drying-out as well as the ambient water content are examined for a large variety of natural soils. Also, the dynamic of soil-drying out under transient heat injection is investigated.

The presented results have been achieved in the framework of an interdisciplinary research project between the High Voltage Laboratories and the Geothermal Science and Technology of TU Darmstadt as well as a German distribution system operator. They have been incorporated into an application tool that has successfully been put into operation.

Kurzfassung

Die durch Verluste hervorgerufene Erwärmung führt, in Kombination mit der maximal zulässigen Leitertemperatur, zur Begrenzung der Übertragungsfähigkeit von Energiekabelsystemen. Zur Ermittlung dieser thermischen Stromtragfähigkeit stehen prinzipiell zwei Methoden zur Verfügung: die Berechnung auf Basis analytischer Ausdrücke oder numerischer Simulationen. Während erstgenannte schnelle Ergebnisse bei geringem Rechenaufwand ermöglichen, sind komplizierte Konfigurationen oder inhomogene Bettungseigenschaften nur näherungsweise durch diese abzubilden. Komplementär hierzu können durch numerische Simulationen beliebige Anordnungen oder Materialeigenschaften abgebildet werden, wobei dies mit einem erhöhten Rechenaufwand einhergeht.

Vor dem Hintergrund veränderter Rahmenbedingungen wie einer fluktuierenden Last durch dezentrale Erzeugungseinheiten, verbesserten Kommunikations- und Messtechniken sowie einer Anreizregulierung, die finanzielle Anreize zur bestmöglichen Auslastung von bestehenden Betriebsmitteln schafft, besteht ein Bedarf an einer Berechnungsmöglichkeit, die beide Vorteile der oben genannten Methoden kombiniert: Erst wenn es möglich ist, die genaue Berechnung beliebiger Konfigurationen und Belastungen mit einem geringem Rechenaufwand zu leisten, können echtzeitfähige Berechnungsmethoden der thermischen Stromtragfähigkeit einen Beitrag zu einer intelligenten Netzführung in Form von flexiblen Grenzwerten, die an die tatsächlichen thermophysikalischen Eigenschaften angepasst sind, leisten.

Da die bisherigen Ansätze für eine echtzeitfähige Berechnung von thermischen Kabelbelastbarkeiten auf analytischen Näherungen basieren, die Einschränkungen bezüglich der Anwendbarkeit mit sich bringen, soll mit der vorliegenden Arbeit die Möglichkeit einer exakten analytischen Methodik ausgelotet werden. Hierzu werden zunächst analytische Lösungen für die Elemente eines Kabelsystems zusammengetragen beziehungsweise vom Autor selbst entwickelt. Sodann wird gezeigt, dass sich mit Hilfe der Methode der thermischen Vierpole die Einzellösungen in ein Gesamtsystem übertragen lassen. Elemente, die sich nicht analytisch berechnen lassen (wie beispielsweise die thermische Kopplung einzelner Kabel in einer nicht-homogenen Bettung) können als numerisch ermittelte Impedanz-Kennlinie in das Netzwerk der thermischen Vierpole integriert werden. Alle drei zeitlichen Abhängigkeitstypen – stationär, periodisch und transient – lassen sich auf Basis der thermischen Vierpole berechnen.

Eine verbesserte Bestimmung der Kabelbelastbarkeit kommt weiterhin nicht ohne ein verbessertes Verständnis des Wärme- und Massetransportes innerhalb der Bettung aus. Mit Hilfe von numerischen Simulationen, die durch experimentelle Versuche validiert wurden, werden die Einflussfaktoren auf eine Bodenaustrocknung und den Umgebungswassergehalt für eine große Bandbreite an natürlichen Böden untersucht. Auch wird die Dynamik von Austrocknungen bei einem transienten Wärmeeintrag durch ein Kabelsystem dargestellt.

Die präsentierten Ergebnisse sind im Rahmen eines interdisziplinären Forschungsprojektes zwischen dem Fachgebiet Hochspannungstechnik, dem Fachgebiet für Angewandte Geothermie sowie einem deutschen Verteilnetzbetreiber entstanden. Sie flossen ein in eine Anwendung, die erfolgreich in den operativen Betrieb des Verteilnetzbetreibers integriert wurde.

1 Motivation and scope of this work

“Calculation of transient cable heating, taking into account a possible soil drying-out”, what could have been the title of this work, is actually the title of a dissertation from the High Voltage Laboratories at TU Darmstadt, published in 1985 [BEY1985]. It not only seems that there has been little progress during the past 35 years: actually, the questions that are addressed in this dissertation are as old as the existence of power transmission by energy cables [HOL2015]. Therefore, a new publication to this area of research must well be justified.

1.1 Motivation

As power is transmitted by cable systems, losses inside the conductor (and, to a minor extent, in the insulation or screen) lead to a generation of heat, which itself causes a rise of temperature of the cable system. However, this temperature rise may endanger the insulation, as an increase of temperature accelerates the ageing mechanisms of the dielectric materials. Consequently, the operating temperature represents one restriction to the capacity of power transmission by energy cables. This thermal limit of the current carrying capacity of power cables is commonly denoted as “ampacity rating”.

As it was said before, research regarding the ampacity rating of power cable systems dates back to the very beginning of the existence of power cables. Starting with the work of Kennelly in 1893 [KEN1893], major advantages have been achieved by Buller [BUL1951], Neher [NEH1953-1], [NEH1953-2], McGrath [GRA1957] and Goldenberg [GOL1958], whose considerations in the 1950s established the principles of the calculation of current carrying capacities. With respect to the German regulations, the contributions by Mainka [MAI1971] and Winkler [WIN1978] in the 1970s form the basis of the DIN-standards that is still valid today. More recently, the extensive work by Brakemann and Anders, whose books are works of reference, is worth pointing out [BRA1985], [AND1997].

This research culminated in the present standards that form the basis of today’s ampacity calculations [IEC60287], [IEC60853], [VDE0276]. Without going into details (which will be done later in chapter 3), it is worth recalling the aim of these standards: first of all, the solutions they provide should be valid for a large number of cases and not just special scenarios. Secondly, the results should basically be on the safe side, and thirdly, the procedures should be relatively “easy” to evaluate.

Against this background, it is a flimsy intent to compare the results that are based on a standard with “more exact” values that have been derived through other tools, namely numerical simulations. A computation, taking into account the details of the input data, will always be more “precise” than results obtained from formulae on pen and paper. This trivial conclusion may – especially in times where computational tools become more and more powerful – lead to the misconception of a certain superiority of numerical calculations over analytical expressions, as indicated by the abundance of publications regarding numerical ampacity calculations.

Without saying that the opposite is true, the advantages of analytical calculations should not be forgotten. Dealing with ampacity calculations always means dealing with uncertainties regarding the geometric configuration of a cable system, its load or the thermal characteristics of the bedding. With respect to these uncertainties, more tangible results are often obtained by the algebraic formulations, because the sensitivities of the results with respect to their input parameters can quickly be evaluated. In contrast to that, the result of a numerical calculation is first and foremost a number, to which the sensitivities must tediously be derived through parameter studies.

As a consequence of the highlighted advantages and inconveniences of the two methods, today's ampacity calculations often englobe both approaches, depending on the requirements of the calculations: for vast medium- and low voltage cable networks, the generalized equations and the assumption of standardized soil parameters are used, whereas for prominent high voltage cable connections (often embedded in thermally stabilized backfill material of well-specified thermal properties), numerical calculations of the temperature fields are common. Furthermore, the analytical expressions provide a valuable source of validation of the numerical models.

However, recent changes in the nature of electric power transmission and distribution question the aforementioned applications: With respect to distribution networks in dense agglomerations areas, the reinforced use of cable routes lead to the presence of several cable systems inside one trench, each of them experiencing different load schemes. The resulting variety of configurations of different cable systems inside one single trench can hardly be covered by tabulated values and is getting increasingly complex with respect to analytical expressions. Regarding distribution networks in rural areas, the increase of dispersed power injection by windfarms or photovoltaic panels lead to significant changes in the load patterns. However, this change of dynamic is – as it will be further highlighted in chapter 3 – insufficiently covered by the present standards. Also, incentive regulation encourages the distribution system operators to make the most efficient use of their infrastructure. Against this background, the conservative assumptions of the standards regarding the current carrying capacity of power cable systems are put into question marks, as the calculated ampacity might be well below the actual possible rating: hence, by assuming too conservative thermal rating limits, inefficient investments are done, so that a more precise calculation of thermal limits is an economical interest of the distribution system operators [BAL2015-2].

Finally, the maximum voltage drop within a distribution grid has been the decisive criterion for dimensioning cable systems for years. However, by the appearance of transformers with voltage regulation by tap changers and an increasing number of high power 110/20 kV power transformer stations, voltage fluctuations (especially voltage rise due to photovoltaic) may more and more be controlled efficiently, shifting the focus back to the rated current limits imposed by thermal restrictions as the bottlenecks of distribution capacities [FGH2014].

As the mentioned changes in the distribution grids seem to be in favour of a more widespread application of numerical computations, there is a development in transmission cable systems that emphasises the advantages of analytical calculations: with a dynamic rating system in the form of a “real time monitoring” providing a surplus of ampacity with respect to static limits [OLS2013-1], the calculation of admissible currents should be done rapidly by the operator in charge, without engaging time consuming FE-calculations. Also, if a direct approach is chosen and the temperature alongside the route is measured with the help of a distributed temperature measurement predictions of the ampacity in the future or the ability of an “emergency” capacity requires fast calculation methods. This is also true with respect to the inclusion of temperature dependent cable properties into load-flow calculations [OLS2015].

As a consequence, to meet the mentioned new exigencies of a “real time ampacity rating”, some new approaches have been implemented, being based on an analytical approximation ([OLS2013-2], [MIL2006] and [AND2003] or numerical computations [EBE2019]. However, the focus of the mentioned contributions lays on the implementation and application of a real time rating algorithm, which goes at the expense of evaluating its theoretical fundamentals and the principle methodologies. As a consequence, [AND2003] relies on the procedures proposed in [IEC60287] and [IEC60283]; [MIL2006] calculates the temperature in the time-domain as a sum of exponential terms (as the

outcome of a ladder network), whose time constants are the results of a comparison with numerical simulations, and [OLS2013] uses a thermal ladder network, in which larger parts such as the insulation of high-voltage power cables or the bedding of the cable system are discretized into several sub-parts. As a justification to the chosen methodologies, the authors of the mentioned contributions take an engineering perspective: '*If it works it is just fine*'.

Although this practical approach is very useful when dealing with many problems, it also entails substantial disadvantages: If an algorithm is based on the procedures of the IEC standards, its application will always be restricted to the scope of these standards. This entails the danger of an utilization to configurations, which are not covered by the standards. Moreover, discretization may lead to long, clumsy expressions, which increase the computing time as well as the question of an adequate number of sub-sections. And finally, the thermal interaction between cables inside one trench, taking into account a drying-out of soil, cannot be implemented correctly by any of the mentioned procedures. Therefore, a universal approach to calculate the temperature of cable systems analytically without the use of rough approximations or simplifications is missing until now. This work will close this gap.

In order to do so, not the actual application of the real time rating is focused, but an approach that is resumed by a citation from Kurt Lewin is taken: *There is nothing so practical than a good theory*¹. Hence, the author would like to counteract the widespread tendency to assume an antagonism between "theory" and "practice" which – even within universities – is more and more commonly expressed, often with the aim of devaluating "theory" in contrast to a somehow more relevant "practice". Not only are the proponents of such a standpoint unable to explain how a "practice" without "theory" is supposed to work, but also – as many examples show – the application of results without understanding the underlying theory can also become very dangerous [TAL2008]. In the present case, it turns out that the ample evaluation of the theory leads to a methodology – the thermal quadrupole – that drastically improves practical applicability.

The basis of deriving a performant method to calculate cable ampacity ratings rapidly without lack of exactness is to review the analytical solutions to the field problems implied by the heating of cable systems. Hence, the first achievement of this work is to provide an overview of solutions – some well-known and used within the existing standards, some derived for the first time by the author – to all types of geometries relevant to the configuration of cable systems. As this is done for all three possible dependencies of time, a collection of this completeness has not yet been provided in the field of cable ampacity rating.

Secondly, it is demonstrated that the method of thermal quadrupoles [MAI2000] is useful to subsume all possible geometries and dependencies in time to one single equivalent circuit. As a consequence, the presented work aims at giving a full portrait of this method, including both its theoretic foundations and application. By doing so, the author proposes to replace the hitherto used approximated thermal ladder networks by their exact formulations.

However, the detailed evaluation of analytical means not only leads to positive results (in the form of closed-form solutions), but also marks their restrictions: The thermal properties of a non-homogenous bedding, including the thermal interactions of multiple cables inside of it, is hard to represent analytically. But instead of using rough approximations or omitting this weak point, the presented method allows to include numerically derived thermal self- and coupling impedances into the network

¹ *Problems of Research in Social Psychology, in: Field Theory in Social Science; Selected Theoretical Papers, D. Cartwright (Hrsg.), Harper & Row, New York 1951. S. 169*

of quadrupoles. The resulting computation achieves, therefore, both requirements of a real-time capable ampacity rating calculation: rapidity and exactness.

Finally, reviewing the method to derive thermal ampacity ratings does not go without reviewing the implementation of the most prominent factor of influence: the bedding of cable systems. During operation, the heat that is injected by the cable into the bedding entails a redistribution of humidity away from the cable. However, as this dried soil in the vicinity of the cable has a lower thermal conductivity as in a wetted state, this “drying-out” of soils entails a significant reduction with respect to the current carrying capacity of the cable system.

Since the late 1970’s, this “drying-out” of soils is included into common ampacity rating calculations with the help of the so-called “two-zone model” [CIG1992]. Furthermore, efforts to calculate the involved heat and mass transfer numerically and by this to refine the static two-zone model have been undertaken ([RAD1984], [AND1988-1],) without resulting in tangible and applicable contributions to the computation of ampacity ratings. Other studies often focus on sands as the primarily used natural bedding material [GRO1984] and rely either on test field measurements [KOS1978] or exclusively on simulations [FRE1996]. Finally, the influence of climate and natural conditions is often mentioned [AND1988-2], without actually studying their effect on the cable bedding in operational conditions.

Therefore, some major questions still exist against the background of a refinement of cable ampacity rating or its use in the framework of a real time monitoring approach: First of all, the possibilities of a soil specific model of the drying-out should be examined. The idea behind this is that by taking soil probes alongside the route, the thermal model of the bedding can be adopted to its actual on-site properties, rather than using the conservative parameters proposed by the present standards. As most soils have a thermal conductivity higher than $1 \text{ W}\cdot\text{m}^{-1}\cdot\text{K}^{-1}$ which is assumed in the standard, this would normally result in an increase of the computed current carrying capacity.

In addition to this, it is worth reviewing whether the inclusion of the dynamics of the drying-out is advantageous. As the time constants of the latter are in the range of weeks (if not months), the possible periods of “emergency currents” may be longer than those derived on a static drying-out. In this context, it is also interesting to further examine the influence of environmental and climate conditions. This would allow conclusions on whether an indirect rating system, i.e. the adoption of the rated transmission current on the basis of measured weather data (as it is already implemented with regard to overhead lines [STE2000]), would also be possible for cable systems.

And finally, it was shown that the existing standards as well as the thermal models proposed by [OLS2012] and [MIL2006] only approximate the effect of the soil drying-out on the thermal coupling between the cables. Insisting on the exactness of the quadrupole approach for the cable elements, it is just congruent to require the implemented soil model to exactly reflect the assumed bedding properties.

In order to address these questions, an interdisciplinary approach in cooperation with a German distribution system operator and the Geothermal Science and Technology of TU Darmstadt was chosen to combine both: The expertise of *geothermal* and *electrical* engineers, the *laboratory equipment* and *measurements* from a field *test* with the *theoretical implementation* and *computation* of the involved physical processes, the profound *understanding of soil physics* with the acknowledgement of limitations with regard to the *practical implementation into the grid operations*. [DRE2016] focuses on the laboratory measurements and experiments, whereas the interpretation of the results with regard to their ramifications to ampacity calculations is done in the scope of this work.

To finish this motivation, it is worth pointing out that the presented methodology was successfully implemented into an application tool that enables the distribution system operator to determine the actual thermal limits of its cable systems more precisely. By doing so, an effective use of the existing infrastructure as well as investments is assured that leads to considerable cost advantages. Moreover, it must be said that the presented methods are applicable also on high-voltage and extra high voltage cables.

1.2 Structure

In order to convey the aforementioned aspects, the presented work is structured as follows:

Chapter 2 starts with a short overview of the physical components of cables as well as the relevant electrical and thermal properties of the involved materials. Also, in chapter 3, the existing standards and recent developments in the field of ampacity rating calculation will be highlighted. This will not only give the reader a good introduction into the basic principles of ampacity rating, but will further highlight the difficulties that are arising by applying analytical concepts to complex configurations of cable systems and non-linear bedding materials.

The following chapter 4 will take a step back and start by a derivation of the constitutive equations of the three different disciplines of physic that play a role in the ampacity calculation: electromagnetism with respect to the calculation of cable losses, thermal conduction with respect to the heat transfer inside the cable elements as well as the combined heat and mass transfer with respect to the diffusion of humidity inside the soil as a consequence of the induced heat by the cable or changing environmental conditions. It is shown that the first two physics can be solved analytically; whereas - due to the strong non-linearity of the involved material properties - the coupled heat and mass transfer will be examined closer in chapter 7. Hence, the resulting equations for the magnetostatic approximation and the conductive heat transfer will be applied to the studied geometries as well as time regimes, namely stationary, periodic or transient conditions. After a short demonstration of the general solution techniques, those will be applied in order to provide solutions to every cable element separately in chapter 5.

At this point, it should be pointed out that the content of chapter 4 and 5 shall not be considered as a simple synthesis of what has already been written in numerous monographs, but many thoughts and effort went into the work of subsuming the abundance of expressions that can be found in this context as an outcome of the underlying equations. And although the ample illustration of the solution techniques may seem “far away” from the actual purpose of this work, it is the author’s conviction that by thoroughly including them, it is helpful to readers outside its actual scope, as this allows the expansion of the results to fields that are not explicitly covered by this work. Moreover, some expressions such as the stationary temperature distribution around a cable inside homogenous bedding with a convective boundary on its surface have been solved for the first time.

Chapter 6 shows that the great variety of solutions from chapter 5 can be subsumed into a network of thermal quadrupoles. Therefore, the concept and the fundamentals of a thermal quadrupole are presented, alongside with the resulting expression for each cable element as well as the homogenous bedding. Furthermore, it is demonstrated that only the solutions for stationary periodic solutions must be taken into account: As the system is assumed to be linear, the solutions for stationary periodic solutions represent the transfer function, with the help of which transient solutions can be obtained by inverse transformation. Then, the procedure to calculate the temperature of the whole cable system is presented. The chapter finishes with the comparison between the results obtained by thermal

quadrupoles to the approximation by Van Wormer [WOR1955], which is commonly employed to reproduce the thermal behaviour of cable elements under periodic boundary constraints.

Turning the attention to the bedding of cable systems, chapter 7 takes a closer look at the complex heat and mass transfer mechanisms that take place inside natural soils by first discussing the assumptions of the two-zone model, i.e. that the thermal behaviour of the natural bedding can be subsumed by a temperature-dependent heat conductivity. Then, the drying-out of beddings under stationary conditions is discussed for all soil types, specified in the draft of the German standard E-DIN 4220. In addition to this, factors of influence such as the maximum temperature inside the bedding, the ambient water saturation level or fluctuations of the hydraulic conductivity of the soils are evaluated on exemplary soils. As the ambient saturation is an important factor, a tangible assumption for all soil types is met and validated by a verified simulation of the water content inside soil throughout a year. Furthermore, the drying-out under stationary periodic or transient heat injection from the cable is studied.

Finally, the key results of this work are lined out in the conclusion together with some perspectives of further improving the computation of cable ratings by quadrupoles themselves as well as the implementation of a refined thermal model of the bedding.

2 Components and Configurations of Single Core Cables

Before delving deeper into the implied physics of ampacity calculation, it is necessary to give a short overview of the components of a cable and to recall their functions. As the presented work focusses on single-core cables with cylindrical components, so will the following explanations. Therefore, all components are symmetric in azimuthal direction, being a cylinder (regarding the conductor) or coaxial hollow cylinder (any other element). The cross section of a single core cable is drafted in Figure 2.1.

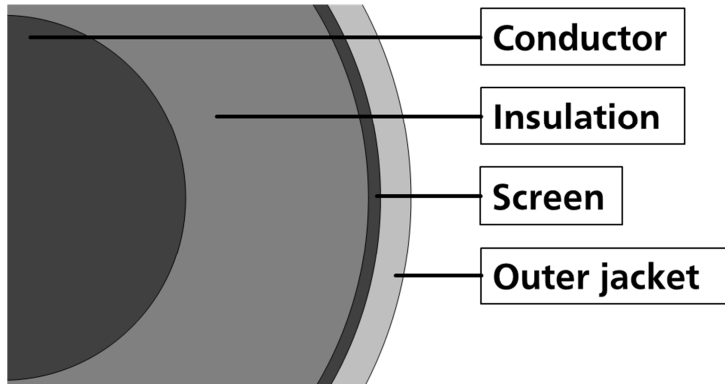


Figure 2.1: Overview of the components of an XLPE single core cable

2.1 Conductor

The main function of a power cable, i.e. the transport of energy, is achieved by the conductor. In general, it can be chosen between aluminium or copper for the conductor material. However, as the ratio between conductivity and price is favourable for aluminium, the latter is chosen whenever possible. Only for bulk power transmission, copper is chosen as the corresponding large cross sections for aluminium would result in mechanical challenges. Also, the fact that copper is less vulnerable to corrosion as aluminium was in the past considered an advantage regarding the reliability of connectors in joints and terminals [LÜC1981]. The main properties are given in Table 2.1.

Table 2.1: Relevant material properties of copper and aluminium [LÜC1981], [CRC2011]

	Copper	Aluminium
Density in $\text{kg}\cdot\text{m}^{-3}$	$8.89\cdot 10^3$	$2.70\cdot 10^3$
Specific heat capacity in $\text{J}\cdot\text{kg}^{-1}\cdot\text{K}^{-1}$	385	879
Specific electric resistivity in $\Omega\cdot\text{m}$	$17.24\cdot 10^{-9}$	$28.26\cdot 10^{-9}$
Specific thermal conductivity in $\text{W}\cdot\text{m}^{-1}\cdot\text{K}^{-1}$	400	238
Temperature coefficient of the resistivity in $1\cdot\text{K}^{-1}$	$3.93\cdot 10^{-3}$	$4.03\cdot 10^{-3}$

For relatively small cross sections in medium and low voltage power cables ($A_c < 150 \text{ mm}^2$), the conductor can be realized as a solid conductor, for larger cross sections, it is composed of separated wires ("stranded conductor"). These wires can also be insulated against each other or even be twisted

in the form of a helix in longitudinal direction in order to reduce the influence of the skin-effect (“Miliken-conductor”). Other than round conductors, there are also sector shaped conductors, hollow conductors (especially for low pressure oil filled cables) as well as oval conductors (for gas pressure cables). It shall be noticed that the nominal cross section does not denote the geometric, but the electric cross section. Therefore, the value for the resistance per unit length shall be taken from the cables specifications rather than being calculated from the geometry and electric conductivity of the conductor material [PIR1999]. The current inside the conductor, i.e. the load current and – to a minor extent – the reactive current, cause ohmic losses inside the conductor. For AC-cables, these losses are increased by the skin- and the proximity effect, which will be treated in detail in chapter 5.1.1.

2.2 Inner and outer semicon layer

In order to homogenize the electric field inside the insulation and prevent high field strengths and partial discharges at the edges of the single wires, the conductor as well as the insulation are surrounded by a conductive layer. For paper-insulated cables, the conductor is often wrapped into several layers of carbon paper (i.e. paper, to which carbon black has been added), whereas a metallized paper (H-Foil) is placed between the insulation and the screen. For cables with an extruded insulation, the semicon material often consists of the same material as the insulation, to which conductive filler such as carbon black have been added. The semicon layer is generally between 1 to 2 mm of thickness.

2.3 Insulation

The insulation of a cable must withstand the voltage from the conductor to the earthed screen. Until the 1980's, the material of choice for the insulation was paper, drowned in a resin for low or medium voltage applications (“mass-impregnated”), or in oil for high-voltage applications (low-pressure oil cables). Today, the insulation of most cables is composed of cross-linked Polyethylene (XLPE), whose advantages are a cheaper production as well as a lower dissipation factor (and therefore lower dielectric losses) than paper insulation. In low-voltage applications, Polyvinylchloride (PVC) is widely used because of its high mechanical robustness. However, due to its high dissipation factor, it is unsuitable for medium- or high voltage applications. Table 2.2 resumes the most important characteristics of common insulation materials.

Due to the effect of polarization, dielectric losses occur inside the insulation. However, these losses can be neglected for cables with $U_m < 123$ kV. The same is true for the ohmic losses due to the leakage current through the insulation.

2.4 Screen

Other than screening the insulation, an important function of the screen is the conduction of the fault current (in the case of a damage of the insulation) and the capacitive current of AC-cables. In Germany, the screen of XLPE-cables is composed of single copper wires in the shape of a helix (connected by a counter-wise running contact helix). If a solid hollow cylinder is intended, as it is often the case for paper-insulated cables in order to protect the insulation from humidity, aluminium or lead is used. While lead has a high bendability and is resistant to chemical reactions, aluminium is much lighter, has a lower electric resistance and is much more resistant to mechanical stresses. Hence, lead screens must always be protected by an armouring, whereas screens from aluminium are generally realised in a curled manner to enhance the mechanical flexibility [PIR1999]. In order to reduce the losses due to induced currents, the screens of a three phase system are interchanged after one and two thirds of the total length (“cross bonding”).

Table 2.2: Relevant material properties of insulation materials [LÜC1981], [CRC2011], [IEC2006-1]

	MI - paper	Oil - paper	PVC	XLPE
Density in $\text{kg}\cdot\text{m}^{-3}$	1000	1000	1450	920
Specific heat capacity in $\text{J}\cdot\text{kg}^{-1}\cdot\text{K}^{-1}$	1000	1000	950	2120
Specific thermal conductivity in $\text{W}\cdot\text{m}^{-1}\cdot\text{K}^{-1}$	0.2	0.2	0.20	0.30
Relative permittivity	4	3.5	8	2.3
Dissipation factor ($\tan \delta$) ²	$10\cdot 10^{-3}$	$3.5\cdot 10^{-3} - 4\cdot 10^{-3}$	$100\cdot 10^{-3}$	$1\cdot 10^{-3}$
Maximum operating temperature in $^{\circ}\text{C}$ ³	55-80	55-80	70	90

2.5 Armouring

In order to protect the cable (especially offshore-cables) against pulling forces or physical damage, there is the possibility to reinforce it with the help of an armouring. This armouring is composed of steel and should be realized in two layers with opposing rotations to equalize torque stresses.

2.6 Outer jacket

The outer jacket of the cable serves as a physical protection against environmental impacts and corrosion of the metallic screen. Before the introduction of polymers into the production of energy cables, the outer jacket was often composed of a mixture of flax and bitumen. Today, the outer jacket for high- and medium voltage cables is usually made from high-density polyethylene (HD-PE) due to its mechanical robustness and relatively low water diffusion constant, whereas PVC is often used in low voltage applications because of its resistance against chemical reactions and its flame retardant properties [VDEW1997].

2.7 Laying Configurations

In general, there are two possibilities of placing three single core cables inside the bedding: Either as a trefoil formation (see Figure 2.2, left) or in lateral formation (Figure 2.2, right). The laying in trefoil-formation demands lesser trench width, reduces induced losses and leads to lower magnetic fields, whereas the lateral formation is favourable with respect to the thermal limits. As a consequence, cables with $U_m < 123 \text{ kV}$ are mostly laid in trefoil formation, high voltage cables with $U_m \geq 123 \text{ kV}$ in lateral formation [SIE1998].

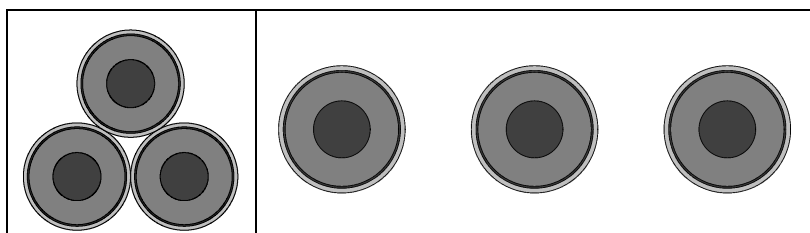


Figure 2.2: Trefoil formation (left) and lateral formation (right) of three single core cables

²The values in IEC 60287-1 are given at the maximum admissible temperature of the cable in order to reflect worst-case conditions. However, the loss factor is highly temperature dependent. As a consequence, values for the loss factors that can be found in various literature are often lower, i.e. a loss factor $0.5\cdot 10^{-3}$ for XLPE for temperatures up to 60°C is often assumed [SIE1998].

³ For paper insulation, the maximum temperature depends on the highest voltage of equipment [VDEW1997].

3 Present standards

As to start with, the content of three major standards (two of them international [IEC60287], [IEC60853], one German [VDE0276-620]) regarding ampacity ratings of cable system is to be highlighted. This will not only convey the main principles and factor of influences of the calculation of current carrying capacities to the reader, but also - as standards always do - resumes the research that has been conducted in this area until now. Moreover, by pointing out that each standard is based on different methodologies and therefore bounded by the corresponding assumptions, the benefit of the later proposed quadrupole approach to cover all possible time regimes, bedding materials and cable configurations will become more evident. In this sense, the following descriptions should not reproduce the content of the standards, but rather unveil the underlying theory.

3.1 IEC 60287

The most prominent standard regarding the calculation of ampacity ratings is IEC 60287. On the one hand side, this is due to the fact that in its first part [IEC60287-1], it gives practicable instructions to the calculation of cable losses, which will be recalled later in section 5.1. On the other hand, the fact that it only deals with stationary conditions, which can serve as a worst case scenario and lead to relatively handsome equations, has contributed to its widespread use. In general, it uses the equivalence between the thermal Fourier law (see equation 4.26) and the electromagnetic Ohm's law to express the temperature drop between the conductor and the reference temperature as the product of the heat flux per unit length with the thermal resistance of the complete cable system. For a homogenous bedding and neglecting the dielectric losses (as it can be done for medium voltage cables), regrouping Fourier's law then leads to the determination of the maximum current for a single, medium voltage cable without armouring under stationary load and no drying-out of the soil

$$I_{\max,60287,\text{hom}} = \sqrt{\frac{T_{\max} - T_{\text{ref}}}{R'_{\text{con},\sim}(T_{\max}) \cdot [R_{\text{th},\text{iso}} + (1 + \lambda_{\text{IEC}}) \cdot R_{\text{th},\text{jac}} + n \cdot (1 + \lambda_{\text{IEC}}) \cdot R_{\text{th},\text{e}}]}} \quad (3.1)$$

With:

$I_{\max,60287,\text{hom}}$: Maximum conductor current for stationary load when neglecting dielectric losses and assuming a homogenous bedding according to IEC 60287

T_{\max} : Maximum conductor temperature

T_{ref} : Temperature at laying depth without the influence of the cable. [VDE0276-620] proposes 20 °C as a worst case assumption

$R'_{\text{con},\sim}(T_{\max})$: Electric AC-resistance per unit length of the conductor at maximum conductor temperature

$R_{\text{th},\text{iso}}$: Thermal resistance of the insulation to a heat flux per unit length

$R_{\text{th},\text{jac}}$: Thermal resistance of the outer jacket to a heat flux per unit length

λ_{IEC} : Loss factor of the screen as defined in equation (5.32)

n : Number of conductors in one cable

$R_{\text{th},\text{e}}$: Thermal resistance of the surrounding bedding to a heat flux per unit length

The computation of the actual thermal resistances is given in the second part of IEC 60287 for a large variety of cables and laying conditions [IEC60287-2]. With respect to the studied single conductor cables, they equal the expressions derived in chapter 5.3.1.

Furthermore, the effect of a drying of the soil can elegantly be incorporated for one single cable or a cable system in trefoil formation into equation (3.1), if the two-zone model (see explanations in chapter 7.2) is assumed [BRA1985]. In this case, the temperature gradient in the region outside of the dried-out zone can be expressed as

$$\text{grad } T = \frac{\vec{q}}{\lambda_{\text{wet}}} \quad (3.2)$$

With:

T : Temperature

\vec{q} : Heat flux density

λ_{wet} : Thermal conductivity of the ambient soil (i.e. the “wet” region) for the two-zone model

Equally, for the dried region, it is

$$\text{grad } T = \frac{\vec{q}}{\lambda_{\text{dry}}} \quad (3.3)$$

Where:

λ_{dry} : Thermal conductivity of soil in the dry region, assuming a two-zone model

The difference between the temperature on the outer jacket at maximum conductor temperature and the reference temperature on the soil surface can therefore be written as

$$\begin{aligned} T_{\max,e} - T_{\text{ref}} &= \int_{|\vec{l}|=0}^{|\vec{l}|=l_{\text{crit}}} \frac{\vec{q}}{\lambda_{\text{wet}}} d\vec{l} + \int_{|\vec{l}|=l_{\text{crit}}}^{|\vec{l}|=l} \frac{\vec{q}}{\lambda_{\text{trocken}}} d\vec{l} \\ &= dT_{\text{crit}} + \frac{\vec{q}}{\lambda_{\text{dry}}} (|\vec{l}| - l_{\text{crit}}) \end{aligned} \quad (3.4)$$

With:

$T_{\max,e}$: Temperature at the outer surface of the cable at maximum conductor temperature

dT_{crit} : Critical temperature rise above the reference temperature, at which drying-out of the soil begins

\vec{l} : Arbitrary path from the soil surface to the cable outer jacket, strictly perpendicular to the isothermals

l_{crit} : Length of an arbitrary path from the soil surface to the beginning of the dried region, strictly perpendicular to the isothermals

The length l_{crit} can further be expressed in terms of the critical temperature rise as

$$dT_{\text{crit}} = \frac{\vec{q}}{\lambda_{\text{wet}}} \cdot l_{\text{crit}} \rightarrow l_{\text{crit}} = dT_{\text{crit}} \cdot \frac{\lambda_{\text{wet}}}{\vec{q}} \quad (3.5)$$

so that insertion from equation (3.5) into (3.4) leads to

$$T_{\max,e} - T_{\text{ref}} = \frac{\vec{q}}{\lambda_{\text{dry}}} \cdot l - dT_{\text{crit}} \left(\frac{\lambda_{\text{wet}}}{\lambda_{\text{dry}}} - 1 \right) \quad (3.6)$$

Regrouping finally yields

$$dT_{\max,e} + dT_{\text{crit}} \left(\frac{\lambda_{\text{dry}}}{\lambda_{\text{wet}}} - 1 \right) = \frac{l}{\lambda_{\text{dry}}} \cdot \vec{q} \quad (3.7)$$

with

$$dT_{\max,e} = T_{\max,e} - T_{\text{ref}} \quad (3.8)$$

As a consequence of equation (3.7), it can be stated that the effect of the drying-out of soil when considering a two-zone model can be incorporated into the calculations as following: The bedding is calculated as if its thermal conductivity were homogenous and equal to λ_{dry} , but the maximum temperature is raised by the second summand on the left hand side of equation (3.7). Therefore, equation (3.1) can simply be re-written as

$$I_{\max,60287} = \sqrt{\frac{dT_{\max} + dT_{\text{crit}} \left(\frac{\lambda_{\text{dry}}}{\lambda_{\text{wet}}} - 1 \right)}{R'_{\text{con},\sim}(T_{\max}) \cdot [R_{\text{th},\text{iso}} + (1+\lambda) \cdot R_{\text{th},\text{jack}} + n \cdot (1+\lambda_{\text{IEC}}) \cdot R_{\text{th},e}]}} \quad (3.9)$$

$I_{\max,60287}$: Maximum conductor current for one single cable or a cable system in trefoil formation under stationary load by neglecting dielectric losses according to IEC 60287

Hence, IEC 60287 provides tangible formulations of the steady state ampacity ratings for a large variety of cables and laying configurations (which are induced in the calculation of $R_{\text{th},e}$). But the drying-out of soil is not taken into account with respect to the mutual heating of cables.

Nonetheless, equation (3.9) is useful to illustrate the importance of the thermal properties of the bedding: Figure 3.1 shows the current $I_{\max,60287}$ for one single aluminium cable system of type NA2XS(F)2Y⁴ with a nominal cross section of $A_c = 150 \text{ mm}^2$, laid in trefoil formation, as a dependency of λ_{wet} for different values of the critical temperature rise dT_{crit} . The thermal conductivity of the dried region is assumed to be $0.4 \text{ W} \cdot \text{m}^{-1} \text{K}^{-1}$ as assumed by [VDE0276-620].

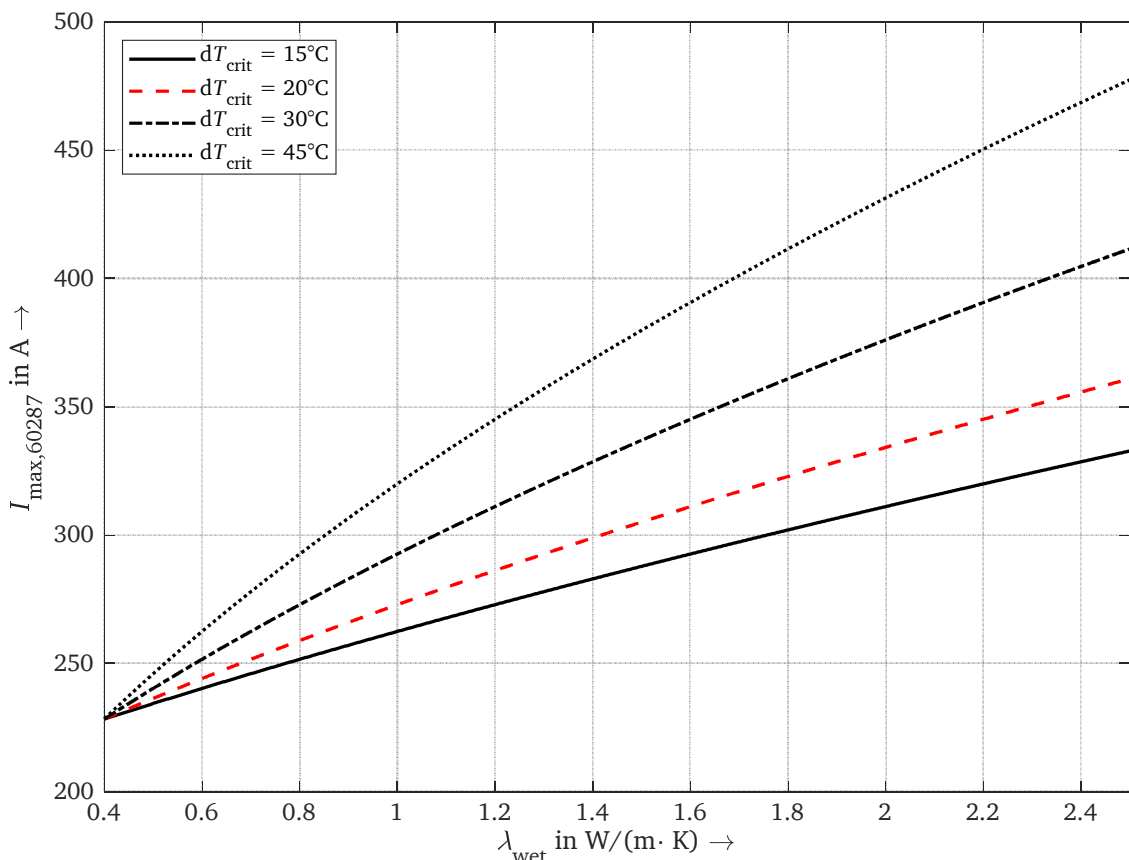


Figure 3.1: $I_{\max,60287}$ for a medium voltage cable system of type NA2XS(F)2Y with $A_c = 150 \text{ mm}^2$ (aluminium) in trefoil formation as a function of the thermal conductivity (λ_{wet}) of the ambient soil for different critical temperatures

⁴ Medium voltage cable according to the German standard, aluminium-conductor with an XLPE-insulation, screen of copper wires and a HD-PE outer jacket.

With respect to Figure 3.1, the interest of a refined determination of the bedding properties of the soil becomes evident. As the German standard [VDE0276-620] assumes a thermal conductivity of the ambient soil to be $1 \text{ W}\cdot\text{m}^{-1}\cdot\text{K}^{-1}$, whereas natural soils tend more towards a value of 1.5 to $2 \text{ W}\cdot\text{m}^{-1}\cdot\text{K}^{-1}$, this would already result in an increase of ampacity of 10 – 17.5 %. Moreover, as soils with a lower fraction of sand grains usually exhibit critical temperatures higher than 15°C , which are assumed by [VDE0276-620] for a constant load, there may also be a high potential of increasing the actual ampacity ratings. The possibility of a more refined selection of the parameters with respect to the soil characteristics is therefore discussed in chapter 7.

3.2 IEC 60853

In addition to the aforementioned considerations under stationary conditions, IEC 60853 provides guidelines to calculate the ampacity rating for cable systems under cyclic load patterns as well as transient conditions (which, under a practical viewpoint, are denoted as “emergency currents”). The first part of this standard [IEC60853-1] is dealing with cyclic rating factors by neglecting the internal thermal capacitances of the cable, which is reasonable for cables having a relatively “small” diameter and on the safe side for larger cables (as the inclusion of the capacitances of the cable elements would reduce the rise of temperature). As a consequence, for arbitrary load cycles, the application of the first part is limited to cable systems with U_m up to 36 kV; for cables of a higher U_m , some restrictions on the load cycles have to be met. However, the second part includes these thermal capacitances into the calculations and covers also transient conditions [IEC60853-2]. In both parts, a possible drying-out of the soil is neglected, so that part three provides an inclusion of a possible soil drying-out [IEC60853-3].

For the first part, the basic methodology consists in explicitly calculating the temperature development for the six hours before the peak temperature (which need not be at the highest current), whereas the influence of the remaining 18 hours is approximated by the loss load factor. The latter is defined as

$$\mu_{\text{IEC}} = \frac{1}{24} \sum_{i=0}^{23} Y_i \quad (3.10)$$

Where:

μ_{IEC} : Loss load factor according to IEC 60853

Y_i : Average normalized squared current during the i -th hour before the time of the highest conductor temperature

$$Y_i = \left(\frac{I_i}{I_{\max,60287,\text{hom}}} \right)^2 \quad (3.11)$$

With:

I_i : Average current in the i -th hour before the peak temperature

In order to clarify the nomenclature, Figure 3.2 shows an exemplary, normalized load cycle, the normalized squared load cycle as well as the marked levels of Y_0 to Y_6 .

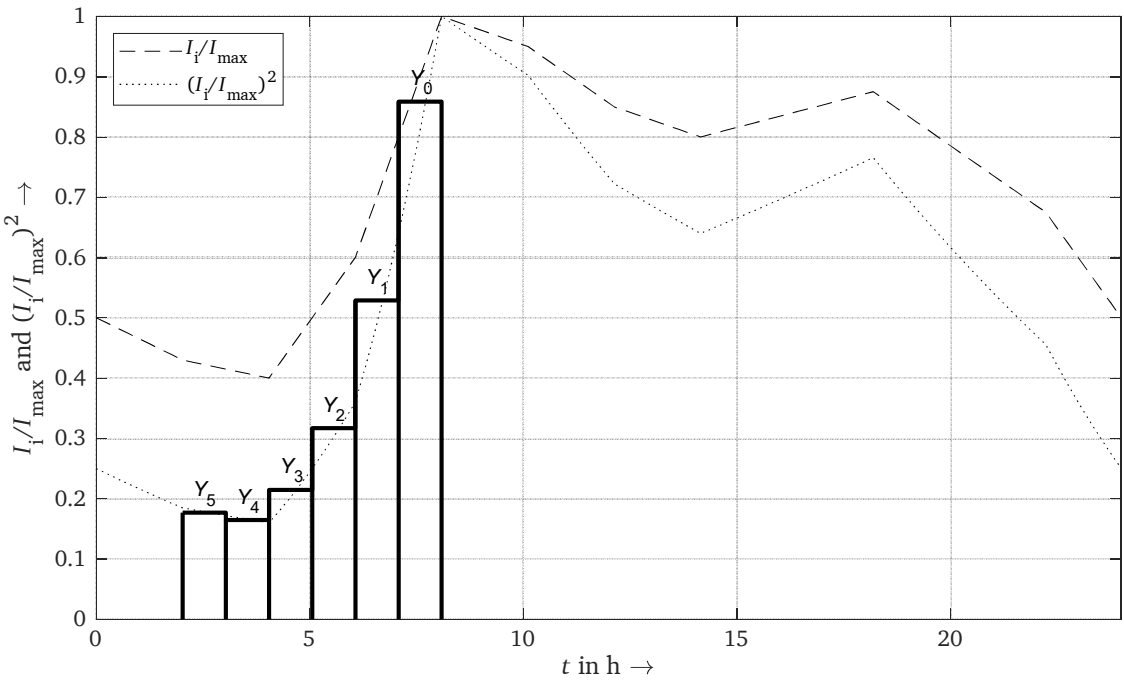


Figure 3.2: Visualisation of the factors Y_5 to Y_0 according to [IEC60853]

The actual temperature calculation due to the six hours of load preceding the maximum temperature is based on the calculation of the temperature field of the transient heating around a line power source. This can be derived with the help of the fundamental solution of the one dimensional heat conduction in cylindrical coordinates, which is given in equation (4.142). Inserting the fundamental solution into the Green's function approach from equation (4.148) and assuming a constant heat injection, starting at $t = 0$, the temperature at a distance $|\vec{r}|$ from the line source can be calculated as [CAR1959]

$$T(t) = \frac{\dot{Q}'}{4\pi\lambda} \int_0^t \frac{1}{(t-t')} e^{-\frac{|\vec{r}|^2}{4\alpha(t-t')}} dt' \quad (3.12)$$

Where:

\dot{Q}' : Heat flux per unit length, injected by a line source

α : Thermal diffusivity

By setting

$$u = \frac{|\vec{r}|^2}{4\alpha(t-t')} \quad (3.13)$$

and replacing t by $3600 \cdot i$ equation (3.12), the latter can be rewritten to [CAR1959, p.261]⁵

$$T(\dot{Q}', i, r) = \frac{\dot{Q}'}{4\pi\lambda} \int_{\frac{r^2}{4\alpha \cdot 3600 \cdot i}}^{\infty} \frac{e^{-u}}{u} du = -\frac{\dot{Q}'}{4\pi\lambda} \text{Ei}\left(-\frac{r^2}{4\alpha \cdot 3600 \cdot i}\right) \quad (3.14)$$

where Ei denotes the exponential integral function. Strictly spoken, the line source must also be mirrored to respect the Dirichlet boundary condition at the ground surface, but with respect to the maximum considered time of six hours, the effect of this boundary on the actual temperature development can be neglected.

⁵ In the referred edition, a factor α^{-1} is given in the denominator, due to the definition of the value of the line source to be $\rho \cdot c_p \cdot \dot{Q}'$

Finally, it must be taken into account that the temperature drop from the conductor to the ground surface is only partly caused by the external resistance. Defining the ratio between the temperature drop throughout the bedding and the maximum steady state conductor temperature as k_{IEC} and neglecting the thermal capacitances of the cable, the transient temperature rise of the conductor due to a current that equals the rated current for a constant load is

$$\theta_R(i) = k \cdot T(P'_{\text{cable}}(T_{\max}), i, r_{\text{cable}}) \quad (3.15)$$

Where:

$\theta_R(i)$: “Conductor temperature rise above ambient at time i hours due to the application of a step function of load current equal to the sustained (100% load factor) rated current” [IEC60853-1]

k_{IEC} : Ratio of the temperature drop across the bedding to the total temperature drop between conductor and ground surface as defined by IEC 60853

$$k_{\text{IEC}} = \frac{P'_{\text{cable}}(T_{\max}) \cdot R_{\text{th,e}}}{\theta(\infty)} \quad (3.16)$$

$P'_{\text{cab}}(T_{\max})$: Total joule losses per cable at maximum operating temperature

$\theta(\infty)$: Conductor steady state temperature rise above ambient due to $P'_{\text{cable}}(T_{\max})$ only (i.e. disregarding dielectric losses) in °C

Therefore, the effect of the step function of amplitude Y_i at the moment of the highest conductor temperature can be calculated by using equation (3.15) as

$$dT_i = Y_i \cdot (\theta_R(i+1) - \theta_R(i)) \quad (3.17)$$

The actual temperature, denoted θ_m , can now be calculated as the sum of the temperatures due to the step functions in addition to the influence of the average temperature. Moreover, the temperature drop within the cable must be taken into account. Hence, with the definition of dT_i from equation (3.17) and under consideration that $\theta_R(0) = 0$, it is

$$\theta_m = \sum_{i=0}^5 dT_i + \mu \cdot (\theta_R(\infty) - \theta_R(6)) + \theta_R(\infty)(1 - k) \quad (3.18)$$

Where:

$\theta_R(\infty)$: “steady state conductor temperature rise due to the sustained (100% load factor) rated current” [IEC60853-1]. If dielectric losses are neglected it is

$$\theta_R(\infty) = \theta(\infty) = T_{\max} - T_{\text{ref}} \quad (3.19)$$

θ_m : “Maximum conductor current for a daily load cycle whose peak current is the [sustained (100% load factor); note from the author] rated current” [IEC60853].

Figure 3.3 shows the result of equation (3.18) in red on the secondary axis for a medium voltage cable system of type NA2XS(F)2Y with $A_c = 150 \text{ mm}^2$ (aluminium) in trefoil formation up to the first current peak of the load scheme. The latter equals the one that is shown in Figure 3.2 (black, primary axis). Moreover, the result of a finite element simulation of the same configuration is shown as a red, dotted line. It can be stated that the result – considering the fact that equation (3.18) is not used to calculate the actual temperature, but to find the maximum current, and that the simulation takes into account the temperature dependency of the conductor losses – is fairly good regarding the peak temperature, with a difference of about 3 °C between the numeric and the analytical calculation. However, regarding the dynamic of the curve, a significant discrepancy between the analytically calculated and the numerically simulated curve can be conceded.

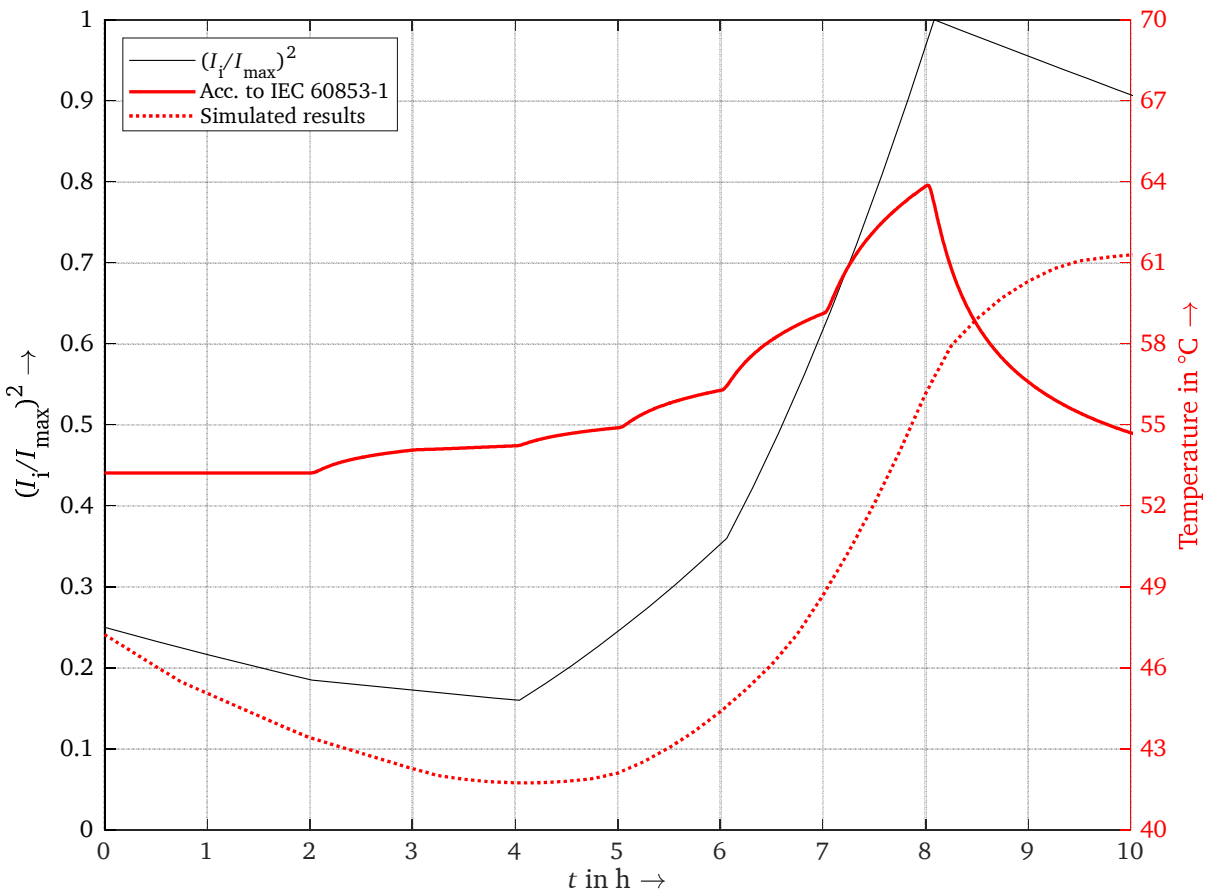


Figure 3.3: Conductor temperature according to the procedure from [IEC60853-1] for a cable of type NA2XS(F)2Y with $A_c = 150 \text{ mm}^2$ (Aluminium) in trefoil formation, subjected to the load pattern from Figure 3.2 with $I_{\max,60287}$ as the peak current amplitude. Dotted Line: Results from a simulation. The soil is supposed to be homogenous with a thermal conductivity of $1 \text{ W} \cdot \text{m}^{-1} \cdot \text{K}^{-1}$

By evaluating the ratio of the temperature θ_m and the maximum admissible conductor temperature, a load factor M_{IEC} is derived, giving the ratio between the rated current in stationary conditions to the admissible current under the evaluated, periodic load scheme

$$I_{\max,60853,\text{hom}} = M_{\text{IEC}} \cdot I_{\max,60287,\text{hom}} \quad (3.20)$$

With:

M_{IEC} : Rating factor due to a cyclic variation of load current

In part two of IEC 60853 [IEC60853-2], the thermal capacitances of the cable components are incorporated into the procedure that is mentioned above. In order to do so, first a ladder network of the cable with π -equivalent circuits is built, following the Van-Wormer-Approach (which will be further highlighted in chapter (6.7)). But instead of calculating the heat generation on the basis of the complete system, the ladder network is split up into two parts: the calculation of the temperature development inside the cable, denoted $\theta_c(t)$, and the temperature development on the surface of the cable, denoted $\theta_e(t)$. This procedure is illustrated in Figure 3.4.

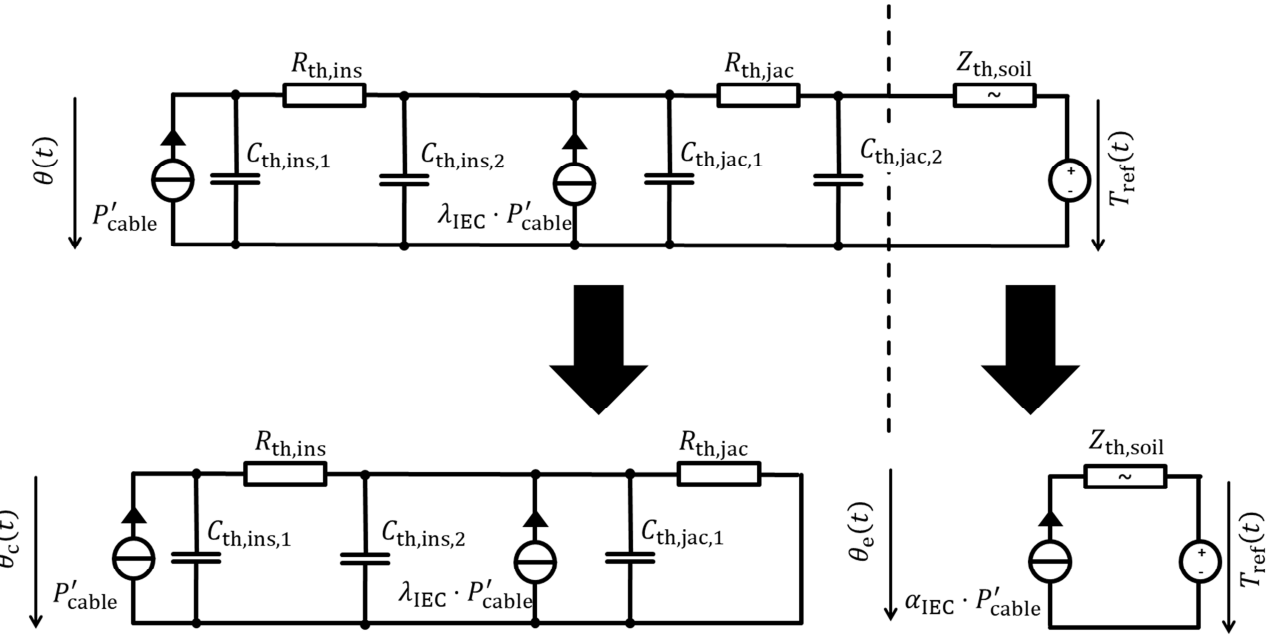


Figure 3.4: Illustration of the decomposition of the overall thermal equivalent circuit of the cable system (in this example, a medium voltage cable of type NA2XS(F)2Y) into two separate parts as proposed by IEC 60853-2. $Z_{th,soil}$ represents the thermal impedance of the soil.

First, the transient temperature rise of the conductor above the temperature on the outer surface of a cable at time t after the application of a unity step function of the nominal stationary current is calculated. This is done using the short-circuited ladder network, shown on the bottom, left side of Figure 3.4. Here, the cable components such as the insulation or the cable jacket can be split into further parts in order to account for shorter-period transients. From the calculation of $\theta_c(t)$, a “conductor to cable surface attainment factor” $\alpha_{IEC}(t)$ is derived as being the ratio between the transient conductor temperature and the steady state temperature for the thermal network, shown down left in Figure 3.4

$$\alpha_{IEC}(t) = \frac{\theta_c(t)}{\theta_c(\infty)} \quad (3.21)$$

Where:

- $\alpha_{IEC}(t)$: Conductor to cable surface attainment factor according to [IEC60853-2]
- $\theta_c(t)$: Transient temperature rise of conductor above the outer surface of a cable at time t after the application of a unity step function of the nominal stationary current
- $\theta_c(\infty)$: Transient temperature rise of conductor above the outer surface of a cable in stationary conditions

In a second step, the factor $\alpha_{IEC}(t)$ is used as a proportionality factor regarding the heat flux into the bedding. Based on the reasoning from part 1 of the standard, the temperature rise of the outer jacket is then supposed to be

$$\theta_e(t) = \alpha_{IEC}(t) \cdot T(P'_cable(T_{max}), t, r_{cable}) \quad (3.22)$$

With:

- $\theta_e(t)$: Transient temperature rise of the outer surface of a cable at time t after the application of a unity step function of the nominal stationary current

Hence, the total conductor temperature can be expressed as the sum of the internal and the external temperature rise

$$\theta(t) = \theta_e(t) + \theta_c(t) \quad (3.23)$$

Where:

$\theta(t)$: Transient temperature rise of conductor above the ambient temperature at time t after the application of a unity step function of the nominal stationary current

From the temperature $\theta(t)$ in equation (3.23), a factor M in analogy to equation (3.20) is derived.

Lastly, the third part of IEC 60853 [IEC60853-3] includes a possible introduction of the soil drying-out into the calculation of the factor M_{IEC} . Here, it must first be checked whether the temperature of the outer jacket exceeds the soil critical temperature during operation. If so, the steady state rating, on which the factor M is applied, is changed in a way that resembles the change from equation (3.1) to equation (3.9). The fact that for a given critical temperature, the dried-out zone under periodical conditions is smaller than under stationary condition is therefore not strictly taken into account, but counterweighted by the default choice of a very high critical temperature of 50 °C. Moreover, the problem of the mutual cable heating under the assumption of a dried-out soil in IEC 60287, which was mentioned before, still persists.

3.3 DIN VDE 0276

Although the German standard DIN VDE 0276 also focuses on periodic load schemes, there are significant differences to the international standard IEC 60283. First and foremost, it is obvious that the German standard aims more on the practical application than the description of the underlying ampacity rating calculations, as no formulae to calculate the temperature is given in the standard, but a table of actual current values for the corresponding cables. Regarding medium voltage distribution cables, the admissible current for a list of different conductor sizes and materials is given in DIN VDE 0276-620. Here, a periodically changing load scheme with a load factor of $m_{VDE} = 0,7$ is assumed, and soil drying-out is considered. It shall be noticed that the load factor m should not be confused with the loss factor from equation (3.10), as the load factor is defined as

$$m_{VDE} = \frac{1}{24} \sum_{i=0}^{23} \frac{I_i}{I_{\max}} \quad (3.24)$$

With:

m_{VDE} : Load factor as defined by [VDE0276-620]

The adoption of the values from DIN VDE 0276 to different environmental conditions (such as the reference temperature and the soil thermal resistivity or the laying inside protection pipes) and an accumulation of multiple cables inside one trench (but all equally loaded) is done via derating factors that can be derived by application of DIN VDE 0276-1000.

Most important is that the German standard does not use the same equations as IEC 60853, but relies on a method that anticipates the analysis of a periodic signal by its frequency components which will be further detailed later on. Here, an equivalent diameter is calculated that reflects the penetration depth of a heat wave with a certain frequency. Then, the actual resistance of the bedding is composed of two parts: The direct component of the losses traverses the ground resistance per unit length, as calculated in equation (3.9), whereas the alternating part takes effect on a thermal resistance that is calculated on the basis of the equivalent diameter. In the case that the equivalent diameter surpasses the drying out of the soil, the latter is quite simply split into two parts in order to take into account the

changes of the thermal properties. For further details of the actual computation, [WIN1978] resumes the work presented in [MAI1971], [WIN1971], [MAI1974-1], [MAI1974-2].

Although this procedure incorporates the calculation of alternating load flow patterns nicely into equation (3.9) and does not necessitate ample calculations of the transients, which is the case for IEC 60853, there are some inconveniences: First of all, the method is only reliable to load schemes with a load factor equal to or higher than 0.5. However load schemes of a power injection of photovoltaic generation typically have a load factor between of $0.3 < m_{VDE} < 0.4$. Moreover, the characterization of the load dynamic by the load factor only leads to very conservative results. As an example, Figure 3.5 shows two load patterns, both with $m_{VDE} = 0.7$, which would lead to the same ampacity rating according to DIN VDE 0276.

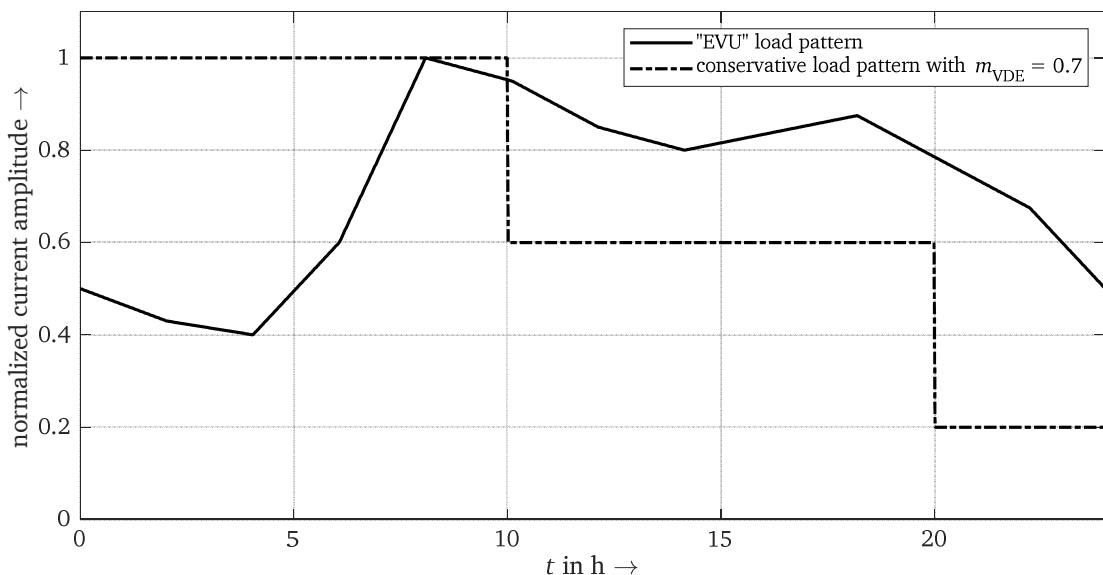


Figure 3.5: Comparison between two normalized daily load patterns of the same load factor $m_{VDE} = 0.7$.

But, by computing the temperature numerically, a difference of the current carrying capacity of more than 10 % is found. As the actual values in the standard are based on the load scheme, which is drawn in a dash-dotted line, and represent a very unfavorable load pattern because of the long lasting of the highest amplitude, this difference may be desired as the standard should always be one the safe side. However, in the sense of an accurate determination of the current carrying capacity, a difference of 10 % is worth of an enhancement.

3.4 Conclusion and assessment of the present standards

As it was demonstrated, the three standards cover a large variety of the three factors of influences on the cable ampacity rating: the geometric configuration of the cable systems, the load dynamic as well as the thermal properties of the bedding and soil. Moreover, they do so by being practical in the sense that no specialized software is needed for their application.

However, this practicality comes at a price: Most obviously, it can be stated that all three standards use different methodologies whereas the underlying theory of heat conduction is the same. This disparity in methods is due to the differences in the dependencies of time, which are covered by the standards, and the exigence that all procedures should be calculable on “pen and paper”. Especially for the calculation of transient and periodic temperatures, as it is proposed by IEC 60853, this necessity leads to a multiplicity of approximate formulae that make the actual process seem adverse.

Furthermore, several assumptions and simplifications are made that are valid from a practical, but less coherent from a theoretical viewpoint: With respect to IEC 60287, the soil drying-out is not taken into consideration regarding the thermal interaction between the cables when calculating their external resistance. The reduction of the maximum temperature rise for one cable due to its own losses because of the mutual heating of cables in the same duct can be integrated into equation (3.1), but this is not specified in the standard itself.

Regarding IEC 60853, the usage of a line source to determine the heating inside the bedding instead of a cylindrical source was already discussed in [BUL1951]. Also, the splitting of the system by first calculating the transient heating of the cable alone and then using α_{IEC} as a proportionality factor for the heat flux into the bedding may be opportune, but is theoretically not correct. And the proposed application of a derating factor due to the drying-out of the soil does not take into account the changes in the dynamic of the heating due to changed thermal properties of the bedding. Also, as the rating factor M is always related to the maximum current values derived in IEC 60287, the problems of determining the mutual heating of cables under the assumption of a dried-out soil persist.

And finally, the restriction of the method behind DIN VDE 0276 to load factors larger than 0.5 is deficient to calculate load schemes due to a power injection from photovoltaic sites.

As a consequence of these different methodologies, the existing standards – as good they may be for their actual scope – cannot serve as the basis of a routine to implement a “real time” computation of cable ampacity ratings, as they are hard to be put into the form of an automatized algorithm. More suitable would be a coherent methodology, even at the price that the solution of the implied expression can only be solved with the help of a computational routine. Furthermore, no restrictions should exist regarding the possible cable configuration and the dynamic of the load.

Such an approach was already presented in [OLS2012] or [MIL2006]. However, they are based on a discretization of the cable elements and – regarding [OLS2012] – of a cylindrical approximation of the outer bedding. Furthermore, the representation of the mutual heating of different cable groups within the presented models and the underlying simplifications are only valid for a limited number of cables. A theoretically concise approach without any restriction regarding the load scheme, bedding properties and cable configurations has therefore been missing until now. But before this gap is filled by this work, the fundamentals of the implied physics will be recalled.

4 Theoretical fundamentals

As different as the involved physics are, their theoretic formulation all lead to a set of similar differential equations, whose deduction will shortly be recalled in the following section. Afterwards, the solution techniques will be presented and finally applied to relevant problems regarding the calculations of cable losses as well as the heat conduction in cable systems.

4.1 Fundamental equations

In the first part of chapter 4, the state equations for the three different disciplines of physic will be derived. This is done with respect to electrodynamics (regarding the conductor and screen losses), heat conduction (regarding the conduction of heat inside cable elements) and heat and mass diffusion inside soils.

4.1.1 Fundamental equations of electrodynamics

In order to formulate the equations that govern the calculation of the cable losses, one must start with the Maxwell equations, whose differential form is [WEI2010]⁶

$$\text{rot } \vec{E}(\vec{r}, t) = -\frac{\partial}{\partial t} \vec{B}(\vec{r}, t) \quad (4.1)$$

$$\text{rot } \vec{H}(\vec{r}, t) = \frac{\partial}{\partial t} \vec{D}(\vec{r}, t) + \vec{J}(\vec{r}, t) \quad (4.2)$$

$$\text{div } \vec{D}(\vec{r}, t) = \varrho(\vec{r}, t) \quad (4.3)$$

$$\text{div } \vec{B}(\vec{r}, t) = 0 \quad (4.4)$$

With:

$\vec{E}(\vec{r}, t)$: Electric field strength

$\vec{D}(\vec{r}, t)$: Displacement field

$\vec{H}(\vec{r}, t)$: Magnetic field strength

$\vec{B}(\vec{r}, t)$: Magnetic flux density

$\vec{J}(\vec{r}, t)$: Current density

In the following, the dependencies of the variables such as time (t) and space (\vec{r}) will be omitted to improve readability. Equation (4.1) is also known as Faraday's law, equation (4.2) as Ampère's law. Equations (4.3) and (4.4) are often referred to as Gauss's law. Moreover, the field strengths and the flux densities are connected via material properties. In the case of an isotropic medium, i.e. there is no dependency of the properties from the direction of fields, and a frequency independent behaviour, one may write

$$\vec{D} = \varepsilon \cdot \vec{E} \quad (4.5)$$

$$\vec{B} = \mu \cdot \vec{H} \quad (4.6)$$

$$\vec{J} = \kappa \cdot \vec{E} \quad (4.7)$$

Where:

ε : Permittivity

μ : Magnetic permeability

κ : Electric conductivity

⁶ If not otherwise indicated, the equations in chapter 4.1.1 are taken from [WEI2010]

Permittivity and permeability are commonly expressed as the product of material related scalars and the properties of vacuum, so that

$$\epsilon = \epsilon_r \cdot \epsilon_0 \quad (4.8)$$

$$\mu = \mu_r \cdot \mu_0 \quad (4.9)$$

Where:

ϵ_0 : Permittivity of vacuum; $\epsilon_0 \approx 8.854 \cdot 10^{-12} \text{ A}\cdot\text{s}\cdot\text{V}^{-1}\cdot\text{m}^{-1}$

μ_0 : Permeability of vacuum; $\mu_0 = 4 \cdot \pi \cdot 10^{-7} \text{ V}\cdot\text{s}\cdot\text{A}^{-1}\cdot\text{m}^{-1}$

With respect to the calculation of losses inside a cable conductor, equation (4.2) can be further simplified: As the displacement-current is much smaller than the current density, one may write

$$\max \left| \frac{\partial}{\partial t} \vec{D} \right| \ll \max |J| \quad (4.10)$$

so that equation (4.2) simplifies to

$$\operatorname{rot} \vec{H} = \vec{J} \quad (4.11)$$

This *quasi stationary approximation* is also valid for regions of non-conducting materials, as the changes in time are much smaller than the propagation velocity of electromagnetic waves if only the basic frequency of 50 Hz is considered. In other words: The examined geometries are much smaller than the associated wavelength of the basic frequency, so that the changes in field can be assumed to be instantaneous throughout the calculation area. As a consequence, the magnetic fields may be regarded as “primary” from whose the electric fields can be derived, neglecting the influence of the latter on the magnetic fields [WEI2010].

Inserting equation (4.7) into (4.11) and regrouping leads to

$$\vec{E} = \frac{1}{\kappa} \operatorname{rot} \vec{H} \quad (4.12)$$

so that inserting equation (4.12) into equation (4.1) and reformulation of the magnetic flux density with the help of equation (4.6) yields

$$\operatorname{rot} \left(\frac{1}{\kappa} \operatorname{rot} \vec{H} \right) = -\mu \cdot \frac{\partial}{\partial t} \vec{H} \quad (4.13)$$

Under consideration of equation (4.4) and a uniform electric conductivity, the left side of the equation above simplifies to

$$\operatorname{rot} \left(\frac{1}{\kappa} \operatorname{rot} \vec{H} \right) = \frac{1}{\kappa} [\operatorname{grad}(\operatorname{div} \vec{H}) - \Delta \vec{H}] = -\frac{1}{\kappa} \Delta \vec{H} \quad (4.14)$$

so that equation (4.13) can be written as

$$\Delta \vec{H} = \kappa \cdot \mu \cdot \frac{\partial}{\partial t} \vec{H} \quad (4.15)$$

Analogically, equation (4.15) can be formulated with respect to the electric field strength, yielding

$$\Delta \vec{E} = \kappa \cdot \mu \cdot \frac{\partial}{\partial t} \vec{E} \quad (4.16)$$

With respect to the given boundary conditions, it may even be helpful to use the vector potential \vec{A} , which is defined as

$$\operatorname{rot} \vec{A} = \vec{B} \quad (4.17)$$

so that equation (4.4) is always fulfilled [LEH1990].

Using a proper gauge choice, i.e. [LEH1990]

$$\operatorname{div} \vec{A} = 0 \rightarrow \operatorname{rot} \operatorname{rot} \vec{A} = \operatorname{grad} \operatorname{div} \vec{A} - \vec{\Delta} \vec{A} = -\vec{\Delta} \vec{A}(\vec{r}, t) \quad (4.18)$$

leads to:

$$\vec{\Delta} \vec{A} = \kappa \cdot \mu \cdot \frac{\partial}{\partial t} \vec{A} \quad (4.19)$$

In areas where the conductivity of the material is zero, equation (4.19) simplifies to

$$\vec{\Delta} \vec{A}(\vec{r}, t) = 0 \quad (4.20)$$

4.1.2 Fundamental equations of heat conduction

With respect to the deviation of the fundamental equation of heat conduction, one starts best with the first law of thermodynamics [SCH2014-2]⁷, applied to an infinitesimal volume without heat generation

$$\frac{\partial H}{\partial t} = -\operatorname{div} \vec{q} \quad (4.21)$$

Where:

H : Enthalpy density⁸

Moreover, the specific enthalpy, i.e. the enthalpy related to the mass, can be expressed by the help of the two state variables, temperature and pressure

$$\frac{H \cdot V}{m} = h = h(T, p) \quad (4.22)$$

With:

m : Mass inside the control volume

h : Specific enthalpy

p : Pressure

Applying the chain rule, it follows that a change in specific enthalpy can be expressed as

$$dh = \left. \frac{\partial h}{\partial T} \right|_p \cdot dT + \left. \frac{\partial h}{\partial p} \right|_T \cdot dp = c_p \cdot dT + \left. \frac{\partial h}{\partial p} \right|_T \cdot dp \quad (4.23)$$

Where:

c_p : Specific heat capacity at constant pressure

Assuming the pressure to be constant, equation (4.23) simplifies to

$$dh = c_p \cdot dT \quad (4.24)$$

Or, with respect to the total enthalpy

$$\frac{\partial H}{\partial t} = \rho \cdot c_p \cdot \frac{\partial T}{\partial t} \quad (4.25)$$

Concerning the right side of equation (4.21), the flow of heat is proportional to the gradient of the temperature, i.e.

$$\vec{q} = -\lambda \cdot \operatorname{grad} T \quad (4.26)$$

Where:

λ : Thermal conductivity

⁷ All derivations in chapter 4.1.2 are based on the explanations in [SCH2014-2]

⁸ For this demonstration, the notation in [KEM1981] is followed, so that H does not denote the total enthalpy (as it is commonly the case)

Equation (4.26) is often referred to as the Fourier-law. Inserting the Fourier-law, equation (4.25) and a possible heat generation into (4.21) then yields the *general heat equation* [HAH2012]

$$\rho \cdot c_p \frac{\partial T}{\partial t} = -\operatorname{div}(\lambda \cdot \operatorname{grad} T) + g \quad (4.27)$$

With:

ρ : Mass density

g : Volumetric heat generation

Assuming the heat conductivity and density of the material to be constant and neglecting the temperature dependency of the latter, this simplifies to

$$\Delta T = \frac{\rho \cdot c_p}{\lambda} \frac{\partial T}{\partial t} - \frac{g}{\lambda} = \frac{1}{\alpha} \frac{\partial T}{\partial t} - \frac{g}{\lambda} \quad (4.28)$$

If there is no heat generation inside the medium, equation (4.28) becomes

$$\Delta T = \frac{1}{\alpha} \frac{\partial}{\partial t} T \quad (4.29)$$

4.1.3 Fundamental equations of coupled heat and mass diffusion within soils

To evaluate the physical changes within bedding materials of power cable systems, the combined transfer of mass (in the form of water and vapour) and heat inside the soil matrix must be derived. In order to do so, it is recommendable to start with the movement of water within soil under isothermal conditions and then expand the theory on water movements under thermal gradients. Finally, the movement of vapour is included into the equations. The derivations in chapter 4.1.3 are mainly based on the explanations in [LOG2001] and [KEM1981] (which, itself resumes the work of [PHI1957] and [VRI1958]), although many expressions have been reformulated to the pressure head instead of the volumetric water content as the state variable, because this improves the stability of numerical calculations.

4.1.3.1 Mass transfer in soils

Starting with water movements inside soils under isothermal conditions, it must be stated that the velocity and tension tensors are hard to be considered regarding the geometry of pore spaces inside the soil. Moreover, the flow rates are very low with respect to free-flow velocities, so that an exact formulation of the flow field using Navier-Stokes equations is less practicable. Nonetheless, as the pore structure is very small compared to the overall geometry, the pressure gradients inside the pore air can be neglected, and it is possible to describe the flow of water macroscopically as a diffusion process. The driving force behind this diffusion is the gradient of hydraulic pressure, hence [LOG2001]

$$\vec{m}_l \sim \frac{1}{g} \operatorname{grad} p_{hy} \quad (4.30)$$

Where:

\vec{m}_l : Mass flux density of liquid water

g : Gravitational acceleration

p_{hy} : Hydraulic pressure

As the following considerations are restricted to water as fluid, it is reasonable to divide equation (4.30) by the density of water, which yields

$$\vec{v}(\vec{r}, t) \sim \frac{1}{g \cdot \rho_w} \operatorname{grad} p_{hy} \quad (4.31)$$

With:

\vec{v} : Darcy velocity

ρ_w : Density of water

The Darcy velocity represents the macroscopic bulk velocity and should not be confused with the actual flow velocity of the water. As the variations in pressure and temperature within the soil have only small effects on the density of water, the latter may be considered to be constant in the following. Moreover, it is useful to combine the hydraulic pressure and the specific weight w_w of water to the so-called hydraulic head h_h , so that

$$h_h = \frac{p_{hy}}{g \cdot \rho_w} = \frac{p_{hy}}{w_w} \quad (4.32)$$

Where:

h_h : Hydraulic head

w_w : Specific weight of water

The hydraulic head, often also denoted as hydraulic potential ϕ , is – considering the unsaturated zone – composed of the effect of gravity (denoted as elevation head) and the pressure head h_{hy} (or hydrostatic potential ψ). The former can be expressed as the distance to a reference potential z_{ref} with the variable of space z (if the coordinate system is chosen such as the gravitational force acts alongside the z -direction), so that it may be written

$$h_h(\vec{r}, t) = h_{hy}(\vec{r}, t) + z - z_{ref} \quad (4.33)$$

With:

h_{hy} : Pressure head

z : Variable of space in the direction of gravitational force

z_{ref} : Height of the reference potential, usually the phreatic level

While the pressure head is positive below the phreatic water surface, water inside the unsaturated zone is exposed to negative pressure due to adsorption and capillary forces.

Inserting equation (4.33) into (4.31) then yields

$$\vec{v} \sim \text{grad } h_h = \text{grad } h_{hy} + \vec{e}_z \quad (4.34)$$

The proportionality factor between the gradient of the hydraulic head and the Darcy velocity is denoted the hydraulic conductivity k . It is in general a function of the water content of the soil and – to a minor extend – of the temperature. Therefore

$$\vec{v} = k \cdot \text{grad } h_h = k \cdot \text{grad } h_{hy} + k \cdot \vec{e}_z \quad (4.35)$$

With:

k : Hydraulic conductivity

Or, in terms of the mass flow of liquid water:

$$\vec{m}_l = -\rho_w [D_{l,h_{hy}} \cdot \text{grad } h_{hy} + k \cdot \vec{e}_z] \quad (4.36)$$

Where:

$D_{l,h_{hy}}$: Diffusion coefficient of liquid water due to gradients of the pressure head

Sometimes, the permeability K of the soil is used instead of the hydraulic conductivity k , as the permeability depends only on the soil (if stated as incompressible) and not the fluid. In the case of water, the relationship between these two parameters is [LAN2003]⁹

$$K = \frac{\mu_w}{\rho_w \cdot g} \cdot k \quad (4.37)$$

With:

K : Permeability

μ_w : Dynamic viscosity of water

In analogy to equation (4.36), the transport equation of water vapour can be formulated, regarding two differences: Firstly, the gravity term in (4.36) can be neglected and secondly, as the partial pressure of water vapour is highly dependent of the temperature, the gradient of the latter is included into the transport equation, leading to

$$\vec{m}_v = -\rho_w \left[D_{v,h_{hy}} \cdot \text{grad } h_{hy} + D_{v,T} \cdot \text{grad } T \right] \quad (4.38)$$

Where:

\vec{m}_v : Mass flux density of water vapour

$D_{v,h_{hy}}$: Diffusion coefficient of water vapour due to gradients of the pressure head

$D_{v,T}$: Diffusion coefficient of water vapour due to gradients of the temperature

The sum of equation (4.36) and (4.38) then leads to the total mass flux density

$$\vec{m} = \vec{m}_l + \vec{m}_v = -\rho_w \cdot \left(\left[D_{h_{hy}} \cdot \text{grad } h_{hy} + D_{v,T} \cdot \text{grad } T + k \cdot \vec{e}_z \right] \right) \quad (4.39)$$

With:

$D_{h_{hy}}$: Diffusion coefficient due to gradients of the pressure head:

$$D_{h_{hy}} = D_{l,h_{hy}} + D_{v,h_{hy}} \quad (4.40)$$

The detailed calculation of the mass diffusion coefficients is given in Appendix A4.

In addition to the flow that is described by equation (4.39), the conservation of mass must be considered: A non-zero balance of the Darcy-velocity on the surface of a control volume leads to a change of the volumetric water content, hence

$$\frac{\partial \theta_l}{\partial t} = -\text{div } \vec{v}_l = \text{div} \left(D_{l,h_{hy}} \cdot \text{grad } h_{hy} \right) + \frac{\partial k}{\partial z} \quad (4.41)$$

With:

θ_l : Volumetric water content as a fraction of the pore space volume

And with respect to water vapour

$$\frac{\partial \theta_v}{\partial t} = -\frac{1}{\rho_w} \text{div } \vec{m}_v = \text{div} \left(D_{v,h_{hy}} \cdot \text{grad } h_{hy} \right) + \text{div} \left(D_{v,T} \cdot \text{grad } T \right) \quad (4.42)$$

Where:

θ_v : Volumetric content of the condensed water vapour in % of the pore space volume

⁹ In the cited German source, K is the hydraulic conductivity ("Durchlässigkeitsbeiwert") and k the permeability. For the following, the definition according to [LOG2001] is kept.

The sum of equation (4.41) and (4.42) then yields the conservation equation for the total mass

$$\frac{\partial \theta_l}{\partial t} + \frac{\partial \theta_v}{\partial t} = \operatorname{div} (D_{h_{hy}} \cdot \operatorname{grad} h_{hy}) + \operatorname{div} (D_{v,T} \cdot \operatorname{grad} T) + \frac{\partial k}{\partial z} \quad (4.43)$$

As the volumetric water content of liquid water is a function of the pressure head as well as – to a lesser extend – of the temperature (further influences on the hydraulic potential such as osmotic or mechanical pressures or changes of the pore volume will not be regarded in the following), one may write

$$h_{hy} = f(\theta_l, T) \quad (4.44)$$

as well as

$$\theta_l = f(h_{hy}, T) \quad (4.45)$$

The same goes for the volumetric content of water vapour, so that

$$\theta_v = f(h_{hy}, T) \quad (4.46)$$

Applying the chain rule for the derivation in time on equations (4.45) and (4.46) therefore leads to

$$\frac{\partial \theta_l}{\partial t} = \left. \frac{\partial \theta_l}{\partial h_{hy}} \right|_T \cdot \frac{\partial h_{hy}}{\partial t} + \left. \frac{\partial \theta_l}{\partial T} \right|_{h_{hy}} \cdot \frac{\partial T}{\partial t} \quad (4.47)$$

$$\frac{\partial \theta_v}{\partial t} = \left. \frac{\partial \theta_v}{\partial h_{hy}} \right|_T \cdot \frac{\partial h_{hy}}{\partial t} + \left. \frac{\partial \theta_v}{\partial T} \right|_{h_{hy}} \cdot \frac{\partial T}{\partial t} \quad (4.48)$$

so that equation (4.43) can be re-written as

$$\begin{aligned} & \left[\frac{\partial \theta_l}{\partial h_{hy}} + \frac{\partial \theta_v}{\partial h_{hy}} \right]_T \cdot \frac{\partial h_{hy}}{\partial t} + \left[\frac{\partial \theta_l}{\partial T} + \frac{\partial \theta_v}{\partial T} \right]_{h_{hy}} \cdot \frac{\partial T}{\partial t} = \\ & c_1 \cdot \frac{\partial h_{hy}}{\partial t} + c_2 \cdot \frac{\partial T}{\partial t} = \operatorname{div} (D_{h_{hy}} \cdot \operatorname{grad} h_{hy}) + \operatorname{div} (D_{v,T} \cdot \operatorname{grad} T) + \frac{\partial k}{\partial z} \end{aligned} \quad (4.49)$$

In difference to equation (4.27) or (4.19), equation (4.49) contains two variables of state: the pressure head as well as the temperature. Therefore, a second equation must be derived to fully determine the distribution of heat and mass. This is done by evaluating the heat transfer mechanisms in the following section.

4.1.3.2 Heat transfer in soils

Regarding the transfer of heat, the equations in section (4.1.2) are still valid for porous media. However, two important differences have to be considered:

Firstly, the heat flux within the soil matrix not only encompasses conduction (as it is the case for solid matters), but also advection, i.e. the transport of inner energy due to the bulk motion of the fluid and vapour. Furthermore, the heat of vaporization or condensation must be taken into account, leading to the formulation of the heat flux

$$\vec{q} = \vec{q}_{\text{con}} + \vec{q}_{\text{adv}} + \vec{q}_{\text{lat}} \quad (4.50)$$

Where:

\vec{q}_{kon} : Heat flux density due to conduction

\vec{q}_{adv} : Heat flux density due to advection

\vec{q}_{lat} : Heat flux density due to the transport of latent heat

For the conductive heat flux, the Fourier-law from equation (4.26) is still valid, although it must be taken into account that the heat conductivity depends strongly on the water content of the soil and is therefore a function of space and time. The advective heat flux is calculated by

$$\vec{q}_{\text{adv}} = c_{p,w} \cdot (T - T_{\text{ref}}) \cdot \vec{m} \quad (4.51)$$

Where:

$c_{p,w}$: Specific heat capacity of liquid water at constant pressure

T_{ref} : Reference temperature

And with regard to the transport of latent heat, it is

$$\vec{q}_{\text{lat}} = L \cdot \vec{m}_v \quad (4.52)$$

Where:

L : Specific heat of vaporization of water

Expressing equation (4.52) in terms of the state variables by inserting equation (4.38) yields

$$\vec{q}_{\text{lat}} = -L \cdot \rho_w \cdot (D_{v,h_{\text{hy}}} \cdot \text{grad } h_{\text{hy}} + D_{v,T} \cdot \text{grad } T) \quad (4.53)$$

Inserting equation (4.26), (4.51) and (4.53) into (4.50), the total heat flux can be written as

$$\vec{q} = -\lambda' \cdot \text{grad } T - L \cdot \rho_w \cdot (D_{v,h_{\text{hy}}} \cdot \text{grad } h_{\text{hy}} + D_{v,T} \cdot \text{grad } T) + c_{p,w} \cdot (T - T_{\text{ref}}) \cdot \vec{m} \quad (4.54)$$

or, after regrouping with respect to the gradients

$$\vec{q} = -(\lambda' + L \cdot \rho_w \cdot D_{T,v}) \cdot \text{grad } T - L \cdot \rho_l \cdot D_{v,h_{\text{hy}}} \cdot \text{grad } h_{\text{hy}} + c_{p,l} \cdot (T - T_{\text{ref}}) \cdot \vec{m} \quad (4.55)$$

As the diffusion of water vapour also appears at small temperature gradients, the heat conductivity λ is often combined with the transport of latent heat to the so-called “apparent thermal conductivity”. This conductivity is “apparent” in the sense that this is the conductivity that is measured by temperature sensors. With its definition

$$\lambda = \lambda' + L \cdot \rho_w \cdot D_{T,v} \quad (4.56)$$

equation (4.55) is reformulated to

$$\vec{q} = -\lambda \cdot \text{grad } T - L \cdot \rho_w \cdot D_{v,h_{\text{hy}}} \cdot \text{grad } h_{\text{hy}} + c_{p,w} \cdot (T - T_{\text{ref}}) \cdot \vec{m} \quad (4.57)$$

Secondly, the fact that a volume of „soil“ is composed out of a solid, liquid and gas must be taken into account by calculation the total enthalpy. Therefore, it is

$$H_{\text{tot}} = \rho_s \cdot c_{p,s} \cdot (T - T_{\text{ref}}) + \rho_w \cdot c_{p,w} \cdot \theta_l \cdot (T - T_{\text{ref}}) + \rho_w \cdot \theta_v \cdot [L + c_{p,w} \cdot (T - T_{\text{ref}})] \quad (4.58)$$

Where:

H_{tot} : Total enthalpy density

ρ_s : Density of the solid fraction of the soil

$c_{p,s}$: Specific heat capacity at constant pressure of the solid fraction of the soil

Hence, the derivation with respect to time of the total enthalpy yields

$$\frac{\partial H_{\text{tot}}}{\partial t} = C_{\text{tot}} \cdot \frac{\partial T}{\partial t} + \rho_w \cdot c_{p,w} \cdot (T - T_{\text{ref}}) \cdot \left[\frac{\partial \theta_l}{\partial t} + \frac{\partial \theta_v}{\partial t} \right] + \rho_w \cdot L \cdot \frac{\partial \theta_v}{\partial t} \quad (4.59)$$

Where:

$$C_{\text{tot}} = \rho_s \cdot c_{p,s} + \rho_w \cdot c_{p,w} \cdot \theta_l + \rho_w \cdot c_{p,w} \cdot \theta_v + \rho_w \cdot \theta_v \cdot \frac{\partial L}{\partial T} \quad (4.60)$$

Inserting equation (4.43) for the derivations with respect to the time gives

$$\frac{\partial H_{\text{tot}}}{\partial t} = C_{\text{tot}} \cdot \frac{\partial T}{\partial t} + \rho_w \cdot c_{p,w} \cdot (T - T_{\text{ref}}) \cdot \left(c_1 \cdot \frac{\partial h_{\text{hy}}}{\partial t} + c_2 \cdot \frac{\partial T}{\partial t} \right) + \rho_w \cdot L \frac{\partial \theta_v}{\partial h_{\text{hy}}} \frac{\partial h_{\text{hy}}(\vec{r}, t)}{\partial t} \quad (4.61)$$

Or, by regrouping

$$\frac{\partial H_{\text{tot}}}{\partial t} = [C_{\text{tot}} + \rho_w \cdot c_{p,w} \cdot (T - T_{\text{ref}}) \cdot c_2] \cdot \frac{\partial T}{\partial t} + [\rho_w \cdot c_{p,w} \cdot (T - T_{\text{ref}}) \cdot c_1 + \rho_w \cdot L \frac{\partial \theta_v}{\partial h_{\text{hy}}}] \cdot \frac{\partial h_{\text{hy}}}{\partial t} \quad (4.62)$$

Finally, the flux equation in (4.57) and the derivation of the total enthalpy from equation (4.62) must be included into equation (4.21). Building the divergence of the heat flux yields

$$-\operatorname{div} \vec{q} = \operatorname{div} (\lambda \cdot \operatorname{grad} T) + \operatorname{div} (L \cdot \rho_l \cdot D_{\theta,v} \cdot \operatorname{grad} \theta_l) - \operatorname{div} (c_{p,w} \cdot (T - T_{\text{ref}}) \cdot \vec{m}) \quad (4.63)$$

Inserting the expression for the flow of mass in (4.38) into (4.63) and setting the reference temperature to zero gets

$$\begin{aligned} -\operatorname{div} \vec{q} &= \operatorname{div} (\lambda \cdot \operatorname{grad} T) + \operatorname{div} (L \cdot \rho_w \cdot D_{h_{\text{hy}},v} \cdot \operatorname{grad} h_{\text{hy}}) \\ &\quad + \operatorname{div} (c_{p,w} \cdot \rho_w \cdot T \cdot ([D_{h_{\text{hy}}} \cdot \operatorname{grad} h_{\text{hy}} + D_{v,T} \cdot \operatorname{grad} T + k \cdot \vec{e}_z])) \end{aligned} \quad (4.64)$$

so that

$$\begin{aligned} \frac{\partial H_{\text{tot}}}{\partial t} &= \operatorname{div} ([\lambda + c_{p,w} \cdot \rho_w \cdot T \cdot D_{v,T}] \cdot \operatorname{grad} T) \\ &\quad + \operatorname{div} (\rho_w \cdot [c_{p,l} \cdot T \cdot D_{h_{\text{hy}}} + L \cdot D_{h_{\text{hy}},v}] \cdot \operatorname{grad} h_{\text{hy}}) + \frac{\partial k}{\partial z} \end{aligned} \quad (4.65)$$

Finally, the derivation in time of the total enthalpy from equation (4.62) can be inserted into equation (4.65). Merging the different terms into functions makes the structure become more clear

$$c_3 \cdot \frac{\partial T(\vec{r}, t)}{\partial t} + c_4 \cdot \frac{\partial h_{\text{hy}}}{\partial t} = \operatorname{div} (c_5 \cdot \operatorname{grad} T) + \operatorname{div} (c_6 \cdot \operatorname{grad} h_{\text{hy}}) + \frac{\partial k}{\partial z} \quad (4.66)$$

Closing remark: The choice of an arbitrary reference temperature can be justified via the help of a different formulation of equation (4.64): If the divergence is built from the product of the flux of mass and the scalar temperature field, it is

$$\begin{aligned} -\operatorname{div} \vec{q} &= \operatorname{div} (\lambda \cdot \operatorname{grad} T) + \operatorname{div} (L \cdot \rho_w \cdot D_{\theta,v} \cdot \operatorname{grad} \theta_l) \\ &\quad + c_{p,w} \cdot \rho_w \cdot (T - T_{\text{ref}}) \cdot \operatorname{div} \vec{m} + c_{p,w} \cdot \rho_w \cdot \vec{m} \cdot \operatorname{grad} T \end{aligned} \quad (4.67)$$

If this is inserted into equation (4.21) by formulating the derivatives of time from water contents as the divergence of the mass flux, so that

$$\frac{\partial H_{\text{tot}}}{\partial t} = C_{\text{tot}} \cdot \frac{\partial T}{\partial t} + \rho_w \cdot c_{p,l} \cdot (T - T_{\text{ref}}) \cdot \operatorname{div} \vec{m} + \rho_w \cdot L \cdot \frac{\partial \theta_v}{\partial t} \quad (4.68)$$

The term including the reference temperature is eliminated

$$\begin{aligned} C_{\text{tot}} \cdot \frac{\partial T}{\partial t} + \rho_l \cdot L \cdot \frac{\partial \theta_v}{\partial t} \\ = \operatorname{div} (\lambda \cdot \operatorname{grad} T) + \operatorname{div} (\rho_w \cdot L \cdot D_{\theta,v} \cdot \operatorname{grad} \theta_l) + c_{p,l} \cdot \rho_w \cdot \vec{m} \cdot \operatorname{grad} (T) \end{aligned} \quad (4.69)$$

4.2 Boundary and initial conditions

Solutions to the derived equations in (4.19), (4.28), (4.49) and (4.66) have not only to be solved inside the regarded domain, but must also fulfil specific conditions on the boundary of the domain. In general, if the state variable to be solved is scalar and denoted as P , the condition on a boundary i can be formulated as [HAH2012]

$$a_i \cdot P(\vec{r}_i, t) + b_i \cdot \frac{\partial}{\partial \vec{n}_i} P(\vec{r}_i, t) = c_i(\vec{r}_i, t) \quad (4.70)$$

Where:

- \vec{r}_i : Position vector of the boundary i
- \vec{n}_i : Normal vector to the boundary i
- a_i, b_i : Factors determining the type of the boundary condition
- $c_i(\vec{r}_i, t)$: Arbitrary function

Depending on the factors a_i and b_i , three different types can be distinguished:

1. If $b_i = 0$ the boundary condition is called a Dirichlet boundary condition, as the value of the state variable is fixed on the boundary.
2. If $a_i = 0$ the boundary condition is classified as a Neumann boundary condition, as the flux perpendicular to the boundary is determined.
3. If $a_i \neq 0$ and $b_i \neq 0$ the boundary is called a Robin- or Cauchy condition, as the flux perpendicular to the boundary is a function of the temperature on it.

Furthermore, if

$$c_i(\vec{r}_i, t) = 0 \quad (4.71)$$

the boundary condition is said to be homogenous, otherwise, it is called non-homogenous.

The rather abstract formulation in equation (4.70) becomes more tangible if it is applied to the actual physics: Considering the temperature field due to heat conduction, a Dirichlet condition fixes the temperature on a boundary. This condition is often applied to the ground surface, as it is a common assumption that the temperature on the ground surface is equal to the “ambient” temperature. Moreover, the thermal interaction between different cables is often calculated by assuming worst case conditions, so that in this case, the temperature on the cable conductor surface is set to the maximum conductor temperature. A Neumann condition comes into play if the heat flux into or out of a component is known. This is the case for the cable components as well as the bedding, which are traversed by the losses of a cable system. And finally, a Robin boundary condition implements a convective boundary condition, as in this case, the heat flux into the ambient fluid is governed by the temperature difference between the surface and the surroundings. Therefore, boundary conditions of the third type must be applied on the outside of cable jackets if they are surrounded by air or – strictly spoken – to the ground surface. The fact that the boundary condition of the ground surface is often replaced by a Dirichlet condition will be discussed in section 5.3.

With respect to the flux of moisture within soils, a Dirichlet condition fixes the pressure head on the boundary. The most prominent boundary would be the phreatic level, as the potential on it is defined to be zero. A Neumann boundary condition must be used if the inflow of water (in the form of the Darcy-velocity) is known, and a Cauchy boundary condition can be used to implement evaporation on the ground surface.

If, however, the state variable is a vector, conditions on boundaries must take into account its direction. This begins with boundaries between two materials with different properties inside the domain: While a scalar state variable is always continuous on the boundaries between two different materials, this is only valid for some components for the state vector. With respect to the quasi-stationary magnetic fields, introduced in section 4.1.1, the conditions on boundaries can be written as the following [WEI2010]:

1. The tangential component of the electric field strength must be continuous, hence

$$\vec{n}_{1,2} \times (\vec{E}_2 - \vec{E}_1) = \vec{0} \quad (4.72)$$

Where:

$\vec{n}_{1,2}$: Normal vector on the boundary from area 1 to area 2

\vec{E}_1, \vec{E}_2 : Electric field strength in area 1 and 2, respectively

2. The difference of the normal component of the displacement field equals the surface charge density on the boundary

$$\vec{n}_{1,2} \cdot (\vec{D}_2 - \vec{D}_1) = \sigma \quad (4.73)$$

Where:

\vec{D}_1, \vec{D}_2 : Displacement field strength in area 1 and 2, respectively

σ : Surface charge density on the boundary

3. The normal component of the magnetic flux must be continuous, hence

$$\vec{n}_{1,2} \cdot (\vec{B}_2 - \vec{B}_1) = \vec{0} \quad (4.74)$$

Where:

\vec{B}_1, \vec{B}_2 : Displacement field strength in area 1 and 2, respectively

4. The difference of the tangential component of the magnetic field intensity equals the surface current density¹⁰ on the boundary

$$\vec{n}_{1,2} \times (\vec{H}_2 - \vec{H}_1) = \vec{J}_s \quad (4.75)$$

Where:

\vec{H}_1, \vec{H}_2 : Magnetic field strength in area 1 and 2, respectively

\vec{J}_s : Surface current density on the boundary

5. From equation (4.17), the application of the rotation and comparison with equation (4.74) leads to the condition of the magnetic vector potential to be

$$\vec{n}_{1,2} \times (\vec{A}_2 - \vec{A}_1) = \vec{0} \quad (4.76)$$

Where:

\vec{A}_1, \vec{A}_2 : Magnetic vector potential in area 1 and 2, respectively

¹⁰ I.e. the current on a surface (perpendicular to the normal vector on the surface)

With respect to boundaries that are restricting the domain, it is common to assume a perfect conductor or a perfect insulator. In the first case, equation (4.72) forces the electric field to be zero inside the domain with $\kappa \rightarrow \infty$, leading to

$$\vec{n}_{1,2} \times \vec{A} = \vec{0} \quad (4.77)$$

In the second case, as no surface current can occur, it is

$$\vec{n}_{1,2} \times \vec{H} = \vec{0} \quad (4.78)$$

Finally, not only the boundaries in space must be considered, but also – for transient problems – the boundary condition in time. Hence, the distribution of the state variable at the initial moment must be known. As this is commonly at $t = 0$, one may write

$$P(\vec{r}, t = 0) = P_i(\vec{r}) \quad (4.79)$$

where P_i is called the initial value distribution.

4.3 Simplifications of the derived partial differential equations

Before solving the aforementioned differential equations, it is equitable to first simplify them with respect to the nature of the examined problem, i. e. the regime of time as well as the geometry of the problem. This will be done in the following section.

4.3.1 Adoption to dependencies in time

In general, the equations that are derived in the foregoing paragraph are valid for transient processes, i.e. the boundary conditions or heat generation within the boundary can undergo arbitrary changes with time. However, if the changes are periodic in time or disappear completely, the resulting equations simplify considerably.

Periodic conditions

If all boundary conditions follow a periodic, sinusoidal dependency on time and all material properties are assumed to be linear, the use of complex phasors represent a powerful tool in simplifying partial differential equations. In this case, all quantities are expressed as the real part of a complex phasor, so that, if a state variable P is considered, one may write [WEI2010]

$$P(\vec{r}, t) = \Re\{\underline{P}(\vec{r}) \cdot e^{j\omega t}\}; \quad \underline{P}(\vec{r}) = |\underline{P}(\vec{r})| \cdot e^{\phi(\vec{r})} \quad (4.80)$$

Where:

ω : Angular frequency

$\phi(\vec{r})$: Phase angle

The advantage of this formulation lays in the simplification of the derivation in time. Deriving the quantity \underline{P} from equation (4.80) with respect to the time yields

$$\frac{\partial}{\partial t} (\underline{P}(\vec{r}) \cdot e^{j\omega t}) = j\omega \cdot \underline{P}(\vec{r}) \cdot e^{j\omega t} \quad (4.81)$$

Hence, the derivation with respect to the time becomes a multiplication with $j\omega$.

The assumption of a periodic condition is valid for the quasistationary computation of losses inside the power cable system, as the current flows sinusoidally and all frequencies other than the base frequency of 50 Hz will be neglected. Therefore, the formulation with respect to the magnetic vector potential in equation (4.19) simplifies to a vector Helmholtz-equation

$$\vec{\Delta} \underline{A}(\vec{r}) = j\omega_{el} \cdot \kappa \cdot \mu \cdot \underline{A}(\vec{r}) \quad (4.82)$$

As power cable systems often experience repeating daily load schemes, the solution of the equation of heat conduction in (4.28) (as well as the moisture migration in equations (4.49) and (4.66)) under the assumption of periodic dependency is equally useful when computing ampacity ratings. With respect to heat conduction, equation (4.28) changes to

$$\Delta \underline{T}(\vec{r}) = \frac{j\omega_{th}}{\alpha} \underline{T}(\vec{r}) - \frac{g(\vec{r})}{\lambda} \quad (4.83)$$

Or, if there is no heat generation within the medium, equation (4.83) simplifies to a scalar Helmholtz equation

$$\Delta \underline{T}(\vec{r}) = \frac{j\omega_{th}}{\alpha} \underline{T}(\vec{r}) \quad (4.84)$$

Stationary conditions

A system is said to be stationary if there is no dependency on time at all, hence

$$\frac{\partial}{\partial t} = 0 \quad (4.85)$$

Strictly spoken, a fully stationary state does not exist when regarding the temperature rise of cable systems, as all parts are subjected to time-variant natural boundary conditions. Moreover, as the variation of time constants can amount to several decades with regard to moisture migration within loamy soils, even the assumption of constant boundary conditions would not lead to a completely stationary state.

Nonetheless, the examination of a stationary state is useful with respect to worst case assumptions: As the thermal impedance of the bedding in stationary conditions is always greater than the one in periodic or instationary conditions, the calculation of the stationary temperature field is a useful estimation on the safe side if the load of the cable system is constant. In this case, insertion of equation (4.85) into (4.28) yields

$$\Delta T(\vec{r}) = -\frac{g(\vec{r})}{\lambda} \quad (4.86)$$

Hence, equation (4.28) becomes an inhomogeneous Poisson equation. If there is no heat generation in the medium, this simplifies further to a homogeneous Poisson equation, also known as Laplace equation

$$\Delta T(\vec{r}) = 0 \quad (4.87)$$

With respect to the moisture migration within soils under a temperature gradient, the assumption of stationary conditions is also advisable as a worst case consideration, as this leads to the largest extension of the dry-out zone. In this case, equation (4.49) simplifies to

$$0 = \operatorname{div} \left(D_{h_{hy}} \cdot \operatorname{grad} h_{hy} \right) + \operatorname{div} \left(D_{v,T} \cdot \operatorname{grad} T \right) + \frac{\partial k}{\partial z} \quad (4.88)$$

4.3.2 Adoption to the geometry

In addition to the simplifications in the paragraph above, the fundamental equations can be further adopted to the studied geometry. The aim is then to reduce the number of degrees of freedom by choosing a coordinate system so that the potential or the flux is parallel or orthogonal to the coordinate direction. As in most cases for ampacity calculation, the problem is invariant in longitudinal direction, a restriction to two-dimensional examination is reasonable. Moreover, with respect to the examination of power cable systems, two coordinate systems provide a substantial reduction of the complexity of the equation. These are shown in Figure (4.1) and will shortly be discussed¹¹.

¹¹ The discussion is based on [WEI2010] and [MOO1971]

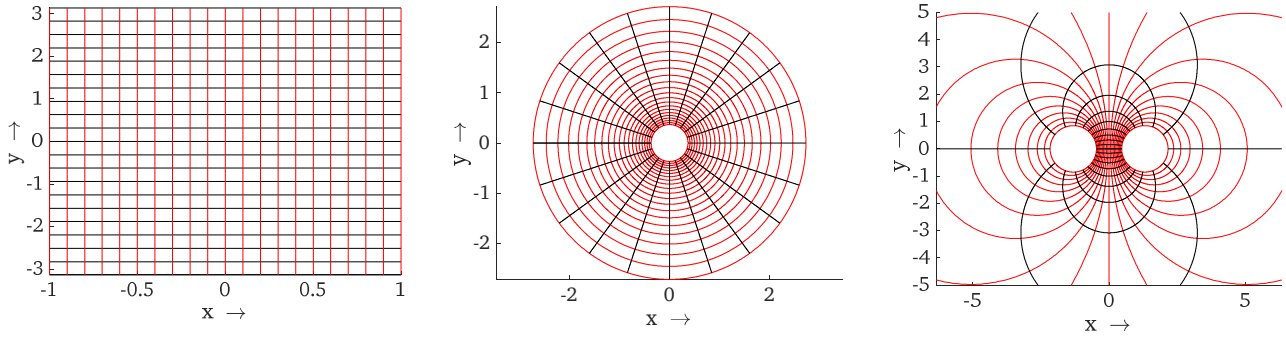


Figure 4.1 Representations of relevant coordinate systems, Left: Cartesian (as lines of constant x and y); Middle: cylindrical (as lines of constant r and φ); Right: bipolar-cylindrical (as lines of constant η and ψ)

Cylindrical coordinate system

As the elements of single core cables have a cylindrical appearance, the application of the cylindrical coordinate system is recommendable to study the losses as well as heat conduction inside of them. If the cable system is laid alongside the z -direction, in which the problem is assumed to be invariant, the position vector can be written as

$$\vec{r} = r \cdot \vec{e}_r + \varphi \cdot \vec{e}_\varphi \quad (4.89)$$

This transformation is achieved by the complex function of the form

$$\underline{z} = e^{j \cdot w} \quad (4.90)$$

where \underline{z} and w are arbitrary complex variables. The function in equation (4.90) maps lines of a constant real part to lines of a constant radius and lines of constant imaginary part to lines of a constant phase angle. If, as an example, a hollow cylinder around the origin with an inner radius of r_i and an outer radius r_a shall be calculated, this area is projected to a rectangle with $r \in [r_i; r_a]$ and $\varphi \in [-\pi; \pi]$.

By decomposition in real and imaginary parts, the conversion to Cartesian system can be written as

$$x = r \cos \varphi \quad \text{and} \quad y = r \sin \varphi \quad (4.91)$$

Or, vice versa

$$r = \sqrt{x^2 + y^2}; \quad \varphi = \arctan \frac{y}{x} + a \quad \text{with} \quad a = \begin{cases} 0 & \text{for } x > 0 \\ \pi & \text{for } x < 0, y \geq 0 \\ -\pi & \text{for } x < 0, y < 0 \end{cases} \quad (4.92)$$

Within the coordinate system, the operations for scalar state variables can be written as

$$\text{grad } P(r, \varphi) = \frac{\partial P}{\partial r} \vec{e}_r + \frac{1}{r} \frac{\partial P}{\partial \varphi} \vec{e}_\varphi \quad (4.93)$$

$$\Delta P(r, \varphi) = \frac{1}{r} \frac{\partial}{\partial r} \left\{ r \frac{\partial P}{\partial r} \right\} + \frac{1}{r^2} \frac{\partial^2 P}{\partial \varphi^2} \quad (4.94)$$

With respect to state variables in the form of a vector in z -direction, it is

$$\Delta(\vec{A} \cdot \vec{e}_z) = \left(\frac{\partial^2 A_z}{\partial r^2} + \frac{1}{r^2} \frac{\partial^2 A_z}{\partial \varphi^2} + \frac{1}{r} \frac{\partial A_z}{\partial r} \right) \cdot \vec{e}_z \quad (4.95)$$

Bipolar – cylindrical coordinate system

To examine the flow of heat through the bedding, i.e. the geometry of a cylinder (that represents the surface of the outer jacket of the cable) in front of a plane (that is the ground surface), the use of a bipolar – cylindrical coordinate system is recommended. In this case, it is

$$\vec{r} = \eta \cdot \vec{e}_\eta + \psi \cdot \vec{e}_\psi \quad (4.96)$$

Where the underlying conformal mapping is

$$z = a \frac{e^\psi + 1}{e^\psi - 1} \quad (4.97)$$

With a as a real parameter [MOO1971]. From this, the transformation to Cartesian coordinates is

$$x = \frac{a \cdot \sinh(\eta)}{\cosh(\eta) - \cos(\psi)}; \quad y = \frac{a \cdot \sin(\psi)}{\cosh(\eta) - \cos(\psi)} \quad (4.98)$$

Or, vice versa

$$\eta = \frac{1}{2} \ln \left[\frac{(x+a)^2 + y^2}{(x-a)^2 + y^2} \right] \quad \text{and} \quad \psi = \pi - 2 \cdot \arctan \left(\frac{2 \cdot a \cdot y}{a^2 - x^2 - y^2 + \sqrt{(a^2 - x^2 - y^2)^2 + 4a^2 y^2}} \right) \quad (4.99)$$

The relation in equation (4.98) can be regrouped as

$$x^2 + [y - a \cdot \cot(\psi)]^2 = a^2 \cdot \csc^2(\psi) \quad (4.100)$$

$$[x - a \cdot \coth(\eta)]^2 + y^2 = a^2 \cdot \operatorname{csch}^2(\eta) \quad (4.101)$$

Where \csc denotes the cosecans with

$$\csc(\psi) = \frac{1}{\sin(\psi)} \quad (4.102)$$

And csch the cosecans hyperbolicus

$$\operatorname{csch}(\eta) = \frac{1}{e^\eta - e^{-\eta}} = \frac{1}{\sinh(\eta)} \quad (4.103)$$

By regarding equation (4.100) and (4.101), it becomes clear that lines of constant ψ form a circle around the point $(0|a \cdot \operatorname{acot}(\psi))$ with a radius of $a \cdot \csc(\psi)$, and lines of constant η form circles around the point $(a \cdot \coth(\eta)|0)$ with a radius of $a \cdot \operatorname{csch}(\eta)$. If, as an example, the area with a boundary at $y = 0$ and a cylinder with a radius r at $x = x_0$ is to be considered, we have

$$a \cdot \coth(\eta) = x_0 \rightarrow \eta = \operatorname{arcoth} \left(\frac{x_0}{a} \right) = \frac{1}{2} \ln \left(\frac{x_0 + a}{x_0 - a} \right) \quad (4.104)$$

and

$$a \cdot \operatorname{csch}(\eta) = r \rightarrow \eta = \operatorname{arcsch} \left(\frac{r}{a} \right) = \ln \left(\frac{a + \sqrt{a^2 + r^2}}{r} \right) \quad (4.105)$$

from which the equation to determine the parameter a is derived

$$\operatorname{arcoth} \left(\frac{x_0}{a} \right) = \operatorname{arcsch} \left(\frac{r}{a} \right) \quad (4.106)$$

As a should be real, equation (3.73) is always fulfilled if

$$a^2 + r^2 = x_0^2 \rightarrow a = \pm \sqrt{x_0^2 - r^2}; \quad |x_0/a| > 1 \quad (4.107)$$

Finally, the operations on scalar state variables changes to

$$\operatorname{grad} P = \frac{1}{a} [\cosh(\eta) - \cos(\psi)] \left(\frac{\partial P}{\partial \eta} \vec{e}_\eta + \frac{\partial P}{\partial \psi} \vec{e}_\psi \right) \quad (4.108)$$

$$\Delta P = \frac{1}{a^2} [\cosh(\eta) - \cos(\psi)]^2 \left(\frac{\partial^2 P}{\partial \eta^2} + \frac{\partial^2 P}{\partial \psi^2} \right) \quad (4.109)$$

4.4 Solution strategies

To finally solve the resulting partial differential equations, two techniques will be applied in the following, i.e.

- Separation of variables
- Use of Green Functions

Before they will be applied to the actual problems, they will shortly be presented in a general form. The third technique that is used – the integral transformation of Sturm-Liouville problems – will not explicitly be explained, as their application resembles the use of the well-known Fourier or Laplace-transformations. For further information, the explanations given in [HAH2012] are recommended.

4.4.1 Separation of variables

The separation of variables constitutes a widely used method to transform PDE of several variables into a set of ordinary (i.e. equations of only one variable) differential equations (ODE) [WEI2010]. The main idea is to represent the solution of the PDE as a product of functions, which depend on one single variable only. Considering an equation with one variable in space, e.g. the x – direction, and a dependency on time of the form

$$\Delta P(x, t) = \frac{\partial}{\partial t} P(x, t) \quad (4.110)$$

The solution would be written as

$$P(x, t) = f_a(x) \cdot f_b(t) \quad (4.111)$$

Inserting the expression in (4.110) into (4.109) then leads to

$$\frac{1}{f_a(x)} \cdot \frac{\partial^2 f_a(x)}{\partial x^2} = \frac{1}{f_b(t)} \cdot \frac{\partial f_b(t)}{\partial t} = -\beta^2 \quad (4.112)$$

so that two ODEs arise, coupled by the separation constant β

$$\frac{1}{f_a(x)} \cdot \frac{\partial^2 f_a(x)}{\partial x^2} = -\beta^2 \quad (4.113)$$

$$\frac{1}{f_b(t)} \cdot \frac{\partial f_b(t)}{\partial t} = -\beta^2 \quad (4.114)$$

Furthermore, it must be considered that the resulting ODEs depend on the underlying coordination system. If cylindrical coordinates are applied, the separation of variables leads to the following equation for the variable in space and time

$$\frac{1}{f_a(\rho)} \cdot \left\{ \frac{\partial^2 f_a(\rho)}{\partial \rho^2} + \frac{1}{\rho} \frac{\partial f_a(\rho)}{\partial \rho} \right\} = -\beta^2 \quad (4.115)$$

$$\frac{1}{f_b(t)} \cdot \frac{\partial f_b(t)}{\partial t} = -\beta^2 \quad (4.116)$$

If the stationary problem consists of two variables in Cartesian space, it is

$$\Delta P(x, y) = 0 \quad (4.117)$$

The solution would be written as

$$P(x, y) = f_a(x) \cdot f_b(y) \quad (4.118)$$

Inserting the expression in (4.118) into (4.117) then leads to

$$\frac{1}{f_a(x)} \cdot \frac{\partial^2 f_a(x)}{\partial x^2} = -\beta^2 \quad (4.119)$$

$$\frac{1}{f_b(y)} \cdot \frac{\partial^2 f_b(y)}{\partial y^2} = \beta^2 \quad (4.120)$$

4.4.2 Solution of ordinary, linear differential equations

As it was demonstrated, the separation of variables reduces one PDE into several ODEs. Still, the latter have to be solved, which will be presented in this section (based on the explanations in [ROC2009]). Generally, linear ordinary differential equations can be written in the form

$$\frac{\partial^2 f(x)}{\partial x^2} + u(x) \cdot \frac{\partial f(x)}{\partial x} + v(x) \cdot f(x) = \zeta(x) \quad (4.121)$$

which are valid in the interval $[x_1, x_2]$ and fulfil the boundary conditions of the two boundaries of the interval. The term of the right hand side is called error term. If it is zero, the equation is called homogeneous

$$\frac{\partial^2 f_h(x)}{\partial x^2} + u(x) \cdot \frac{\partial f_h(x)}{\partial x} + v(x) \cdot f_h(x) = 0 \quad (4.122)$$

It can now be demonstrated that every solution of the homogenous equation can be written as a linear combination of functions that form the *fundamental system* of the equation. These functions can be interpreted as the position vectors of the solution space whose dimension is equal to the order of the ODE. Therefore, if the solution to a homogenous, ordinary equation of second degree is denoted f_h , one may write

$$f_h(x) = \varsigma_1 \cdot f_1(x) + \varsigma_2 \cdot f_2(x) \quad (4.123)$$

Where:

ς_1, ς_2 : Real constants

$f_1(x), f_2(x)$: Fundamental solution system

Before finding the actual fundamental solution, one must determine its actual nature – or answer the question, whether there actually exists one. This is done by including the boundary constraints in the examination. Inserting equation (4.123) into the general form of the boundary conditions (see equation 4.70) on the edges of the interval $[x_1, x_2]$ then leads to the so called *system matrix* of the form

$$\begin{pmatrix} a_1 \cdot f_1(x_1) + b_1 \cdot \frac{\partial f_1}{\partial x}(x_1) & a_1 \cdot f_2(x_1) + b_1 \cdot \frac{\partial f_2}{\partial x}(x_1) \\ a_2 \cdot f_1(x_2) + b_2 \cdot \frac{\partial f_1}{\partial x}(x_2) & a_2 \cdot f_2(x_2) + b_2 \cdot \frac{\partial f_2}{\partial x}(x_2) \end{pmatrix} \cdot \begin{pmatrix} \varsigma_1 \\ \varsigma_2 \end{pmatrix} = \begin{pmatrix} c_1 \\ c_2 \end{pmatrix} \quad (4.124)$$

From equation (4.124), it becomes clear that a boundary value problem may have none, exactly one or an infinite number of solutions: If the determinant of the system matrix is unequal to zero, it can be inverted, and the real constant can explicitly be determined. If equation (4.123) is under-determined, there is an infinite number of solutions, if it is over-determined, there is in general none (or one, if the boundary conditions are chosen such as they are a solution of the problem).

Once the solution to the homogenous equation in (4.123) is found, the solution to the corresponding inhomogenous equation in (4.122) can be written as the sum of the homogenous and the so called particular solution $f_p(x)$, so that

$$f(x) = f_h(x) + f_p(x) \quad (4.125)$$

where the particular solution (under homogenous boundary conditions) can be derived by the method of variation of constants or a Green's function approach. Hence, the problem is to find the fundamental systems of the homogenous equation in (4.123). This, however, can only be done for a specific class of differential equations in a systematic manner, which will be presented in the next section, alongside with all the relevant fundamental systems that will occur in the course of the computations.

If the two functions u and v in equation (4.122) are independent of x , equation (4.122) is denoted as an ordinary differential equation of second degree with constant coefficients. In this case, the equation can be re-written as a system of two linear differential equations of first degree, i.e.

$$\vec{f}_h' = \begin{pmatrix} f_1(x) \\ f_2(x) \end{pmatrix}' = \begin{pmatrix} 0 & 1 \\ -v & -u \end{pmatrix} \cdot \begin{pmatrix} f_1(x) \\ f_2(x) \end{pmatrix} = [A] \cdot \vec{f}_h = 0 \quad (4.126)$$

Each line in (4.125) is solved by

$$f_n(x) = e^{\xi_n \cdot x} \quad (4.127)$$

Where:

ξ_n : Eigenvalue, i.e. the root of the characteristic polynomial from equation (4.126)

As the columns of the matrix in (4.126) are evidently linearly independent, there are two different Eigenvalues to be found, from which the corresponding two Eigenvectors can be derived. Therefore, the solution can be written as

$$\vec{f}_h = e^{\xi_1 \cdot x} \cdot \vec{\xi}_1 + e^{\xi_2 \cdot x} \cdot \vec{\xi}_2 \quad (4.128)$$

With:

$\vec{\xi}_1, \vec{\xi}_2$: Eigenvectors of the matrix in equation (4.126)

Depending on the functions $u(x)$ and $v(x)$ in equation (4.122), the fundamental systems can be found with the help of the aforementioned relations. The results are shown in the Appendix A.1 for the following relevant cases:

$$\begin{array}{lll} u(x) = 0; & v(x) = 0 & u(x) = 0; \quad v(x) = +\beta^2 \\ u(x) = \frac{1}{x}; & v(x) = 0 & u(x) = \frac{1}{x}; \quad v(x) = \beta^2 - x^2 \\ u(x) = 0; & v(x) = -\beta^2 & u(x) = \frac{1}{x}; \quad v(x) = x^2 - \beta^2 \end{array}$$

4.4.3 Green's functions

Other than splitting them into ODEs through separation of variables, the use of Green's functions represent another powerful method to solve PDEs. In order to work out the basic idea behind these functions, their use will first be demonstrated regarding the stationary case from equation (4.86) before being extended to time-dependent, multidimensional problems. The following explanations are based on the descriptions in [COL2011], [NOL2013] and [LEH1990].

Starting point for the derivation of the use of Green's function are the so called fundamental solutions. With respect to the Laplace equation of stationary heat conduction, a fundamental solution solves the following equation

$$\Delta T(\vec{r}) = -\frac{Q}{\lambda} \delta(\vec{r} - \vec{r}') \quad (4.129)$$

Where:

$\delta(\vec{r} - \vec{r}')$: Dirac-delta distribution

Q : Heat source in three dimension in W

The Dirac-delta distribution is defined by:

$$\delta(\vec{r} - \vec{r}') = \begin{cases} 0 & \text{for } \vec{r} \neq \vec{r}' \\ \infty & \text{for } \vec{r} = \vec{r}' \end{cases} \quad (4.130)$$

Integrating the product of the delta-distribution and a function over a volume leads to

$$\iiint_{-\infty}^{\infty} P(\vec{r}) \cdot \delta(\vec{r} - \vec{r}') dV = P(\vec{r}') \quad (4.131)$$

Hence, the fundamental solution of (4.129) can be interpreted as the temperature field around a point source (in three dimensions), a line source (in two dimensions) or a surface source (in one dimension) in an infinite space. The corresponding expressions are:

$$F_{3D,=}(\vec{r}, \vec{r}') = \frac{1}{4\pi\lambda} \frac{\dot{Q}}{|\vec{r}-\vec{r}'|} + \varsigma \quad (4.132)$$

$$F_{2D,=}(\vec{r}, \vec{r}') = -\frac{\dot{Q}'}{2\pi\lambda} \ln(\vec{r} - \vec{r}') + \varsigma \quad (4.133)$$

$$F_{1D,=}(\vec{r}', \vec{r}') = -\frac{\dot{Q}''}{2\lambda} (\vec{r} - \vec{r}') + \varsigma \quad (4.134)$$

Where:

$\dot{Q}, \dot{Q}', \dot{Q}''$: Heat flux, heat flux per unit length and heat flux density¹²

In the case of several sources inside an infinite space and zero temperature for $\vec{r} \rightarrow \infty$, the temperature field can then be expressed as the sum of the corresponding fundamental solutions, or – for a heat generation density – as the integral over the corresponding solution. E.g. for the three dimensional space

$$T(\vec{r}) = \int_V \frac{F_{3D,=}(\vec{r}, \vec{r}')}{\dot{Q}} \cdot g(\vec{r}') dV' = \frac{1}{4\pi\lambda} \int_V \frac{g(\vec{r}')}{|\vec{r}-\vec{r}'|} dV' \quad (4.135)$$

However, as the final solution of any ODE is influenced by the charge distribution inside the domain as well as the conditions on the boundaries, the impact of the latter has to be included into equation (4.135). In order to do so, the fundamental solution is extended with an ordinary function that solves the homogenous Laplace equation, to the so-called Green's function. Again, in three dimensions, this leads to

$$G_{3D,=}(\vec{r}, \vec{r}') = \frac{1}{4\pi\lambda} \frac{1}{|\vec{r}-\vec{r}'|} + u(\vec{r}, \vec{r}') \quad (4.136)$$

$$\Delta u(\vec{r}, \vec{r}') = 0 \quad (4.137)$$

By inserting equation (4.135) into the so-called Green's identities, the solution of equation (4.68) in three dimensions under the consideration of the boundary constraints can be written as [COL2011]¹³

$$\begin{aligned} T(\vec{r}) &= \frac{1}{\lambda} \int G_{3D,=}(\vec{r}, \vec{r}') \cdot g(\vec{r}') \cdot dV' \\ &+ \sum_{i=1}^m \int f_i(\vec{r}'_i) \cdot G_{3D,=}(\vec{r}, \vec{r}'_i) dA'_i \\ &- \lambda \sum_{i=1}^n \int f_i(\vec{r}'_i) \cdot \left. \frac{\partial G_{3D,=}(\vec{r}, \vec{r}')}{\partial \vec{n}_i} \right|_{\vec{r}'=\vec{r}'_i} dA'_i \end{aligned} \quad (4.138)$$

Where:

$f_i(\vec{r}_i)$: Boundary condition on the i -th surface

A_i : Area of the i -th surface

¹² In this case, \dot{Q}'' denotes the total heat flux density, i.e. on both sides of the surface. Hence, if a boundary condition is regarded equation (4.134) must be divided by 2.

¹³ As [COL2011] excludes the material properties from the Green's function, the division by lambda is included into their formulation of equation (4.138) rather than (4.137). However, this is just a matter of definition.

This form nicely demonstrates the different components of a solution to equation (4.68): The first part in (4.138) represents the contribution of the heat generation inside the domain, whereas the second integral accounts for the boundary conditions of second and third type, the third integrals for all boundary conditions of the first kind.

The Green's function approach is equally useful for periodic and non-stationary problems. In the first case, the fundamental solution for a two dimensional problem must satisfy

$$\Delta \underline{T} - \frac{j\omega_{th}}{\alpha} \cdot \underline{T} = -\frac{\dot{Q}'}{\lambda} \delta(\vec{r} - \vec{r}') \quad (4.139)$$

Where:

\dot{Q}' : Heat flux per unit length in two dimensions in $\text{W}\cdot\text{m}^{-1}$

Equation (4.139) is solved by [CAR1959]¹⁴

$$F_{2D,\sim}(\vec{r}', \vec{r}') = \frac{\dot{Q}'}{2\pi\lambda} \cdot K_0 \left[\sqrt{\frac{j\omega_{th}}{\alpha}} \cdot (r - r') \right] \quad (4.140)$$

In the transient case, the fundamental solution must satisfy

$$\Delta T(\vec{r}, t) = \frac{1}{\alpha} \frac{\partial T(\vec{r}, t)}{\partial t} - \frac{\dot{Q}'}{\lambda} \delta(t - \tau) \cdot \delta(\vec{r} - \vec{r}') \quad (4.141)$$

Where:

Q' : Heat source per unit length in two dimensions in $\text{J}\cdot\text{m}^{-1}$

The corresponding two-dimensional fundamental solutions can be found with the help of a Fourier-transformation to be

$$F_{2D,\tau}(\vec{r}', t, \vec{r}', \tau) = \frac{Q'}{4\pi\lambda(t-\tau)} e^{-\frac{(r-r')^2}{4\alpha(t-\tau)}} \quad (4.142)$$

Hence, all the difficulty lies in finding the Green's function for a given geometry and set of boundary constraints. Without going into details, the Green's functions that will be applied in the following chapters will be named.

With respect to the calculation the stationary temperature distribution inside a cylinder or hollow cylinder of an outside radius of r_o , taking into account volumetric heat generation, the following Green's function will be used [COL2011]

$$G_{1D,\sim}(r, r') = \frac{1}{2\pi} \begin{cases} \ln \frac{r_o}{r'} & \text{for } r < r' \\ \ln \frac{r_o}{r} & \text{for } r > r' \end{cases} \quad (4.143)$$

In terms of the one-dimensional Green's function in periodic condition, the formulation for cylindrical coordinates will be used in section 5.2.2. Here, it is [COL2011]

$$G_{1D,\sim}(r, r', \omega_{th}) = \frac{1}{2\pi\alpha \cdot (1 - S_1 S_2)} \begin{cases} [S_2 I_0(\beta r') + K_0(\beta r')] \cdot [I_0(\beta r) + S_1 K_0(\beta r)] & \text{for } r < r' \\ [S_2 I_0(\beta r) + K_0(\beta r)] \cdot [I_0(\beta r') + S_1 K_0(\beta r')] & \text{for } r > r' \end{cases} \quad (4.144)$$

Where the expressions S_1 and S_2 are chosen according to the geometry and the boundary conditions.

¹⁴ For equation (4.141) as well as (4.142), Carslaw gives the formula with the thermal diffusivity in the denominator (instead of the thermal conductivity, as it is done here). This is due to the definition of the liberated heat flux as $\rho c_p \cdot \dot{Q}'$ or instantaneous heat $\rho c_p \cdot Q'$. The two formulations are thus equal.

For transient problems, there is another, powerful way to derive the Green's functions: Assuming a problem with homogenous boundary conditions and no heat generation inside the domain, the Green's function approach for a one dimensional problem in cylindrical coordinates simplifies to [HAH2011]

$$T(\vec{r}, t) = \int_{r=r_i}^{r_o} G_{1D,\tau}(r, t, r', 0) \cdot T_i(r') \cdot r' dr' \quad (4.145)$$

However, as it will be seen later on, the described problem can often be expressed in such an integral form that the Green's function can be established by comparing the two equations.

In order to obtain the temperature distribution as a consequence of the volumetric heat generation at homogenous boundary conditions, the Green's functions from equation (4.143) and (4.144) must be evaluated by the following equations:

For the stationary conditions in cylindrical coordinates with a dependency on r only and homogenous boundary conditions, it is [COL2011]

$$T(r) = \frac{1}{\lambda} \int_0^{r_o} g(r') \cdot G_{1D,=}(r, r') \cdot 2\pi r' \cdot dr' \quad (4.146)$$

As well as for steady-periodic conditions

$$\underline{T}(r, \omega_{th}) = \frac{\alpha}{\lambda} \int_{r_i}^{r_o} g(r', \omega_{th}) \cdot \underline{G}_{1D,\sim}(r, r', \omega_{th}) 2\pi r' \cdot dr' \quad (4.147)$$

And for transients with non-homogenous boundary conditions [HAH2012]¹⁵

$$\begin{aligned} T(r, t) = & \int_{r=r_i}^{r_o} G_{1D,\tau}(r, t, r', 0) \cdot T_i(r') \cdot r' dr' \\ & + \frac{\alpha}{\lambda} \int_{\tau=0}^t \int_{r_i}^{r_o} G_{1D,\tau}(r, t, r', \tau) \cdot g(r', \tau) \cdot r' \cdot dr' d\tau \\ & + \frac{\alpha}{\lambda} \sum_{i=1}^m [r' \cdot G_{1D,\tau}(r, t, r', \tau)]_{r'=r_i} \cdot f_i(r_i, \tau) d\tau \\ & + \alpha \sum_{i=1}^m \left[r' \cdot \frac{\partial G_{1D,\tau}(r, t, r', \tau)}{\partial \vec{n}_i} \right]_{r'=r_i} \cdot f_i(r_i, \tau) d\tau \end{aligned} \quad (4.148)$$

Hence, this chapter first derives the potential equations for the three physical disciplines that are involved in the ampacity rating of power cable systems: electromagnetism, heat conduction and the diffusion process of heat and mass inside soils. Furthermore, methodologies to simplify and solve these potential equations are presented: The adoption of the formulation to the geometry and dependency in time as well as the method of separation of variables and the Green's function approach. In the following chapter, the latter will be used to find explicit analytical solutions to the geometries that have to be considered for single core cables: full and hollow cylinders as well as the bedding.

¹⁵ Whether to incorporate the factor 2π , arising from the integration alongside the φ -direction, into the Green's function itself or the equation of its application is just a matter of definition. Hence, the formulations from equation (4.146) and (4.148) are equal.

5 Solutions to relevant geometries

The aforementioned theory is finally used to calculate the solutions of the fundamental equations in (4.1.1) and (4.1.2) for relevant geometries with respect to power cable systems. Because single core cables will be considered, these geometries are:

- Full and hollow cylinders
- One single cable or a group of single cables inside a semi-infinite medium

As it will be demonstrated later in chapter 7.1, the material parameters that are involved in the equations of the heat and mass transfer are strongly non-linear, so that their straightforward, exact analytical calculation is not possible. Therefore, in order to solve equations (4.49) and (4.66), a numerical approach will be demonstrated in chapter 7.

5.1 Calculation of cable losses

First and foremost, the losses inside a cable system have to be calculated. This includes the losses inside the conductor due to the conductor currents, losses inside the dielectric due to polarization effects as well as the losses inside the sheaths due to induced currents. The current dependent losses inside the conductor and the sheath will be derived on the basis of the equations from part 4.1.1: First, one single, circular conductor will be regarded in order to calculate the losses due to the current flow inside it, including the skin effect. Secondly, the circular sheath will be added in order to examine the current induced losses inside of it. However, as the thickness of the screen is much smaller than the penetration depth of the current at network frequency, the skin effect inside the sheath can be neglected. Hence, the actual current density distribution need not be considered, so that the full formulation of the problem need not be considered. Therefore, the calculation by the induced currents with the help of the method of the mean average distances [BAL2009], which assumes a homogenous current distribution, is sufficient for the calculation of sheath and armour losses.

5.1.1 Calculation of the conductor losses

As a first step, the losses inside a single, circular conductor with the outer radius of r_c , an electrical conductivity κ and a permeability μ which is traversed by a periodically oscillating current of the angular frequency ω_{el} will be derived. With respect to chapter 4.3.1, equation (4.19) simplifies to

$$\vec{\Delta}\underline{A}(\vec{r}) = j\omega_{el} \cdot \kappa \cdot \mu \cdot \vec{A}(\vec{r}) = \underline{k}^2 \cdot \vec{A}(\vec{r}, t) = (1 + j)\sqrt{\frac{\omega_{el}\mu\kappa}{2}} \cdot \vec{A}(\vec{r}, t) \quad (5.1)$$

Regarding the geometry, the use of cylindrical coordinates is suitable, so that

$$\vec{A}(\vec{r}) = \underline{A}_r \cdot \vec{e}_r + \underline{A}_\varphi \cdot \vec{e}_\varphi + \underline{A}_z \cdot \vec{e}_z \quad (5.2)$$

and equation (5.1) becomes

$$\begin{pmatrix} \Delta\underline{A}_\varphi - \frac{1}{r^2}\underline{A}_r - \frac{2}{r^2}\frac{\partial\underline{A}_\varphi}{\partial\varphi} \\ \Delta\underline{A}_r - \frac{1}{r^2}\underline{A}_r - \frac{2}{r^2}\frac{\partial\underline{A}_\varphi}{\partial\varphi} \\ \Delta\underline{A}_z \end{pmatrix} - \underline{k}^2 \cdot \begin{pmatrix} \underline{A}_r \\ \underline{A}_\varphi \\ \underline{A}_z \end{pmatrix} = 0 \quad (5.3)$$

Furthermore, it can be stated that the problem is indifferent in the direction of φ and z , hence

$$\frac{\partial}{\partial\varphi} = \frac{\partial}{\partial z} = 0 \quad (5.4)$$

Applying the scalar Laplacian operator under the premise of equation (5.4) then leads to three decoupled partial differential equations for the three components of the magnetic vector potential

$$\vec{0} = \begin{pmatrix} \frac{\partial^2 \underline{A}_r}{\partial r^2} + \frac{1}{r} \frac{\partial \underline{A}_r}{\partial r} - \left[\frac{1}{r^2} + \underline{k}^2 \right] \\ \frac{\partial^2 \underline{A}_\varphi}{\partial r^2} + \frac{1}{r} \frac{\partial \underline{A}_\varphi}{\partial r} + \left[\underline{k}^2 - \frac{1}{r^2} \right] \\ \frac{\partial^2 \underline{A}_z}{\partial r^2} + \frac{1}{r} \frac{\partial \underline{A}_z}{\partial r} - \left[\frac{0}{r^2} + \underline{k}^2 \right] \end{pmatrix} \quad (5.5)$$

With respect to the Appendix A1.5 and A1.6, the solution to equation (5.5) is

$$\underline{\vec{A}} = \begin{pmatrix} \varsigma_1 \cdot I_1(\underline{kr}) + \varsigma_2 \cdot K_1(\underline{kr}) \\ \varsigma_3 \cdot J_1(\underline{kr}) + \varsigma_4 \cdot Y_1(\underline{kr}) \\ \varsigma_5 \cdot I_0(\underline{kr}) + \varsigma_6 \cdot K_0(\underline{kr}) \end{pmatrix} \quad (5.6)$$

The solution must stay finite in the entire domain, whereas

$$\lim_{r \rightarrow 0} K_1(\underline{kr}) = \lim_{r \rightarrow 0} Y_1(\underline{kr}) = \lim_{r \rightarrow 0} K_0(\underline{kr}) = \infty \quad (5.7)$$

Hence, it follows that

$$\varsigma_2 = \varsigma_4 = \varsigma_6 = 0 \quad (5.8)$$

Furthermore, as the surrounding medium of the conductor is assumed to be of conductivity zero, the current density in radial direction on the outer boundary must be zero due to

$$\vec{E} = j\omega_{el} \cdot \vec{A} \quad (5.9)$$

As the magnetic vector potential is of the same direction as the current density, it follows that

$$\underline{A}_r(r = r_{con}) = 0 \rightarrow \varsigma_1 \cdot I_1(\underline{kr}_{con}) = 0 \quad (5.10)$$

However, as the modified Bessel function of first kind does not possess a root for $r > 0$, it is

$$\varsigma_1 = 0 \quad (5.11)$$

As a result of equation (5.8) and (5.11), the magnetic vector potential (and therefore the current density) can only encompass components in the direction of φ and z . However, as the induced current as “primary” source of the quasi-magnetostatic field is composed only of components in the z -direction, the azimuthal component is zero in this example. The last degree of freedom is eliminated by the application of the Gauß-theorem on the outer boundary of the conductor. If the total current inside the conductor is denoted I , it follows

$$\int_{\varphi=0}^{\varphi=2\pi} \underline{H}_\varphi \cdot r \cdot d\varphi = \int_{\varphi=0}^{2\pi} \frac{1}{\mu} (\text{rot } \underline{\vec{A}} \cdot \vec{e}_\varphi) \cdot r \cdot d\varphi = I \quad (5.12)$$

with

$$\text{rot } \underline{\vec{A}} = -\frac{\partial \underline{A}_z}{\partial r} \cdot \vec{e}_\varphi = -\varsigma_5 \cdot \underline{k} \cdot I_1(\underline{kr}) \quad (5.13)$$

it follows from equation (5.12) that

$$-2\pi \cdot \varsigma_5 \cdot \underline{k} \cdot I_1(\underline{kr}_{con}) \cdot r_{con} = \mu \cdot I \rightarrow \varsigma_5 = -\frac{\mu \cdot I}{2\pi \cdot \underline{k} \cdot r_{con}} \cdot \frac{1}{I_1(\underline{kr}_{con})} \quad (5.14)$$

Therefore, it is [KÜP2006]

$$\underline{\vec{H}} = \frac{1}{\mu} \text{rot } \underline{\vec{A}} = -\frac{1}{\mu} \frac{\partial \underline{A}_z}{\partial r} \cdot \vec{e}_\varphi = -\varsigma_5 \frac{\underline{k}}{\mu} I_0(\underline{kr}) \cdot \vec{e}_\varphi = \frac{I}{2\pi \cdot r_c} \cdot \frac{I_1(\underline{kr})}{I_1(\underline{kr}_{con})} \cdot \vec{e}_\varphi \quad (5.15)$$

$$\underline{\vec{E}} = -j\omega \cdot \underline{\vec{A}} = (1 + j) \sqrt{\frac{\omega \mu}{2\kappa}} \frac{I}{2\pi \cdot r_{con}} \cdot \frac{I_0(\underline{kr})}{I_1(\underline{kr}_{con})} \cdot \vec{e}_z \quad (5.16)$$

With regard to low frequencies, the Bessel function can be approximated with

$$I_0(\underline{k}r) \approx 1; \quad I_1(\underline{k}r) \approx \frac{\underline{k}r}{2} \quad \text{for } \underline{k}r \ll 1 \quad (5.17)$$

so that the fields become

$$\vec{H}_{\underline{k}r \ll 1} = \frac{I}{2\pi r_c^2} \cdot r \cdot \vec{e}_\varphi \quad \vec{E}_{\underline{k}r \ll 1} = \frac{I}{\kappa \cdot \pi \cdot r_c^2} \cdot \vec{e}_z \quad \text{for } \underline{k}r \ll 1 \quad (5.18)$$

which corresponds to the solutions of the stationary current density field. By dividing equation (5.16) with the result in (5.18), the supplementary resistance due to eddy currents can be determined to be

$$1 + y_s = \Re \left\{ \frac{\underline{k} \cdot r_{\text{con}}}{2} \frac{I_0(\underline{k} \cdot r_{\text{con}})}{I_1(\underline{k} \cdot r_{\text{con}})} \right\}; \quad (5.19)$$

Where:

y_s : skin effect factor

By defining

$$\Re \left\{ \frac{\underline{k} \cdot r_{\text{con}}}{2} \right\} = r_{\text{con}} \cdot \sqrt{\frac{\mu \cdot \omega \cdot \kappa}{8}} \stackrel{\text{def}}{=} x_s \quad (5.20)$$

the expression in equation (5.19) can be developed with a Taylor-Series

$$1 + y_s = 1 + \frac{1}{3} \cdot x_s^4 \quad \text{für } x < 1 \quad (5.21)$$

$$1 + y_s = x_s + \frac{1}{4} + \frac{3}{64 \cdot x_s} \quad \text{für } x > 1 \quad (5.22)$$

As in most cases the DC-resistance $R'_{c,\text{DC}}$ per unit length of the conductor is known rather than the material properties, the factor x_s is commonly expressed as

$$x_s^2 = \pi \cdot f \frac{10^{-7}}{R'_{c,\text{DC}}} \quad (5.23)$$

In IEC60287, equation (5.21) is used, albeit a correction term in the denominator is included

$$y_{s,\text{IEC}} = \frac{x_{\text{IEC}}^4}{192 + 0.8 \cdot x_{\text{IEC}}^4} \quad \text{für } y_{s,\text{IEC}} < 2.8 \quad (5.24)$$

where

$$x_{\text{IEC}}^2 = \frac{8\pi f}{R'_{c,\text{DC}}} \cdot 10^{-7} \cdot k_s \quad (5.25)$$

The term k_s reflects the impact of the properties of the conductor, such as the use of oxidized and therefore insulated single wires. A comparison of equation (5.23) and (5.25) yields

$$\frac{x_{\text{IEC}}}{x_s} = \sqrt{8} \approx 2.8 \quad (5.26)$$

so that the conditions of use in equations (5.21) and (5.24) are the same. The proximity effect, i.e. the effect of adjacent conductors on the current density across the conductor surface, can generally be neglected, as the induced currents inside the screens lead to a decoupling of the phases.

5.1.2 Dielectric losses inside the insulation

In addition to the current depending losses inside the conductor, voltage dependent losses inside the insulation due to polarization effects must in principle be considered. As a consequence, the current into the insulation is not exclusively capacitive, but consists of a resistive part as well. The latter is generally expressed as

$$\underline{I}_r = \tan(\delta) \cdot \underline{I}_{\text{ins}} \quad (5.27)$$

Where:

$\underline{I}_{\text{ins}}$: Capacitive component of the current into the insulation

\underline{I}_r : Resistive component of the current into the insulation

$\tan(\delta)$: Dissipation factor

Inserting the expression of the capacitive current

$$P_{\text{ins}}' = \frac{|\underline{U}_m|^2}{3} \cdot \omega_{\text{el}} C' \cdot \tan(\delta) \quad (5.28)$$

Where:

P_{ins}' : Dielectric losses per unit length

\underline{U}_m : Highest voltage for equipment

C' : Capacitance per unit length of a single cable

Equation (5.28) can be used to check whether the dielectric losses are relevant with regard to the total heating of the cable. Usually, this is not the case for cables with $\underline{U}_m \leq 123$ kV. If dielectric losses do represent a considerable heat source, the expression of the volumetric dielectric losses as a function of the field strength [KÜC2011]

$$g_{\text{di}} = \omega_{\text{el}} \cdot \epsilon'' \cdot (\vec{E})^2 \sim \zeta \cdot \frac{1}{r^2} \quad (5.29)$$

With:

g_{di} : Volumetric heat generation by dielectric losses

ϵ'' : Imaginary part of the permittivity

will be used in section 5.2.1 to derive the impact of the temperature distribution within the insulation.

5.1.3 Losses inside the screen

In principle, the approach that was followed in section 5.1.1 can be extended to calculate the current distribution inside the conductor as well as the screen for a three-phase cable system in lateral or trefoil formation. However, as the problem is no longer indifferent to the φ – direction, a separation of variables with regard to φ and r has to be carried out. A solution to this problem is presented in [FER1996], in which the adjacent cables are approximated by line sources.

However, the involved expressions become rather complex, especially when considering the fact that only the base frequency of 50 Hz is considered, so that – as it was mentioned earlier – the skin effect inside the screen has not been taken into account. Therefore, the aim of calculating the induced currents inside the screen and the resulting screen losses is best to be achieved by considering the inductive coupling between the different conductors, based on the method of mean geometric distances [BAL2016]. Here, the ratio between the screen and the conductor current can be determined to be:

$$\frac{I_{sc}}{I} = - \frac{j\omega_{el} \frac{\mu_0}{2\pi} \cdot \ln\left(\frac{2 \cdot r_{jac}}{r_{sc}}\right)}{R'_{sc} + j\omega_{el} \frac{\mu_0}{2\pi} \mu_0 \ln\left(\frac{2 \cdot r_{jac}}{r_{sc}}\right)} \quad (5.30)$$

Where:

I_{sc} : Total electric current inside the screen

r_{jac} : Outer radius of the outer jacket of the cable

r_{sc} : Mean radius of the cable screen

R'_{sc} : Resistance per unit length of the cable screen

With respect to a system in trefoil formation, the ratio of equation (5.30) for the screen of the outer cables changes to

$$\frac{I_{sc}}{I} = -e^{j\frac{2}{3}\pi} \cdot \frac{j\omega_{el} \frac{\mu_0}{2\pi} \cdot \ln\left(\frac{d}{r_{sc}}\right)}{R'_{sc} + j\omega_{el} \frac{\mu_0}{2\pi} \mu_0 \ln\left(\frac{d}{r_{sc}}\right)} \quad (5.31)$$

With:

d : Distance between the center of two adjacent cables

With the help of equations (5.30) and (5.31), the ratio of the screen losses to the conductor losses can be determined to be

$$\frac{P'_{sc}}{P'_{con}} = \frac{R'_{sc}}{R'_{con}} \cdot \left(\frac{I_{sc}}{I} \right)^2 = \lambda_{IEC} \quad (5.32)$$

5.2 Calculation of heat conduction inside cable elements

The heat that is generated by the losses inside a cable conductor, insulation or screen traverses other parts of the cable as well as the bedding in which the cable system is laid. Inside the cable system, this happens exclusively by heat conduction and – as exclusively single core cables are considered – inside a cylindrical geometry. Therefore, equation (4.28) must be solved in a cylindrical coordinate system. This will be done for three relevant dependencies of time: stationary, periodic and transient dependencies.

5.2.1 Stationary conditions

Adopting equation (4.86) to the symmetry of the configuration in cylindrical coordinate system, i.e.

$$\frac{\partial}{\partial \varphi} = \frac{\partial}{\partial z} = 0 \quad (5.33)$$

leads to

$$\frac{\partial^2 T(r)}{\partial r^2} + \frac{1}{r} \frac{\partial T(r)}{\partial r} = -\frac{g(r)}{\lambda} \quad (5.34)$$

which has to be solved with respect to the different cable elements. As it was described in chapter 4.4.2, this is done by first finding the temperature distribution T_h that solves the homogeneous equation and respects the boundary constraints. Secondly, the particular solution T_p under homogeneous boundary constraints is found, so that the final solution is expressed as

$$T(r) = T_h(r) + T_p(r) \quad (5.35)$$

With respect to appendix A1.2, the solution of the homogeneous equation has the form [CAR1959]

$$T_h(r) = \varsigma_1 \cdot \ln r + \varsigma_2 \quad (5.36)$$

Considering a cylindrical conductor with an outer radius r_o and a Dirichlet boundary condition $T = T_o$ on the outer radius, it becomes clear that

$$\varsigma_1 = 0 \quad (5.37)$$

as the solution must stay finite. Hence, the value of the second constant is directly derived to be

$$\varsigma_2 = T_o \quad (5.38)$$

The solution of the particular equation under a homogeneous boundary condition that incorporates the constant volumetric heat generation inside the conductor is derived from the Green's function in equation (4.143), so that

$$T_p(r) = \frac{g_o}{2\pi\lambda} \int_{\varphi=0}^{2\pi} \left[\int_{r'=0}^r \ln\left(\frac{r_o}{r'}\right) r' dr' + \int_{r'=r}^{r_o} \ln\left(\frac{r_o}{r'}\right) r' dr' \right] d\varphi \quad (5.39)$$

Evaluating the integrals leads to

$$T_p(r) = \frac{g}{4\lambda} (r_o^2 - r^2) \quad (5.40)$$

Assuming a hollow cylinder with an inner radius r_i and an outer radius r_o for the insulation or the cable screen, the system matrix is

$$\begin{pmatrix} a_1 \cdot \ln(r_o) - \frac{b_2}{r_o} & a_1 \\ a_1 \cdot \ln(r_i) - \frac{b_2}{r_i} & a_2 \end{pmatrix} \cdot \begin{pmatrix} \varsigma_1 \\ \varsigma_2 \end{pmatrix} = \begin{pmatrix} c_1 \\ c_2 \end{pmatrix} \quad (5.41)$$

Assuming a heat flux \vec{q}_i on the inner and a temperature T_o on the outer boundary, the coefficients of the homogenous solution can therefore be derived by

$$\begin{pmatrix} \varsigma_1 \\ \varsigma_2 \end{pmatrix} = -\frac{r_i}{\lambda} \begin{pmatrix} 1 & 0 \\ -\ln(r_o) & -\lambda/r_i \end{pmatrix} \cdot \begin{pmatrix} \vec{q}_i \cdot \vec{e}_r \\ T_o \end{pmatrix} \quad (5.42)$$

With respect to the cable screen, the losses can be assumed constant over the surface, so that

$$g(r) = g \quad (5.43)$$

Therefore, the particular solution with a homogeneous Neuman boundary condition on the inner and a homogenous Dirichlet condition on the outer radius is found with the Greens function from equation (4.143) to be

$$T_p(r) = \frac{g}{2\pi\lambda} \int_{\varphi=0}^{2\pi} \left[\int_{r'=r_i}^r \ln\left(\frac{r_o}{r'}\right) r' dr' + \int_{r'=r}^{r_o} \ln\left(\frac{r_o}{r'}\right) r' dr' \right] d\varphi \quad (5.44)$$

Evaluating the integrals leads to

$$T_p(r) = \frac{g}{\lambda} \left[\frac{1}{4} (r_o^2 - r^2) - \frac{r_i^2}{2} \ln\left(\frac{r_o}{r}\right) \right] \quad (5.45)$$

Considering dielectric losses inside the insulation, it was shown that they are proportional to the inverse of the radius, so that the heat generation can be written as

$$g(r) = \frac{g}{r^2} \quad (5.46)$$

The analogy to equation (5.44) under the assumption of (5.46) is then

$$T_p(r) = \frac{g}{2\pi\lambda} \int_{\varphi=0}^{2\pi} \left[\int_{r'=r_i}^r \frac{1}{r'} \cdot \ln\left(\frac{r_o}{r'}\right) dr' + \int_{r'=r}^{r_o} \frac{1}{r'} \cdot \ln\left(\frac{r_o}{r'}\right) dr' \right] d\varphi \quad (5.47)$$

Evaluating the integrals leads to

$$T_p(r) = \frac{g}{\lambda} \left[\ln\left(\frac{r_o}{r}\right) \cdot \ln\left(\frac{r}{r_i}\right) + \frac{1}{2} \cdot \ln^2\left(\frac{r_o}{r}\right) \right] \quad (5.48)$$

If the heat generation can be neglected – as it is in general the case for the dielectric losses for cables with $U_m < 123$ kV – or if no losses appear – as it is the case for the outer jacket – the temperature distribution is still given by equation (5.35) with $T_p = 0$.

Finally, a Robin condition on the outer radius of the cable jacket is considered, as it is suitable for cables hanging in air and therefore experiencing a convective heat transfer to their surrounding. Then, the system matrix from equation (5.41) changes to

$$\begin{pmatrix} -\lambda/r_i & 0 \\ \ln(r_o) + \frac{\lambda}{h_{rob} \cdot r_a} & 1 \end{pmatrix} \cdot \begin{pmatrix} \varsigma_1 \\ \varsigma_2 \end{pmatrix} = \begin{pmatrix} \vec{q}_i \cdot \vec{e}_r \\ T_o \end{pmatrix} \quad (5.49)$$

Where:

h_{rob} : Convection coefficient

Therefore, the determination of the coefficients from equation (5.42) changes to:

$$\begin{pmatrix} \varsigma_1 \\ \varsigma_2 \end{pmatrix} = -\frac{r_i}{\lambda} \begin{pmatrix} 1 & 0 \\ -\ln(r_o) - \frac{\lambda}{h_{rob} \cdot r_o} & -\lambda/r_i \end{pmatrix} \cdot \begin{pmatrix} \vec{q}_i \cdot \vec{e}_r \\ T_o \end{pmatrix} \quad (5.50)$$

5.2.2 Periodic conditions

With respect to periodic boundary conditions and heat generation, the geometric symmetries from equation (5.33) have to be applied to equation (4.83), leading to

$$\frac{\partial^2 T(r)}{\partial r^2} + \frac{1}{r} \frac{\partial T(r)}{\partial r} - \frac{j\omega}{\alpha} T(r) = \frac{1}{\lambda} g(r) \quad (5.51)$$

which has, according to appendix A1.5, the solution for the homogenous equation

$$T_h(r) = \varsigma_1 \cdot I_0(\underline{\beta} \cdot r) + \varsigma_2 \cdot K_0(\underline{\beta} \cdot r) \quad (5.52)$$

with

$$\underline{\beta} = \sqrt{\frac{j\omega_{th}}{\alpha}} \quad (5.53)$$

Considering a cylindrical conductor with uniform heat generation, the homogeneous solution (i.e. the temperature field that is imposed only by the boundary condition) leads to

$$\varsigma_2 = 0 \quad (5.54)$$

as the solution must stay finite for $r \rightarrow 0$. The second coefficient is found according to the boundary condition on the outer radius of the conductor. If a Dirichlet-condition with $T(r_o) = T_o$ is applied, it is

$$T_o = \varsigma_1 \cdot I_0(\underline{\beta} \cdot r_o) \rightarrow \varsigma_1 = \frac{T_o}{I_0(\underline{\beta} \cdot r_o)} \quad (5.55)$$

so that [CAR1959]

$$T_h(r) = T_o \cdot \frac{I_0(\underline{\beta} \cdot r)}{I_0(\underline{\beta} \cdot r_o)} \quad (5.56)$$

In order to take into account the influence of the heat generation, the particular solution is derived with the help of a Green's function approach. With reference to equation (4.144) and choosing

$$\underline{S}_1 = 0 \quad (5.57)$$

because $r_i \rightarrow 0$ as well as

$$\underline{S}_{2,D} = -\frac{K_0(\underline{\beta}r_o)}{I_0(\underline{\beta}r_o)} \quad (5.58)$$

due to an assumed homogenous Dirichlet-condition on the outer radius of the conductor. Inserting equation (5.57) and (5.58) into (4.144) leads to the following expression for the temperature distribution:

$$\begin{aligned} T_p(r, S_2) &= \frac{g}{\lambda} \int_{r'=0}^r [S_2 \cdot I_0(\underline{\beta}r') + K_0(\underline{\beta}r)] \cdot I_0(\underline{\beta}r') \cdot r' dr' \\ &\quad + \frac{g}{\lambda} \int_{r'=r}^{r_o} I_0(\underline{\beta}r) \cdot [S_2 \cdot I_0(\underline{\beta}r') + K_0(\underline{\beta}r')] \cdot r' dr' \end{aligned} \quad (5.59)$$

Solving the integrals with the help of the following relations

$$\int I_0(\underline{\beta}r') \cdot r' dr' = \frac{r'}{\underline{\beta}} I_1(\underline{\beta}r') \quad (5.60)$$

$$\int K_0(\underline{\beta}r') \cdot r' dr' = -\frac{r'}{\underline{\beta}} K_1(\underline{\beta}r') \quad (5.61)$$

and the approximations of the Bessel-functions for small arguments [COL2011]

$$I_1(\underline{\beta}r') = \frac{1}{2} \underline{\beta}r' \cdot \frac{1}{\Gamma(2)} \quad (5.62)$$

as well as the Wronski determinant

$$I_0(\underline{\beta}r') \cdot K_1(\underline{\beta}r') + K_0(\underline{\beta}r') \cdot I_1(\underline{\beta}r') = \frac{1}{\underline{\beta}r'} \quad (5.63)$$

yields

$$T_p(r, S_2) = \frac{g_o}{\lambda} \left(\frac{r_c}{\underline{\beta}} [S_2 I_1(\underline{\beta}r_o) - K_1(\underline{\beta}r_o)] \right) \cdot I_0(\underline{\beta}r) + \frac{1}{\underline{\beta}^2} \quad (5.64)$$

Just like in the stationary case, the total solution is then given by the sum of the homogeneous and the particular solution

$$\underline{T}(r) = \underline{T}_h(r) + \underline{T}_p(r) \quad (5.65)$$

For reasons that will be explained later in chapter 6.4.1, the solution of the partial problem with a homogeneous Neuman-condition is also of interest. In this case, equation (5.64) is still valid, only equation (5.58) changes to

$$\underline{S}_{2,N} = \frac{K_1(\underline{\beta}r_o)}{I_1(\underline{\beta}r_o)} \quad (5.66)$$

Inserting equation (5.66) into (5.64) yields that the solution for a homogeneous Neumann boundary condition in this case is independent of r and equals

$$\underline{T}_p(r, S_{2,N}) = \frac{g}{\lambda} \frac{1}{\underline{\beta}^2} \quad (5.67)$$

Regarding a hollow cylinder with no heat generation, the system matrix of equation (5.52) is:

$$\begin{pmatrix} a_1 \cdot I_0(\underline{\beta} \cdot r_i) + b_2 \cdot \underline{\beta} \cdot I_1(\underline{\beta} \cdot r_i) & a_1 \cdot K_0(\underline{\beta} \cdot r_i) - b_1 \cdot \underline{\beta} \cdot K_1(\underline{\beta} \cdot r_i) \\ a_2 \cdot I_0(\underline{\beta} \cdot r_o) + b_2 \cdot \underline{\beta} \cdot I_1(\underline{\beta} \cdot r_o) & a_2 \cdot K_0(\underline{\beta} \cdot r_o) - b_2 \cdot \underline{\beta} \cdot K_1(\underline{\beta} \cdot r_o) \end{pmatrix} \cdot \begin{pmatrix} \zeta_1 \\ \zeta_2 \end{pmatrix} = \begin{pmatrix} c_1 \\ c_2 \end{pmatrix} \quad (5.68)$$

If a Neumann-condition is on its inner boundary, and a Dirichlet condition is assumed at its outer boundary, equation (5.68) simplifies to

$$\begin{pmatrix} -\lambda \cdot \underline{\beta} \cdot I_1(\underline{\beta} \cdot r_i) & \lambda \cdot \underline{k} \cdot K_1(\underline{\beta} \cdot r_i) \\ I_0(\underline{\beta} \cdot r_o) & K_0(\underline{\beta} \cdot r_o) \end{pmatrix} \cdot \begin{pmatrix} \zeta_1 \\ \zeta_2 \end{pmatrix} = \begin{pmatrix} \vec{q}_i \cdot \vec{e}_r \\ T_o \end{pmatrix} \quad (5.69)$$

so that the two constants can be derived from

$$\begin{pmatrix} \zeta_1 \\ \zeta_2 \end{pmatrix} = \frac{-1}{\det S} \begin{pmatrix} -K_0(\underline{\beta} \cdot r_o) & \lambda \cdot \underline{\beta} \cdot K_1(\underline{\beta} \cdot r_i) \\ I_0(\underline{\beta} \cdot r_o) & \lambda \cdot \underline{\beta} \cdot I_1(\underline{\beta} \cdot r_i) \end{pmatrix} \cdot \begin{pmatrix} \vec{q}_i \cdot \vec{e}_r \\ T_o \end{pmatrix} \quad (5.70)$$

where

$$\det S = -\lambda \underline{\beta} \cdot [I_1(\underline{\beta} \cdot r_i) \cdot K_0(\underline{\beta} \cdot r_o) + I_0(\underline{\beta} \cdot r_o) \cdot K_1(\underline{\beta} \cdot r_i)] \quad (5.71)$$

Considering a constant heat generation of value g_0 across the surface as it is the case for the screen, the partial solution can equally be determined via the Green's function approach from equation (4.144). In this case, the two coefficients S_1 and S_2 of the Green's function are

$$S_1 = \frac{I_1(\underline{\beta} r_i)}{K_1(\underline{\beta} r_i)} \quad (5.72)$$

$$S_{2,D} = -\frac{K_0(\underline{\beta} r_o)}{I_0(\underline{\beta} r_o)} \quad (5.73)$$

so that the expression for determining the temperature distribution becomes

$$\begin{aligned} T_p(r) = & \frac{g}{\lambda(1-S_1S_{2,D})} \int_{r'=r_i}^r [S_2 \cdot I_0(\underline{\beta} r') + K_0(\underline{\beta} r)] \cdot I_0(\underline{\beta} r') \cdot r' dr' \\ & + \frac{g}{\lambda(1-S_1S_{2,D})} \int_{r'=r_i}^r [S_1 \cdot S_2 \cdot I_0(\underline{\beta} r) + S_1 \cdot K_0(\underline{\beta} r)] \cdot K_0(\underline{\beta} r') \cdot r' dr' \\ & + \frac{g}{\lambda(1-S_1S_{2,D})} \int_{r'=r}^{r_o} I_0(\underline{\beta} r) \cdot [S_2 \cdot I_0(\underline{\beta} r') + K_0(\underline{\beta} r')] \cdot r' dr' \\ & + \frac{g}{\lambda(1-S_1S_{2,D})} \int_{r'=r}^{r_o} S_1 \cdot K_0(\underline{\beta} r) \cdot [S_2 \cdot I_0(\underline{\beta} r') + K_0(\underline{\beta} r')] \cdot r' dr' \end{aligned} \quad (5.74)$$

Solving the integral and simplifying the expressions with the help of the relations in (5.60) to (5.64) yields

$$\begin{aligned} T_p(r) = & \frac{g}{\lambda \cdot \underline{\beta} \cdot (1-S_1S_{2,D})} \left(r_i \cdot [S_2 I_0(\underline{\beta} r) + K_0(\underline{\beta} r)] [S_1 K_1(\underline{\beta} r_i) - I_1(\underline{\beta} r_i)] \right. \\ & \left. + r_o \cdot [I_0(\underline{\beta} r) + S_1 K_0(\underline{\beta} r)] [S_2 I_1(\underline{\beta} r_o) - K_1(\underline{\beta} r_o)] + \frac{1}{\underline{\beta}} [1 - S_1 S_2] \right) \end{aligned} \quad (5.75)$$

If a convective boundary condition is assumed at the outer boundary, as it is the case for cables hanging in air, the system matrix from equation changes to

$$\begin{pmatrix} -\lambda \cdot \underline{\beta} \cdot I_1(\underline{\beta} \cdot r_i) & \lambda \cdot \underline{\beta} \cdot K_1(\underline{\beta} \cdot r_i) \\ I_0(\underline{\beta} \cdot r_o) + \frac{\lambda}{h_{rob}} \cdot \underline{\beta} \cdot I_1(\underline{\beta} \cdot r_o) & K_0(\underline{\beta} \cdot r_o) - \frac{\lambda}{h_{rob}} \cdot \underline{\beta} \cdot K_1(\underline{\beta} \cdot r_o) \end{pmatrix} \cdot \begin{pmatrix} \zeta_1 \\ \zeta_2 \end{pmatrix} = \begin{pmatrix} \vec{q}_i \cdot \vec{e}_r \\ T_o \end{pmatrix} \quad (5.76)$$

so that the calculation of the coefficients changes to

$$\begin{pmatrix} \varsigma_1 \\ \varsigma_2 \end{pmatrix} = \frac{1}{\det S} \begin{pmatrix} K_0(\underline{\beta} \cdot r_o) - \frac{\lambda}{h} \cdot \underline{\beta} \cdot K_1(\underline{\beta} \cdot r_o) & -\lambda \cdot \underline{\beta} \cdot K_1(\underline{\beta} \cdot r_i) \\ -I_0(\underline{\beta} \cdot r_o) - \frac{\lambda}{h} \cdot \underline{\beta} \cdot I_1(\underline{\beta} \cdot r_o) & -\lambda \cdot \underline{\beta} \cdot I_1(\underline{\beta} \cdot r_i) \end{pmatrix} \cdot \begin{pmatrix} \vec{q}_i \cdot \vec{e}_r \\ T_o \end{pmatrix} \quad (5.77)$$

where

$$\begin{aligned} \det S = & \lambda \underline{\beta} \cdot I_1(\underline{\beta} \cdot r_i) \cdot \left[\frac{\lambda}{h} \cdot \underline{\beta} \cdot K_1(\underline{\beta} \cdot r_o) - K_0(\underline{\beta} \cdot r_o) \right] \\ & - \lambda \underline{\beta} \cdot K_1(\underline{\beta} \cdot r_i) \left[\frac{\lambda}{h} \cdot \underline{\beta} \cdot I_1(\underline{\beta} \cdot r_o) + I_0(\underline{\beta} \cdot r_o) \right] \end{aligned} \quad (5.78)$$

5.2.3 Transient conditions

As it follows from section 4.4.3, the solution to transient problems can be achieved by finding the Greens's function that corresponds to the actual geometry and boundary constraints. In order to do so, first the solution to the homogenous problem (i.e. assuming the heat generation inside the domain to equal zero) will be solved. Then, by comparing the resulting expression with the equation in (4.145), the Green's function can be derived. This will be done for the cylinder – representing the conductor – as well as a hollow cylinder – representing all other cable elements such as the insulation or outer jacket. The calculations for the cylinder have been taken from [HAH2012].

With respect to the cable elements, the separation of variables in cylindrical coordinates (as explained in chapter 4.4.1) has to be applied. Taking into account the symmetries in equation (5.33), this leads to the fundamental system of the function of space to be

$$f_a(r) = \varsigma_1 \cdot J_0(\beta_n \cdot r) + \varsigma_2 \cdot Y_0(\beta_n \cdot r) \quad (5.79)$$

Considering a cylinder for the cable conductor, it follows directly that

$$\varsigma_2 = 0 \quad (5.80)$$

as the solution must stay finite for $r = 0$. The Eigenvalues of the solution are found by the help of the Dirichlet-condition on the outer radius, it follows

$$T|_{r=r_o} = 0 \rightarrow \varsigma_1 \cdot J_0(\beta_n \cdot r_o) = 0 \text{ for } n = 1, 2, 3 \dots \quad (5.81)$$

Including the solution of the dependency in time from equation (4.116), which is

$$f_b(t) = e^{-\alpha \cdot \beta_n^2 \cdot t} \quad (5.82)$$

the overall solution takes the form

$$T(r, t) = \sum_{n=1}^{\infty} \varsigma_{1,n} \cdot J_0(\beta_n \cdot r) \cdot e^{-\alpha \cdot \beta_n^2 \cdot t} \quad (5.83)$$

The constant $\varsigma_{1,n}$ is finally derived using the orthogonality of the implied Bessel functions at initial conditions. Multiplying equation (5.83) with $J_0(\beta_m \cdot r)$ and integrating in space for $t = 0$ leads to

$$\int_{r=0}^{r_o} T_i(r) \cdot J_0(\beta_n \cdot r) \cdot r \, dr = \sum_{n=1}^{\infty} \int_{r=0}^{r_o} \varsigma_{1,n} \cdot J_0(\beta_n \cdot r) \cdot J_0(\beta_n \cdot r) \cdot r \, dr \quad (5.84)$$

where [HAH2012]

$$\int_{r=0}^{r_o} \varsigma_{1,n} \cdot J_0(\beta_n \cdot r) \cdot J_0(\beta_n \cdot r) \cdot r \, dr = \begin{cases} 0 & \text{if } n \neq m \\ N(\beta_n) & \text{if } n = m \end{cases} \quad (5.85)$$

The term $N(\beta_n)$ denotes the normalized integral. For the fundamental system in equation (5.79), it is

$$N(\beta_n) = \int_{r=0}^{r_o} J_0^2(\beta_n \cdot r) \cdot r \, dr = \frac{r_o^2}{2} [J_1(\beta_n \cdot r_o)]^2 \quad (5.86)$$

Due to the orthogonality in equation (5.85), the summation in (5.84) vanishes and the constant can be expressed as

$$\varsigma_{1,n} = \frac{1}{N(\beta)} \int_{r'=r_i}^{r_o} T_i(r') \cdot J_0(\beta_n \cdot r) \cdot r' \cdot dr' \quad (5.87)$$

Inserting equation (5.87) into (5.83) leads to the solution of a cylinder without heat generation and a homogeneous Dirichlet-condition for $r = r_o$ as a function of the initial temperature distribution

$$T(r, t) = \sum_{n=1}^{\infty} \frac{1}{N(\beta)} \int_{r'=r_i}^{r_o} T_i(r') \cdot J_0(\beta_n \cdot r) \cdot r' \cdot dr' \cdot J_0(\beta_n \cdot r) \cdot e^{-\alpha \cdot \beta_n^2 \cdot t} \quad (5.88)$$

Reformulating equation (5.88) and comparing it to the general form in (4.145) leads to the Green's function

$$G(r, t | r', \tau) = \frac{2}{r_o} \sum_{n=1}^{\infty} \frac{1}{[J_1(\beta_n \cdot r_o)]^2} J_0(\beta_n \cdot r') \cdot J_0(\beta_n \cdot r) \cdot e^{-\alpha \cdot \beta_n^2 \cdot (t-\tau)} \quad (5.89)$$

With the help of equation (5.89) as well as the general formulation of the Green's function solution approach in (4.148), the temperature distribution inside the cylinder, following an instantaneous heat generation at zero initial temperature, i.e.

$$g(r, t) = g \quad (5.90)$$

$$T_i(r') = 0 \quad (5.91)$$

and a homogenous Dirichlet-condition for $r = r_o$ can be derived as

$$T(r, t) = \frac{\alpha}{\lambda} g \int_{\tau=0}^t \int_{r'=0}^{r_o} \frac{2}{r_o} \sum_{n=1}^{\infty} \frac{1}{[J_1(\beta_n \cdot r_o)]^2} J_0(\beta_n \cdot r') \cdot J_0(\beta_n \cdot r) \cdot e^{-\alpha \cdot \beta_n^2 \cdot (t-\tau)} \cdot r' \cdot dr' d\tau \quad (5.92)$$

Using the expression [LEH1990]

$$\int \beta_n \cdot r \cdot J_0(\beta_n \cdot r) dx = \beta_n \cdot r \cdot J_1(\beta_n \cdot r) \quad (5.93)$$

the integral in equation (5.92) can be solved to

$$T(r, t) = \frac{2g}{\lambda \cdot r_o} \left(\sum_{n=1}^{\infty} \frac{1}{\beta_n^3} \cdot \frac{J_0(\beta_n \cdot r)}{J_1(\beta_n \cdot r_o)} \cdot [1 - e^{-\alpha \cdot \beta_n^2 \cdot t}] \right) \quad (5.94)$$

As the exponential function vanishes for $t \rightarrow \infty$, it can be demonstrated that the solution in equation (5.94) converges to the one given in equation (5.40). Furthermore, the heat flux density across the boundary can be calculated as

$$\vec{q}_h(r_o, t) = -\lambda \frac{\partial T(r, t)}{\partial r} \Big|_{r=r_o} = 2 \frac{g}{r_o} \left(\sum_{n=1}^{\infty} \frac{1}{\beta_n^2} \cdot [1 - e^{-\alpha \cdot \beta_n^2 \cdot t}] \right) \quad (5.95)$$

Furthermore, it shall be noticed that equation (5.94) represents the inverse Laplace transformation of (5.64), where the heat generation term is the Laplace-transformation of the step function in time. However, with respect to the material properties of the conductor materials as well as the geometric dimensions, it becomes clear that the transient state lasts for seconds only. Therefore, the error which is induced by neglecting the transient heating of the conductor is small.

Considering a hollow cylinder for the insulation or other cable elements, the homogeneous Neumann-condition of the inner boundary leads to

$$-\lambda \cdot \frac{\partial T(r, t)}{\partial r} \Big|_{r=r_i} = 0 \rightarrow \varsigma_2 = -\varsigma_1 \cdot \frac{J_1(\beta_n \cdot r_i)}{Y_1(\beta_n \cdot r_i)} \quad (5.96)$$

so that

$$f_a(r) = \frac{\varsigma_1}{Y_1(\beta_n \cdot r_i)} \cdot [Y_1(\beta_n \cdot r_i) \cdot J_0(\beta_n \cdot r) - J_1(\beta_n \cdot r_i) \cdot Y_0(\beta_n \cdot r)] \quad (5.97)$$

The homogeneous Dirichlet-condition on the outer boundary leads to the possible Eigenvalues of the function to be

$$T|_{r=r_o} = 0 \rightarrow Y_1(\beta_n \cdot r_i) \cdot J_0(\beta_n \cdot r_o) - J_1(\beta_n \cdot r_i) \cdot Y_0(\beta_n \cdot r_o) = 0 \text{ for } n = 1, 2, 3 \dots \quad (5.98)$$

Including the solution of the dependency in time from equation (4.116), which is

$$f_b(t) = e^{-\alpha \cdot \beta_n^2 \cdot t} \quad (5.99)$$

the overall solution takes the form

$$T(r, t) = \sum_{n=1}^{\infty} \frac{\varsigma_n}{Y_1(\beta_n \cdot r_i)} \cdot (Y_1(\beta_n \cdot r_i) \cdot J_0(\beta_n \cdot r) - J_1(\beta_n \cdot r_i) \cdot Y_0(\beta_n \cdot r)) \cdot e^{-\alpha \cdot \beta_n^2 \cdot t} \quad (5.100)$$

The constants ς_n now have to be determined with the help of the initial value distribution, i.e.

$$T_i(r) = \sum_{n=1}^{\infty} \frac{\varsigma_n}{Y_1(\beta_n \cdot r_i)} (Y_1(\beta_n \cdot r_i) \cdot J_0(\beta_n \cdot r) - J_1(\beta_n \cdot r_i) \cdot Y_0(\beta_n \cdot r)) \quad (5.101)$$

Integrating equation (5.101) in space and using the orthogonality described in [HAH2012], it is

$$\varsigma_n \cdot N(\lambda_n) = \int_{r_i}^{r_o} T_i(r') \cdot \{Y_1(\beta_n \cdot r_i) \cdot J_0(\beta_n \cdot r') - J_1(\beta_n \cdot r_i) \cdot Y_0(\beta_n \cdot r')\} \cdot r' \cdot dr' \quad (5.102)$$

It is not by accident that the equation resembles the form of a Fourier-Cosinus (or Fourier-Sinus) function. In fact, equation (5.102) also represents an integral transformation of the initial value distribution, in this case the finite Hankel Transformation [CIN1965]. The Norm in this case is

$$N(\beta_n) = \frac{2}{\pi^2} \frac{[J_1(\beta_n \cdot r_i)]^2 - [J_0(\beta_n \cdot r_o)]^2}{\beta_n^2 \cdot [J_0(\beta_n \cdot r_o)]^2} = \frac{2}{\pi^2} \frac{1}{\beta_n^2} \left\{ \frac{[J_1(\beta_n \cdot r_i)]^2}{[J_0(\beta_n \cdot r_o)]^2} - 1 \right\} \quad (5.103)$$

Moreover, the term inside the curled brackets in equation (5.102) can be expressed as

$$f_{a,n}(\beta_n, r, r_i) = Y_1(\beta_n \cdot r_i) \cdot J_0(\beta_n \cdot r) - J_1(\beta_n \cdot r_i) \cdot Y_0(\beta_n \cdot r) \quad (5.104)$$

leading to

$$T(r, t) = \sum_{n=1}^{\infty} \left\{ \frac{1}{N(\beta_n)} \int_{r'}^{r_o} F(r') \cdot f_{a,n}(\beta_n, r', r_i) \cdot r' \cdot dr' \right\} \cdot f_{a,n}(\beta_n, r, r_i) \cdot e^{-\alpha \cdot \beta_n^2 \cdot t} \quad (5.105)$$

Changing the sequence of summation and integration as well as reordering the terms leads to a form similar to the one in equation (4.145), from which the Green's function can be derived as

$$G(r, t, r', t') = \sum_{n=1}^{\infty} \frac{f_{\delta,n}(\beta_n, r', r_i) \cdot f_{\delta,n}(\beta_n, r, r_i)}{N(\beta_n)} \cdot e^{-\alpha \cdot \beta_n^2 \cdot (t-t')} \quad (5.106)$$

Inserting equation (5.106) in the general formula in (4.148) then leads to the final expression of the temperature as a function of time and space. If, for example, the initial temperature-distribution inside the hollow cylinder as well as the Dirichlet-condition on the outer boundary is zero, and for $t = 0$ a constant heat flux is introduced inside the inner boundary, the temperature on the inside of the inner boundary is given by

$$T(\rho, t) = \vec{q} \cdot \vec{e}_r \cdot \frac{r_i}{\lambda} \sum_{n=1}^{\infty} \frac{1}{|N(\beta_n)| \cdot \beta_n^2} \cdot f_{\delta,n}(\beta_n, r_i, r_i)^2 \cdot (1 - e^{-\alpha \cdot \beta_n^2 \cdot t}) \quad (5.107)$$

In the case of a Robin boundary condition for $r = r_a$, the Norm in equation (5.103) changes to

$$N(\beta_n) = \frac{2}{\pi^2} \frac{[J_1(\beta_n \cdot r_i)]^2 (h_{rob}^2 + \beta_n^2) - [h_{rob} \cdot J_0(\beta_n \cdot r_o) - \beta_n \cdot J_1(\beta_n \cdot r_o)]}{\beta_n^2 \cdot [h_{rob} \cdot J_0(\beta_n \cdot r_o) - \beta_n \cdot J_1(\beta_n \cdot r_o)]^2} \quad (5.108)$$

and the equation for the determination of the Eigenvalues (5.81) changes to

$$\begin{aligned} & J_1(\beta_n \cdot r_i) \cdot [h \cdot Y_0(\beta_n \cdot r_o) - \beta_n \cdot Y_1(\beta_n \cdot r_o)] \\ & - Y_1(\beta_n \cdot r_i) \cdot [h \cdot J_0(\beta_n \cdot r_o) - \beta_n \cdot J_1(\beta_n \cdot r_o)] = 0 \text{ für } n = 1, 2, 3 \dots \end{aligned} \quad (5.109)$$

5.3 Calculation of heat conduction inside the homogenous bedding

When heat leaves the cable surface, it must traverse the bedding in order to be finally released from the ground surface into the surrounding air – leading to a temperature rise of the cable with respect to the “undisturbed” soil temperature at the same depth. Equally, changes of temperature on the ground surface can lead to changes of temperature in the laying depth of the cable. Considering the heat transfer inside the bedding to take place only via conduction and assuming the bedding to be of a material of homogeneous properties, expressions to calculate the temperature rise due to both effects will be presented, in stationary, periodic as well as transient time regimes. The final temperature is the superposition of both solutions.

5.3.1 Stationary conditions

Considering the temperature rise on the outer cable jacket due to the heat that is injected from the cable into the bedding in the first place, the use of bipolar cylindrical coordinates is suitable. In this case, the problem described by equation (4.87) takes the form

$$\Delta T(\eta, \psi) = \frac{1}{a^2} [\cosh(\eta) - \cos(\psi)]^2 \left(\frac{\partial^2 T}{\partial \eta^2} + \frac{\partial^2 T}{\partial \psi^2} \right) = 0 \quad (5.110)$$

If a Dirichlet-condition is assumed on both, the outer cable jacket as well as the ground surface, the problem is indifferent to the ψ -direction, so that the equation (5.110) simplifies to

$$\Delta T(\eta, \psi) = \frac{1}{a^2} [\cosh(\eta) - \cos(\psi)]^2 \cdot \frac{\partial^2 T}{\partial \eta^2} = 0 \rightarrow \frac{\partial^2 T}{\partial \eta^2} = 0 \quad (5.111)$$

With respect to Appendix A1.1, the solution of equation (5.111) takes the form

$$T(\eta) = \varsigma_1 \cdot \eta + \varsigma_2 \quad (5.112)$$

Considering first two Dirichlet-conditions on the cable surface, T_i , and the ground surface, T_o , respectively, the system matrix becomes

$$\begin{pmatrix} -\eta_1 & 1 \\ 0 & 1 \end{pmatrix} \cdot \begin{pmatrix} \varsigma_1 \\ \varsigma_2 \end{pmatrix} = \begin{pmatrix} T_i \\ T_o \end{pmatrix} \quad (5.113)$$

so that the two constants in equation (5.112) can be calculated according to

$$\begin{pmatrix} \varsigma_1 \\ \varsigma_2 \end{pmatrix} = \frac{1}{\eta_1} \begin{pmatrix} -1 & 1 \\ 0 & \eta_1 \end{pmatrix} \cdot \begin{pmatrix} T_o \\ T_i \end{pmatrix} \quad (5.114)$$

Expressing equation (5.112) in Cartesian coordinates lead to

$$T(\eta) = \frac{\varsigma_1}{2} \ln \left[\frac{(x+a)^2 + y^2}{(x-a)^2 + y^2} \right] + \varsigma_2 \quad (5.115)$$

Comparing this to the fundamental solution in two dimensions from equation (4.133), it becomes obvious that this represents the temperature field of a line source, mirrored at the ground surface. Therefore, the same results could have been achieved by finding the Green’s function as mentioned in chapter 4.4.3 by the method of images.

If, however, a constant heat flux density on the cable surface is assumed, the problem is no longer indifferent to the ψ -direction, and equation (5.110) must be solved. In order to do so, separation of variables is applied, leading to a fundamental system of the following form

$$f_a(\psi) = \varsigma_1 \cdot \cos(\beta_n \cdot \psi) + \varsigma_2 \cdot \sin(\beta_n \cdot \psi) \quad (5.116)$$

The boundary condition for $\psi = 0$ leads directly to

$$\varsigma_2 = 0 \quad (5.117)$$

The solution for $\psi = 2\pi$ yields the Eigenvalues to be

$$\beta_n = \frac{n}{2}; n = 0, 1, 2 \dots \quad (5.118)$$

The approach for the function of η is therefore

$$f_b(\eta) = \varsigma_3 \cdot \cosh(\beta_n \cdot \eta) + \varsigma_4 \cdot \sinh(\beta_n \cdot \eta) \quad (5.119)$$

The condition for $\eta = 0$ yields

$$\varsigma_4 = 0 \quad (5.120)$$

so that the temperature can be expressed as

$$T(\eta, \psi) = \varsigma_0 \cdot \eta + \sum_{n=1}^{\infty} \varsigma_n \cdot \sinh\left(\frac{n}{2} \cdot \eta\right) \cdot \cos\left(\frac{n}{2} \cdot \psi\right) \quad (5.121)$$

The remaining coefficients will be determined via the heat flux condition on the outer jacket of the cable, hence

$$-\frac{\lambda}{a} [\cosh(\eta) - \cos(\psi)] \cdot \frac{\partial T(\eta, \psi)}{\partial \eta} \Big|_{\eta=\eta_1} = \vec{q}_h \rightarrow \frac{\partial T(\eta, \psi)}{\partial \eta} \Big|_{\eta=\eta_1} = -\frac{a}{\lambda} \frac{|\vec{q}_h|}{[\cosh(\eta_1) - \cos(\psi)]} \quad (5.122)$$

Where:

\vec{q}_h : Heat flux density on the cable surface into the bedding

which leads to

$$\varsigma_0 + \sum_{n=1}^{\infty} \varsigma_n \cdot \frac{n}{2} \cdot \cosh\left(\frac{n}{2} \cdot \eta_1\right) \cdot \cos\left(\frac{n}{2} \cdot \psi\right) = -\frac{a}{\lambda} \frac{|\vec{q}_h|}{[\cosh(\eta_1) - \cos(\psi)]} \quad (5.123)$$

With the help of the orthogonality of the implied functions, it is

$$\begin{aligned} \int_0^{2\pi} \varsigma_0 + \sum_{n=1}^{\infty} \varsigma_n \cdot \frac{n}{2} \cdot \cosh\left(\frac{n}{2} \cdot \eta_1\right) \cdot \cos\left(\frac{n}{2} \cdot \psi\right) \cos\left(\frac{m}{2} \cdot \psi\right) d\psi \\ = \begin{cases} \varsigma_n \frac{n \cdot \pi}{2} \cosh\left(\frac{n}{2} \cdot \eta_1\right) & \text{for } n = m \\ 0 & \text{else} \end{cases} \end{aligned} \quad (5.124)$$

So that finally

$$\varsigma_n = -\frac{2a}{\lambda \cdot n \cdot \pi} \frac{\vec{q}_h}{\cosh\left(\frac{n}{2} \cdot \eta_1\right)} \int_0^{2\pi} \frac{\cos\left(\frac{n}{2} \cdot \psi\right)}{[\cosh(\eta_1) - \cos(\psi)]} d\psi; n = 1, 2, 3 \dots \quad (5.125)$$

$$\varsigma_0 = -\frac{a}{2\pi \cdot \lambda} \vec{q}_h \int_0^{2\pi} \frac{1}{[\cosh(\eta_1) - \cos(\psi)]} d\psi \quad (5.126)$$

Regarding the question whether the Dirichlet-condition (i.e. a constant temperature) or the Neumann condition (i.e. a constant heat flux) is the “right” condition for the outer jacket, one can argue that this depends on the nature of the jacket, i.e. the heat conductivity or its thickness: Usually, the underlying copper screen entails a nearly constant temperature on the outer jacket as well. In contrast, a thick outer jacket with poor heat conductivity may better be approximated by a constant heat flux. However, a significant difference between these two assumptions only appears for values of η_1 that are significantly larger than typical cable diameters.

In contrast to the widely used Dirichlet-condition on the ground surface, the physically correct boundary condition on the ground surface would be of a Robin-type, as the heat is transferred from the ground surface to the air via convection. As the formulation of the gradient in bipolar cylindrical

coordinates complicates the implementation of the Robin-boundary condition, the Green's function approach is applied instead. Hence, a Green's function has to solve the following problem

$$\frac{\partial^2 T(x,y)}{\partial x^2} + \frac{\partial^2 T(x,y)}{\partial y^2} = Q' \cdot \delta(x) \cdot \delta(y - y_0) \quad (5.127)$$

and to respect the boundary constraint on the ground surface

$$-\lambda \frac{\partial T(x,y)}{\partial y} \Big|_{y=0} = h_{\text{rob}} \cdot T(x,y) \Big|_{y=0} \quad (5.128)$$

In a first step, the problem is reformulated as follows: The domain is cut in half, with a homogenous Neumann condition for $x = 0, y < 0$ as well as limited to a width L . Using the integral transformation of a Sturm-Liouville boundary problem (see [HAH2012]), equation (5.127) is reformulated to

$$\frac{\partial^2 \bar{T}(y,\beta_n)}{\partial y^2} - \beta_n^2 \cdot \bar{T}(y,\beta_n) = \bar{g}(y,\beta_n) \quad (5.129)$$

where

$$\bar{T}(y,\beta_m) = \int_{x=0}^L f_n(x,\beta_n) \cdot T(x,y) \, dx \quad (5.130)$$

$$\bar{g}(y,\beta_n) = \int_{x=0}^L f_n(x,\beta_n) \cdot g(x,y) \, dx \quad (5.131)$$

with the corresponding Eigenfunction

$$f_n(x,\beta_n) = \cos(\beta_n x) \quad (5.132)$$

From equation (5.132) and the boundary condition at $x = L$, the Eigenvalues can directly be derived

$$\cos(\beta_n \cdot L) = 0 \rightarrow \beta_n = \left(n - \frac{1}{2} \right) \cdot \frac{\pi}{L}; n = 1, 2, 3, \dots \quad (5.133)$$

Regarding the source term in equation (5.127) and taking into account that only half the heat has to be considered, it is

$$\bar{g}(y,\beta_m) = \frac{Q'}{2} \cdot \delta(y - y_0) \int_{x=0}^L \cos(\beta_m \cdot x) \cdot \delta(x) \, dx = \frac{Q'}{2} \cdot \delta(y - y_0) \quad (5.134)$$

Inserting equation (5.134) into (5.129), the resulting equation can be solved with the help of a one-dimensional Green's function, whose systematic derivation is presented in [COL2011]. For the present case, the solution is given by

$$\frac{2 \cdot \lambda}{Q'} \cdot \bar{T}(y,\beta_n) = \begin{cases} \varsigma_1 \cdot e^{\beta_n y} + \varsigma_2 \cdot e^{-\beta_n y} & \text{for } y > y_0 \\ \varsigma_3 \cdot e^{\beta_n y} + \varsigma_4 \cdot e^{-\beta_n y} & \text{for } y < y_0 \end{cases} \quad (5.135)$$

Inserting the Dirichlet boundary condition for $y \rightarrow -\infty$ leads to

$$\varsigma_4 = 0 \quad (5.136)$$

as well as the Robin condition at $y = 0$ yields

$$\varsigma_1 = \frac{\lambda \cdot \beta_n - h_{\text{rob}}}{\lambda \cdot \beta_n + h_{\text{rob}}} \cdot \varsigma_2 = \varsigma(\lambda, h_{\text{rob}}) \cdot \varsigma_2 \quad (5.137)$$

Including the condition of continuity as well as the jump condition for the derivations leads to the solution in the image domain

$$\frac{2 \cdot \lambda}{Q'} \cdot \bar{T}(y,\beta_n) = \begin{cases} \frac{1}{2 \cdot \beta_n} [\varsigma(\lambda, h_{\text{rob}}) \cdot e^{\beta_n(y+y_0)} + e^{\beta_n(y_0-y)}] & \text{for } y > y_0 \\ \frac{1}{2 \cdot \beta_n} [\varsigma(\lambda, h_{\text{rob}}) \cdot e^{\beta_n(y+y_0)} + e^{\beta_n(y-y_0)}] & \text{für } y < y_0 \end{cases} \quad (5.138)$$

The final solution is then found by retransforming the expression in equation (5.138) to the original domain by

$$T(x, y) = \sum_{n=1}^{\infty} \frac{f_n(x, \beta_n)}{N(\beta_n)} \cdot \bar{T}(y, \beta_n) \quad (5.139)$$

where the Norm of the Eigenfunction equals

$$N(\beta_n) = \int_{x=0}^L \cos^2(\beta_n \cdot x) dx = \frac{L}{2} \quad (5.140)$$

The solution in equation (5.139) may be transformed to the solution of the semi-infinite domain by expanding L to infinity. This leads to the transition from discrete Eigenvalues in equation (5.133) to a continuous spectrum, as well as the Norm in equation (5.140) changes to

$$N(\beta_n) = \frac{\pi}{2} \quad (5.141)$$

Equation (5.139) is altered to

$$T(x, y) = \frac{2}{\pi} \int_{\beta=0}^{\infty} \cos(\beta \cdot x) \cdot \bar{T}(y, \beta_n) d\beta \quad (5.142)$$

which is nothing else but the reverse cosine transform with respect to x .

Considering the influence of the temperature on the ground surface to the temperature of the cable, the domain to be dealt with is a one-dimensional, semi-infinite one. Assuming the ground to expand in negative y -direction and locating the ground surface at $y = 0$ at a temperature of T_0 , Cartesian coordinates are chosen, which simplifies the equation to be solved to

$$\Delta T(y) = \frac{\partial^2 T}{\partial y^2} = 0 \quad (5.143)$$

According to Appendix A1.1, the fundamental system for this equation is

$$T(y) = \varsigma_1 \cdot y + \varsigma_2 \quad (5.144)$$

However, as the temperature must stay finite for $y \rightarrow \infty$, it directly follows that

$$\varsigma_1 = 0 \quad (5.145)$$

Furthermore, the boundary condition leads to

$$\varsigma_2 = T_0 \quad (5.146)$$

so that the temperature is a constant and equal to the reference temperature on the ground surface.

5.3.2 Periodic conditions

As the two-dimensional Helmholtz equation from equation (4.84) is not separable in bipolar-cylindrical coordinates, the solution for the temperature field under the assumption of a periodic heat injection from the cable will be found with the help of a Green's function. Referring to the fundamental solution from equation (4.140), the Green's function to implement a homogenous Dirichlet boundary condition on the ground surface can be found via a mirror image to be [CAR1956]

$$\underline{G}(x, y, x', y') = \frac{\dot{Q}'}{2\pi} \cdot \left(K_0 \left[\underline{\beta} \sqrt{(x-x')^2 + (y-y')^2} \right] - K_0 \left[\underline{\beta} \sqrt{(x+x')^2 + (y+y')^2} \right] \right) \quad (5.147)$$

However, in contrast to the stationary case, it is no longer possible to shift the sources in such a way that a Dirichlet-condition on the outer jacket of the cable is fulfilled. However, deviations of the temperature alongside the outer jacket are small if the laying depth of the cable is considerably larger

than the outer diameter, as it is also stated in IEC 60287, so that the position of the line source in the centre of the cable is a valid approximation.

Considering the effect of a convectional boundary condition on the ground surface, it is not possible to employ the same procedure as in the stationary case. This is because the resulting formulation arising from equation (4.84) does not represent a Sturm-Liouville Problem so that the modified Bessel-functions (which form the fundamental system) are not orthogonal.

Hence, a Green's function approach will also be employed to solve the problem of a periodically oscillating line source in front of a convective boundary condition: Applying the Fourier transformation with regard to x , equation (4.84) simplifies to an ordinary differential equation

$$\Delta \underline{T}(y) - (s_F^2 + \underline{\beta}^2) \underline{T} = P_v \cdot \delta(y - y_0) \quad (5.148)$$

This procedure is already proposed in [PUR2014], albeit the execution is incorrect: The geometry is correctly transformed (as the term of the right hand side in equation (5.148) corresponds to a surface charge), but the Laplace-equation as a whole must be transformed – and not be built in the image section. Therefore, the fundamental system mentioned in equation (A15) from Appendix A1.3 is the correct one, not the one mentioned in [PUR2014].

Hence, the Green's function for the one-dimensional equation in (5.148) can be written as

$$\underline{G}(y, y') = \begin{cases} \zeta_1 \cdot e^{s_F \cdot y} + \zeta_2 \cdot e^{-s_F \cdot y} & \text{for } y_0 < y \\ \zeta_3 \cdot e^{s_F \cdot y} + \zeta_4 \cdot e^{-s_F \cdot y} & \text{for } -\infty < y < y_0 \end{cases} \quad (5.149)$$

Following the steps of the derivation of the Green's function in one dimension [COL2011], the temperature in the image section for $y > y_0$ can be written as

$$\begin{aligned} \underline{T}(y > y_0, s_F^2) = & \frac{h_{\text{rob}}/\lambda}{\sqrt{s_F^2 + \underline{\beta}^2} \cdot (\sqrt{s_F^2 + \underline{\beta}^2} + h_{\text{rob}}/\lambda)} e^{\sqrt{s_F^2 + \underline{\beta}^2} \cdot (y_0 + y)} \\ & - \frac{1}{2 \cdot \sqrt{s_F^2 + \underline{\beta}^2}} \cdot \left(e^{\sqrt{s_F^2 + \underline{\beta}^2} \cdot (y_0 + y)} + e^{\sqrt{s_F^2 + \underline{\beta}^2} \cdot (y_0 - y)} \right) \end{aligned} \quad (5.150)$$

An inverse transformation of equation (5.150) as a closed formulation has not been found. However, it should be noted that for $h_{\text{rob}} \rightarrow \infty$, the result is the Fourier transformation of the sum of modified Bessel-functions K_0 from equation (5.147).

Regarding the influence of a periodically changing temperature on the ground surface on the reference-temperature at lying depth of a cable system, the one dimensional equation to be solved is

$$\frac{\partial^2 \underline{T}(y)}{\partial y^2} = \frac{j\omega_{\text{th},2}}{\alpha} \cdot \underline{T}(y) = \left[(1 + j) \sqrt{\frac{\omega_{\text{th},2}}{2 \cdot \alpha}} \right]^2 \cdot \underline{T}(y) = \underline{\beta}^2 \cdot \underline{T}(y) \quad (5.151)$$

Where:

$\omega_{\text{th},2}$: Angular frequency of the temperature change at the ground surface

Regarding Appendix A1.3, equation (5.151) has the fundamental system of

$$\underline{T}(y) = \zeta_1 \cdot e^{\underline{\beta} \cdot y} + \zeta_2 \cdot e^{-\underline{\beta} \cdot y} \quad (5.152)$$

As the temperature has to stay finite for $y \rightarrow -\infty$, it follows directly that

$$\zeta_2 = 0 \quad (5.153)$$

The other coefficient is determined via the boundary condition at the ground surface, so that

$$\underline{T}(y = 0) = \underline{T}_o \rightarrow \varsigma_1 = \underline{T}_o \quad (5.154)$$

Therefore, the real part of the temperature at laying depth, $-y_0$, can be written as

$$\begin{aligned} T(y_0) &= \Re\{\underline{T}(y_0) \cdot e^{j\omega_{th,2} \cdot t}\} = \Re\{\underline{T}_o \cdot e^{-\beta \cdot y_0} \cdot e^{j\omega_{th,2}}\} \\ &= T_o \cdot e^{-y_0 \cdot \sqrt{\frac{\omega_{th,2}}{2 \cdot \alpha}}} \cdot \cos\left(\omega \cdot t - y_0 \cdot \sqrt{\frac{\omega_{th,2}}{2 \cdot \alpha}}\right) \end{aligned} \quad (5.155)$$

Hence, the temperature experiences an exponentially decreasing damping as well as a phase shift. If the boundary condition on the ground surface is a Robin-condition to the reference temperature T_o , equation (5.154) changes to

$$-\lambda \frac{\partial \underline{T}(y=0)}{\partial y} = h_{rob} \cdot (\underline{T}(y=0) - \underline{T}_o) \rightarrow \varsigma_1 = \frac{h_{rob}}{h_{rob} + \beta \cdot \lambda} \cdot T_o \quad (5.156)$$

so that the result from equation (5.155) is altered to

$$T(y_0) = T_o \cdot \frac{h_{rob}}{h_{rob} + \beta \cdot \lambda} \cdot e^{-y_0 \cdot \sqrt{\frac{\omega_{th,2}}{2 \cdot \alpha}}} \cdot \cos\left(\omega \cdot t - y_0 \cdot \sqrt{\frac{\omega_{th,2}}{2 \cdot \alpha}}\right) \quad (5.157)$$

which, for $h_{rob} \rightarrow -\infty$, converges towards equation (5.155).

5.3.3 Transient conditions

As it was already mentioned before, the Helmholtz equation is not separable in cylindrical-bipolar coordinates, so that a solution of the transient heating inside a bedding is once again based on the Green's function approach. In analogy to the periodic conditions, the losses inside the conductor can be approximated as a line source. Therefore, the two dimensional fundamental solution of the time dependent heat equation can be used to describe the temperature field around a buried power cable. Based on equation (4.142), the Green's function for a line source of Q' inside an infinite medium is

$$G(r, t, r', t') = \frac{Q'}{4\pi\alpha(t-t')} e^{-\frac{(r-r')^2}{4\alpha(t-t')}} \quad (5.158)$$

Where:

Q' : Instantaneous heat per unit length, released by a line source

Inserting equation (5.158) into equation (4.148) then yields the result already derived in (3.14). However, this only approximates the actual results, as the time that it takes for the heat to traverse the cable elements (i.e. from the conductor surface to the surface of the outer jacket) should not be part of the solution. Moreover, the thermal properties inside the cable are not the same as for the bedding as it is assumed in equation (3.14). As a consequence, equation (3.14) exhibits a delay to the correct solution that increases with growing cable diameter.

In order to address these shortcomings, it is possible to place line sources of the amplitudes $\dot{Q}' \cdot d\varphi$ alongside the cable's outer diameter and to integrate in azimuthal direction. For an instantaneous release of $\rho c_p \cdot 2\pi r_{jac} Q'$ of heat, this yields the solution [CAR1959]

$$\begin{aligned} T(r, r_{jac} t) &= \frac{Q' r_{jac}}{4\pi\alpha t} \int_0^{2\pi} e^{-\frac{r^2 + (r_{jac})^2 - 2rr_{jac} \cos\varphi}{4\alpha t}} d\varphi \\ &= \frac{Q' r_{jac}}{4\pi\alpha t} e^{-\frac{r^2 + r_{jac}^2}{4\alpha t}} \int_0^{2\pi} e^{-\frac{rr_{jac} \cos\varphi}{2\alpha t}} d\varphi = \frac{Q'}{4\pi\alpha t} e^{-\frac{r^2 + r_{jac}^2}{4\alpha t}} \cdot I_0\left(\frac{r \cdot r_{jac}}{2\alpha t}\right) \end{aligned} \quad (5.159)$$

Equation (5.159) is an improvement to equation (3.14) in the sense that at $t = 0$, the heat is actually liberated at the surface of the outer jacket of the cable. However, the convolution of equation (5.159) with respect to time, i.e. the temperature development inside the bedding due to an applied step function of heat injection, has not been found as closed form expression. Moreover, equation (5.159) is still an approximation in the sense that the outer surface of the cable is not a boundary from which heat is injected strictly perpendicular, but the outer surface of the cable represents a cylindrical source, whose heat is emitted also into the cable.

As a consequence, the exact solution of a circular boundary inside an infinite medium, into which heat is injected strictly perpendicularly, is derived in the following. In analogy to the calculations in chapter 5.2.3, the used separation of variables in cylindrical coordinates yields for the dependency of the special variable

$$f_a(r, \beta_n, r_i) = J_0(\beta \cdot r) \cdot Y_1(\beta \cdot r_i) - J_1(\beta \cdot r_i) \cdot Y_0(\beta \cdot r) \quad (5.160)$$

as well as for the dependency in time

$$f_b(t, \beta) = e^{-\alpha\beta^2 \cdot t} \quad (5.161)$$

Assuming an infinite medium instead of the bounded hollow cylinder from chapter 5.2.3, the Eigenvalues are no longer distinct values, but become a spectrum. Equally, the Norm changes to [CIN1965]

$$N(\beta, r_i) = J_1^2(\beta \cdot r_i) + Y_1^2(\beta \cdot r_i) \quad (5.162)$$

As a consequence, the solution can be written as

$$T(r, t) = \int_{\beta=0}^{\infty} \beta \cdot \frac{f_a(r, \beta)}{N(\beta)} \cdot e^{-\alpha\beta^2 \cdot t} \int_{r'=r_i}^{\infty} r' \cdot f_a(r', \beta) \cdot T_i(r') dr' d\beta \quad (5.163)$$

Interchanging the order of the integration and a comparison to equation (4.145) yields the Green's function

$$G(r, t, r', t') = \int_{\beta=0}^{\infty} \frac{\beta}{N(\beta)} f_a(r, \beta) \cdot f_a(r', \beta) \cdot e^{-\alpha\beta^2 \cdot (t-t')} d\beta \quad (5.164)$$

With the help of the Green's function from (5.164) and equation (4.148), the temperature development under any arbitrary form of heat injection in time can be derived. As an example, if heat is injected in the form of a Heaviside step function, the resulting temperature field is

$$T(r, t) \int_{\beta=0}^{\infty} \frac{\beta}{N(\beta)} f_a(r, \beta) \cdot f_a(r_i, \beta) (1 - e^{-\alpha\beta^2 \cdot t}) d\beta \quad (5.165)$$

For the sake of completeness, [GOL1959] gives the following Green's function for a transient heating of a line source in front of a convective boundary condition

$$\begin{aligned} G(x, y, t, x', y', t') &= \frac{Q'}{4\pi\alpha(t-t')} \left(e^{-\frac{(y-y')^2}{4\alpha(t-t')}} + e^{-\frac{(y+y')^2}{4\alpha(t-t')}} \right) \cdot e^{-\frac{(x+x')^2}{4\alpha(t-t')}} \\ &\quad - \frac{h_{rob}}{2\sqrt{\pi\alpha(t-t')}} \operatorname{erfc} \left(\frac{(y+y')}{2\sqrt{\alpha(t-t')}} + h_{rob}\sqrt{\alpha(t-t')} \right) \cdot e^{h_{rob}(y+y')+\alpha h^2(t-t')-\frac{(x-x')^2}{4\alpha(t-t')}} \end{aligned} \quad (5.166)$$

where it should be noted that the position of the line source is assumed to be positive, so that $y_0 > 0$.

Hence, in chapter 5, all solutions for every relevant geometry (homogeneous and particular for the conductor, insulation and screen) for every dependency in time is presented – some of them well established, some of them derived and presented by the author himself.

6 The use of thermal quadropoles

In the previous chapter, analytical expressions for all relevant physical problems in the corresponding geometric configurations and possible time dependencies have been presented. However, the abundancy of the resulting mathematical expressions may leave the reader perplexed: At this point, it is unclear how the rating of a complete system should be based on the multitude of equations from chapter 5.

What therefore is missing is an approach to not only reduce the complexity of the expressions itself, but to merge the calculations of the separate components into the description of one *system*. This is undertaken in the following chapter, with the aim to lead the excessive mathematical equations back to a form that mirrors the clarity and simplicity of the equations mentioned in chapter 4.1.

6.1 The definition of input and output variables

In order to reduce the complexity of the involved expressions, it is helpful to recognize that they provide information that is not really of an interest: Albeit the temperature distribution within the whole domain can be determined, what really matters are the conditions on the boundaries. Or, in other words: The temperature inside the bedding at different distances to the cable is not as relevant (for one single cable) as the temperature on the outside of the cable jacket that follows from an injection of heat flux into it.

As either the state variable itself (in the case of a Dirichlet boundary condition) or its gradient (regarding a Neumann boundary condition) or its relation (in the case of the Robin boundary condition) is fixed, the complementary quantity is determined via the properties of what is “between” the two boundaries – i.e. the partial differential equation that describes the regarded physical process as well as the implied geometry and material properties. Taking the stationary heat conduction inside a hollow cylinder as an example, it is derived in section (5.2.1) that the solution for the temperature takes the form

$$T(r) = \varsigma_1 \ln r + \varsigma_2 \quad (6.1)$$

Or, regarding the heat flux density

$$\vec{q}(r) = -\lambda \cdot \text{grad } T(r) = -\frac{\lambda \cdot \varsigma_1}{r} \quad (6.2)$$

Putting equations (6.1) and (6.2) into the form of a matrix leads to

$$\begin{pmatrix} T(r) \\ \vec{q}(r) \end{pmatrix} = \begin{pmatrix} \ln r & 1 \\ -\lambda/r & 0 \end{pmatrix} \cdot \begin{pmatrix} \varsigma_1 \\ \varsigma_2 \end{pmatrix} \quad (6.3)$$

If the heat flux density on the inner radius as well as the reference temperature on the outer radius is prescribed, the temperature on the inner boundary as well as the heat flux density on the outer boundaries are the results of the “behaviour” of the hollow cylinder with respect to the stationary heat conduction. Hence

$$\begin{pmatrix} T(r_i) \\ \vec{q}(r_o) \end{pmatrix} = \begin{pmatrix} \ln r_i & 1 \\ -\lambda/r_o & 0 \end{pmatrix} \cdot \begin{pmatrix} \varsigma_1 \\ \varsigma_2 \end{pmatrix} \quad (6.4)$$

Inserting equation (6.3) for the particular coefficients into equation (6.4) and multiplying of the involved matrices yields

$$\begin{pmatrix} T(r_i) \\ \vec{q}(r_o) \cdot \vec{e}_r \end{pmatrix} = \begin{pmatrix} \ln(r_i/r_o) & 1 \\ r_i/r_o & 0 \end{pmatrix} \cdot \begin{pmatrix} \vec{q}(r_i) \cdot \vec{e}_r \\ T(r_o) \end{pmatrix} \quad (6.5)$$

Hence, the resulting equation in (6.5) delivers a direct link between the *input variables* – i.e. the determined boundary constraints – and the *output variables* – i.e. the complementary quantities on the boundary. The matrix on the right hand side characterises therefore “everything in between the boundaries”, representing the geometry as well as the material properties of the domain (the latter are, in the concrete example of equation (6.5), not relevant due to the choice of the boundary conditions and the stationary consideration).

A reader with a background in electrical engineering may be familiar with the form of the equation (6.5): The connection between the state variable (a potential) and its derivation (a flux) at two different points via a matrix that represents a certain “connection” between these two points is a method to describe electric networks, since 1921 known as “quadropoles”, a term introduced by the German engineer Franz Breisig [WUN1985]. In fact, defining the variables of interest and summarizing the behaviour of the system into a matrix was a reasoning already undertaken by no one less than Küpfmüller, the founder of the system analysis [KÜP2006]. In the following, a short overview of this concept is given.

6.2 Introduction to quadropoles

In general, quadropoles can be assumed as “black boxes”, connecting fluxes into or out of systems with the corresponding potentials at its terminals. A representation with the temperature T as state variable and the total heat flux \dot{Q} as flux variable is shown in Figure 6.1. All following definitions have been taken from [KRE1967].

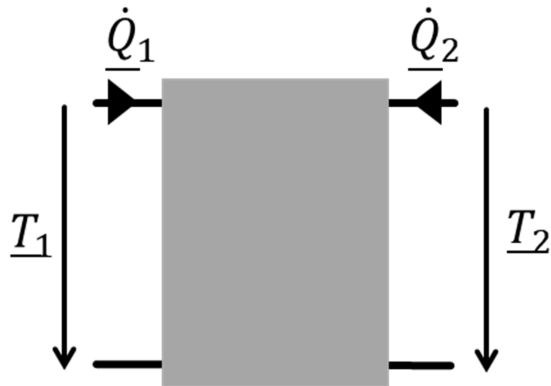


Figure 6.1: Illustration of a general quadrupole with temperature (T) as state variable and the total heat flux (\dot{Q}) as flux variable.

For linear and passive quadropoles (i.e. quadropoles with no internal energy source), the relation between the fluxes and the potentials can be given in a matrix form. In the analogy to the Ohmic law, the equation of the form

$$\begin{pmatrix} \dot{Q}_1 \\ \dot{Q}_2 \end{pmatrix} = \begin{pmatrix} y_{1,1} & y_{1,2} \\ y_{2,1} & y_{2,2} \end{pmatrix} \cdot \begin{pmatrix} T_1 \\ T_2 \end{pmatrix} = [Y] \cdot \begin{pmatrix} T_1 \\ T_2 \end{pmatrix} \quad (6.6)$$

With:

\dot{Q}_1, \dot{Q}_2 : Phasors of the total heat fluxes into a thermal quadrupole (with the direction indicated in Figure 5.1)

T_1, T_2 : Phasors of the temperatures at a thermal quadrupole

is denoted as the quadrupole equation in admittance form [SCH2014-1]. A quadrupole is called reciprocal if

$$\underline{y}_{2,1} = \underline{y}_{1,2} \quad (6.7)$$

In this case, it is

$$\left. \frac{\dot{Q}_1}{T_2} \right|_{T_1=0} = - \left. \frac{\dot{Q}_2}{T_1} \right|_{T_2=0} \quad (6.8)$$

If also

$$\underline{y}_{1,1} = \underline{y}_{2,2} \quad (6.9)$$

the quadrupole is called symmetrical, so that it can be mirrored with regard to its vertical axis. Apart from its representations as a matrix, quadrupoles can also be illustrated by equivalent circuit diagrams. In Figure 6.2, the π -equivalent circuit of a symmetrical quadrupole is shown.

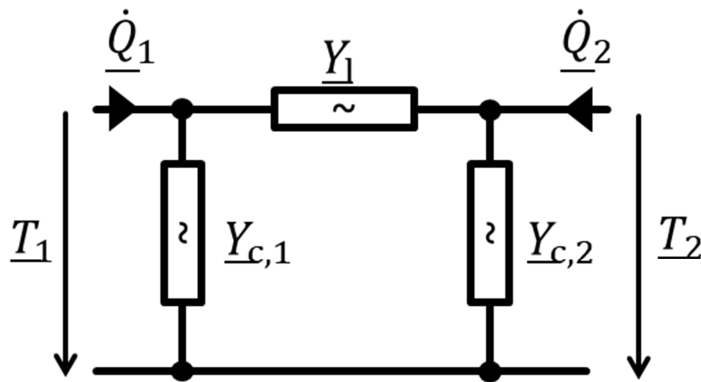


Figure 6.2: π -equivalent circuit of a thermal quadrupole

From the admittance form of the quadrupole equation in (6.6), the thermal admittances in Figure 6.2 can be derived as following

$$Y_{c,1} = \underline{y}_{1,1} + \underline{y}_{1,2} \quad Y_{c,2} = \underline{y}_{2,2} + \underline{y}_{1,2} \quad Y_l = -\underline{y}_{1,2} \quad (6.10)$$

In analogy to the admittance form, it also exists an impedance form of the quadrupole matrix with

$$\begin{pmatrix} T_1 \\ T_2 \end{pmatrix} = \begin{pmatrix} Z_{1,1} & Z_{1,2} \\ Z_{2,1} & Z_{2,2} \end{pmatrix} \cdot \begin{pmatrix} \dot{Q}_1 \\ \dot{Q}_2 \end{pmatrix} = [\underline{Z}] \cdot \begin{pmatrix} \dot{Q}_1 \\ \dot{Q}_2 \end{pmatrix} \quad (6.11)$$

from which the T-equivalent circuit for symmetrical quadrupoles in Figure 6.3 can be derived

$$Z_{l,1} = \underline{z}_{1,1} - \underline{z}_{1,2} \quad Z_{l,2} = \underline{z}_{2,2} - \underline{z}_{1,2} \quad Z_c = \underline{z}_{1,2} \quad (6.12)$$

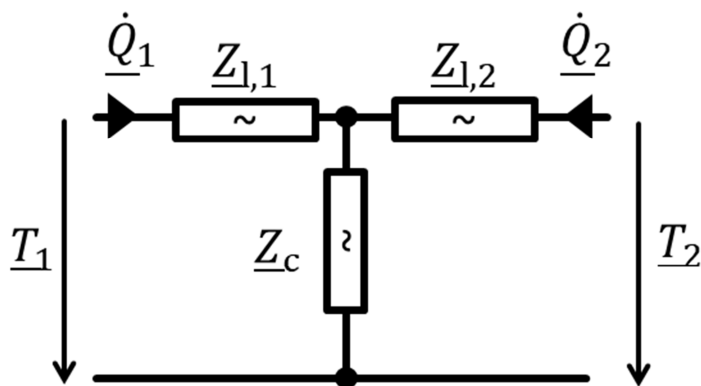


Figure 6.3: T-equivalent circuit of a thermal quadrupole

With respect to the following application, the chain form of a quadrupole is of high importance. This form is defined by

$$\begin{pmatrix} \underline{T}_1 \\ \underline{\dot{Q}}_1 \end{pmatrix} = \begin{pmatrix} \underline{a}_{1,1} & \underline{a}_{1,2} \\ \underline{a}_{2,1} & \underline{a}_{2,2} \end{pmatrix} \cdot \begin{pmatrix} \underline{T}_2 \\ -\underline{\dot{Q}}_2 \end{pmatrix} = [\underline{A}] \cdot \begin{pmatrix} \underline{T}_2 \\ -\underline{\dot{Q}}_2 \end{pmatrix} \quad (6.13)$$

The transformation between the chain- and the admittance form is given by

$$[\underline{Y}] = \frac{1}{\underline{a}_{1,2}} \begin{pmatrix} \underline{a}_{2,2} & -\det[\underline{A}] \\ -1 & \underline{a}_{1,1} \end{pmatrix} \quad [\underline{A}] = -\frac{1}{\underline{y}_{2,1}} \begin{pmatrix} \underline{y}_{2,2} & 1 \\ \det[\underline{Y}] & \underline{y}_{1,1} \end{pmatrix} \quad (6.14)$$

The advantage of the formulation in chain form is that a series connection of two quadrupoles can be calculated by a multiplication of the two matrices A. If, as an example, two quadrupoles with

$$\begin{pmatrix} \underline{T}_1 \\ \underline{\dot{Q}}_1 \end{pmatrix} = [\underline{A}]_a \cdot \begin{pmatrix} \underline{T}_2 \\ -\underline{\dot{Q}}_2 \end{pmatrix} \quad \begin{pmatrix} \underline{T}_3 \\ \underline{\dot{Q}}_3 \end{pmatrix} = [\underline{A}]_b \cdot \begin{pmatrix} \underline{T}_4 \\ -\underline{\dot{Q}}_4 \end{pmatrix} \quad (6.15)$$

are connected in series, i.e.

$$\begin{pmatrix} \underline{T}_2 \\ -\underline{\dot{Q}}_2 \end{pmatrix} = \begin{pmatrix} \underline{T}_3 \\ \underline{\dot{Q}}_3 \end{pmatrix} \quad (6.16)$$

it is

$$\begin{pmatrix} \underline{T}_1 \\ \underline{\dot{Q}}_1 \end{pmatrix} = [\underline{A}]_a \cdot \begin{pmatrix} \underline{T}_2 \\ -\underline{\dot{Q}}_2 \end{pmatrix} = [\underline{A}]_a \cdot [\underline{A}]_b \cdot \begin{pmatrix} \underline{T}_4 \\ -\underline{\dot{Q}}_4 \end{pmatrix} = [\underline{A}]_{a,b} \cdot \begin{pmatrix} \underline{T}_4 \\ -\underline{\dot{Q}}_4 \end{pmatrix} \quad (6.17)$$

Finally, a form that arises frequently from the assumed boundary conditions is the so-called H-Form with

$$\begin{pmatrix} \underline{T}_1 \\ \underline{\dot{Q}}_2 \end{pmatrix} = \begin{pmatrix} \underline{h}_{1,1} & \underline{h}_{2,1} \\ \underline{h}_{1,2} & \underline{h}_{2,2} \end{pmatrix} \cdot \begin{pmatrix} \underline{\dot{Q}}_1 \\ \underline{T}_2 \end{pmatrix} \quad (6.18)$$

from which the other forms can be derived by

$$[\underline{A}] = \frac{1}{\underline{h}_{2,1}} \begin{pmatrix} -\det[\underline{H}] & -\underline{h}_{1,1} \\ -\underline{h}_{2,2} & -1 \end{pmatrix} \quad [\underline{Y}] = \frac{1}{\underline{h}_{1,1}} \begin{pmatrix} 1 & -\underline{h}_{1,2} \\ \underline{h}_{2,1} & \det[\underline{H}] \end{pmatrix} \quad (6.19)$$

As a consequence, the different geometries of a cable system can be subsumed into the form of quadrupoles, which allows a rapid calculation of the parameters of the system as a whole. Before giving the actual form of the matrices, it must first be found a way to equally subsume the different *dependencies from time* (i.e. stationary, periodic and transient conditions) that have been regarded separately so far under one general perspective. This will be done in the following chapter.

6.3 The use of the frequency domain

By comparing the solutions of the stationary as well as periodic solutions to the expressions found for the transient solutions, it may be noticed that the latter do not possess the same *algebraic structure* between the input and the output variables as it is the case for the stationary or periodic solutions. Therefore, it is the question whether and how the quadrupole approach can also be applied to transient problems.

In order to answer this question, it is helpful to recall that in principle, the input variable, assumed as being a time-dependent total heat flux $Q_i(t)$, and the output variable, supposed to be a time dependent temperature $T_o(t)$ are related via a differential operator [MAT1987]

$$L\left(\frac{d}{dt}\right)(T_o(t)) = Q_i(t) \quad (6.20)$$

Where:

$L\left(\frac{d}{dt}\right)$: Differential operator

$Q_i(t)$: Time dependent total heat flux as input variable

$T_o(t)$: Time dependent temperature as output variable

Furthermore, an inverse operator of L is assumed with

$$T_o(t) = L^{-1}(Q_i(t)) \quad (6.21)$$

Using the properties of the Dirac-delta distribution, the input function can be written as

$$Q_i(t) = \int_0^\infty Q_i(\tau) \cdot \delta(t - \tau) d\tau \quad (6.22)$$

Using the linearity of the operators, one may write

$$T_o(t) = L^{-1}\left(\int_0^\infty Q_i(\tau) \cdot \delta(t - \tau) d\tau\right) = \int_0^\infty Q_i(\tau) \cdot L^{-1}(\delta(t - \tau)) d\tau \quad (6.23)$$

The expression

$$L^{-1}(\delta(t - \tau)) \stackrel{\text{def}}{=} G(t) \quad (6.24)$$

is, as it was already mentioned, the Green's function with respect to time, and can therefore be interpreted as the “response” of the system described by (6.20) to a Dirac incitation. Furthermore, the integral relation in (6.23) is called convolution. Hence, equation (6.23) can be re-written as

$$T_o(t) = Q_i(t) * G(t) \quad (6.25)$$

However, with the help of the Laplace transformation that is defined by

$$\mathcal{L}\{f(x)\}(s_L) = \int_0^\infty f(x) \cdot e^{-x \cdot s_L} dx \quad (6.26)$$

the convolution in equation (6.25) can be transformed to a multiplication

$$\mathcal{L}\{T_o(t)\} = T_o(s_L) = \mathcal{L}\{Q_i(t)\} \cdot \mathcal{L}\{G(t)\} = Q_i(s_L) \cdot G(s_L) \quad (6.27)$$

Hence, the relation between the input and the output signal for transients in the image-section is of the same algebraic form as the one for stationary or periodic signals in the time domain. Therefore, the quadrupole approach can easily be used on the spectrum of the input variable. Afterwards, the solution $T_o(s_L)$ has to be transformed back into the time domain to obtain $T_o(t)$. Figure 6.4 summarizes the procedure [MAT1987].

Finally, in order to find the function $G(s_L)$, it is not necessary to explicitly transform the solution found in the time domain, but it can directly be derived from the already established transfer function for periodic signals by interchanging the variable as follows

$$j\omega \rightarrow s_L \quad (6.28)$$

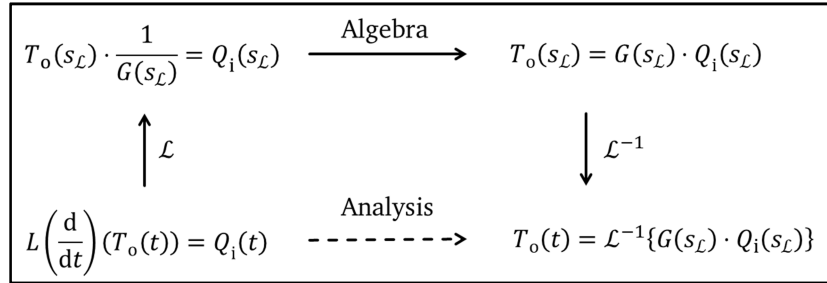


Figure 6.4: Illustration of the use of the Laplace-function, taken from [MAT1987]

Under a historical perspective, equation (6.28) follows the chronology, as the “Heaviside calculus” was the extension of the “symbolic method” derived by Steinmetz for stationary oscillations on non-stationary processes [KÜP2006]. The extensive theory behind this “simple” change of variable (which, as [MAT1987] puts it, is actually the formal equality of a rational function of an *operator* s_L to an expression of the *complex variable* s_L) shall not be given at this point. For further information, the referred sources are to be consulted.

Hence, the input signals, i.e. the losses inside the cable system, have to be transformed into the frequency domain. As the Fast-Fourier transformation (FFT) offers a rapid numerical implementation of the decomposition of the signal into its frequencies, it is helpful to consider the Fourier Transformation instead of the Laplace-Transformation. The latter is defined as

$$\mathcal{F}\{f(x)\}(s_F) = \int_{-\infty}^{\infty} f(x) \cdot e^{-jx \cdot s_F} dx \quad (6.29)$$

In this case, non-stationary processes can be implemented in practice by simply adding “sufficient” zeros for $t < 0$ at the time-series.

6.4 Calculation of thermal quadrupoles

As a consequence of the previous explanations, the thermal quadrupoles of the calculated geometries from chapter 5 shall be derived for stationary periodic as well as for stationary conditions. For homogeneous problems, this can be done in a formalized manner, as the solution (i.e. the temperature distribution) can always be written in terms of the fundamental system of the corresponding PDE. Taking the cylindrical coordinate system as an example, it is

$$\underline{T}(r) = \underline{\varsigma}_1 \cdot f_1(r) + \underline{\varsigma}_2 \cdot f_2(r) \quad (6.30)$$

The associated heat flux density is calculated by Fourier’s law from equation (4.30)

$$\vec{\underline{q}}(r) = -\lambda \cdot \text{grad } \underline{T}(r) = -\lambda \cdot [\underline{\varsigma}_1 \cdot f'_1(r) + \underline{\varsigma}_2 \cdot f'_2(r)] \quad (6.31)$$

Or, in a combined form

$$\begin{pmatrix} \underline{T}(r) \\ \vec{\underline{q}}(r) \end{pmatrix} = \begin{pmatrix} f_1(r) & f_2(r) \\ -\lambda \cdot f'_1(r) & -\lambda \cdot f'_2(r) \end{pmatrix} \cdot \begin{pmatrix} \underline{\varsigma}_1 \\ \underline{\varsigma}_2 \end{pmatrix} \quad (6.32)$$

The coefficients $\underline{\varsigma}_1$ and $\underline{\varsigma}_2$ can directly be derived from equation (6.32). Assuming the same boundary constraints as in the example from chapter 5.1 (i.e. a Neuman boundary constraint for $r = r_i$ and a Dirichlet boundary constraint at $r = r_o$) and denoting the inverse of the system matrix as $[S]^{-1}$, one may write

$$\begin{pmatrix} \underline{T}(r) \\ \vec{\underline{q}}(r) \end{pmatrix} = \begin{pmatrix} f_1(r) & f_2(r) \\ -\lambda \cdot f'_1(r) & -\lambda \cdot f'_2(r) \end{pmatrix} \cdot [S]^{-1} \cdot \begin{pmatrix} \vec{\underline{q}}(r_i) \cdot \vec{e}_r \\ \underline{T}(r_o) \end{pmatrix} \quad (6.33)$$

with

$$[S]^{-1} = \frac{1}{\lambda[f_2(r_o)f'_1(r_i) - f_1(r_o)f'_2(r_i)]} \cdot \begin{pmatrix} -f_2(r_o) & -\lambda \cdot f'_2(r_i) \\ f_1(r_o) & \lambda \cdot f'_1(r_i) \end{pmatrix} \quad (6.34)$$

Hence, the unknown values for the temperature on the inner boundary as well as the heat flux density on the outer boundary can directly be derived by

$$\begin{pmatrix} \underline{T}(r_i) \\ \vec{\underline{q}}(r_o) \cdot \vec{e}_r \end{pmatrix} = \begin{pmatrix} f_1(r_i) & f_2(r_i) \\ -\lambda \cdot f'_1(r_o) & -\lambda \cdot f'_2(r_o) \end{pmatrix} \cdot [S]^{-1} \cdot \begin{pmatrix} \vec{\underline{q}}(r_i) \cdot \vec{e}_r \\ \underline{T}(r_o) \end{pmatrix} = [H]^* \cdot \begin{pmatrix} \vec{\underline{q}}(r_i) \cdot \vec{e}_r \\ \underline{T}(r_o) \end{pmatrix} \quad (6.35)$$

This already recalls the form of the H-Matrix of the quadrupoles, although the direction of the fluxes from Figure 6.2 must be taken into account. Furthermore, for the considered application, the use of the total heat flux per unit length \dot{Q}' across the boundaries rather than the heat flux density is of interest. As the heat flux is perpendicular to the considered boundaries, this integration simplifies to a multiplication

$$\begin{pmatrix} \underline{T}(r_i) \\ \dot{Q}'(r_o) \end{pmatrix} = \begin{pmatrix} 1 & 0 \\ 0 & -2\pi r_o \end{pmatrix} \cdot \begin{pmatrix} \underline{T}(r_i) \\ \vec{\underline{q}}(r_o) \cdot \vec{e}_r \end{pmatrix} \quad (6.36)$$

$$\begin{pmatrix} \vec{\underline{q}}(r_i) \cdot \vec{e}_r \\ \underline{T}(r_o) \end{pmatrix} = \begin{pmatrix} \vec{e}_r & 0 \\ 0 & 1 \end{pmatrix} \cdot \begin{pmatrix} \dot{Q}'(r_i) \\ \underline{T}(r_o) \end{pmatrix} \quad (6.37)$$

so that, with the discussed boundary constraints, the H-Form of the thermal quadrupole under the consideration of the enounced boundary constraints and geometry can directly be given by

$$\begin{pmatrix} \underline{T}(r_i) \\ \dot{Q}'(r_o) \end{pmatrix} = \begin{pmatrix} 1 & 0 \\ 0 & -2\pi r_o \end{pmatrix} \cdot [H]^* \cdot \begin{pmatrix} \vec{e}_r \\ 2\pi r_i \end{pmatrix} \cdot \begin{pmatrix} \dot{Q}'(r_i) \\ \underline{T}(r_o) \end{pmatrix} = [H] \cdot \begin{pmatrix} \dot{Q}'(r_i) \\ \underline{T}(r_o) \end{pmatrix} \quad (6.38)$$

From the H-Form in equation (6.38), the corresponding admittance, impedance or chain matrices as well as the components of the equivalent circuits can then be derived. It shall also be noted that the quadrupole expressions can be derived from any other combination of valid boundary constraints.

For inhomogenous problems, equation (6.30) is expanded with the particular solution, leading to

$$\underline{T}(r) = \underline{\zeta}_1 \cdot f_1(r) + \underline{\zeta}_2 \cdot f_2(r) + f_p(r) \quad (6.39)$$

where the term f_p denotes the particular solution. Then, regarding the heat flux density, it is

$$\vec{\underline{q}}(r) = -\lambda \cdot [\underline{\zeta}_1 \cdot f'_1(r) + \underline{\zeta}_2 \cdot f'_2(r) + f'_p(r)] \quad (6.40)$$

Hence, equation (4.32) can be re-written to

$$\begin{pmatrix} \underline{T}(r_i) \\ \vec{\underline{q}}(r_o) \end{pmatrix} = \begin{pmatrix} f_1(r_i) & f_2(r_i) \\ -\lambda \cdot f'_1(r_o) & -\lambda \cdot f'_2(r_o) \end{pmatrix} \cdot \begin{pmatrix} \underline{\zeta}_1 \\ \underline{\zeta}_2 \end{pmatrix} + \begin{pmatrix} f_p(r_i) \\ -\lambda \cdot f'_p(r_o) \end{pmatrix} \quad (6.41)$$

As a consequence of equation (6.41), the thermal quadrupole can – in the case of existing volumetric heat generation within the geometry – complemented by a temperature source in series due to the increase of temperature on the inner boundary as well as a flux source due to the increase of heat flux across the outer boundary of the geometry. An example is shown in Figure 6.4 with

$$dT_1 = f_p(r_i) \quad (6.42)$$

$$d\underline{Q}'_1 = -2\pi \cdot \lambda \cdot f'_p(r_o) \quad (6.43)$$

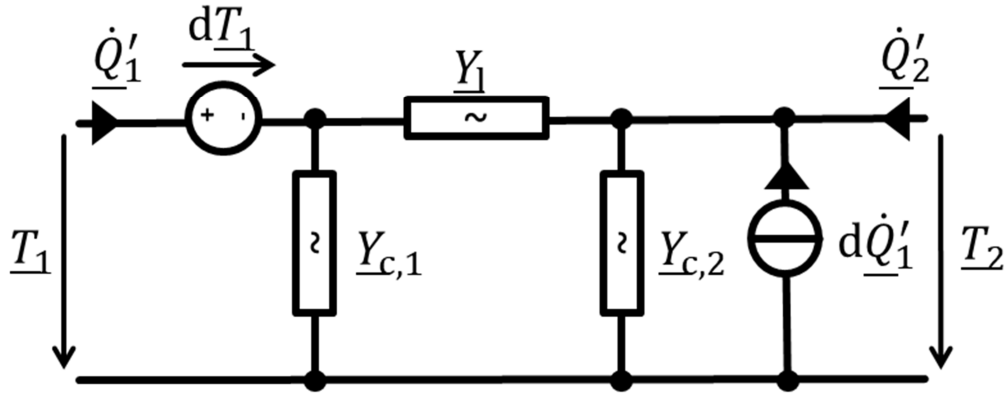


Figure 6.4: π -equivalent circuit of a thermal quadrupole with a volumetric loss generation

The general procedure that was just highlighted will now be applied on each component of a cable system in order to derive the corresponding thermal quadrupole. Afterwards, the computation of the total system will be presented.

6.4.1 Conductor

With respect to the aforementioned procedure to derive the components of the thermal quadrupole, the conductor poses a problem: As it is only bounded by one boundary – i.e. the outer radius – there can be no heat influx into it. Hence, the flux \underline{Q}'_1 must always be zero.

This condition is best achieved by starting with the impedance form from equation (6.11). By assuming the components $\underline{z}_{1,1}$ and $\underline{z}_{2,1}$ close to infinity, the heat flux \underline{Q}'_1 is forced to zero in order to obtain finite values for the temperature \underline{T}_1 (which, in this case, denotes the temperature in the center of the conductor). The components $\underline{z}_{1,2}$ and $\underline{z}_{2,2}$ are derived with the help of the homogenous solution from equation (5.56) (by taking into account the direction of the heat flux \underline{Q}'_2) as following

$$\underline{z}_{1,2} = \frac{\underline{T}_1}{\underline{Q}'_2} \Big|_{\underline{Q}'_1=0} = \frac{1}{2\pi r_{\text{con}} \cdot \lambda \cdot \beta \cdot I_1(\beta \cdot r_{\text{con}})} \quad (6.44)$$

$$\underline{z}_{2,2} = \frac{\underline{T}_2}{\underline{Q}'_2} \Big|_{\underline{Q}'_1=0} = \frac{1}{2\pi r_{\text{con}} \cdot \lambda \cdot \beta} \cdot \frac{I_0(\beta \cdot r_{\text{con}})}{I_1(\beta \cdot r_{\text{con}})} \quad (6.45)$$

where

$$\underline{T}_1 = T_h(r=0) \quad \underline{T}_2 = T_h(r=r_{\text{con}}) \quad (6.46)$$

and

$$\underline{Q}'_2 = \lambda \int_{\varphi=0}^{2\pi} \text{grad } T_h(r=r_{\text{con}}) r \, d\varphi \quad (6.47)$$

As a consequence from choice of $\underline{z}_{1,1}$ and $\underline{z}_{2,1}$, the resulting quadrupole is asymmetric. However, as the heat flux \underline{Q}'_1 is zero, there is no supplementary voltage source to be considered [KRE1967], so that the T-equivalent circuit equals the one shown in Figure 6.3, with $Z_{1,1}$ close to infinity.

In order to take into account the heat generation inside the conductor, the supplementary flux- and temperature source from Figure 6.4 must be derived. The flux source is found by calculating the total heat flux across the boundary of the particular solution, imposing a homogeneous boundary condition of Dirichlet type (as this resembles a short-circuit at port two). Hence, based on equations (5.58) and (5.64), it is:

$$\begin{aligned} d\dot{Q}'_1 &= -\lambda \int_{\varphi=0}^{2\pi} \frac{dT_p(r, S_{2,D})}{dr} \Big|_{r=r_{con}} d\varphi \\ &= -2\pi r_{con}^2 \cdot g_{con} [S_{2,D} I_1(\underline{\beta} r_{con}) - K_1(\underline{\beta} r_{con})] \cdot I_1(\underline{\beta} r_{con}) \end{aligned} \quad (6.48)$$

The value of the equivalent temperature source can also be derived from equations (5.58) and (5.64): As no heat is flowing inside the quadrupole, the temperature difference between both sides of the equivalent circuit (i.e. the center and the outer boundary of the conductor) must be due solely on the value of the temperature curve. Hence, it is

$$dT_1 = dT_p(r = 0, S_{2,D}) = \frac{g_{con}}{\lambda} \left[\frac{r_{con}}{\underline{\beta}} \cdot (S_{2,D} I_1(\underline{\beta} r_{con}) - K_1(\underline{\beta} r_{con})) + \frac{1}{\underline{\beta}^2} \right] \quad (6.49)$$

However, as it was already mentioned before, the impedance $Z_{1,1}$ can be considered close to infinity, so that the left part of the quadrupole can be considered as decoupled from the right side. Furthermore, as the temperature at the insulation is important for the actual cable rating, the temperature in the center of the conductor would – if there were a large difference from the temperature on the outer radius – of no importance. Hence, the conductor can be considered as a one port device, or - more specifically - a Norton equivalent source, shown in Figure 6.5.

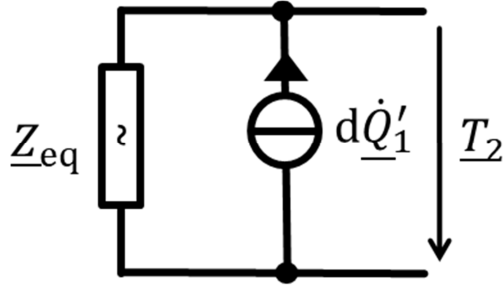


Figure 6.5: Norton equivalent source circuit for a cable conductor

And the equivalent impedance can be determined via

$$Z_{eq} = Z_{2,2} = \frac{T_p(0, S_{2,N})}{\dot{Q}'_{eq}} = -\frac{1}{c_{p,c} \cdot \rho_{con}} \cdot \frac{1}{2j\pi\omega_{th} \cdot r_{con}^2 \cdot I_1(\underline{\beta} r_{con}) \cdot [S_{2,D} I_1(\underline{\beta} r_{con}) - K_1(\underline{\beta} r_{con})]} \quad (6.50)$$

Z_{eq} : Equivalent impedance of a thermal Norton source

However, the expressions significantly simplify if the dimensions of the geometries, the regarded frequencies of the heat generation as well as the high thermal conductivity of the conductor material are taken into consideration: As it can be demonstrated by the development for the involved Bessel-functions for small arguments [COL2011], it is

$$I_1(\underline{\beta} r_{con}) \cdot [S_{2,D} I_1(\underline{\beta} r_{con}) - K_1(\underline{\beta} r_{con})] \Big|_{\underline{\beta} \cdot r_{con} \ll 1} = -\frac{1}{2} \quad (6.51)$$

Therefore, it is justified to write

$$Z_{eq} \approx \frac{1}{j\omega \cdot C'_{th,con}} \quad (6.52)$$

Where:

$C'_{th,con}$: Geometric heat capacitance per unit length of the conductor

$$C'_{th,con} = \pi \cdot r_{con}^2 \cdot c_{p,con} \cdot \rho_{con} \quad (6.53)$$

With:

r_{con} : Radius of the conductor

$c_{p,\text{con}}$: Specific heat of the conductor material

ρ_{con} : Density of the conductor material

as well as for the equivalent flux source per unit length

$$d\dot{Q}'_1 = \pi r_{\text{con}}^2 \cdot g_{\text{con}} = P'_{\text{con}}(\omega) \quad (6.54)$$

Hence, the conductor can be implemented as a current source, in parallel with a shunt admittance. The chain matrix representation of the latter is

$$[A] = \begin{pmatrix} 1 & 0 \\ 1/j\omega \cdot C_{\text{th}} & 1 \end{pmatrix} \quad (6.55)$$

Considering the expressions for stationary conditions, one may start by deriving the H-Matrix from equation (6.38). Based on the homogenous solution from chapter (5.21) and following the steps mentioned in the chapter before, it can be shown that

$$[H] = \begin{pmatrix} 0 & 1 \\ 0 & 0 \end{pmatrix} \quad (6.56)$$

As a consequence, no Y or Z matrix (and therefore no equivalent circuit diagram) can be derived by the proposed procedure. However, taking a physical perspective, one can argue that it is evident that no heat flux arises for the homogeneous problem from equation (5.40), whereas the two temperatures (in the center of the conductor and on its outer boundary) are equal. Therefore, the representation in Figure 6.6 is proposed for the stationary case with no inner heat conduction.

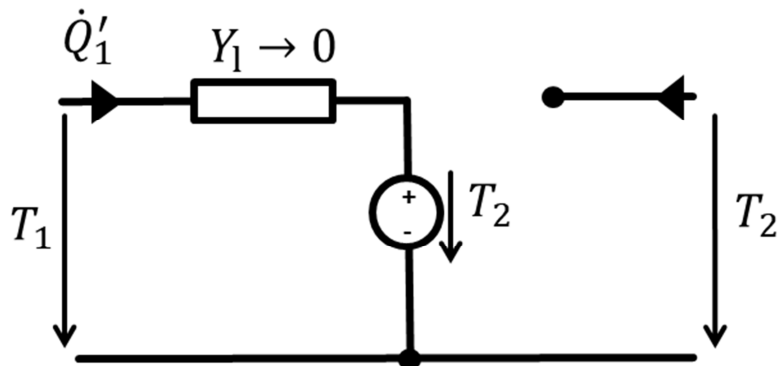


Figure 6.6: Equivalent circuit for a cable conductor in the stationary case without heat generation

The equivalent circuit in Figure 6.6 must finally be completed with the flux- and temperature source in order to implement the stationary case with a uniform heat generation. Using the presented solution with a homogenous Dirichlet-boundary condition on the outer radius, the amplitude of the flux source is derived by

$$d\dot{Q}'_1 = -\lambda \cdot \int_{\varphi=0}^{2\pi} \frac{\partial T_p(r)}{\partial r} r d\varphi \Big|_{r=r_{\text{con}}} = g_{\text{con}} \pi r_{\text{con}}^2 \quad (6.57)$$

It shall be noticed that the result from equation (6.57) equals the integral of g on the conductor surface. The value of the voltage source is equally derived from equation (5.40) to be

$$dT_1 = T_p(0) = \frac{g_{\text{con}}}{4\lambda} r_{\text{con}}^2 \quad (6.58)$$

The complete equivalent circuit diagram is shown in Figure 6.7. However, with respect to the thermal conductivities of copper or aluminium, it is appropriate to neglect the equivalent resistance. In this case, R_{eq} from equation (6.51) is zero whereas Z_{eq} from equation (6.45) is infinite, resulting in a parallel current source which represents the stationary conductor losses.

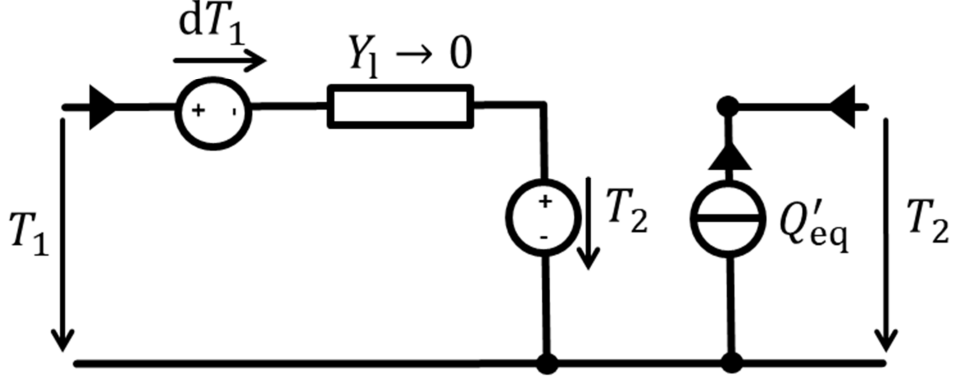


Figure 6.7: Equivalent circuit for a cable conductor in the stationary case with heat generation. The values for \dot{Q}'_{eq} and dT_1 can be determined by equation (6.48) and (6.49)

6.4.2 Insulation

Following the steps that are shown at the beginning of this chapter, the H-matrix for the insulation can be derived from the expressions from a hollow cylinder from chapter 5.2.2. This yields

$$[\underline{H}] = \begin{pmatrix} \frac{\underline{h}_{1,1}^*}{2\pi r_{i,ins}} & \underline{h}_{1,2}^* \\ -\frac{r_{o,ins}}{r_{i,ins}} \underline{h}_{2,1}^* & -2\pi r_{o,ins} \underline{h}_{2,2}^* \end{pmatrix} \quad (6.59)$$

with

$$\underline{h}_{1,1}^* = \frac{K_0(\underline{\beta} \cdot r_{i,ins}) I_0(\underline{\beta} \cdot r_{o,ins}) - K_0(\underline{\beta} \cdot r_{o,ins}) I_0(\underline{\beta} \cdot r_{i,ins})}{\lambda \underline{\beta} \cdot [K_0(\underline{\beta} \cdot r_{o,ins}) I_1(\underline{\beta} \cdot r_{i,ins}) + K_1(\underline{\beta} \cdot r_{i,ins}) I_0(\underline{\beta} \cdot r_{o,ins})]} \quad (6.60)$$

$$\underline{h}_{1,2}^* = \frac{I_0(\underline{\beta} \cdot r_{i,ins}) K_1(\underline{\beta} \cdot r_{i,ins}) + I_1(\underline{\beta} \cdot r_{i,ins}) K_0(\underline{\beta} \cdot r_{i,ins})}{I_0(\underline{\beta} \cdot r_{o,ins}) K_1(\underline{\beta} \cdot r_{i,ins}) + I_1(\underline{\beta} \cdot r_{i,ins}) K_0(\underline{\beta} \cdot r_{o,ins})} \quad (6.61)$$

$$\underline{h}_{2,1}^* = \frac{I_1(\underline{\beta} \cdot r_{o,ins}) K_0(\underline{\beta} \cdot r_{o,ins}) + I_0(\underline{\beta} \cdot r_{o,ins}) K_1(\underline{\beta} \cdot r_{o,ins})}{I_1(\underline{\beta} \cdot r_{i,ins}) K_0(\underline{\beta} \cdot r_{o,ins}) + I_0(\underline{\beta} \cdot r_{o,ins}) K_1(\underline{\beta} \cdot r_{i,ins})} \quad (6.62)$$

$$\underline{h}_{2,2}^* = \frac{\underline{\beta} \cdot \lambda [K_1(\underline{\beta} \cdot r_{o,ins}) I_1(\underline{\beta} \cdot r_{i,ins}) + K_1(\underline{\beta} \cdot r_{i,ins}) I_1(\underline{\beta} \cdot r_{o,ins})]}{K_0(\underline{\beta} \cdot r_{o,ins}) I_1(\underline{\beta} \cdot r_{i,ins}) + K_1(\underline{\beta} \cdot r_{i,ins}) I_0(\underline{\beta} \cdot r_{o,ins})} \quad (6.63)$$

With the help of the expressions in the equation (6.59) to (6.63), the coefficients of the chain matrix can be derived as

$$\underline{a}_{11} = -\frac{1}{\underline{h}_{2,1}} (\underline{h}_{1,2} \cdot \underline{h}_{2,1} - \underline{h}_{1,1} \cdot \underline{h}_{2,2}) \quad (6.64)$$

$$\underline{a}_{1,2} = -\frac{\underline{h}_{1,1}}{\underline{h}_{2,1}} \quad (6.65)$$

$$\underline{a}_{2,1} = -\frac{\underline{h}_{2,2}}{\underline{h}_{2,1}} \quad (6.66)$$

$$\underline{a}_{2,2} = -\frac{1}{\underline{h}_{2,1}} \quad (6.67)$$

and the parameters of the admittance matrix are

$$\underline{y}_{11} = \frac{1}{\underline{h}_{1,1}} \quad (6.68)$$

$$\underline{y}_{1,2} = -\frac{\underline{h}_{1,2}}{\underline{h}_{1,1}} \quad (6.69)$$

$$\underline{y}_{2,1} = \frac{\underline{h}_{2,1}}{\underline{h}_{1,1}} \quad (6.70)$$

$$\underline{y}_{2,2} = \frac{\det[\underline{H}]}{\underline{h}_{1,1}} \quad (6.71)$$

Hence, the components of the π -equivalent circuit can be calculated as

$$\underline{Y}_{c,1,\text{iso}} = \frac{1}{\underline{h}_{1,1}} (1 - \underline{h}_{1,2}) \quad (6.72)$$

$$\underline{Y}_{c,2,\text{iso}} = \frac{1}{\underline{h}_{1,1}} (\det[\underline{H}] - \underline{h}_{1,2}) \quad (6.73)$$

$$\underline{Y}_{l,\text{iso}} = \frac{\underline{h}_{1,2}}{\underline{h}_{1,1}} \quad (6.74)$$

In order to prevent numerical inconveniences, it is recommended to evaluate the quadrupole parameters for $\omega_{\text{th}} = 0$ by the help of the stationary expressions. In this case, the expressions simplify to a series resistance, whose chain matrix can directly be given by

$$A = \begin{pmatrix} 1 & \frac{1}{2\pi\lambda} \ln\left(\frac{r_{o,\text{ins}}}{r_{i,\text{ins}}}\right) \\ 0 & 1 \end{pmatrix} \quad (6.75)$$

The resulting admittance matrix is

$$Y = 2\pi\lambda \left[\ln\left(\frac{r_{o,\text{ins}}}{r_{i,\text{ins}}}\right) \right]^{-1} \cdot \begin{pmatrix} 1 & -1 \\ -1 & 1 \end{pmatrix} \quad (6.76)$$

with the corresponding values of the π -equivalent circuit

$$Y_{c,1,\text{ins}}(\omega_{\text{th}} = 0) = y_{11} + y_{12} = 0 \quad (6.77)$$

$$Y_{c,2,\text{ins}}(\omega_{\text{th}} = 0) = y_{22} + y_{12} = 0 \quad (6.78)$$

$$Y_{l,\text{ins}}(\omega_{\text{th}} = 0) = -y_{12} = 2\pi\lambda \left[\ln\left(\frac{r_{o,\text{ins}}}{r_{i,\text{ins}}}\right) \right]^{-1} \quad (6.79)$$

If the dielectric losses are to be considered, the resulting temperature rise at the inner boundary as well as the supplementary heat flux across the outer boundary can directly be implemented as constant voltage or current sources, as they are independent of the load flow of the cable. The resulting expression can directly be determined from equation (5.48) so that, for the value of the series voltage source (referring to Figure 6.4), it can be found

$$dT_{1,\text{ins}} = T_p(r) \Big|_{r=r_{i,\text{ins}}} = \frac{\pi \cdot g_{\text{di}}}{\lambda} \cdot \ln^2 \left(\frac{r_{o,\text{ins}}}{r_{i,\text{ins}}} \right) \quad (6.80)$$

The supplementary heat flux per unit length in Figure 6.4 is formally derived from the expression in equation (5.48) to be

$$dQ'_{2,\text{ins}} = -\lambda \frac{\partial T_p(r)}{\partial r} \Big|_{r=r_{o,\text{ins}}} = 2\pi \cdot g_{\text{di}} \ln \left(\frac{r_{o,\text{ins}}}{r_{i,\text{ins}}} \right) \quad (6.81)$$

which, of course, equals the total volumetric losses

$$\int_{r=r_{i,ins}}^{r_{o,ins}} \int_{\varphi=0}^{2\pi} \frac{g_{di}}{r^2} \cdot r \, dr \, d\varphi = 2\pi \cdot g_{di} \ln \left(\frac{r_{o,ins}}{r_{i,ins}} \right) \quad (6.82)$$

Nonetheless, for medium voltage cable systems, dielectric losses can generally be neglected.

6.4.3 Screen or armour

The parameters of the quadrupole or the thermal equivalent circuit for a screen (assumed as a hollow cylinder) or the armour are the same as for the insulation in equation (6.72) to (6.74). However, with regard to the current dependent losses, the expressions for the equivalent voltage and current sources in (6.80) as well as (6.81) must be derived on the basis of equation (5.45), as they are no longer constant in time but oscillating with ω_{th} . Therefore, the supplementary voltage source is

$$d\underline{T}_{1,sc} = \frac{g_{scr}}{\lambda \cdot \beta \cdot (1 - S_1 S_2)} \left[r_{i,sc} \cdot [S_2 I_0(\underline{\beta} r_{i,sc}) + K_0(\underline{\beta} r_{i,sc})] [S_1 K_1(\underline{\beta} r_{i,sc}) - I_1(\underline{\beta} r_{i,sc})] \right. \\ \left. + r_{o,sc} \cdot [I_0(\underline{\beta} r_{i,sc}) + S_1 K_0(\underline{\beta} r_{i,sc})] [S_2 I_1(\underline{\beta} r_{o,sc}) - K_1(\underline{\beta} r_{o,sc})] + \frac{1}{\underline{\beta}^2} [1 - S_1 S_2] \right] \quad (6.83)$$

and the supplementary current source becomes

$$d\underline{Q}'_{2,sc} = -\lambda \frac{\partial T_p(r)}{\partial r} \Big|_{r=r_{o,iso}} = \frac{g_{scr}}{\lambda \cdot \underline{\beta} \cdot (1 - S_1 S_2)} \left[r_{i,sc} \cdot \underline{\beta} [S_2 I_1(\underline{\beta} r_{o,sc}) - K_1(\underline{\beta} r_{o,sc})] [S_1 K_1(\underline{\beta} r_{i,sc}) - I_1(\underline{\beta} r_{i,sc})] \right. \\ \left. + r_{o,sc} \cdot \underline{\beta} [I_1(\underline{\beta} r_{o,sc}) - S_1 K_1(\underline{\beta} r_{o,sc})] [S_2 I_1(\underline{\beta} r_{o,sc}) - K_1(\underline{\beta} r_{o,sc})] + \frac{1}{\underline{\beta}^2} [1 - S_1 S_2] \right] \quad (6.84)$$

However, with respect to the thickness of the components and the thermal conductivity of copper, aluminium or steel, it is more than appropriate to neglect the implied thermal impedances and capacitances and to reduce the screen to a simple parallel current source as shown in Figure 6.8

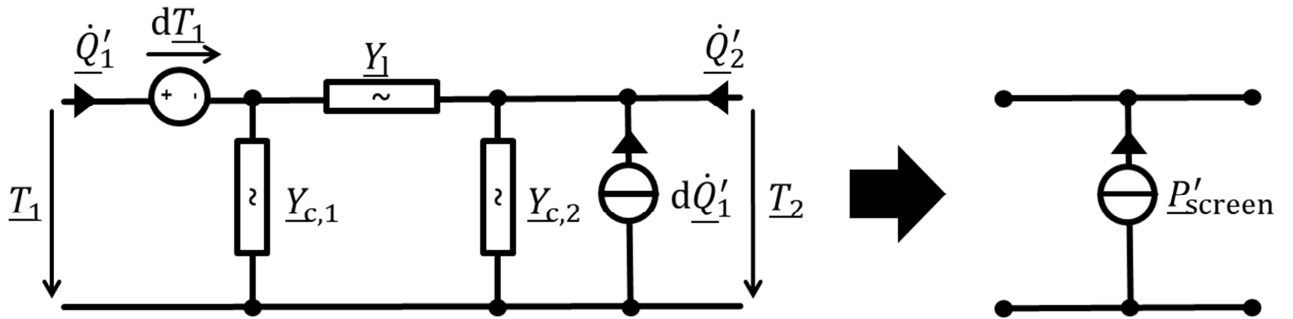


Figure 6.8: Simplification of the thermal quadrupole of the screen of a hollow cylinder with volumetric heat generation to a parallel current source

6.4.4 Outer jacket

As no heat is generated inside the outer jacket, the quadrupole parameters for directly buried cables consist of the homogenous parameters from chapter 6.4.2. However, as cables may also hang in air, a convective or Robin boundary condition on the outer radius shall be considered. In this case, the parameters for the H-Matrix from equations (6.60) to (6.63) change to

$$h_{1,1}^* = \frac{1}{\det S} \left\{ I_0(\underline{\beta} \cdot r_{i,jac}) [K_0(\underline{\beta} \cdot r_{o,jac}) - \frac{\lambda}{h_{rob}} \cdot k \cdot K_1(\underline{\beta} \cdot r_{o,jac})] \right. \\ \left. - K_0(\underline{\beta} \cdot r_{i,jac}) [I_0(\underline{\beta} \cdot r_{o,jac}) + \frac{\lambda}{h_{rob}} \cdot k \cdot I_1(\underline{\beta} \cdot r_{o,jac})] \right\} \quad (6.85)$$

$$\underline{h}_{1,2}^* = \frac{-\lambda\beta}{\det S} \left\{ K_1(\underline{\beta} \cdot \underline{r}_{i,jac}) I_0(\underline{\beta} \cdot \underline{r}_{i,jac}) + I_1(\underline{\beta} \cdot \underline{r}_{i,jac}) K_0(\underline{\beta} \cdot \underline{r}_{i,jac}) \right\} \quad (6.86)$$

$$\begin{aligned} \underline{h}_{2,1}^* &= \frac{-\lambda\beta}{\det S} \left\{ I_1(\underline{\beta} \cdot \underline{r}_{o,jac}) \left[K_0(\underline{\beta} \cdot \underline{r}_{o,jac}) - \frac{\lambda}{h_{rob}} \cdot \underline{k} \cdot K_1(\underline{\beta} \cdot \underline{r}_{o,jac}) \right] \right. \\ &\quad \left. + K_1(\underline{\beta} \cdot \underline{r}_{o,jac}) \left[I_0(\underline{\beta} \cdot \underline{r}_{o,jac}) + \frac{\lambda}{h_{rob}} \cdot \underline{k} \cdot I_1(\underline{\beta} \cdot \underline{r}_{o,jac}) \right] \right\} \end{aligned} \quad (6.87)$$

$$\underline{h}_{2,2}^* = \frac{(\lambda\beta)^2}{\det S} \left\{ K_1(\underline{\beta} \cdot \underline{r}_{i,jac}) I_1(\underline{\beta} \cdot \underline{r}_{o,jac}) - K_1(\underline{\beta} \cdot \underline{r}_{o,jac}) I_1(\underline{\beta} \cdot \underline{r}_{i,jac}) \right\} \quad (6.88)$$

from which all relevant matrix forms and components of the equivalent circuits can be derived. The chain matrix for the stationary case from equation (6.65) then changes to

$$[A] = \begin{pmatrix} 1 & \frac{1}{2\pi\lambda} \cdot \ln\left(\frac{r_{o,jac}}{r_{i,jac}}\right) + \frac{1}{2\pi h_{rob} \cdot r_{o,jac}} \\ 0 & 1 \end{pmatrix} \quad (6.89)$$

from which the admittance matrix can be derived to be

$$[Y] = 2\pi\lambda \cdot \left[\ln\left(\frac{r_{o,jac}}{r_{i,jac}}\right) + \frac{\lambda}{h_{rob} \cdot r_{o,jac}} \right]^{-1} \begin{pmatrix} 1 & -1 \\ -1 & 1 \end{pmatrix} \quad (6.90)$$

In analogy to equations (6.67) to (6.69), the components of the π -equivalent circuit change to

$$Y_{c,1,jac} = Y_{c,2,jac} = 0 \quad (6.91)$$

$$Y_{l,jac} = 2\pi\lambda \cdot \left[\ln\left(\frac{r_{o,jac}}{r_{i,jac}}\right) + \frac{\lambda}{h_{rob} \cdot r_{o,jac}} \right]^{-1} \quad (6.92)$$

6.4.5 Soil

As the heat flux across the ground surface into the air is of no importance to the calculation of the ampacity rating, the soil can be implemented as a simple series impedance instead of a quadrupole. The impedance must only reproduce the relation between the heat flux from the outer cable jacket into the bedding and its temperature rise. Therefore, the chain matrix of the soil can directly be given by

$$[\underline{A}] = \begin{pmatrix} 1 & \underline{Z}_{th,soil} \\ 0 & 1 \end{pmatrix} \quad (6.93)$$

from which the admittance matrix can be derived to be

$$[\underline{Y}] = \frac{1}{\underline{Z}_{th,soil}} \begin{pmatrix} 1 & -1 \\ -1 & 1 \end{pmatrix} \quad (6.94)$$

and, furthermore, the components of the π -equivalent circuit

$$\underline{Y}_{c,1,soil} = \underline{Y}_{c,2,soil} = 0 \quad (6.95)$$

$$\underline{Y}_{l,soil} = \frac{1}{\underline{Z}_{th}} \quad (6.96)$$

where \underline{Z}_{th} depicts the ratio between the heat flux inside the bedding and the resulting temperature rise.

Considering a homogenous bedding, the relevant expressions as a function of the frequency are given in chapter 5.3.2. As the difference between a Dirichlet and a Robin boundary condition on the ground surface is of minor extent, it is recommended to use the simpler equation for a Dirichlet boundary condition. Hence, for one single cable

$$Z_{th,soil} = \frac{1}{2\pi\lambda} \cdot \left(K_0(\underline{\beta} r_{o,jac}) - K_0(\underline{\beta}[r_{o,jac} + 2 \cdot y_0]) \right) \quad (6.97)$$

With respect to a system of single core cables in trefoil formation, the outer radius of the jacket in equation (6.87) can be replaced by an equivalent radius with

$$r_{o,\Delta} = 1.75 \cdot r_{o,jac} \quad (6.98)$$

if the resulting impedance from equation (6.87) is afterwards multiplied by a factor 3. For the stationary case, the expression in (5.98) can be used, as it was shown that the type of the boundary condition on the cable jacket is equally of minor importance. Therefore

$$Z_{th}(\omega = 0) = \frac{1}{2\pi\lambda_{soil}} \cdot \ln\left(\frac{2 \cdot y_0}{r_{o,jac}}\right) \quad (6.99)$$

With respect to a system in trefoil formation, equation (6.89) from IEC 60287 can be used, which is based on the computations on [GOL1969]

$$Z_{th}(\omega = 0) = \frac{1}{2\pi\lambda_{soil}} \cdot \left[\ln\left(\frac{2 \cdot y_0}{r_{o,jac}}\right) + 2 \cdot \ln\left(\frac{y_0}{r_{o,jac}}\right) \right] \quad (6.100)$$

In this case, Z_{th} has not to be multiplied by 3. Cable systems in lateral formation can be implemented according to the procedure from chapter 6.6, with respect to non-homogenous beddings, the thermal impedances can be determined numerically.

6.4.6 Reference temperature

Finally, the network of thermal quadrupoles must be terminated by a reference temperature. This reference temperature is equal to the temperature at laying depth without the influence of the cable, so that its amplitude is given by equation (5.155) for homogenous beddings

$$T_{ref} = T_o \cdot e^{(1+j)\sqrt{\frac{\omega T_{soil}}{2\alpha_{soil}}} \cdot y_0} \quad (6.101)$$

where T_o depicts the spectrum of the temperature on the ground surface. However, with respect to the uncertainties of the thermal properties inside the bedding, the choice of a constant temperature of $T_0 = 20^\circ\text{C}$ is reasonable.

6.5 Complete equivalent circuit for one cable

Following the explanations for the separate parts of the cable system, the equivalent circuit diagram for the complete system is given by connecting the quadrupoles and relevant sources of heat fluxes in series. For a single medium voltage cable, the complete circuit is given in Figure 6.9.

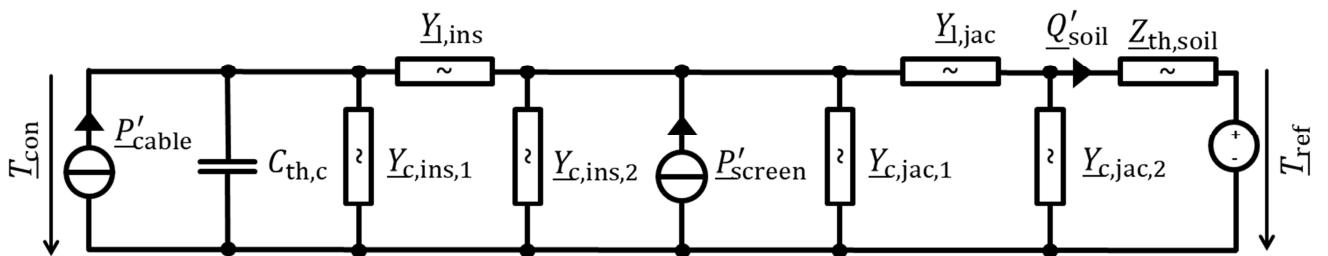


Figure 6.9: Representation of the thermal equivalent circuit of thermal quadrupoles for one single core cable or three single core cables in trefoil formation

In order to calculate the total temperature rise of the cable, the effect of the different sources (i.e., for the example shown in Figure 6.9, the conductor as well as the screen losses) can be regarded separately and superimposed afterwards. By multiplying the chain matrices of the quadrupoles and

summarizing the resulting quadrupoles into one equivalent thermal impedance, the temperature rise of the conductor for one specific angular frequency can then be calculated by

$$\underline{T} - \underline{T}_{\text{ref}} = d\underline{T}_{\text{con}} = \underline{Z}_{\text{eq,a}} \cdot \underline{P}'_{\text{con}} + \underline{Z}_{\text{eq,b}} \cdot \underline{P}'_{\text{screen}} \quad (6.102)$$

Where:

$\underline{Z}_{\text{eq,a}}$: Equivalent thermal impedance with respect to the conductor losses current source

$\underline{Z}_{\text{eq,b}}$: Equivalent thermal impedance with respect to the screen losses current source

By repeating the calculation of equation (6.102) with different angular frequencies, the spectrum of the conductor temperature can be derived, which finally must be transformed into the time domain to get the final result, i.e. the conductor temperature as a function of time.

6.6 Total equivalent circuit for a group of cables

Considering one three phase cable system in lateral formation or multiple cable systems inside the same trench, equation (6.102) must be expanded to a matrix formulation in order to account for the thermal coupling between the different cables. Hence, it is

$$\begin{pmatrix} d\underline{T}_{\text{con},1} \\ d\underline{T}_{\text{con},2} \\ \vdots \\ d\underline{T}_{\text{con},n} \end{pmatrix} = \begin{pmatrix} \underline{Z}_{1,1}^{\text{eq,a}} & \underline{Z}_{1,2}^{\text{eq,a}} & \dots & \underline{Z}_{1,n}^{\text{eq,a}} \\ \underline{Z}_{2,1}^{\text{eq,a}} & & & \\ \vdots & & \ddots & \\ \underline{Z}_{n,1}^{\text{eq,a}} & & & \underline{Z}_{n,n}^{\text{eq,a}} \end{pmatrix} \cdot \begin{pmatrix} \underline{P}'_{\text{con},1} \\ \underline{P}'_{\text{con},2} \\ \vdots \\ \underline{P}'_{\text{con},n} \end{pmatrix} + \begin{pmatrix} \underline{Z}_{1,1}^{\text{eq,b}} & \underline{Z}_{1,2}^{\text{eq,b}} & \dots & \underline{Z}_{1,n}^{\text{eq,b}} \\ \underline{Z}_{2,1}^{\text{eq,b}} & & & \\ \vdots & & \ddots & \\ \underline{Z}_{n,1}^{\text{eq,b}} & & & \underline{Z}_{n,n}^{\text{eq,b}} \end{pmatrix} \cdot \begin{pmatrix} \underline{P}'_{\text{screen},1} \\ \underline{P}'_{\text{screen},2} \\ \vdots \\ \underline{P}'_{\text{screen},n} \end{pmatrix} \quad (6.103)$$

The coupling impedances are derived with the help of the external coupling impedances of the bedding as well as the ratio of the heat flux that leaves the outer surface of the cable and penetrates the bedding. The external coupling impedance can be calculated by equation (5.130) as

$$\underline{Z}_{m,n}^{\text{th,soil}} = \frac{1}{2\pi\lambda} \cdot \left(K_0(\beta d_{m,n}) - K_0\left(\beta\sqrt{d_{m,n}^2 + (2 \cdot y_0)^2}\right) \right) \quad (6.104)$$

Where

$\underline{Z}_{m,n}^{\text{th,soil}}$: External coupling impedances of the bedding between cables m and n

$d_{m,n}$: Distance between cable m and n

The ratio between the heat flux that leaves the cable and the total heat generation inside the cable must then be determined via the network analysis of the ladder network from Figure 6.9. With

$$\dot{Q}'_e = \dot{Q}'_{e,P'_{\text{con}}} + \dot{Q}'_{e,P'_{\text{scr}}} \quad (6.105)$$

Where:

\dot{Q}'_e : Heat flux per unit length through the outer jacket of the cable into the bedding in $\text{W} \cdot \text{m}^{-1}$

$\dot{Q}'_{e,P'_{\text{con}}}$: Heat flux per unit length through the outer jacket of the cable into the bedding due to conductor losses in $\text{W} \cdot \text{m}^{-1}$

$\dot{Q}'_{e,P'_{\text{scr}}}$: Heat flux per unit length through the outer jacket of the cable into the bedding due to screen losses in $\text{W} \cdot \text{m}^{-1}$

the thermal coupling between two cables can therefore be written as

$$Z_{m,n}^{\text{eq,a}} = \frac{Q'_e P'_{\text{con},n}}{P'_{\text{con},n}} \cdot Z_{m,n}^{\text{th,soil}} \quad (6.106)$$

$$Z_{m,n}^{\text{eq,b}} = \frac{Q'_e P'_{\text{screen},n}}{P'_{\text{screen},n}} \cdot Z_{m,n}^{\text{th,soil}} \quad (6.107)$$

Furthermore, it must not be forgotten that the conductor and screen losses are temperature dependent – with a difference of about 30 % between the calculation at 20 °C and 90 °C. Without eliminating this non-linearity analytically, there are two possibilities to take this dependency into account: Either the losses are calculated directly at the maximum temperature or the calculation of the conductor temperature is performed iteratively, using the outcome of the proceeding calculation as the basis for the calculation of losses for the next iteration.

6.7 Comparison of quadrupoles and the Van Wormer representation

By comparing the thermal networks from Figure 6.9 to the one in Figure 3.4, it becomes obvious that the use of thermal quadrupoles is already implicitly applied by using thermal resistances and capacitances. As the latter are often calculated on the basis of a Van Wormer approximation [WOR1955], this chapter closes with a comparison of this approach and the results gained by the application of thermal quadrupoles. But before doing so, the thoughts behind the Van Wormer approximation are illustrated. Taking a cable insulation as an example, the main idea is to separate the geometric capacitance, i.e.

$$C_{\text{th,iso}} = \pi \cdot c_{\text{p,ins}} \cdot \rho_{\text{iso}} \cdot (r_{\text{o,ins}}^2 - r_{\text{i,ins}}^2) \quad (6.108)$$

such that the stored energy at temperature levels on the inside and the outside radius equals the energy at a logarithmic temperature distribution within the insulation. This leads to

$$Y_{c,1,\text{iso}} \approx C_{1,\text{ins,Wor}} = p_{\text{Wor}} \cdot C_{\text{th,ins}} \quad (6.109)$$

$$Y_{c,2,\text{iso}} \approx C_{2,\text{ins,Wor}} = (1 - p_{\text{Wor}}) \cdot C_{\text{th,ins}} \quad (6.110)$$

where the longitudinal component is the stationary resistance from equation (6.79). By equalling the stored energy, the weighting factor p is derived to be

$$p_{\text{Wor}} = \frac{1}{2} \left[\ln \left(\frac{r_{\text{o,ins}}}{r_{\text{i,ins}}} \right) \right]^{-1} - \left[\left(\frac{r_{\text{o,ins}}}{r_{\text{i,ins}}} \right)^2 - 1 \right]^{-1} \quad (6.111)$$

For short term transients, i. e. transients between 10 min and 1 h, the geometric heat capacitance is further derived at radius

$$r_{\text{mid,ins}} = \sqrt{r_{\text{o,ins}} \cdot r_{\text{i,ins}}} \quad (6.112)$$

so that the thermal resistance is simply halved. Then, equations (6.109) and (6.110) are applied to the two resulting geometric capacitances with

$$C_{\text{th,ins}}^{\text{a}} = \pi \cdot c_{\text{p,ins}} \cdot \rho_{\text{ins}} \cdot (r_{\text{mid,ins}}^2 - r_{\text{i,ins}}^2) \quad (6.113)$$

$$C_{\text{th,ins}}^{\text{b}} = \pi \cdot c_{\text{p,ins}} \cdot \rho_{\text{ins}} \cdot (r_{\text{o,ins}}^2 - r_{\text{mid,iso}}^2) \quad (6.114)$$

As an example, Figure 6.10 shows the Nyquist-plots of the input impedances of an XLPE cable insulation, based on a quadrupole approach as well as a first and a second order Van Wormer approximation. Starting from the stationary value for low frequencies, the curves diverge significantly with rising frequency. It must be pointed out that, by further dividing the insulation into several sub-parts, the result of the Van Wormer approximation can be approached to the actual behaviour, as it is also the case for a discretization of the whole system (which is done in [OLS2012]). However, the exact result from a concise representation can only be obtained via the thermal quadrupole approach.

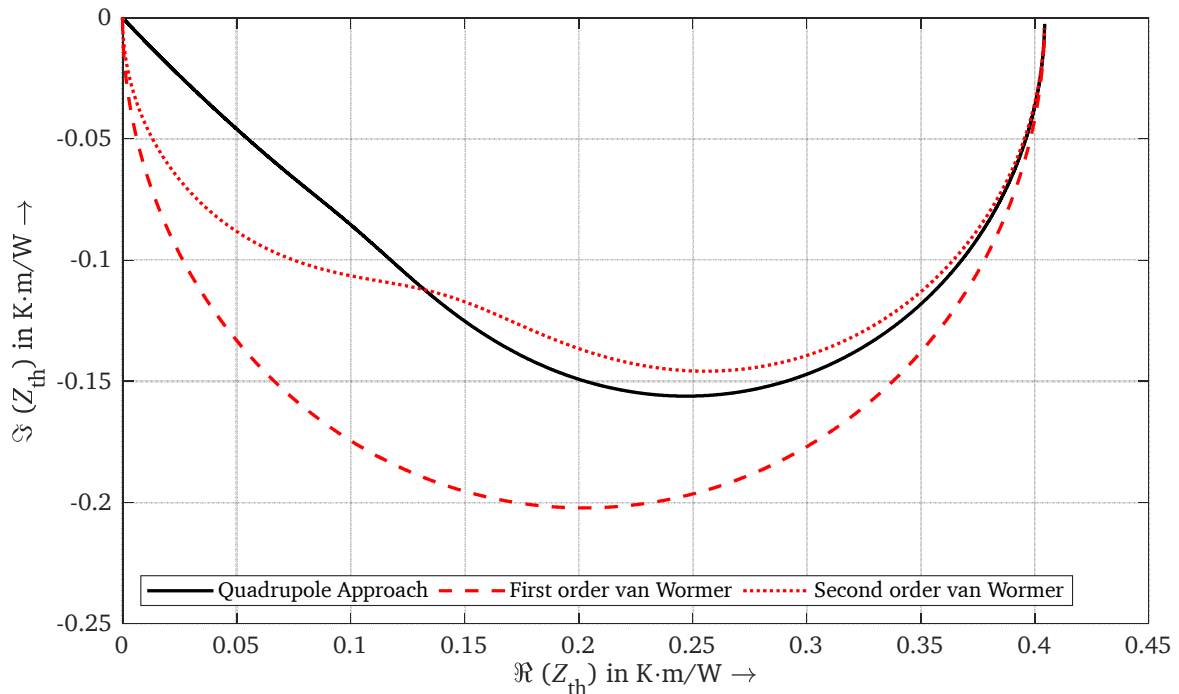


Figure 6.10: Comparison of the Nyquist-plots of the input impedance of a cable insulation (type NA2XS(F)2Y), computed with a quadrupole approach (black, full line) as well as a first order Van Wormer (red, dashed line) and second order Van Wormer (red, dotted line) approximation.

7 Possibilities of a refined thermal model of the bedding

So far, the thermal characteristics of the bedding have been assumed to be homogenous, that means constant throughout the geometry. This assumption, however, is only a rough approximation, as “soil” is nowhere near a homogenous solid, but a highly complex structure, including a solid pore structure of high tortuosity¹⁶, filled to different degrees with water and water vapour [SCH2010]. As a consequence, parameters such as the pore space volume, the level of compaction as well as the water content, which all vary throughout the bedding or alongside a cable route, exert a high influence on the resulting thermal conductivity of soil [CAM1994].

Moreover, the heat that is injected by cable systems into the bedding during operation initiates movements of water and water vapour, which leads to a redistribution of humidity away from the cable to colder regions. Studies on this phenomenon are legion (e.g. [TAY1954], [BAC1992]), and the strong influence on the current carrying capacity that is entailed by this change in thermal properties spurred electrical engineers to use the findings from experimental studies with regard to cable ampacity ratings [DON1979], [KOO1989]. The following chapter will closer examine the ramifications of these water movements on the ampacity rating of power cables.

7.1 Introduction

As the constitutive equations have already been presented in section 4.1.3, the following explanations will focus more on the understanding of the underlying processes that actually lead to the redistribution of humidity away from the cable as well as the involved magnitudes – those of the input variables as well as the time constant. This is essential for the understanding and the assessment of the results that will be presented later.

However, before going into details, the term “soil” that has been used so far needs to be further specified. For the following evaluation, a pedological perspective is taken, classifying a soil according to its grain size distribution as it is proposed by [E-DIN4220]. Here, three soil particles sizes are distinguished: clay (all particles smaller than 2 µm), silt (grain size between 2 and 63 µm) and sand (between 63 µm and 2 mm). With the help of the grain size distribution, a soil can therefore be assigned to one of the four main-soil texture classes (sand, loam, silt and clay) and the corresponding soil sub-texture classes through the illustration in Figure 7.1, where a soil is classified by the fractions of clay (on the abscissa) and silt particles (on the ordinate).

With respect to the numerical implementation of the combined heat and mass transfer inside natural beddings, it is vital to recall the soil characteristics that find their way into the equations from chapter 4.1.3. These characteristics are:

- the water retention characteristic, i.e. the function that connects the pressure head to the corresponding volumetric water content of the soil.
- the hydraulic conductivity characteristic, i.e. the proportionality factor between the gradient of the hydraulic head and the Darcy velocity.
- the thermal conductivity characteristics, i.e. the proportionality factor between the gradient of the temperature and the heat flux.

As it was already mentioned in chapter 4.1.3, all three characteristics are, amongst others, highly dependent on the water content, making an analytical solution of the resulting equations impossible without strong simplifications.

¹⁶ A good definition of this property is “ratio of the diffusivity in the free space to the diffusivity in the porous medium” [LAT1995]

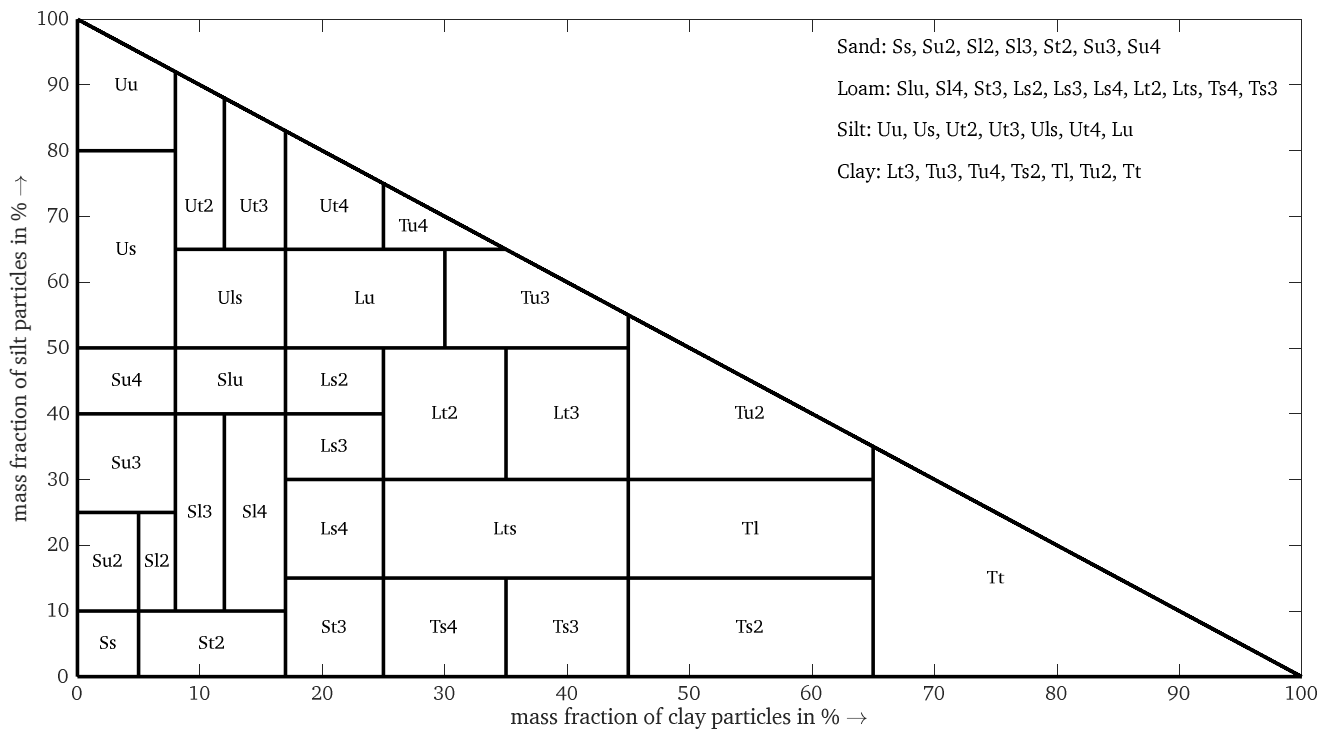


Figure 7.1: Classification of a soil as a function of its mass grain size distribution of clay particles (abscissa) and silt (ordinate) according to [E-DIN4220]

With the help of an evaporation test device [DRE2017] that was developed at the Geothermal Science and Technology of TU Darmstadt, all three characteristics can be recorded simultaneously over a wide range of volumetric water contents. However, with respect to a numerical simulation, a continuous function rather than separated measured values are of interest. As a consequence, the numerical simulation relies on shape functions whose parameters can be fitted to the experimental results. These shape functions will shortly be recalled.

7.1.1 Water retention characteristic

With respect to water content, it is common to express the water content in terms of the effective saturation, which is defined as

$$S_{\text{eff}} = \frac{\theta_l - \theta_r}{\theta_s - \theta_r} \quad (7.1)$$

Where:

- S_{eff} : Effective saturation
- θ_l : Volumetric water content
- θ_s : Saturation water content
- θ_r : Residual water content

One popular description of a continuous function of the saturation is the limited, unimodal Van Genuchten model with [GEN1980]

$$S_{\text{eff}}(h_{\text{hy}}) = \frac{1}{(1 + [\alpha_{\text{Gen}} \cdot |h_{\text{hy}}|]^{n_{\text{Gen}}})^{1-1/n_{\text{Gen}}} \quad (7.2)}$$

With:

- $\alpha_{\text{Gen}}, n_{\text{Gen}}$: Fitting parameter

7.1.2 Hydraulic conductivity

With respect to the hydraulic conductivity, the model according to Mualem finds widespread application [MUA1976]. As a function of the saturation from equation (7.1), this can be written as

$$k = k_{\text{sat}} \cdot S_{\text{eff}}^{\tau} \cdot \left[1 - \left(1 - S_{\text{eff}}^{1/m} \right)^m \right]^2 \quad (7.3)$$

where

$$m = 1 - \frac{1}{n_{\text{Gen}}} \quad (7.4)$$

and

k_{sat} : Saturated hydraulic conductivity

τ : Parameter of tortuosity

Hence, six parameters are necessary in order to describe the water retention curve as well as the hydraulic conductivity. [E-DIN4220] provides estimations for the corresponding soils, which are listed in Appendix A2 and will be used in the course of the following calculations.

7.1.3 Thermal conductivity

Considering thermal conductivity of the soil as a function of the water content, the model of [LU2014] with the adoption to different soil texture groups by [MAR2017] was included in the calculations. In this case, the function is described by

$$\lambda(\theta_l) = e^{\beta-\theta^{-\delta}} + \lambda_{\text{dry}} \quad (7.5)$$

with

$$\beta = p_5 \cdot \chi_{\text{Sand}} + p_6 \cdot \rho_b + p_7 \cdot \rho_b \cdot \chi_{\text{Sand}} + p_8 \quad (7.6)$$

$$\delta = p_3 \cdot \chi_{\text{clay}} + p_4 \quad (7.7)$$

$$\lambda_{\text{dry}} = p_1 + p_2 \cdot \varepsilon_{\text{soil}} \quad (7.8)$$

Where:

$p_1 \dots p_8$: Fitting parameters

$\chi_{\text{clay}}, \chi_{\text{Sand}}$: Fraction of mass of the corresponding particle sizes

$\varepsilon_{\text{soil}}$: Porosity, it is

$$\varepsilon_{\text{soil}} = \left(1 - \frac{\rho_b}{\rho_p} \right) \quad (7.9)$$

and

ρ_s : Particle density, in $\text{g} \cdot \text{cm}^{-3}$, describing the density of the solid phase of the soil. Measurements showed that the value of $\rho_s = 2,65 \text{ g} \cdot \text{cm}^{-3}$ as proposed by [E-DIN4220] is a good assumption for all natural soils.

ρ_b : Bulk density, in $\text{g} \cdot \text{cm}^{-3}$, describing the density of the oven-dried soil. [E-DIN4220] provides approximations for the different soil types as a function of the on-site density (LD). With respect to natural beddings, LD = 3, is a valid assumption that will be used in the following. The corresponding values are given in Appendix A3.

As a consequence of the three equations (7.2), (7.3) and (7.5), the three important functions for exemplary soil can be derived solely from the information found in [E-DIN4220]. These curves are shown in Figure 7.2 (water retention curve), Figure 7.3 (hydraulic conductivity) and Figure 7.4 (thermal conductivity) for all soil types specified by [E-DIN4220].

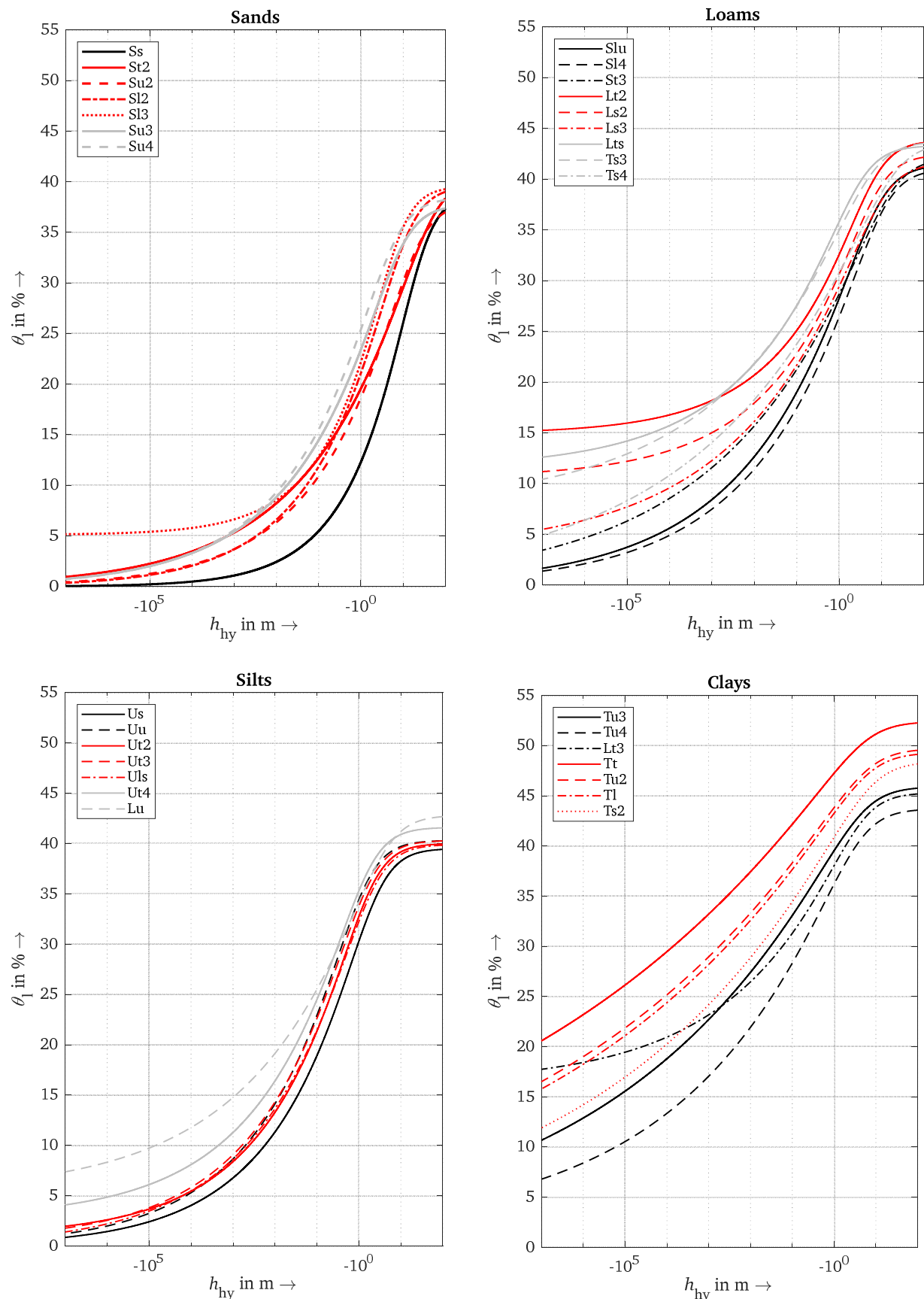


Figure 7.2: Volumetric water content (θ_1) as a function of the pressure head (h_{hy}), based on equation (7.2) and the parameters specified in [E-DIN4220], for all relevant soil types

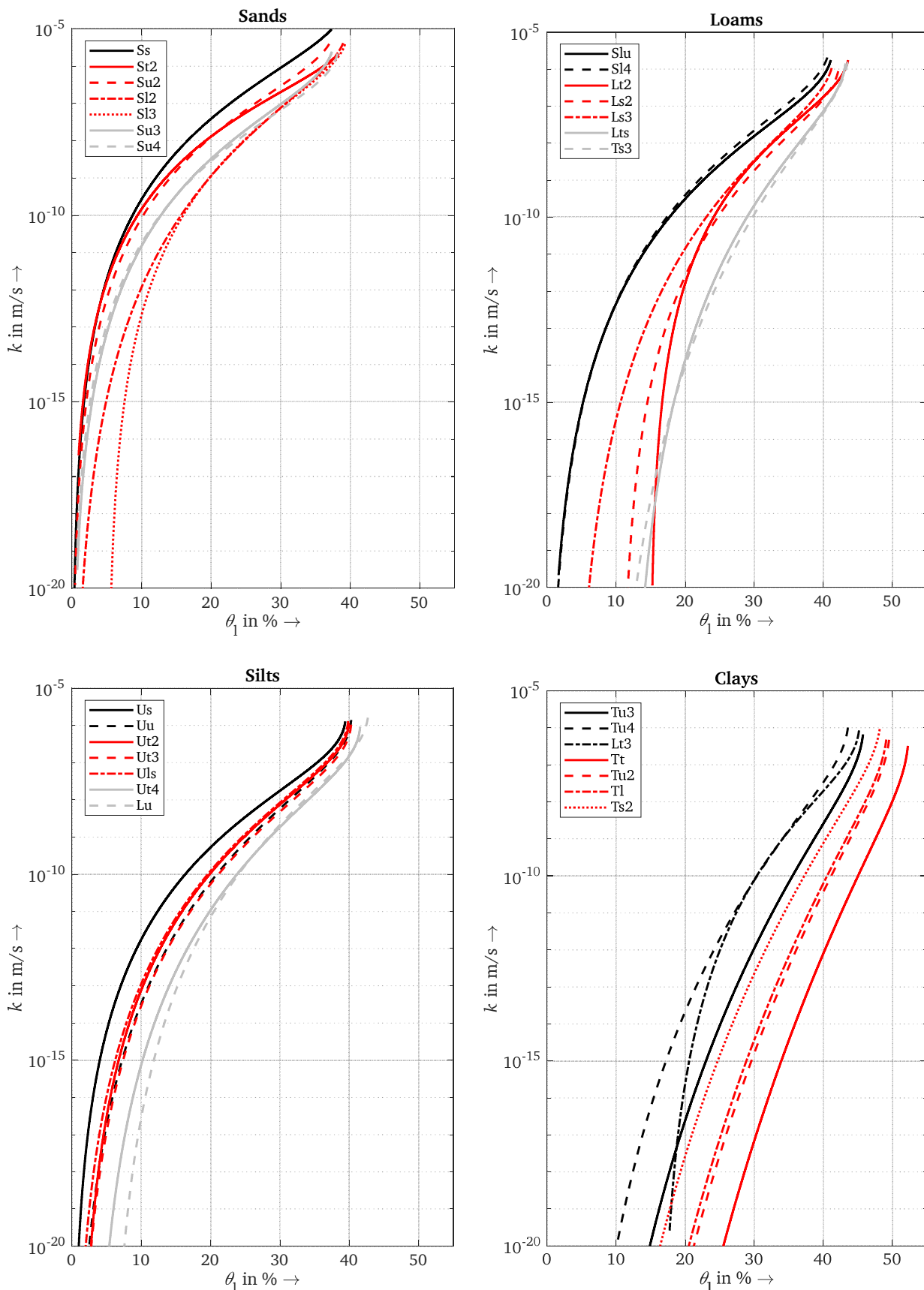


Figure 7.3: Hydraulic conductivity (k) as a function of the volumetric water content (θ_1), based on equation (7.3) and the parameters specified in [E-DIN4220], for all relevant soil types

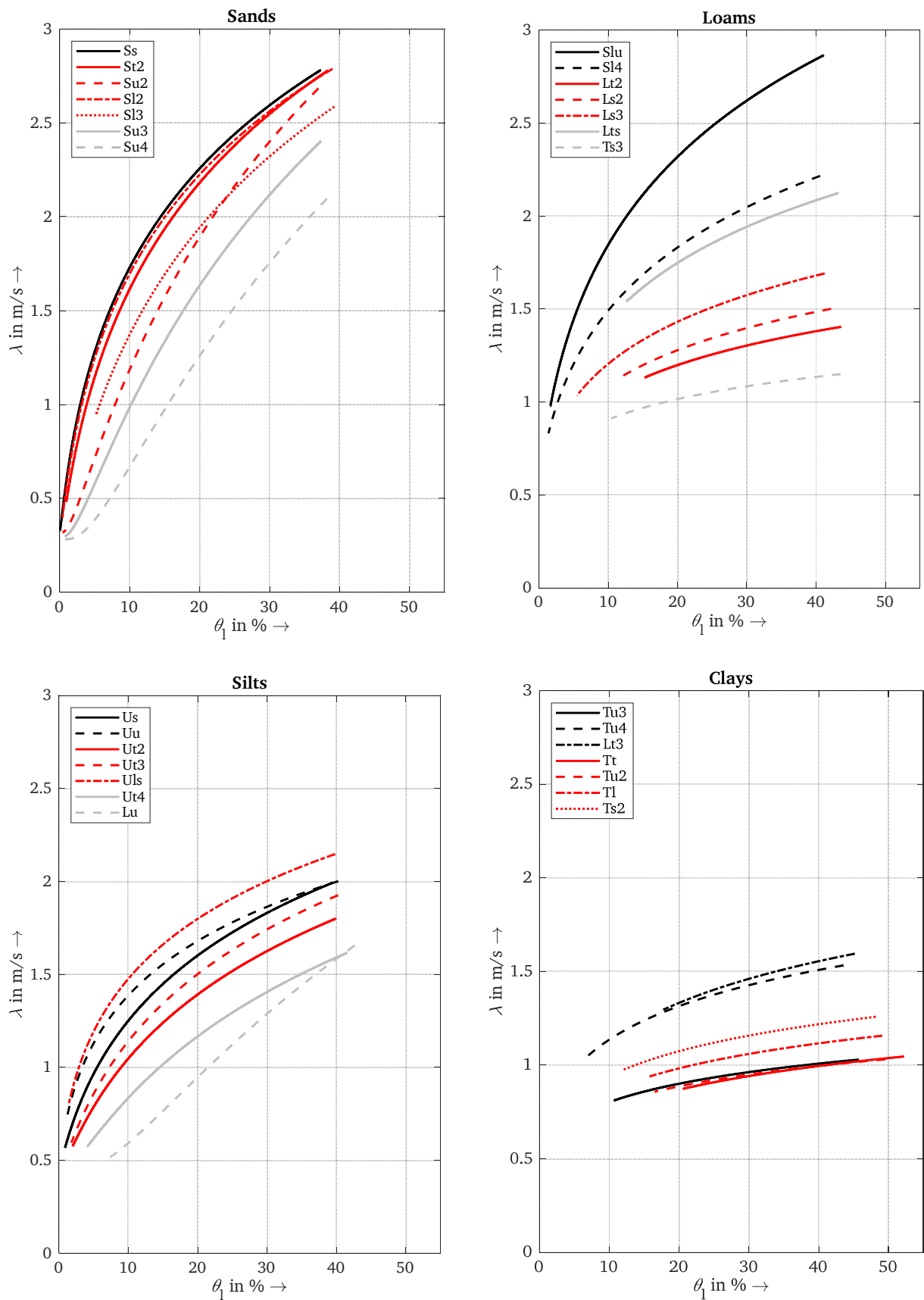


Figure 7.4: Thermal conductivity (λ) as a function of the volumetric water content (θ_1), based on equation (7.5) and the parameters specified in [E-DIN4220], for all relevant soil types

7.1.4 The drying-out of soils

Following the derivations in Appendix A4, the diffusion coefficients from equation (4.39) can be derived from the three soil characteristics in Figures 7.2 to 7.4. This is done for three exemplary soils in Figure 7.6 with respect to the volumetric water content as the state variable, as this dependency is the more common (and vivid) illustration than the used dependency to the hydraulic height. The latter curves are to be found in Appendix A6.

With the help of the shown curves of the diffusion coefficients, the mechanism behind the redistribution of water content from hotter to colder regions inside the bedding can be illustrated, following the explanations in [BRA1985]: Assuming stationary conditions, i.e. the flux of mass equals zero, and taking the volumetric water content as variable of state, equation (4.49) can be rewritten as

$$\text{grad } \theta_l = -\frac{1}{D_{\theta_l}} (D_T \cdot \text{grad } T + k \cdot \vec{e}_z) \quad (7.10)$$

Considering the temperature gradients that usually appear in the vicinity of power cables, the gravitational term in equation (7.10) can be neglected, leading to

$$\text{grad } \theta_l = -\frac{D_T}{D_{\theta_l}} \cdot \text{grad } T \quad (7.11)$$

Hence, the relation between the gradients of the volumetric water content and the temperature is coupled via the quotient of the two diffusion coefficients. This relation is given in Figure 7.5 for the three exemplary soils. If – in a first step – the thermal conductivity is assumed to be independent of the saturation (which, of course, represents only a rough approximation) and therefore the gradient of the temperature to be constant, a rise in the gradient of saturation occurs if the volumetric water content approaches 10 % regarding the pure sand (Ss), 17.5% regarding the pure silt (Uu) and 45% with respect to the pure clay (Tt).

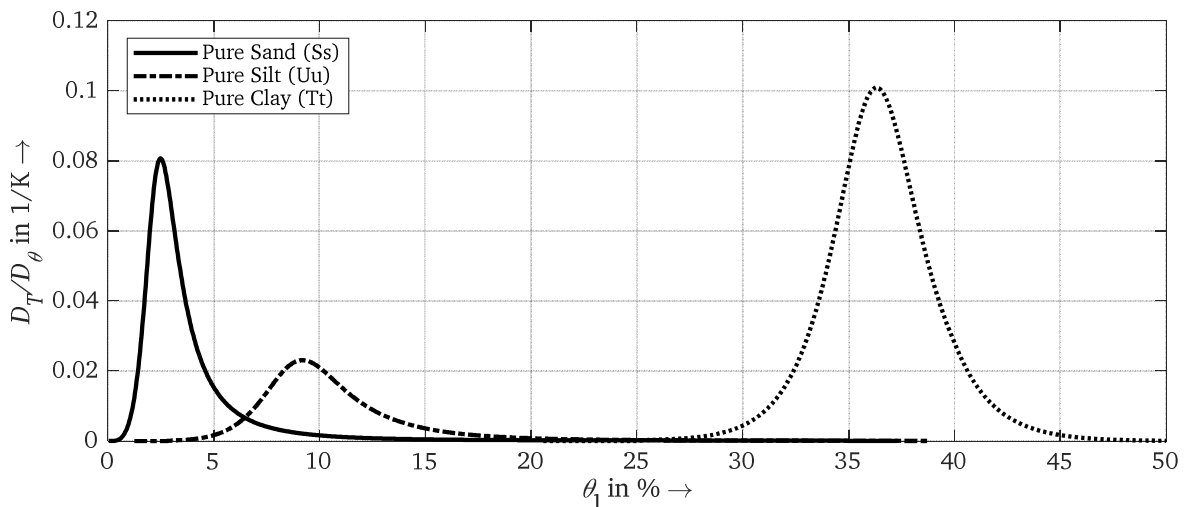


Figure 7.5 Ratio of the diffusion coefficients from equation (7.11) for the three exemplary soils

In reality, this mechanism is further amplified by the fact that the thermal conductivity of soil decreases with the reduction of volumetric water content. Rewriting equation (7.11) by expressing the temperature gradient with the help of the heat flux leads to

$$\text{grad } \theta_l = -\frac{D_T}{D_{\theta_l}} \cdot \frac{\vec{q}}{\lambda(\theta)} \quad (7.12)$$

Hence, a reduction of thermal conductivity due the reduction of water content further increases the gradient of the water content, leading to a more pronounced “drying-out”.

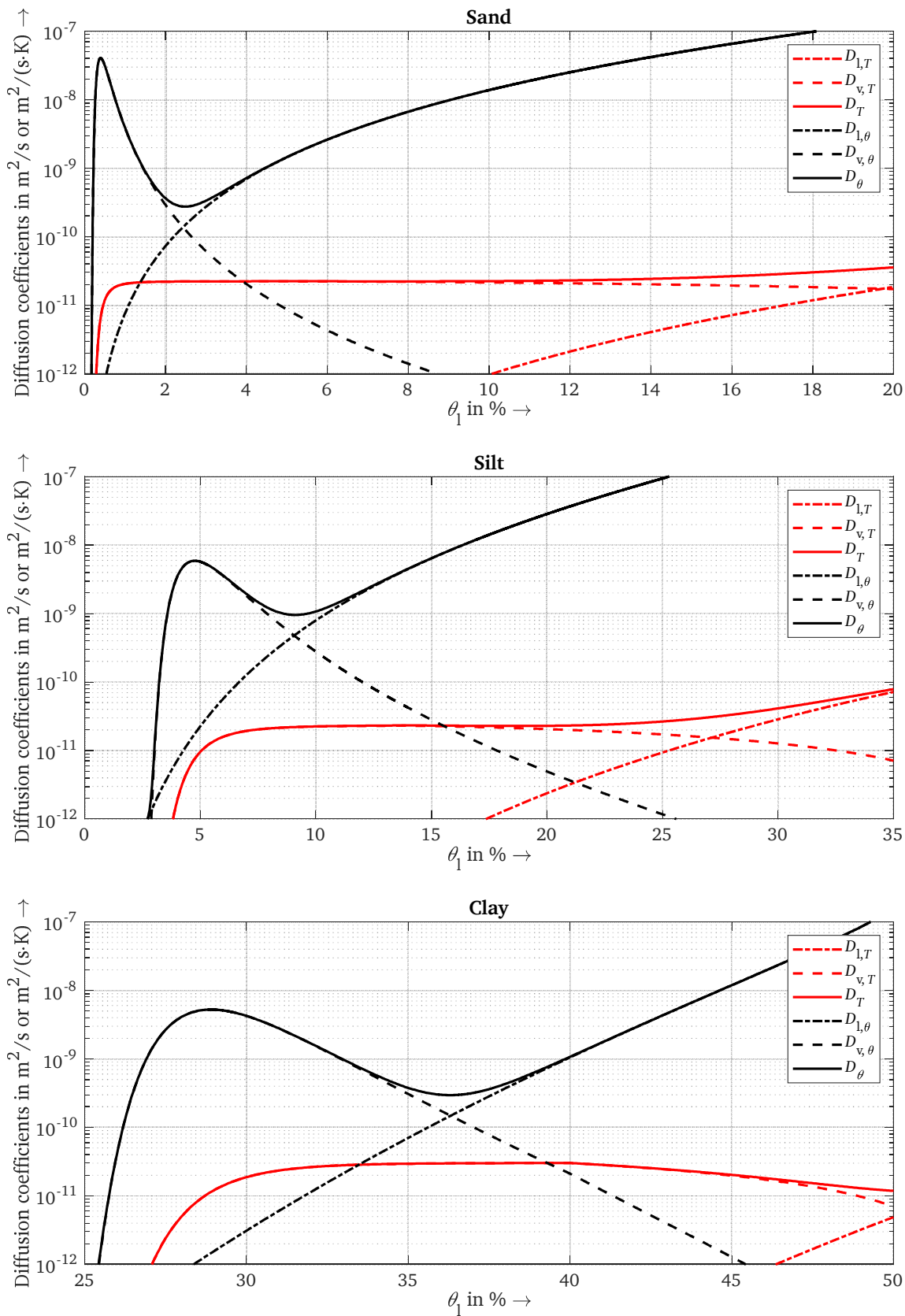


Figure 7.6: Diffusion coefficients as a function of the volumetric water content (θ_1) for a pure Sand (Ss), a pure silt (Uu) and a pure clay (Tt), based on the parameters specified in [E-DIN4220]

7.2 Implementation of soil drying-out into ampacity calculations by the two-zone model

With respect to the implementation of the aforementioned mechanisms into the calculation of the temperature rise of power cable systems, equation (7.11) is of a fundamental importance: As isotherms (i.e. lines of equal temperatures) collide with lines of equal water content (which are also lines of equal thermal conductivity), it is possible to define a temperature dependent thermal conductivity of the bedding.

Regarding the form of this function, the so-called two-zone model has imposed itself as the state of the art in implementing the drying-out of soils into ampacity calculations [CIG1992]. This model is based on the assumption that the redistribution of moisture within the soil leads to two distinctive zones, each of them exhibiting a homogenous thermal conductivity: A “dry” zone with very low moisture content (and hence poor thermal conductivity) around the cable as well as a “wet” zone with ambient moisture content (and therefore considerably higher thermal conductivity). The boundary between these two-zones is marked by the “critical temperature rise” (above the reference temperature) dT_{crit} .

Hence, three parameters of the bedding must be specified when the two-zone model is applied: the thermal conductivity of the bedding in “dry” and “wet” conditions, denoted as λ_{dry} and λ_{wet} , as well as the value of the critical temperature rise, dT_{crit} . As an example, German standard [DIN0276] assumes the following values for stationary conditions

$$\lambda_{\text{dry}} = 0.4 \frac{\text{W}}{\text{m} \cdot \text{K}} \quad (7.13)$$

$$\lambda_{\text{wet}} = 1 \frac{\text{W}}{\text{m} \cdot \text{K}} \quad (7.14)$$

$$dT_{\text{crit}} = 15 \text{ K} \quad (7.15)$$

The resulting curve of the thermal conductivity as function of the temperature for a reference temperature of 20 °C is given in Figure 7.7.

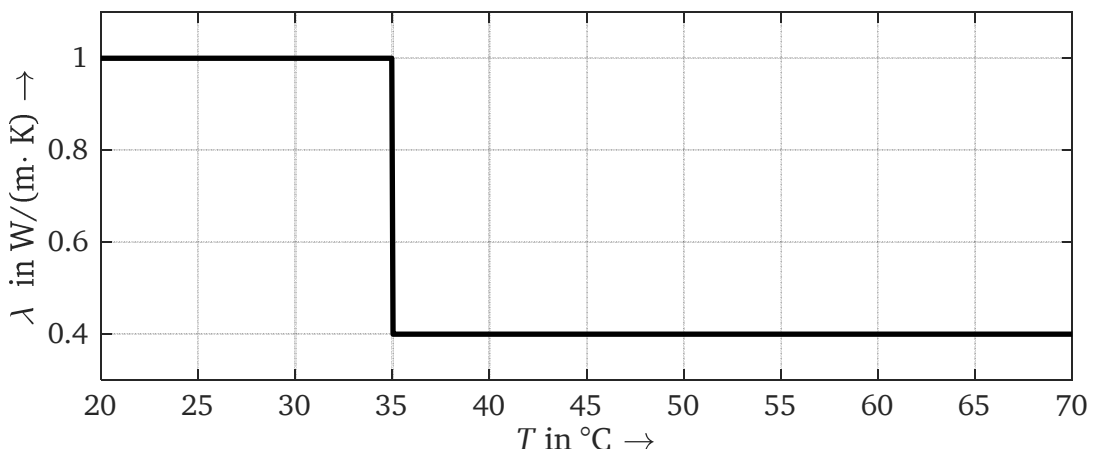


Figure 7.7 Thermal conductivity (λ) of the bedding material as a function of the temperature (T) according to the two-zone model and the parameters proposed by [DIN0276] for constant load, see equations (7.13) to (7.15)

The advantages of the two-zone model are obvious: It reduces the complex consideration of heat and mass transfer mechanisms, described in chapter 4.1.3, to the determination of the three parameters in equation (7.13) to (7.15). Furthermore, it allows the inhomogeneity of the thermal conductivity to be relatively easily included in the equations of ampacity ratings, and [CIG1992] proposes a procedure to calculate the three necessary parameters as a function of soil specific parameters with the help of analytical equations. This procedure will be highlighted in the following.

7.2.1 Present adoption of the two-zone models to specific soils

Regarding the three parameters from equations (7.13) to (7.15), the thermal conductivities may be determined as following: The thermal conductivity in dry conditions can either be measured directly inside an oven-dried soil probe or determined with the help of the presented approximations [MAR2017]. Regarding the thermal conductivity of the “wet” region, [CIG1992] recommends to estimate the thermal conductivity at half the value of the volumetric water content of the undisturbed soil. Again, this value can be calculated using equation (7.5) or measured directly.

More complicated is the determination of the critical temperature rise. As a starting point, [DON1979] assumes that the values of the diffusion coefficients (with the saturation as state variable) depend only on the porosity $\varepsilon_{\text{soil}}$ and the saturation S_{eff} according to

$$D_T \approx D_{v,T} \approx D_{v,T,0}(\varepsilon_{\text{soil}}) \cdot (1 - S_{\text{eff}}) \quad (7.16)$$

$$D_\theta \approx D_{l,\theta} \approx D_{l,\theta,0}(\varepsilon_{\text{soil}}) \cdot (S_{\text{eff}} - s_{\text{cr}})^2 \quad (7.17)$$

Where:

s_{cr} : Critical saturation, i.e. value of saturation where the water bridges between the soil particles break up, see Appendix A4 for further explanation.

Inserting equations (7.16) and (7.17) into (7.11) yields

$$\frac{1}{\eta_D} \cdot \frac{(S_{\text{eff}} - s_{\text{cr}})^2}{(1 - S_{\text{eff}})} \nabla S_{\text{eff}} = -\nabla T \quad (7.18)$$

with

$$\eta_D = \frac{D_{T,v,0}(\varepsilon_{\text{soil}})}{D_{\theta,l,0}(\varepsilon_{\text{soil}})} \quad (7.19)$$

Integrating equation (7.18) perpendicularly to the isotherms alongside the path \vec{l} (already defined for equation (3.4)) from the undisturbed soil surface at reference temperature T_{ref} and ambient saturation leads to

$$\int_s^{s_a} \frac{1}{\eta_D} \cdot \frac{(S_{\text{eff}} - s_{\text{cr}})^2}{(1 - S_{\text{eff}})} dS_{\text{eff}} = - \int_T^{T_a} dT \quad (7.20)$$

Where:

s_a : Ambient saturation

Inserting the primitives on both sides yields

$$-\frac{1}{2 \cdot \eta_D} (S_{\text{eff}} - 1)(3 - 4 \cdot s_{\text{cr}} + S_{\text{eff}}) - (s_{\text{cr}} - 1)^2 \ln(S_{\text{eff}} - 1)|_s^{s_a} = T|_T^{T_{\text{ref}}} \quad (7.21)$$

From equation (7.21), the equation to determine the critical temperature rise, at which the critical saturation level¹⁷ is reached (or, in other words, at which drying-out occurs) is derived to be

$$T_{\text{cr}} = T_{\text{ref}} - \frac{1}{\eta_D} \left[\frac{1}{2} (s_a^2 - s_{\text{cr}}^2) + (s_a - s_{\text{cr}})(1 - 2s_{\text{cr}}) + (1 - s_{\text{cr}})^2 \ln \left(\frac{1 - s_a}{1 - s_{\text{cr}}} \right) \right] \quad (7.22)$$

Hence, on paper, equation (7.22) provides an expression to derive the critical temperature rise as a function of the critical and ambient saturation of the soil as well as a parameter η_D . However, in order to be useful, this expression must both be valid with regard to its application and not to sensitive with respect to the input parameters. This will be investigated in the following.

¹⁷ See the discussion on page 123 for the definition of the critical saturation level

7.2.2 Shortcomings of the two-zone model

In order to start with the validation of the expression from equation (7.22), the approximation in equations (7.16) and (7.17) will first be examined. Taking the sand “Ss” as an example, Figure 7.8 shows the comparison of the curves derived from the extensive calculations in Appendix A4 and the functions in (7.16) and (7.17). Following the explanations in Appendix A4, the critical saturation was set to be the saturation level, at which the hydraulic conductivity falls below $10^{-12} \text{ m}\cdot\text{s}^{-1}$. The values of $D_{v,T,0}$ and $D_{l,\theta,0}$ have been derived with the help of a non-linear regression for all values $S_{\text{eff}} > s_{\text{cr}}$.

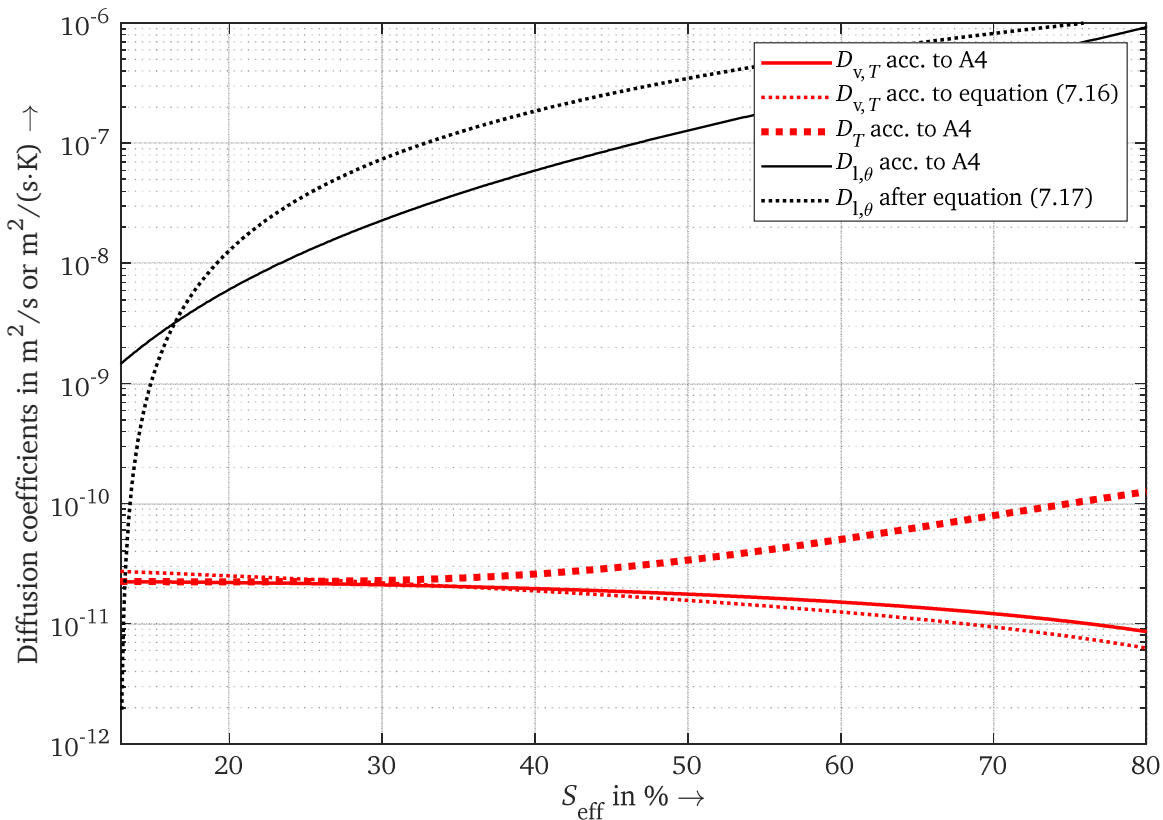


Figure 7.8 Comparison of the curves of the diffusion coefficients for sand (Ss) as a function of the effective saturation (S_{eff}), calculated according to Appendix A4, and the approximations according to equations (7.16) and (7.17)

With respect to the approximation of the curves, it must be said that in the range of the critical saturation, there is a fairly good accordance between the calculation based on equation (7.16) and (7.17) as well as the extensive derivation from Appendix A4. However, two important remarks have to be made: First of all, by including the curve for D_T into the consideration, the assumption that the mass transport due to the temperature gradient is only driven by the transport of vapour is not valid for relatively high degrees of saturation. And secondly, as it is shown in Figure 7.9, a significant error is induced by omitting the temperature dependency of the involved diffusion coefficients.

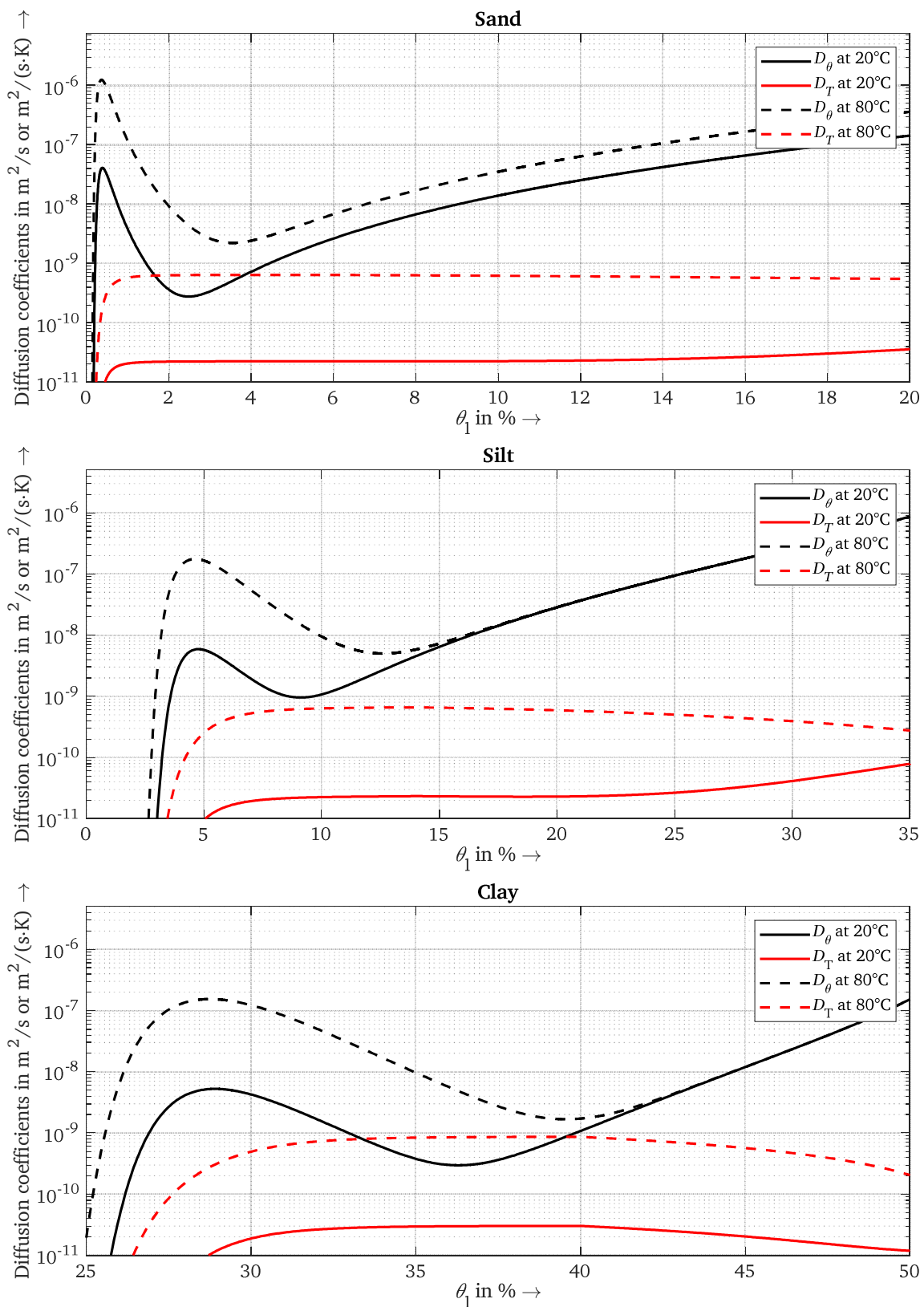


Figure 7.9: Illustration of the effect of the temperature on the diffusion coefficients of the sand "Ss", silt "Uu" and clay "Tt" with the parameters specified by [E-DIN4220]

But the main problem is not the approximation from equation (7.16) and (7.17): As equation (7.22) gives the critical temperature as a function of the critical saturation, the ambient saturation and the parameter η (see equation (7.19)), it should be possible to adopt – together with the values of the thermal conductivities for the dried-out and ambient soil – the two-zone model to the specific characteristics of the natural bedding.

However, the point is that equation (7.22) reacts very sensitively to its input parameters: Given the sand Ss as an example, Figure 7.10 shows the result of the critical temperature as a function of the ambient water content for two different values of η_D . As it is explained in Appendix A4, the critical volumetric water content is assumed to be 5 %, the value for $\eta_D = 1.24 \cdot 10^{-5} \text{ K}^{-1}$ is the result from the regression from Figure 7.8, $\eta_D = 10^{-4} \text{ K}^{-1}$ is a value proposed by [BRA1985].

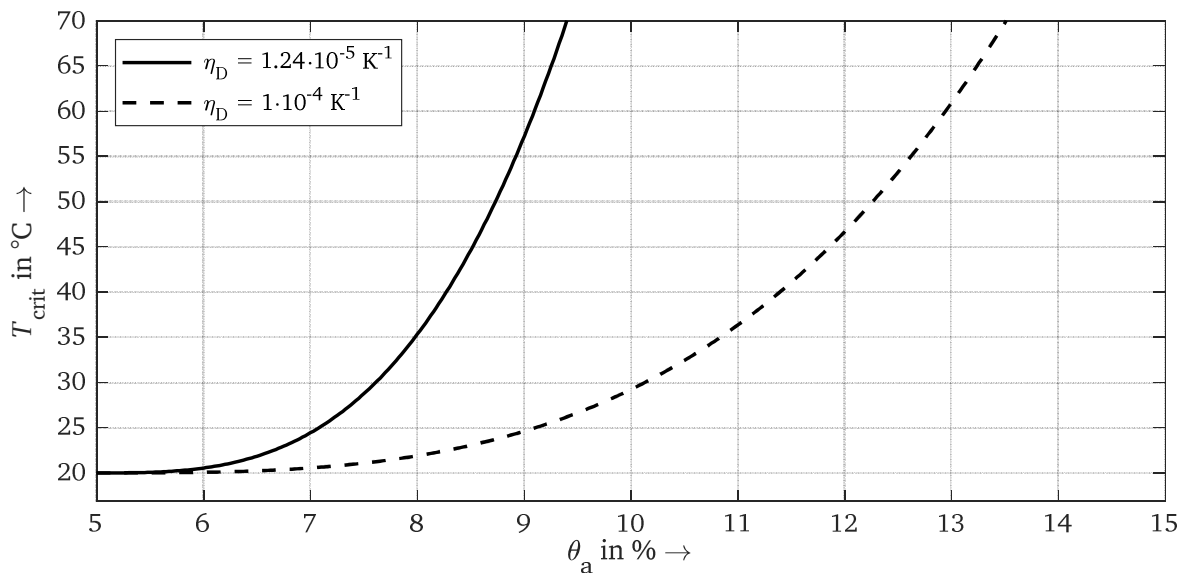


Figure 7.10: Critical temperature (T_{crit}) as a function of the ambient water content (θ_a) according to equation (7.22) for two different values of η

Values of the ambient water content in laying depths of cable systems in sandy soils can oscillate between 5 % and up to 20 %. With reference to Figure 7.10, the high deviations in the calculated critical temperature are far too high to make a reliable statement. The same goes for the other two parameters: Within the range of plausible values for the critical saturation as well as η , almost any critical temperature between 20 °C and 90 °C can be “calculated”. As a consequence, the practical usefulness of equation (7.22) is to be contested.

Therefore, it should be further examined whether the sensitivity of the results from equation (7.22) comes from deficiencies of the underlying calculations or whether they have a physical background. Furthermore, the re-evaluation of the drying-out of natural beddings invites to the following questions:

- The abrupt change in thermal conductivity that is assumed by the two-zone model may be validated for sandy soils. However, most natural beddings are mixtures of grains of different sizes, so that a uniform grain size distribution may result in a “flatter” degeneration of thermal conductivity with rising temperature. Hence, it should be examined whether the two-zone model is valid for all types of soils. Furthermore, the main influencing factors on the course of the curve have to be examined.
- Little is known about the dynamics of the involved heat and mass transport mechanisms. There are indications of the long time-constants involved in the soil drying-out [FRE1996], but no further investigations.

- A simulative evaluation of the drying-out under realistic boundary conditions, i.e. by taking into account the natural fluctuations of ambient water contents due to precipitation and evapotranspiration by plants is unknown to the author.

The aforementioned open questions will be examined with the help of a verified numerical model [DRE2017] that implements the equations from chapter 4.1.3 in the already employed distinction between the three principal regimes of time: stationary, periodic and transient conditions.

7.3 Results in stationary conditions

Strictly spoken, stationary conditions with respect to the distribution of humidity would never appear inside natural beddings. Not only is the heat injected by the cable often fluctuating, but also the environmental conditions such as precipitations or weather changes are anything but constant. Nonetheless, the evaluation of stationary conditions is important with respect to two arguments: On the one hand side, stationary results are most appropriate to study the factor of influences on the drying-out of soils, as the differences between the boundary conditions are most pronounced in the stationary results. This, on the other hand, is also the reason why the stationary results are very important for the ampacity rating of cable systems: Assuming a stationary load is the worst case assumption with respect to the resulting drying-out, so that the stationary conditions are an estimation of the behaviour of the bedding on the safe side.

Evaluating the influencing factors of the soil drying-out, it is of interest – with respect to the temperature dependency of the diffusion coefficients shown in Appendix A5 – to calculate the soil drying-out at different maximum temperature drops between the cable and the soil surface. Furthermore, it seems plausible – with respect to Figure 7.10 – to consider the ambient saturation as a variable input parameter. And finally, the influence of the hydraulic conductivity on the overall results is worth evaluating, as this characteristic is difficult to measure while being very sensitive to the result.

All three evaluations will be conducted for the geometry that is shown in Figure 7.11. It resembles the configuration of a directly buried cable system at a lying depth of $y_0 = -0.7$ m, where the ground surface at $y = 0$ is set to a temperature of 20 °C and the inner boundary (representing the outer jacket of the cable) is set to $T_{\max,e}$. If not otherwise specified, it is assumed that

$$T_{\max,e} = 80 \text{ } ^\circ\text{C} \quad (7.23)$$

With respect to the mass transport equations, the ground surface as well as the other outer boundaries are implemented as Dirichlet conditions at ambient saturation level. The inner boundary is of type “no flow”, the initial values are the reference temperature and the ambient saturation. In order to properly define an “ambient saturation” at the reference ground surface, the effect of gravity was disregarded in the calculations of the two dimensional configuration, as it is proposed by [BRA1985]. The width and depth of the domain is chosen to be 10 m so that the domain represents a good approximation of a semi-infinite domain.

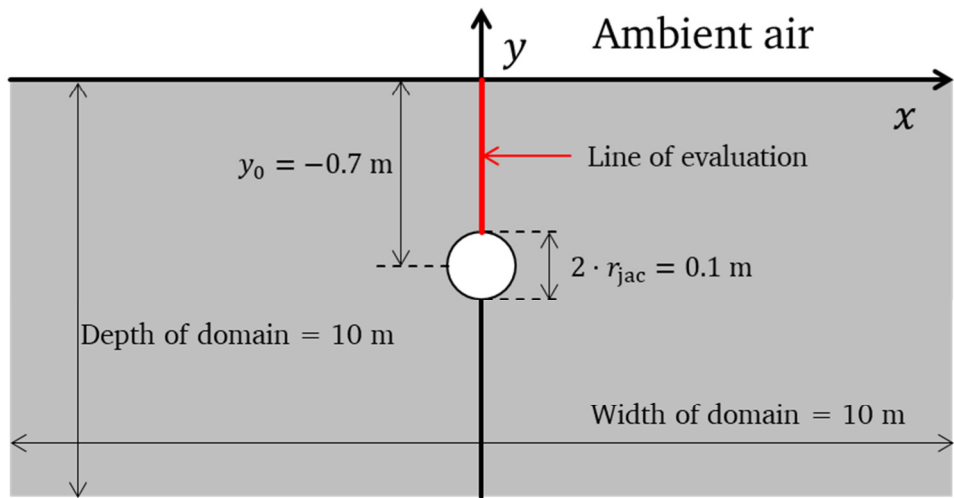


Figure 7.11 Studied geometry (not to scale) for the derivations of the temperature dependent thermal conductivities of the different soils in the following chapters

The shown curves (Figures 7.12 and 7.13) of the relation between the temperature and the thermal conductivity of the bedding material are recorded alongside the y-direction, from the inner boundary at $x = 0 \text{ m}$ and $y = -0.65 \text{ m}$ to the soil surface. In accordance to equation (7.11), it was proven that this relation is the same for every path of the bedding – as long as the ground surface is implemented as a Dirichlet condition at ambient saturation. If the ground surface is implemented as a no-flow boundary, the temperature gradients lead to a minor accumulation of moisture in the vicinity of the ground surface, resulting in a slight deviation of the relation between the temperature and the thermal conductivity of the material.

7.3.1 Influence of the maximum temperature

In a first step, the influence of the temperature $T_{\max,e}$ on the inner boundary of the bedding is studied, as the temperature dependency of the diffusion coefficients (referring to Appendix A5) may lead to the conclusion that the relation between the temperature and the thermal conductivity is itself dependent on the overall temperature level inside the bedding. Therefore, the geometry from Figure 7.11 was simulated for three different maximum temperatures on the inner bedding for the three monofractional soils; the ambient saturation was assumed to equal field capacity, which amounts to circa 15 % volumetric water content for the sand of type Ss, 36.5 % for the silt of type Uu and 49 % for the clay of type Tt.

The resulting curves are shown in Figure 7.12. It can be stated that differences between the results at different maximum temperatures do not exist or are negligible. Hence, the relationship between temperature and thermal conductivity inside the bedding is independent of the maximum temperature of the cable outer jacket. Also are indicated the positions of the zone of transition between “wet” and “dry” state.

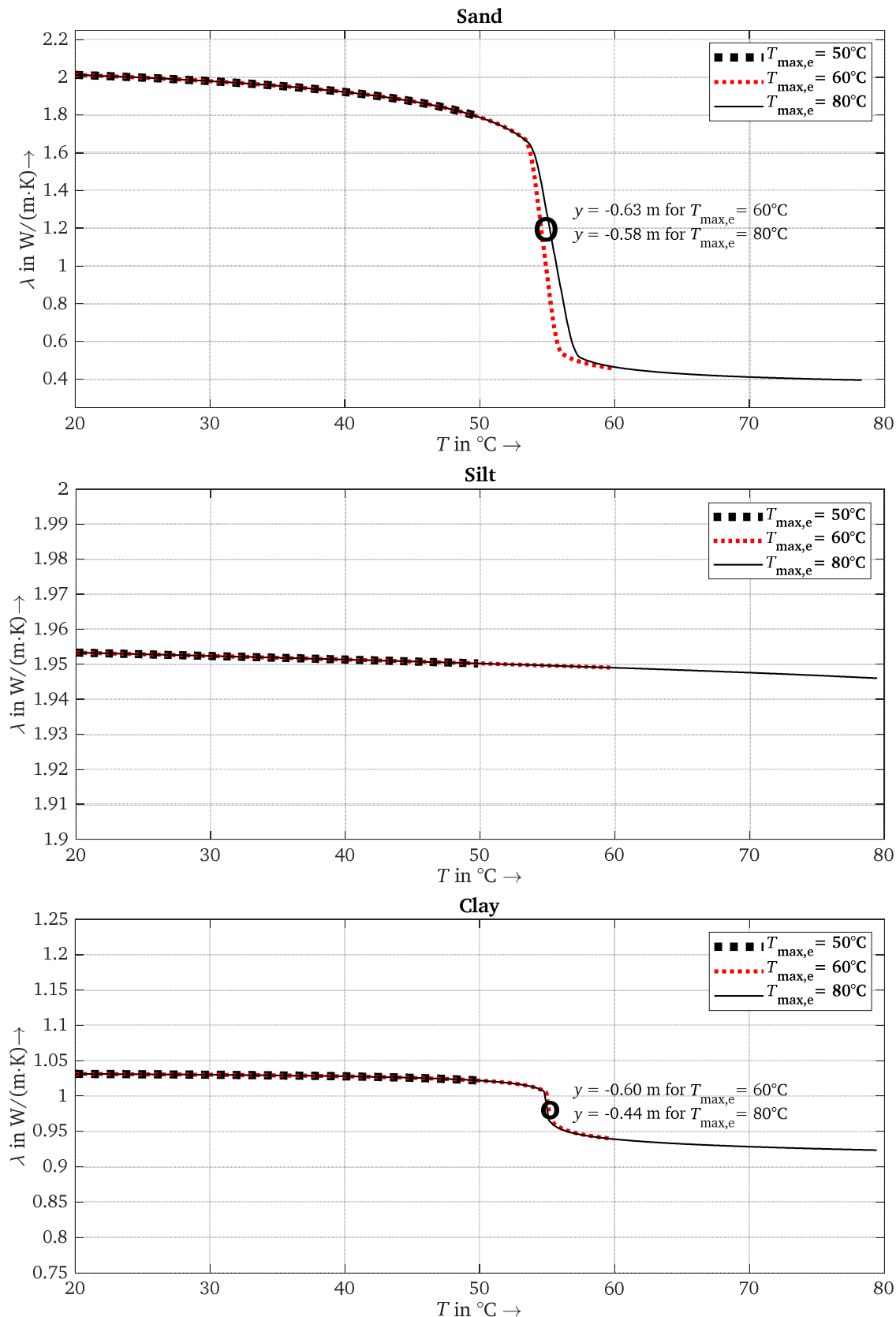


Figure 7.12: Simulated thermal conductivities (λ) as a function of the temperature (T) for different temperatures on the cable outer jacket ($T_{\max,e}$) of a pure sand (Ss), a pure silt (Uu) and a pure clay (Tt). The ambient saturation equals field capacity. For sand and clay, the positions of the zone of transition between "wet" and "dry" state are equally given.

7.3.2 Influence of the ambient water content

As it was mentioned before, equation (7.22) shows a high dependency of the ambient water content of the bedding on the critical temperature rise. As a consequence, it seems necessary to study this sensitivity with the help of the numerical simulations, so that the temperature dependent thermal conductivity for the soils from Figure 7.12 has been recalculated with different values of the ambient saturations. The results are shown in Figure 7.13.

It becomes clear that the high sensitivity of the ambient saturation level is not a shortcoming of the analytical expression in equation (7.22), but is confirmed by the numerical outcome – if there is a drying-out of the soil. Against the background of the robustness of a soil specific thermal model of the bedding, this result is very inconvenient as already in natural conditions, the soils are subjected to high fluctuations in water content – measurements from the test field at TU Darmstadt [BAL2017-1] showed that the water content in sandy soils oscillated between 7.5 % and 20 %, see Figure 7.14.

This, however, poses the question of a “reasonable” assumption of the ambient water content: It must be stated that the assumption of an ambient water content at field capacity is – with respect to the natural conditions – too optimistic. On the other hand, assuming the minimum water content in the course of a year as ambient water content would lead to very conservative results that surely lay below the actual standards with regard to the admissible current carrying capacity.

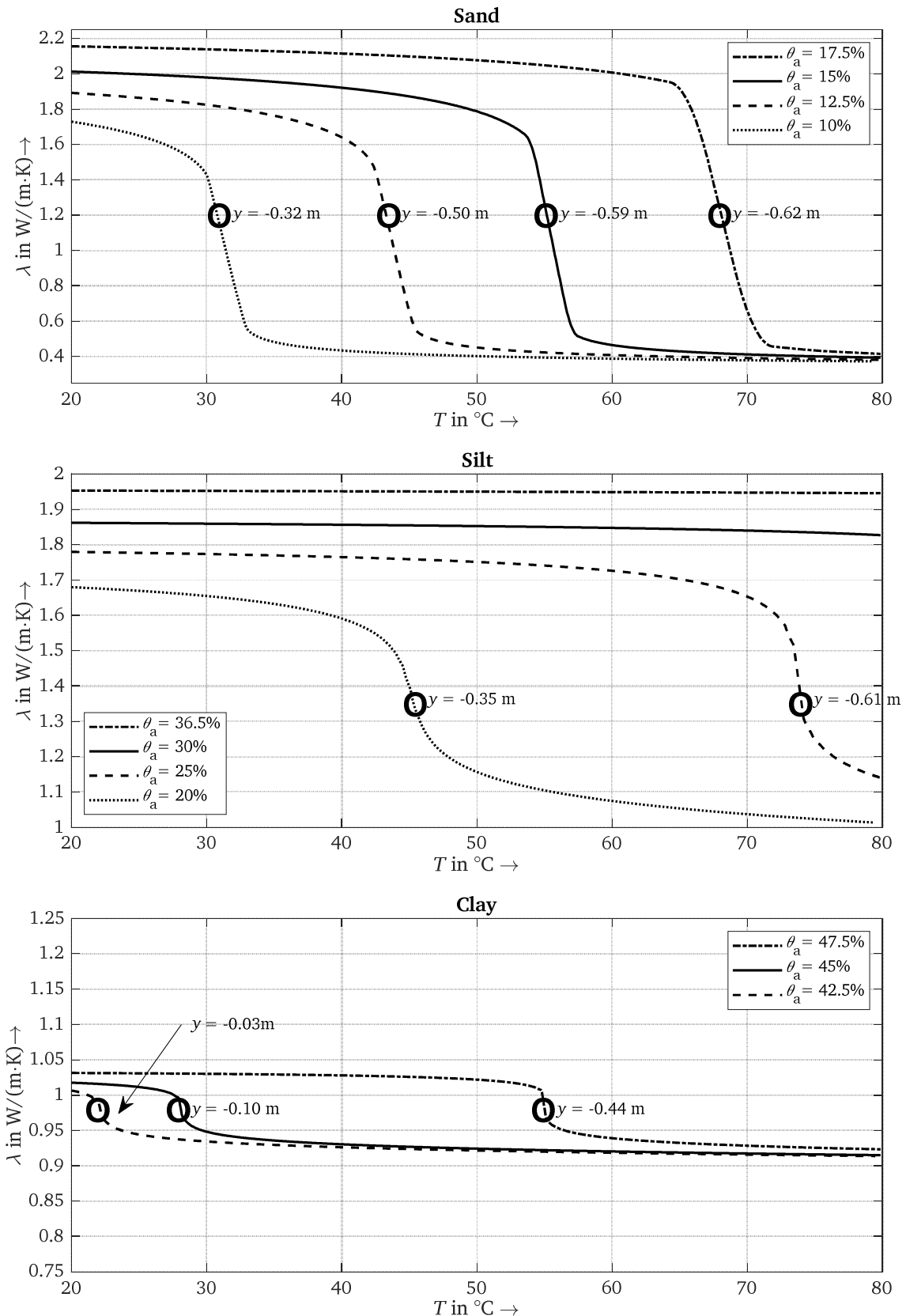


Figure 7.13: Simulated thermal conductivities (λ) as a function of the temperature (T) for different values of the ambient water content of a pure sand (Ss), a pure silt (Uu) and a pure clay (Tt). Also, the positions of the zone of transition between “wet” and “dry” state are equally given.

A loophole of this dilemma may be the definition of a “fresh soil” that can be found in [BLU2011]. With the definitions of the permanent wilting point (pwp) and the available water capacity (awc), it is

$$\text{sandy soils: } \theta_{\text{fresh}} = \theta_{\text{pwp}} + \frac{1}{3} \cdot \theta_{\text{awc}} \quad (7.24)$$

$$\text{loamy soils: } \theta_{\text{fresh}} = \theta_{\text{pwp}} + \frac{1}{2} \cdot \theta_{\text{awc}} \quad (7.25)$$

$$\text{clay soils: } \theta_{\text{fresh}} = \theta_{\text{pwp}} + \frac{2}{3} \cdot \theta_{\text{awc}} \quad (7.26)$$

In order to validate the assumption that a water content at “fresh” condition is a reasonable assumption for the ambient water content of natural soils at laying depth of cable systems, a simulation of the yearly fluctuations of the water content was implemented. The methodology is based on the propositions of [FAO1998], which is recommended by the world food organization to calculate the soil moisture content during the course of the year. The simulation incorporated measured data for the net solar radiation, air temperature and pressure as well as wind speed and precipitations for Darmstadt or adjacent stations, extracted from the climate data center of Deutscher Wetterdienst¹⁸. The model was first verified by a comparison of simulated and measured time series for bare soils of type Ss (sand), Ut2 (mixture of loam and silt) and Ls2 (silt with a proportion of clay). The measurements originated from a test field at TU Darmstadt between October 2016 and June 2017, the simulations implemented the movement of liquid water only. The soil characteristics had been derived from measurements of the soils rather than the propositions of [E-DIN4220] in order to validate the model itself. If the propositions from [E-Din4220] for the soil characteristics had been used, further errors by these approximations would have been introduced. Results are shown in Figure 7.14.

As it can be seen, the model reflects well the dynamic as well as the quantity of soil water content inside the sand. With respect to the soil of type Ut2 and Ls2, the absolute level of the computed water content coincides with the measurements, whereas the dynamics differ. By sensitivity studies, it was found that this difference is largely due to the high influence from the hydraulic conductivity on the results, which itself is highly dependent on the compaction. As a consequence, it seems plausible to assume that the differences between the measured and the simulated dynamics are more likely to be attributed to differences between the measured and the actual hydraulic conductivity (or differences of the compaction in vertical direction) rather than to the model itself. Hence, as the model should provide an idea of the typical range of water contents inside different types of soils instead of reproducing or predicting the exact values, differences between the simulated and measured data seem tolerable.

¹⁸ To be found under: <https://cdc.dwd.de/portal/>

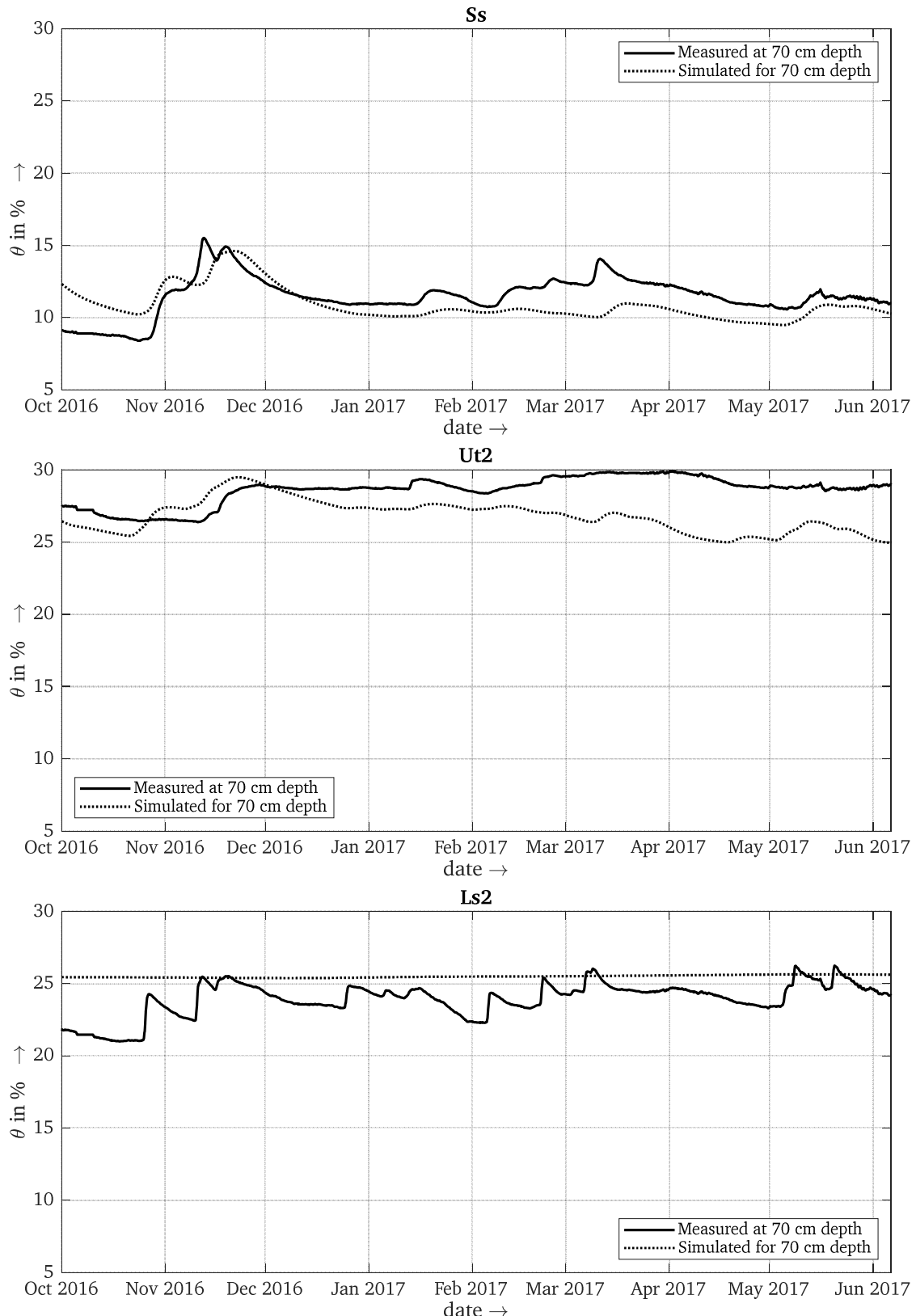


Figure 7.14: Comparison of the measured (full line) and the simulated (dotted line) water content at 70 cm beneath a bare soil surface for three types of soil: sandy soil (Ss), mixture of loam and silt (Ut2) and silt with a proportion of clay (Ls2). The measured data were recorded on the test field of TU Darmstadt [BAL2017-1], the simulation implemented the approach from [FAO1998] and is based on measured climate data.

Therefore, the water contents of all types of soils from Figure 7.1 at a depth of 0.7 m have been simulated based on the yearly climate data of Darmstadt from October 2016 to October 2017. Regarding the ground surface covering, turf with a rooting depth of 15 cm is assumed. The resulting evapotranspiration, i.e. the water transport from the soil to the surrounding air by evaporation from the soil surface as well as transpiration from plants, was implemented according to the methods presented in [FAO1998]. During the simulated year, the cumulative precipitations equal 620 mm, which represents a reasonable choice for middle Europe. In total, a time span of ten years was simulated, guaranteeing “steady state” conditions.

The results as the ratio between the simulated water contents and the “fresh”-content as defined by equations (7.24) to (7.26) are shown as box plots in Figure 7.15, illustrating the minimum and maximum values during the course of the year, as well as the 25 % and 75 % percentile (lower and upper end of the box) and the median value (in red).

With respect to Figure 7.15, one may conclude that the assumption of a “fresh” ambient water content reflects the actual conditions nicely: Most mean values can be found to be close, but above the fresh water content. Therefore, the “fresh” approach is a quite reasonable choice on the safe side. Only for sands, deviations are considerable, with simulated mean values considerably higher than θ_{fresh} . However, with respect to longer periods of draught, it is reasonable to assume the water content of sands more conservatively than for more cohesive soils. Under this perspective, θ_{fresh} as defined by equations (7.24) to (7.26) is an appropriate choice for the ambient water content.

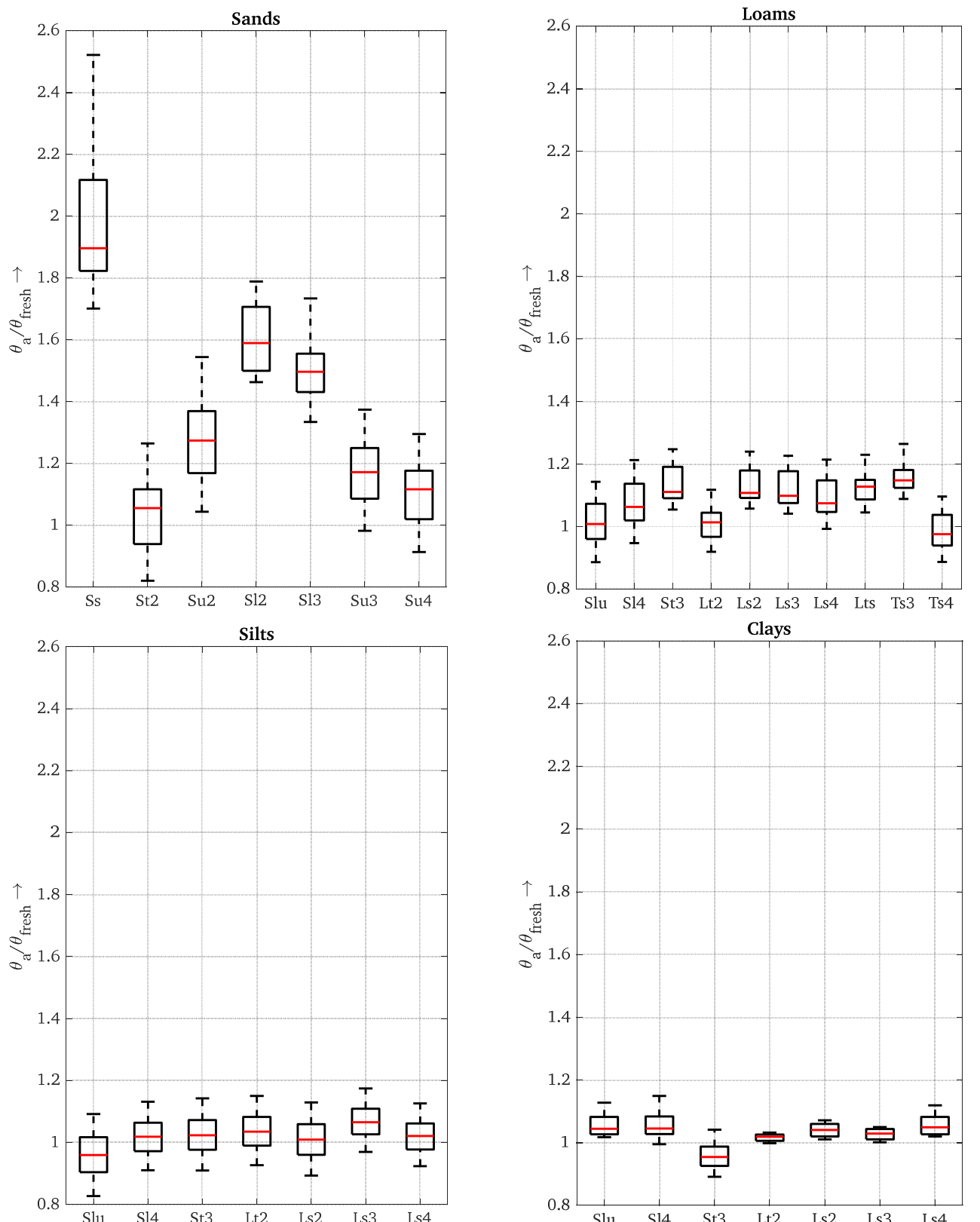


Figure 7.15: Quotient of the simulated ambient water content (θ_a) to the “fresh” water content (θ_{fresh}) from equations (7.23) to (7.25). Shown are the minimum and maximum values, 25 % and 75 % percentiles (lower and upper ends of the box) and the median value (in red).

7.3.3 Influence of the hydraulic conductivity

Finally, the influence of changes of the hydraulic conductivity will be regarded for the three exemplary soils. The background of this evaluation is that, from the three soil characteristics, from which the diffusion coefficients are derived (namely: the water retention curve, the thermal as well as hydraulic conductivity as functions of water content), the hydraulic conductivity is by far the most difficult to measure: Not only do the low flow rates from 10^{-6} to $10^{-10} \text{ m}\cdot\text{s}^{-1}$ make errors in the range of one order in magnitude very likely, but also is the hydraulic conductivity very sensitive to changes of compaction: Despite great care, the soil fabric inside a soil probe may already be altered with respect to its in-situ properties. Therefore, it is helpful to obtain estimations about the influence of the hydraulic conductivity on the heat conductivity as a function of temperature.

Results are shown in Figure 7.16 for the three exemplary soils, assuming field capacity as ambient water content. Unsurprisingly, it can be stated that the hydraulic conductivity has – if drying-out does take place – a very high influence on the resulting relation between temperature and thermal conductivity. This is due to the fact that the diffusion coefficient $D_{l,\theta}$ equals the hydraulic conductivity. Moreover, the high influence of the ambient water content, which was described in the section before, is actually a consequence of the high influence of the hydraulic conductivity, as the latter increases drastically with the ambient water content.

With respect to the aim of developing a soil specific thermal model, this result might deal a blow to the hopes of a practical applicability: With the hydraulic conductivity as an influencing factor that is very hard to measure, but having a large influence on the result, the derivation of the temperature dependent thermal conductivity from measurements seems unachievable. Already by extracting the soil probe, changes in the soil fabric can be produced, which consequently change the hydraulic conductivity significantly. Moreover, measurements of the same probe tend to deviate by one order in magnitude, which, according to Figure 7.16, has substantial influence on the result. As a consequence, high standards on the measurement procedures are required.

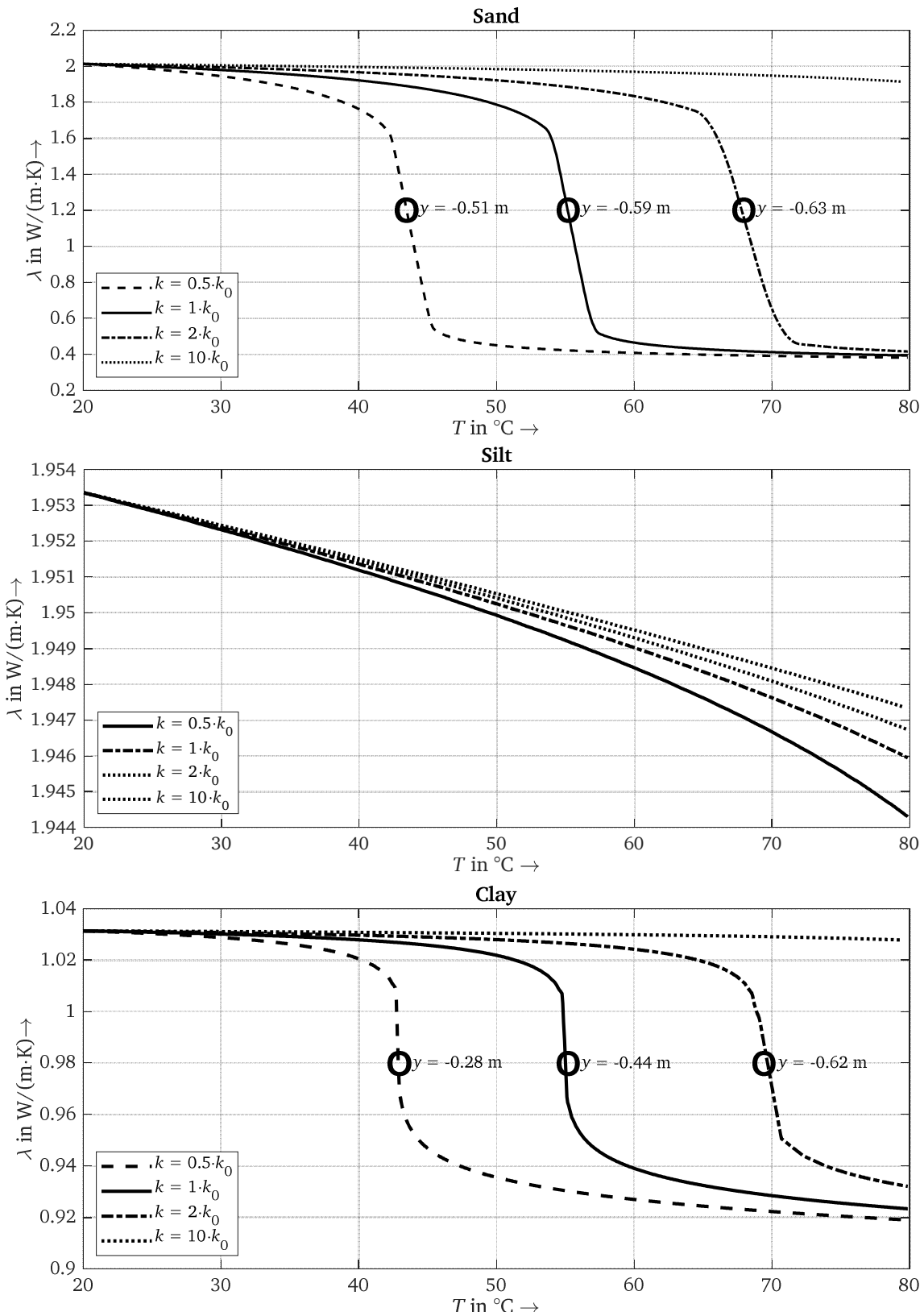


Figure 7.16: Simulated thermal conductivities (λ) as a function of the temperature (T) for different values of the hydraulic conductivity of a pure sand (S_s), a pure silt (U_u) and a pure clay (T_t). k_0 denotes the hydraulic conductivity as assumed by [E-DIN4220]. For sand and clay, the positions of the zone of transition between "wet" and "dry" state are equally given.

7.3.4 Influence of the soil types

To close the evaluation of the stationary case, the thermal conductivity as a function of temperature at an ambient water content θ_{fresh} has been calculated for all soil types from Figure 7.1. These curves are shown in Figure 7.17.

With regard to the aforementioned question, most characteristics can well be approximated by the two-zone model, which means that the transition between a “wet” and a “dry” region is rather pronounced. Moreover, as it would have been expected, the critical temperature rises with the average size of the particles – from sand with very low critical temperature rises to loamy and silt soils. The very low critical temperatures for some sands are the result of the fact that θ_{fresh} is close to the critical temperature rise, which – considering longer dry periods – is not an unrealistic assumption. However, apart from some sands, it becomes also clear that the values from equations (7.13) to (7.15) that are proposed by the standard are very (if not: too) conservative.

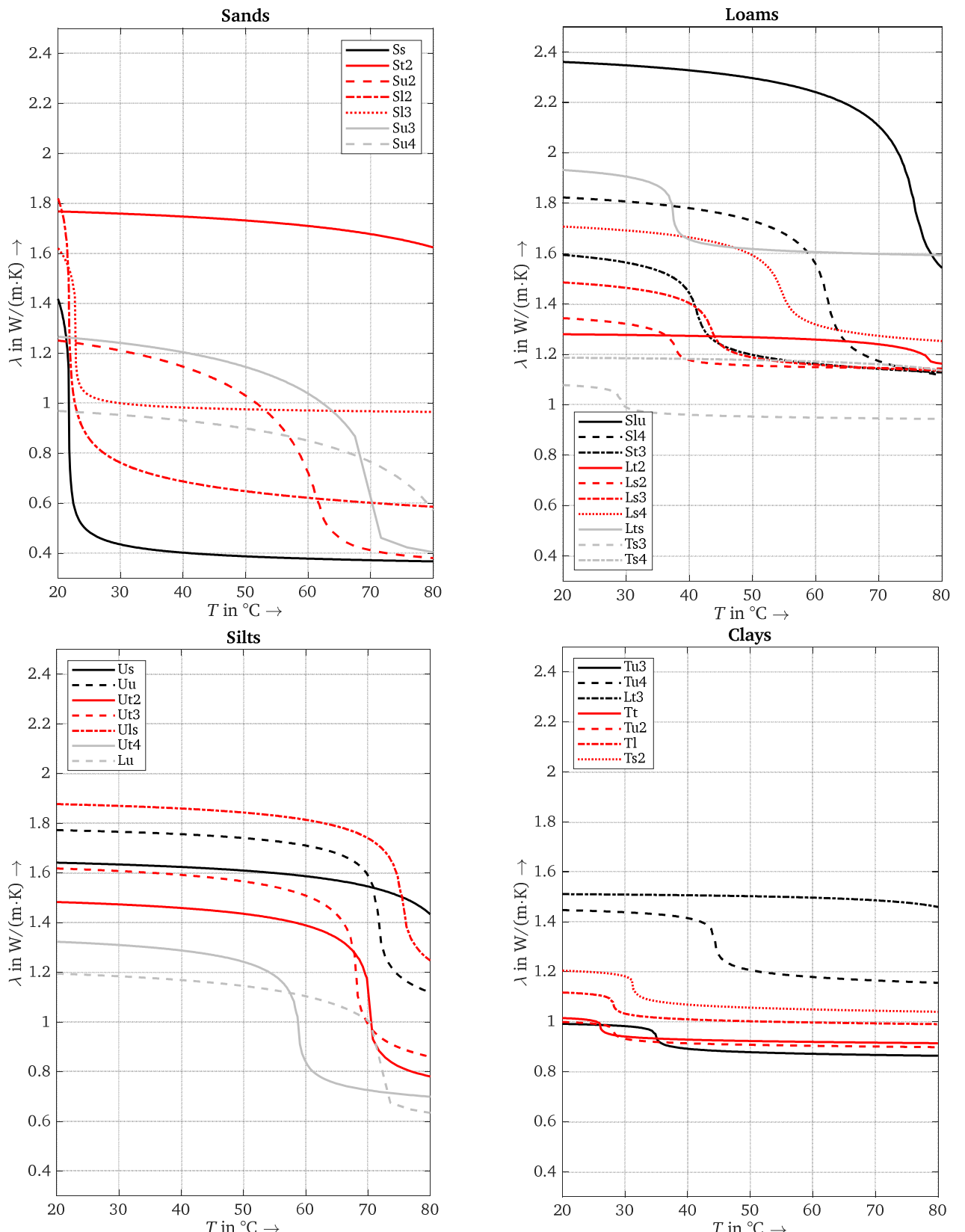


Figure 7.17: Simulated thermal conductivities (λ) as a function of the temperature (T) at an ambient water content θ_{fresh} for all soil types of Figure 7.1

7.4 Results under stationary periodic conditions

Rather than stationary loads, cable systems in distribution and transmission grids are mostly subjected to daily load schemes. As a consequence, the drying-out of soil must also be considered under a periodic heat injection from the cable.

The German standard VDE 0276 takes into account the effect of the periodic load scheme by proposing a change in the critical temperature rise: Instead of 15 K for stationary loads, periodic loads with $m_{VDE} = 0.7$ shall be calculated by assuming a static drying-out with a critical temperature rise of 25 K. However, the characteristic of the soil itself does not change, but the reference frame does.

In order to understand this, Figure 7.18 compares the stationary temperature dependent thermal conductivity of the soil Ss at $\theta_a = 12.5\%$ with the results calculated for the same soil, but with a rectangular-shaped heat injection at the inner boundary with $m_{VDE} = 0.5$, i.e. full load for 12 hours of the day and no load for the consecutive 12 hours. As abscissa, the average temperature during one load cycle is chosen, the ordinate values are the corresponding average thermal conductivities.

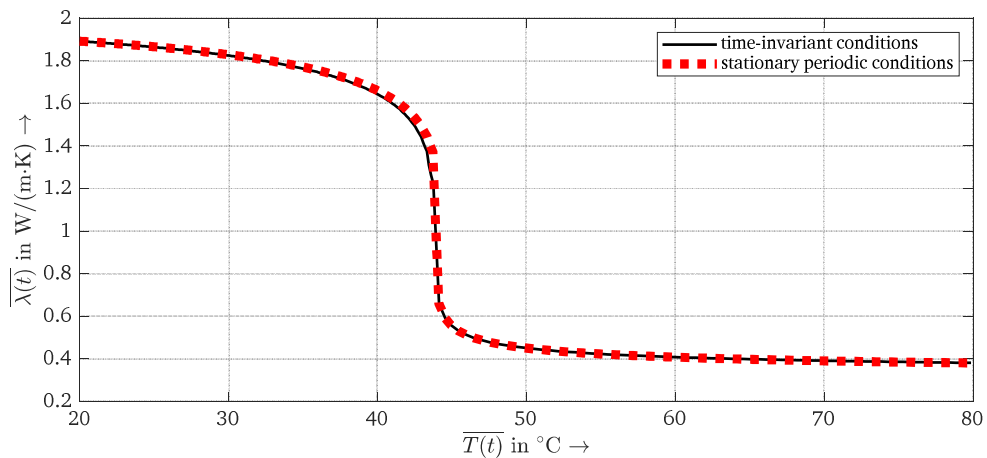


Figure 7.18: Average thermal conductivity (λ) as a function of the average temperature (\bar{T}) for a sand of type Ss with $\theta_a = 12.5\%$ for a stationary load (black, full line) and a periodic, rectangular-shaped heat injection with $m = 0.5$ (red, dotted line)

As it can be conceded, the two characteristics are very close to each other. Therefore, it is fair to say that the relation between the thermal conductivity and the temperature does not change under periodic load conditions if the daily average temperature is chosen as reference.

However, it shall be kept in mind that the temperature field itself is changing: Considering only conduction, the penetration of the heat waves into the bedding diminish if a periodic heat injection is considered. Therefore, if the soil drying-out is calculated from a static temperature distribution, the critical temperature must rise in order to result in the same geometric distribution of the thermal conductivity. Therefore, the change in critical temperature from stationary to periodic loads does not reflect different physical states, but a shift of the reference frame of the temperature dependent thermal conductivity (i.e. the temperature), from the actual maximum temperature distribution (under periodic heat injection) to the temperature distribution in stationary conditions.

And finally, it is worth pointing out that the numerical model, from which the result in Figure 7.18 is taken, does not incorporate the hysteresis effects of the water retention curve in the case of a recurrent drying and re-wetting.

7.5 Results under transient conditions

Finally, the transient heating of a power cable system under consideration of the transient heat and mass transfer inside the bedding is evaluated. In order to illustrate the involved dynamics, the temperature development on the inner boundary of the geometry from Figure 7.11 (which represents the temperature T_e on the surface of the outer cable jacket) under a constant heat injection is calculated for three different implementations of the thermal characteristics of the bedding (which is assumed to be a sand of type Ss with $\theta_a = 12.5\%$). The results are shown in Figure 7.19.

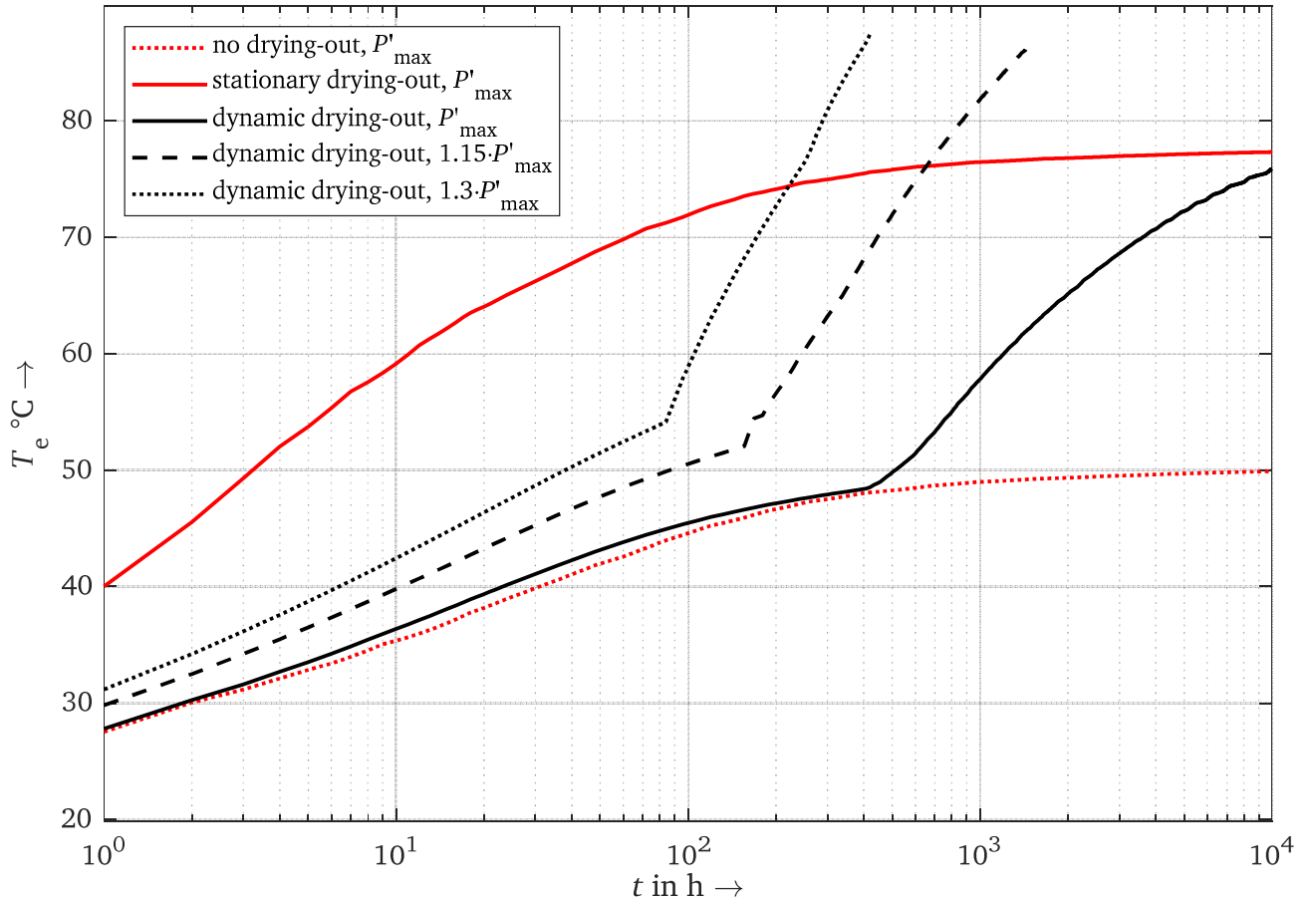


Figure 7.19: Temperature development on the inner boundary of the geometry from Figure 7.11 (T_e) as a function of time (t) when a constant heat flux is injected on the same boundary. In black, full line: Implementation of the temperature dependent heat and mass transfer mechanisms within the bedding. In red, full line: Conductive heat transfer computation, assuming the soil drying-out under stationary conditions. And in red, dotted line: Conductive heat transfer mechanism, assuming no drying-out.

In a first step, the temperature development was calculated based on a purely conductive consideration in two ways: In Figure 7.19, the red, dotted line is the result of a computation, assuming a homogenous thermal conductivity of the bedding that equals the thermal conductivity at ambient water content. Hence, this represents the temperature at the outer surface of a single cable if no soil drying-out takes place. In red, as a full line in Figure 7.19 is drawn the curve, based on the distribution of the thermal conductivity of the bedding at a stationary, maximum drying-out (i.e. the drying out that would occur if the conductor is continuously at its maximum temperature of 90 °C). Therefore, this reflects the procedure that is proposed by VDE 0276 and is an assumption on the safe side regarding the thermal resistance of the overall bedding. For both cases, the heat injection equals P'_{\max} , which is the heat flux per unit length at maximum conductor temperature in stationary condition (and assuming a stationary, maximum drying-out of the bedding).

Finally, in black, was calculated the temperature development on the base of the full implementation of the involved heat and mass diffusion equations. As a consequence, the full line nicely describes the transition from the beginning of the soil drying-out (after about 500 h) to the stationary conditions (after more than 10^4 h). With respect to the long time constant of transition, it is once more proven that the assumption of the standards are too conservative to meet the requirements of today's dynamic operating conditions.

Moreover, as black, dashed and dotted lines, are shown the curves for an increase of heat injection by 15 % and 30 % with respect to the maximum stationary load. With respect to Figure 7.19, it can be stated that the drying-out always starts when the temperature of the outer jacket reaches about 50 °C, which is a little bit more than the stationary critical temperature for this type of sand and ambient water content. As a consequence, one way of simulating the thermal runaway in a simplified manner would be to calculate the transient heating, based on the stationary dependency between the thermal conductivity and the temperature inside the bedding.

In order to compare these three implementations, Figure 7.20 shows the maximum possible operating time (t_{\max}) if the cable is subjected to a load higher than its actual stationary ampacity limit, P'_{\max} . The maximum time is defined as the time at which the temperature T_e reaches 80 °C, which for a medium voltage cable would result in a conductor temperature of about 90 °C.

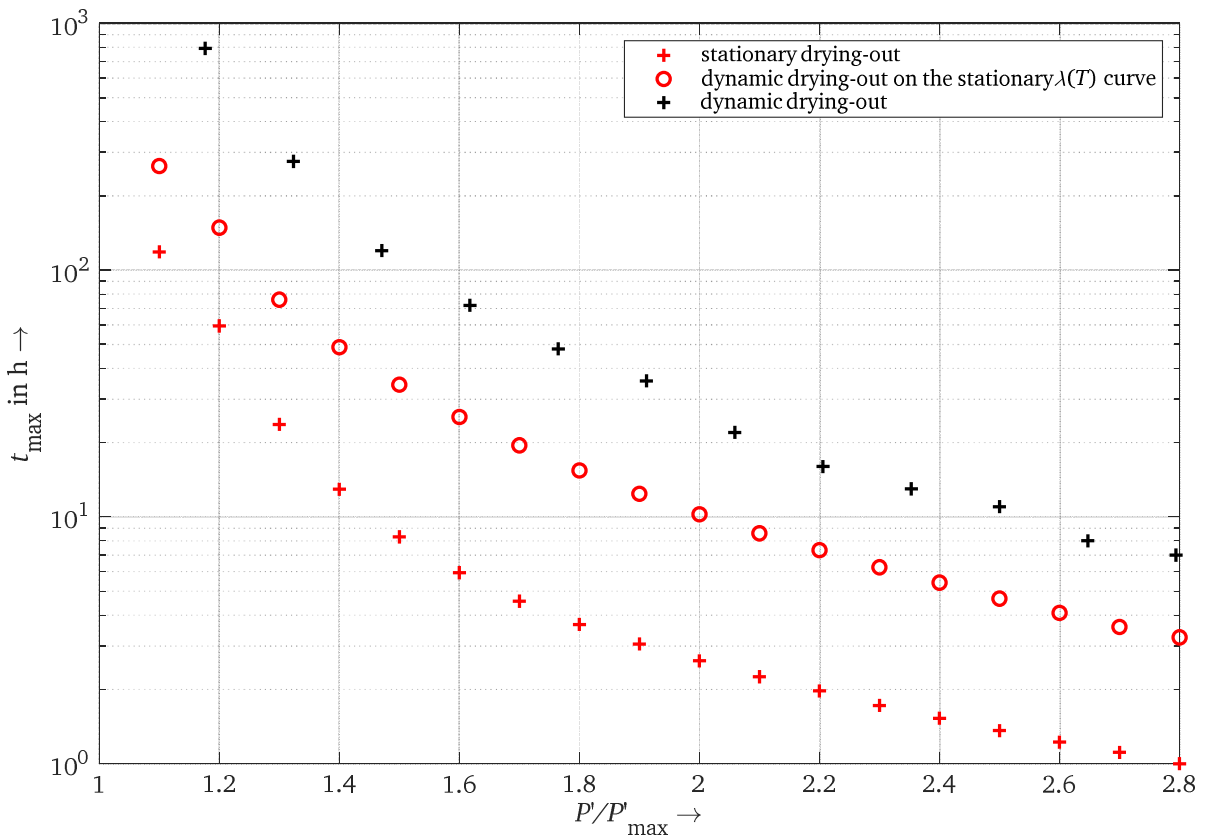


Figure 7.20: Time (t_{\max}) at which the temperature on the inner boundary from Figure 7.10 (T_e) reaches 80°C under the assumption of a constant heat injection P' for three um heat flux per unit length under stationary conditions.

The results shown in Figure 7.20 give an idea about the potential of a dynamic implementation of the soil drying-out in ampacity calculations. For a ratio $P'/P'_{\max} = 2$, the admissible time under the assumption of a stationary drying-out is 3 h, whereas the consideration of the dynamics of drying-out would lead to $t_{\max} \sim 30$ h.

However, the durations for the dynamic calculations of the soil drying-out shown in Figure 7.20 are only valid under the presumption that at the start of the heat injection, there was no prevailing soil drying-out. This leads to the last aspect that is evaluated within the framework of this work: The inclusion of natural precipitation and evapotranspiration into ampacity calculations.

An illustration of the possible benefits of taking the natural fluctuations of soil water contents into consideration is shown in Figure 7.21. Here, the water content at the inner boundary of the geometry that is shown in Figure 7.11 was calculated for a mono-fractional sand (“Ss”) under the following assumptions: Starting from a complete drying-out (i.e. the stationary distribution of the volumetric water content) for $T_{\max,e} = 80^\circ\text{C}$, the heat injection stopped at the first of October. In red, full line is drawn the water content (primary axis), including the effect of precipitation (black bars, secondary axis) and the evapotranspiration of a turf cover. In red, dotted, is shown the simulated curve excluding these effects, i.e. under the influence of static ambient conditions.

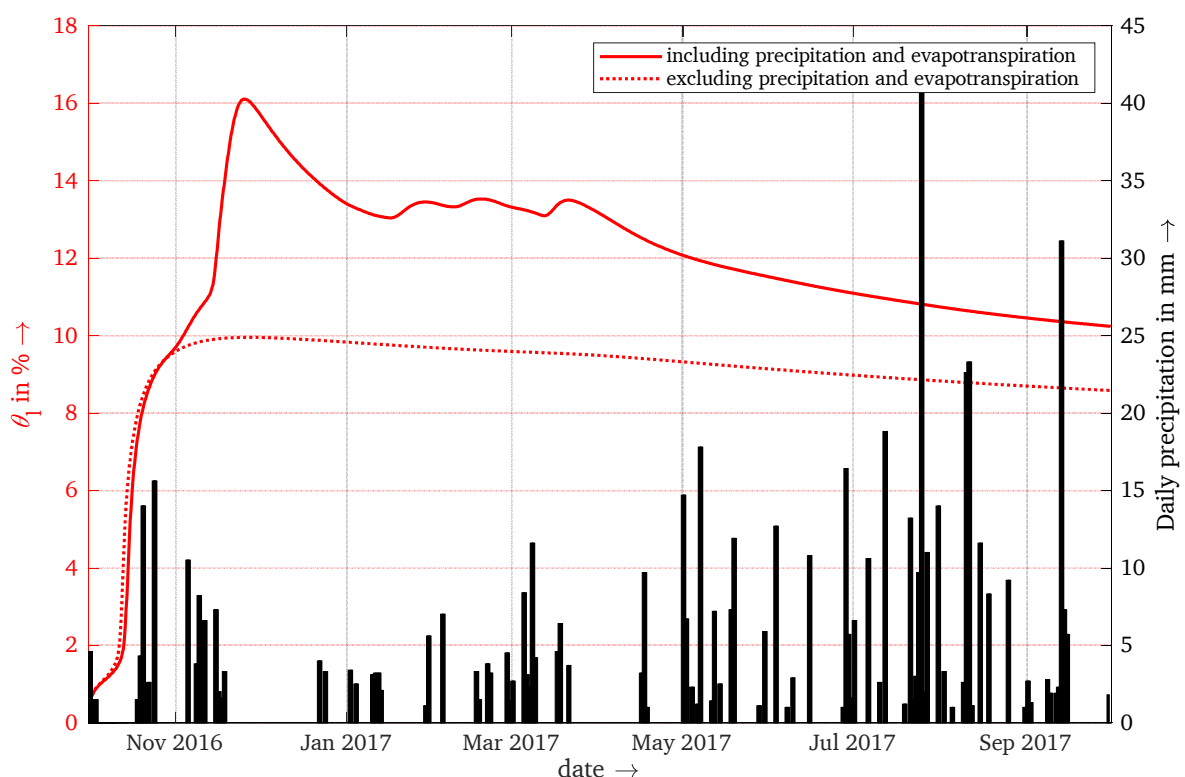


Figure 7.21: Simulated volumetric water content (θ_1) at the inner boundary of the geometry in Figure 7.10 as a function of date. At 1st of October, a complete drying-out was assumed whereas no heat is injected during the simulated period. As red, full line, are shown the results if precipitation and evapotranspiration of a turf cover is considered, as a dotted line is shown the result under stationary conditions. In black bar is shown the daily precipitation (secondary axis)

In both cases, it takes about one month for the soil to re-moisten to a volumetric water content of 10%. However, the benefit of the incorporation of environmental conditions becomes clear during the course of the winter: Due to increasing rainfalls at the end of November, the water content increases further to finally 14 % if actual precipitation data are considered. This is very important with regard to the regeneration of natural beddings for cable systems that are connected to photovoltaics: As in this case, the load is expected to be considerably lower during winters, a regeneration of soils can be assumed. However, with regard to Figure 7.21, it is also worth noticing that the rainfalls during summer are mostly absorbed by the vegetation and do not contribute to a wetting of the soil in the laying depth of the cable.

8 Resumé and outlook

The existing approaches of cable ampacity ratings by analytical formulations or numerical computations provide valid results with respect to their domain of applications: The former is used by the present standards to derive general, conservative results, which tend to underestimate the actual current carrying capacity. The latter provides exact results for the studied configuration, given a well-known set of input variables and a correct implementation.

However, the trivial finding that *changed conditions require new measures* also applies for the calculation of ampacity ratings: As an increase of dispersed power injection from renewable energies lead to unprecedeted load flows, the idea of a periodically recurring, daily load scheme must be abandoned in favour of the expectation of highly variable dynamics. Moreover, the widespread use of communication techniques within the grid paves the way for new, agile processes regarding the operation of a system. And finally, incentive based regulations are pushing the transmission and distribution system operators to make the best use of their existing infrastructure and to plan new lines and cable connections as efficient as possible. In order to do so, an enhanced understanding of the thermophysical processes within soils as well as the progression in measurement techniques makes it possible to refine the hitherto existing, simplified models of the soil thermal properties and ampacity calculations in general.

Hence, a revision of the cable ampacity rating imposes itself, replacing static limits by variable ones, which are permanently updated by the means of embedded calculations, taking into account real time data of cable loads and environmental conditions. Against this background, the present work aims at laying the foundation of an enhanced determination of the current carrying capacity of power cable systems. This was done in the following steps.

8.1 Resumé

As it was presented in chapter 2 of this work, the existing standards do not provide a helpful input when it comes to finding a method that combines the rapidity of analytical formulations with the exactness and flexibility of numerical computations.

One major difficulty in finding a method that meets the aforementioned requirements of a renewed ampacity calculation is the fact that from a theoretical point of view, three different physical disciplines are involved: electromagnetism with respect to the cable losses, heat conduction regarding the transfer of heat inside cable elements and heat and mass diffusion inside the soils. Therefore, the development of a new method to calculate the current carrying capacity of cable systems must start with recalling the theoretic fundamentals of the implied physics, which is done in chapter 4. From the formulation of the three resulting state equations, it becomes clear that, due to linearity of the material properties, the cable losses and the heat conduction inside the cable elements can be calculated analytically, whereas the diffusion of heat and mass is best done numerically due to the strong non-linear behaviour of the implied soil characteristics. The techniques to solve the derived state equations analytically are also presented in chapter 4.

Chapter 5 deals with applying the solution techniques to the relevant configurations: the calculation of losses inside the cable conductor, the insulation as well as the screen and the heat conduction inside all cable elements and a homogenous bedding. Solutions are found for stationary, periodic as well as transient time dependencies. Regarding the bedding, expressions for different assumptions on the outer cable jacket as well as the soil surface are derived.

As a consequence of the abundance of the expressions in chapter 5, the use of thermal quadrupoles [MAI2000] is introduced in chapter 6. It is shown that with the help of this concept, the different geometries of the cable system as well as different dependencies in time can be subsumed into one network of quadrupoles. The calculation of the thermal quadrupoles for each element is presented, together with the procedure to calculate the cable conductor temperature (from which the ampacity can be derived) in a fast and exact manner that is not subjected to restrictions regarding geometries or dependencies in time. This is due to the fact that for complicated geometries such as configurations of multiple cables inside non-homogenous beddings, the required thermal spectra can be calculated numerically and then be integrated into the quadrupole approach.

Turning the attention to the impact of the heat that is injected from the cable into the bedding, chapter 6 shows the conclusion that can be drawn from an interdisciplinary project from the High Voltage Laboratories and the Geothermal Science and Technology at TU Darmstadt. It is shown that the diffusion processes can be modelled based on three soil specific characteristics: the volumetric water content as a function of the pressure head (also known as retention curve), the hydraulic conductivity as a function of volumetric water content and the thermal conductivity as a function of the volumetric water content. Based on these characteristics, the temperature dependent thermal conductivity of 31 soil types (specified in [E-DIN4220]) was derived, using a numerical model that has been validated through extensive laboratory tests [DRE2016]. Considering these results, it becomes evident that the hitherto assumed parameters of the two-zone models are very, not to say too conservative.

With respect to deriving a soil specific thermal model, it was also shown that the results are very sensitive to both, the ambient saturation level as well as the hydraulic conductivity of the bedding. While the ambient saturation level highly depends on the environmental and climatic conditions during the year, the hydraulic conductivity is highly dependent on the in-situ compactness, hard to measure, and it may already be changed by the extraction of a suitable probe. The final conclusion may therefore seem disillusioning: In the eyes of the author, a tangible, soil specific thermal model of the bedding is not practicable – on the base of the approximated soil specifics from [E-DIN4220]. It is therefore necessary to cover the diversity of soil characteristics alongside a cable route through measurements and – if necessary – to use thermally stabilized backfill material that would guarantee a minimum value of heat conductivity.

Whereas for this work, the drying-out of the soil is still assumed stationary and implemented into the quadrupole approach via a numerically determined thermal impedance, the fact that the effort of determining the soil characteristics more specifically is worth undertaking is also demonstrated by the examination of the transient heating of the cable: By assuming a dynamic model of the drying-out, the emergency rating can be expanded considerably, both in time and amplitude. Moreover, it is shown that the inclusion of the regeneration of soils due to precipitation can lead the way towards an indirect online monitoring of cable routes.

Considering the extensive research that has been conducted in the field of power cable ampacity rating until now, it is worth closing this resumé by pointing out the proper achievements of this work:

- In chapter 4, solutions for the thermal equation in all relevant geometries (cylinder, hollow cylinder and bipolar-cylindrical) for all three dependencies of time (stationary, periodic and transient) are presented.
- In chapter 5, the principle of thermal quadrupoles was applied for the first time to the calculation of ampacity ratings. For this purpose, the exact matrices of the thermal quadrupoles and the parameters of the associated thermal equivalent circuit diagrams for all elements of a

cable system are derived. Moreover, the extension of the calculation of one single cable to the representation of configurations that consist of multiple cable systems as a matrix form is shown. The thermal coupling between the systems in arbitrary configurations inside a non-homogenous bedding is incorporated with the help of numerically deduced thermal spectrums.

The result is a methodology that enables a fast and exact calculation of every possible configuration for every load dependency of time (considering a static drying-out). This innovative approach has been implemented successfully in the framework of a cooperation with a German distribution system operator. It is applicable to low and medium as well as high voltage cable systems.

- In chapter 6, the focus is turned to the refined implementation of the complex behaviour of soils into ampacity calculation. This englobes the following innovations:
 - Examination of the validity regarding the existing procedures to calculate the critical temperature for the two-zone model
 - Illustration of the temperature dependency of the diffusion coefficients of heat and mass inside soils and their evaluation with respect to the impact of the maximum temperature, the ambient water content and the hydraulic conductivity of the soil.
 - Validation of the assumption of a “fresh” ambient water content with the help of a verified seasonal simulation of evapotranspiration for all soil types mentioned in [EDIN4220]
 - Simulation of the temperature dependent thermal conductivity for all soil types mentioned in [EDIN4220]
 - Comparison of the transient heating of cable systems between the results of the implementation of the dynamic soil drying-out, the static drying out and the dynamic, temperature dependent thermal conductivity.

8.2 Outlook

In the sense that this work aims primarily at laying the foundations of a fast and tangible methodology for the calculation of ampacity ratings, the possibilities of refinements are abundant: This includes the insertion of the impact of cable crossings or the laying in protection pipes [BAL2015-1] into the general network. But most importantly, the inclusion of the dynamic changes of the soil properties into quadrupole grids, whether they are caused by climatic changes or the heat injection from the cable, represents the biggest challenge to come. This will open the door for a truly universal tool, including not only all possible dependencies of time with respect to the load flow, but also the dependency of time for the natural conditions.

The inclusion of the dynamically changing properties of the bedding into the thermal quadrupole approach also necessitates further research in the domain of the physical understanding of heat and mass transport mechanisms within soils. First and foremost, the inclusion of the hysteresis regarding the relation between the hydraulic height and the water content should be included in numerical simulations in order to fully evaluate the impact of fluctuations of the ambient water content. Also, the inclusion of an exact formulation of the vapour permeability (instead of the reduction factors proposed by [KEMA1981]) is worth considering. Furthermore, little is known about the thermal contact resistance between the outer surface of the cable and its bedding: Due to the loss in water content, shrinkage may appear in cohesive soils, leading to air pockets between the surface of the outer jacket and the bedding. Keeping in mind the mechanical stresses that go along with the distortion of the

cable system under a fluctuating temperature, it is worth considering to evaluate these supplemental thermal resistances at the boundary between cable and bedding.

And finally, from the perspective of the grid operator, the effects of higher cable temperatures, which appear as a consequence of higher ampacity rating, must be evaluated. This includes the cost of higher ohmic losses as well as possible ramifications of the ageing of the equipment – both for the cable systems as well as for joints and other devices inside the grid.

Appendix

In the following section, additional information to the presented work is provided. This includes the calculation of the used fundamental systems, soil parameters from E-DIN4220 as well as details of the calculation of the diffusion coefficients.

A1 Additional information to relevant fundamental systems

With respect to chapter 4.4.2, relevant fundamental system are derived in the following. They are sorted by the values of the function $u(x)$ and $v(x)$ in equation (4.120), as an example, the resulting fundamental systems are drawn with $\varsigma_1 = 1$ and $\varsigma_2 = 1$.

A1.1 $u(x) = 0$ and $v(x) = 0$

The resulting equation is

$$\frac{\partial^2 f_h(x)}{\partial x^2} = 0 \quad (\text{A.1})$$

In this case, the solution follows directly by integrating equation (9.1) twice to be

$$f_h(x) = \varsigma_1 \cdot x + \varsigma_2 \quad (\text{A.2})$$

The system from equation (A.2) is drawn in Figure A.1 for $\varsigma_1 = \varsigma_2 = 1$.

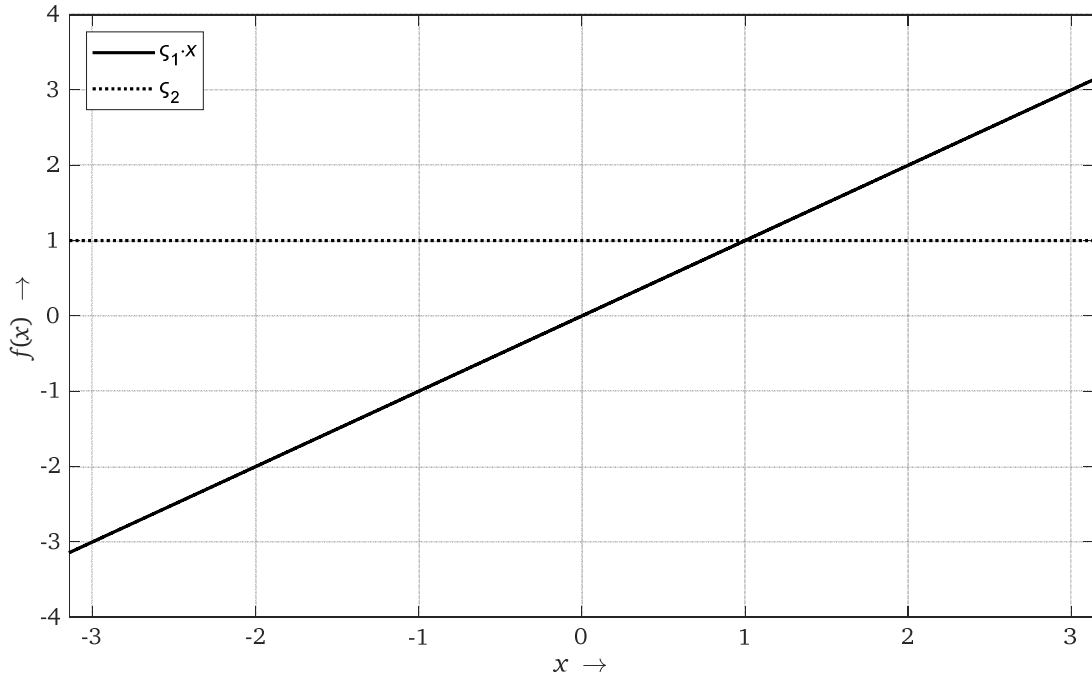


Figure A1: Fundamental system from equation (A.1) with $\varsigma_1 = 1$ and $\varsigma_2 = 1$

A1.2 $u(x) = c(x)$ and $v(x) = 0$

The resulting equation is

$$\frac{\partial^2 f_h(x)}{\partial x^2} + c(x) \cdot \frac{\partial f_h(x)}{\partial x} = 0 \quad (\text{A.3})$$

In this case, a substitution of variables, i.e.

$$\frac{\partial f_h(x)}{\partial x} = f_h^*(x) \quad (\text{A.4})$$

reduces equation (A.3) to a first order differential equation. Hence, the solution can again be obtained by integration

$$\frac{\partial f_h^*(x)}{\partial x} + c(x) \cdot f_h^*(x) = 0 \quad (\text{A.5})$$

Integrating yields

$$f_h^*(x) = \varsigma_1 \cdot \exp \left[- \int_{x_0}^x \varsigma(x') dx' \right] \quad (\text{A.6})$$

or, with respect to $f_h(x)$

$$f_h(x) = \varsigma_1 \cdot \int \exp \left[- \int_{x_0}^{x'} \varsigma(x'') dx'' \right] dx' + \varsigma_2 \quad (\text{A.7})$$

Taking

$$c(x) = \frac{1}{x} \quad (\text{A.8})$$

As an example, equation (A.7) yields

$$f_h(x) = \varsigma_1 \ln(x) + \varsigma_2 \quad (\text{A.9})$$

The system from equation (A.9) is drawn in Figure A.2 for $\varsigma_1 = \varsigma_2 = 1$.

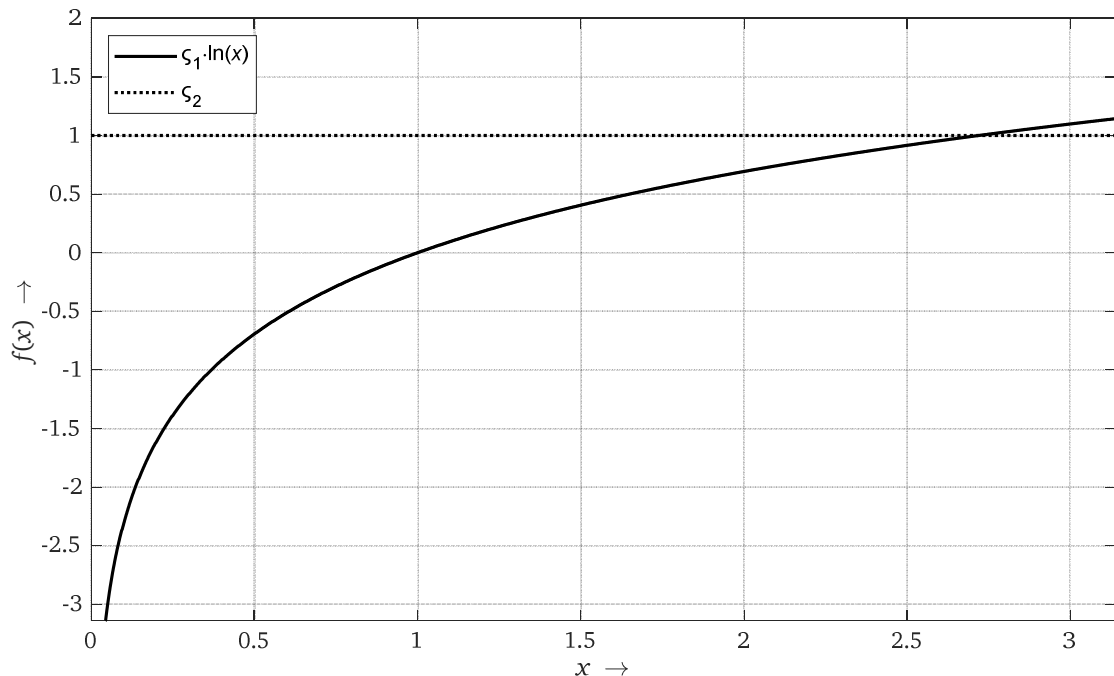


Figure A2: Fundamental system from equation (A.9) with $\varsigma_1 = 1$ and $\varsigma_2 = 1$

A1.3 $u(x) = 0$ and $v(x) = -\beta^2$

The resulting equation is

$$\frac{\partial^2 f_h(x)}{\partial x^2} - \beta^2 \cdot f_h(x) = 0 \quad (\text{A.10})$$

Reformulation as in equation (4.125) yields

$$\vec{f}_h' = \begin{pmatrix} 0 & 1 \\ \beta^2 & 0 \end{pmatrix} \cdot \vec{f}_h = 0 \quad (\text{A.11})$$

Hence, the Eigenvalues are

$$\xi_1 = \beta \quad \xi_2 = -\beta \quad (\text{A.12})$$

with the corresponding Eigenvectors

$$\vec{\xi}_1 = \begin{pmatrix} 1 \\ \beta \end{pmatrix} \quad \vec{\xi}_2 = \begin{pmatrix} 1 \\ -\beta \end{pmatrix} \quad (\text{A.13})$$

Therefore, the solution of (A.11) is

$$\vec{f}_h = e^{\beta \cdot x} \begin{pmatrix} 1 \\ \beta \end{pmatrix} + e^{-\beta \cdot x} \begin{pmatrix} 1 \\ -\beta \end{pmatrix} \quad (\text{A.14})$$

so that fundamental system can be written as

$$f_h(x) = \xi_1 \cdot e^{\beta \cdot x} + \xi_2 \cdot e^{-\beta \cdot x} \quad (\text{A.15})$$

Sometimes, the formulation of equation (A.15) by hyperbolic functions is more appropriate for bounded domains. In this case, it is

$$\xi_1 \cdot \cosh(\beta \cdot x) + \xi_2 \cdot \sinh(\beta \cdot x) \quad (\text{A.16})$$

The system from equation (A.9) is drawn in Figure A.3 for $\xi_1 = \xi_2 = 1$ as well as $\beta = 1$.

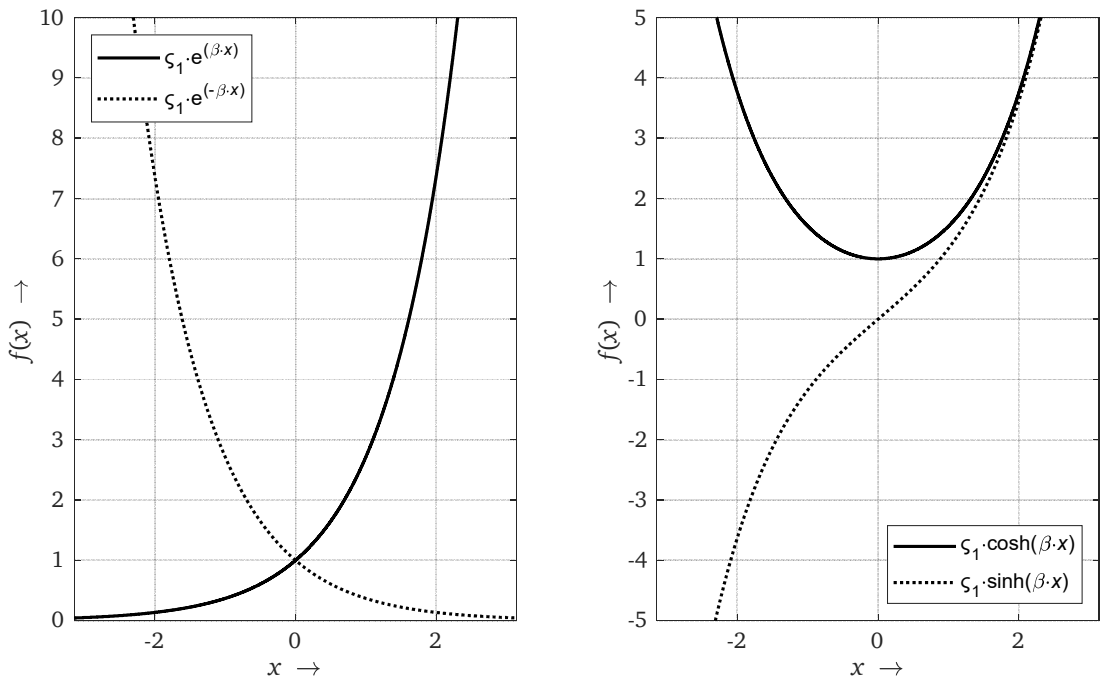


Figure A3: Fundamental system from equation (A.15), left, and (A.16), right, with $\xi_1 = 1$, $\xi_2 = 1$ and $\beta = 1$

A1.4 $u(x) = 0$ and $v(x) = +\beta$

The resulting equation is

$$\frac{\partial^2 f_h(x)}{\partial x^2} + \beta^2 \cdot f_h(x) = 0 \quad (\text{A.17})$$

Reformulation as in equation (4.125) yields

$$\vec{f}_h' = \begin{pmatrix} 0 & 1 \\ -\beta^2 & 0 \end{pmatrix} \cdot \vec{f}_h = 0 \quad (\text{A.18})$$

Hence, the Eigenvalues are

$$\underline{\xi}_1 = j \cdot \beta \quad \underline{\xi}_2 = -j \cdot \beta \quad (\text{A.19})$$

with the corresponding Eigenvectors

$$\underline{\xi}_1 = \begin{pmatrix} 1 \\ j \cdot \beta \end{pmatrix} \quad \underline{\xi}_2 = \begin{pmatrix} 1 \\ -j \cdot \beta \end{pmatrix} \quad (\text{A.20})$$

Therefore, the solution of (A.18) is

$$\vec{f}_h = e^{\beta \cdot x} \begin{pmatrix} 1 \\ \beta \end{pmatrix} + e^{-\beta \cdot x} \begin{pmatrix} 1 \\ -\beta \end{pmatrix} \quad (\text{A.21})$$

so that fundamental system can be written as

$$\vec{f}_h = e^{j \cdot \beta \cdot x} \left[\begin{pmatrix} 1 \\ 0 \end{pmatrix} + j \cdot \begin{pmatrix} 0 \\ \beta \end{pmatrix} \right] + e^{-j \cdot \beta \cdot x} \left[\begin{pmatrix} 1 \\ 0 \end{pmatrix} + j \cdot \begin{pmatrix} 0 \\ -\beta \end{pmatrix} \right] \quad (\text{A.22})$$

The real part of (A.22) is

$$\Re(\vec{f}_h) = \begin{pmatrix} \cos(\beta \cdot x) \\ -\beta \cdot \sin(\beta \cdot x) \end{pmatrix} + \begin{pmatrix} \sin(\beta \cdot x) \\ \beta \cdot \cos(\beta \cdot x) \end{pmatrix} \quad (\text{A.23})$$

So that the real fundamental system is

$$f_h(x) = \varsigma_1 \cdot \cos(\beta \cdot x) + \varsigma_2 \cdot \sin(\beta \cdot x) \quad (\text{A.24})$$

which is given in Figure A4 for $\varsigma_1 = \varsigma_2 = 1$ as well as $\beta = 1$.

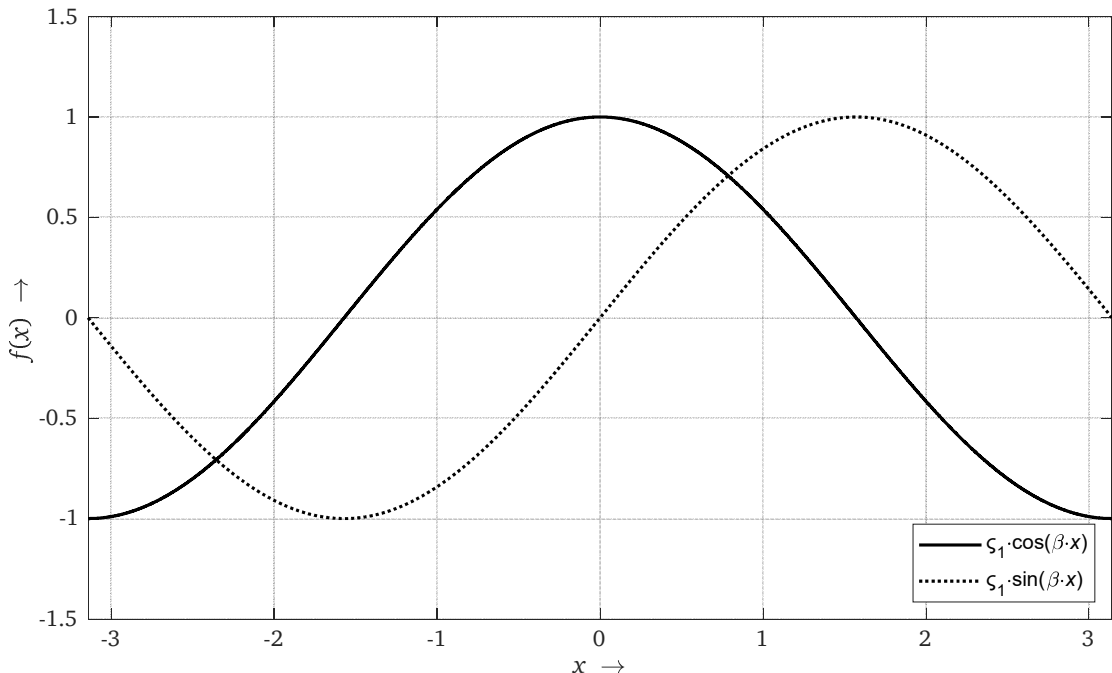


Figure A3: Fundamental system from equation (A.24) with $\varsigma_1 = 1$, $\varsigma_2 = 1$ and $\beta = 1$

A1.5 $u(x) = x^{-1}$ and $v(x) = \beta^2 - n^2 \cdot x^{-2}$

The fundamental system of the resulting equation is

$$\frac{\partial^2 f_h(x)}{\partial x^2} + \frac{1}{x} \cdot \frac{\partial f_h(x)}{\partial x} + \left[\beta^2 - \left(\frac{n}{x} \right)^2 \right] f_h(x) = 0 \quad (\text{A.25})$$

can be found by a power series solution to be

$$f_h(x) = \varsigma_1 \cdot J_n(\beta \cdot x) + \varsigma_2 \cdot Y_n(\beta \cdot x) \quad (\text{A.26})$$

With:

J_n : Bessel function of first kind of order n

Y_n : Bessel functions of second kind of order n .

Regarding the derivations of zero order, it is

$$\frac{d}{dx} \{J_0(\beta \cdot x)\} = -\beta \cdot J_1(x) \text{ and } \frac{d}{dx} \{Y_0(x)\} = -\beta \cdot Y_1(x) \quad (\text{A.27})$$

In the same manner in which the system from equation (A.15) has been reformulated to equation (A.16), the system from (A.26) with $\varsigma_1 = 1$ und $\varsigma_2 = \pm j$ is subsumed by the so-called Hankel-functions. In this case, it is

$$H_n^{(1)}(\beta \cdot x) = J_n(\beta \cdot x) + j \cdot Y_n(\beta \cdot x) \quad (\text{A.30})$$

$$H_n^{(2)}(\beta \cdot x) = J_n(\beta \cdot x) - j \cdot Y_n(\beta \cdot x) \quad (\text{A.31})$$

Where:

$H_n^{(1)}$: Hankel function of first kind of order n

$H_n^{(2)}$: Hankel function of second kind of order n

The real parts from the fundamental system in equation (A.26), (A.30) and (A.31) for order zero and one are shown in Figure A4 $\varsigma_1 = \varsigma_2 = 1$ as well as $\beta = 1$.

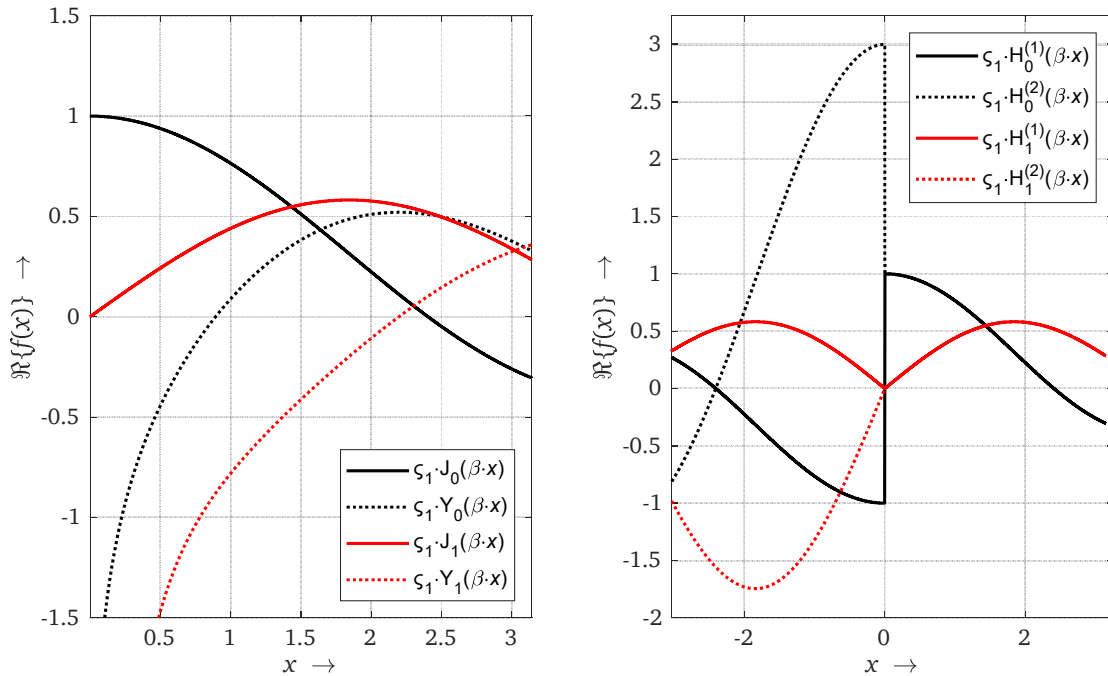


Figure A4: Fundamental system from equation (A.26), left, and (A.30) and (A.31), right, with $\varsigma_1 = 1$, $\varsigma_2 = 1$ and $\beta = 1$

A1.6 $u(x) = x^{-1}$ and $v(x) = n^2 \cdot x^2 - \beta^2$

In analogy to equation (A.26), the fundamental solution of

$$\frac{\partial^2 f_h(x)}{\partial x^2} + \frac{1}{x} \cdot \frac{\partial f_h(x)}{\partial x} - \left[\beta^2 + \left(\frac{n}{x} \right)^2 \right] f_h(x) = 0 \quad (\text{A.32})$$

can be given by

$$f_h(x) = \varsigma_1 \cdot I_n(\beta \cdot x) + \varsigma_2 \cdot K_n(\beta \cdot x) \quad (\text{A.33})$$

With:

I_n : Modified Bessel function of first kind of order n

K_n : Modified Bessel functions of second kind of order n .

The relation between the modified and the regular Bessel functions is given by

$$I_n(\beta \cdot x) = \frac{1}{j} J_n(j\beta \cdot x) \quad (\text{A.34})$$

$$K_n(\beta \cdot x) = \frac{\pi}{2} \cdot j^{n+1} H_n^{(1)}(j\beta \cdot x) = \frac{\pi}{2} \cdot (-j)^{n+1} H_n^{(2)}(-j\beta \cdot x) \quad (\text{A.35})$$

The derivations of functions of order zero is

$$\frac{d}{dx} \{I_0(\beta \cdot x)\} = \beta \cdot I_1(x) \text{ and } \frac{d}{dx} \{K_0(x)\} = -\beta \cdot K_1(x) \quad (\text{A.36})$$

The real parts from the fundamental system in equation (A.33) for order zero and one are shown in Figure A5 $\varsigma_1 = \varsigma_2 = 1$ as well as $\beta = 1$.

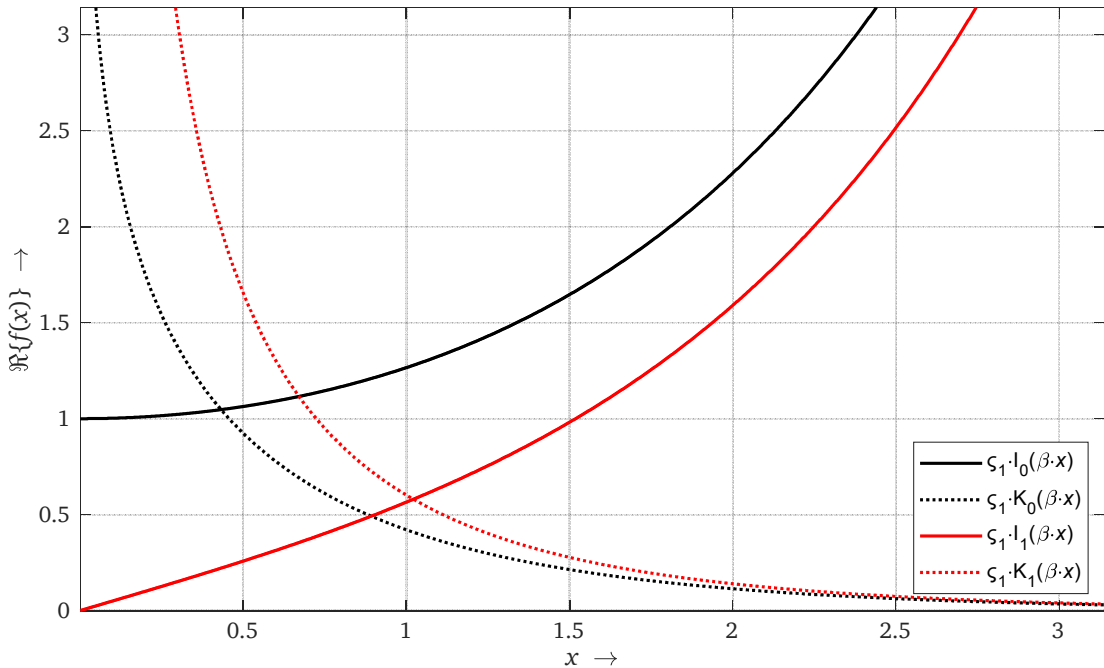


Figure A5: Fundamental system from equation (A.33) with $\varsigma_1 = 1$, $\varsigma_2 = 1$ and $\beta = 1$

A2 Van Genuchten parameters from E-DIN 4220

Soil type	θ_R	θ_R	α_{Gen} in $\frac{1}{\text{hP}}$	n	τ	k_{sat} in $\frac{\text{cm}}{\text{d}}$
Ss	0	0.388	0.264	1.352	-0.59	512.1
Sl2	0	0.395	0.116	1.254	0.00	192.9
Sl3	0.051	0.395	0.071	1.351	0.00	89.8
Sl4	0	0.410	0.105	1.184	-3.24	141.3
Slu	0	0.414	0.082	1.177	-3.92	109.5
St2	0	0.405	0.485	1.188	-6.19	420.4
St3	0	0.421	0.180	1.132	-3.42	305.8
Su2	0	0.379	0.204	1.235	-3.34	285.5
Su3	0	0.377	0.089	1.214	-3.61	119.9
Su4	0	0.384	0.060	1.222	-3.74	83.3
Ls2	0.106	0.424	0.077	1.221	-2.07	38.4
Ls3	0.034	0.416	0.111	1.157	-3.23	98.2
Ls4	0.025	0.417	0.130	1.159	-3.60	169.9
Lt2	0.149	0.438	0.070	1.246	-3.18	62.5
Lt3	0.163	0.453	0.049	1.170	-4.10	44.3
Lts	0.115	0.433	0.034	1.194	0.00	52.0
Lu	0.053	0.428	0.043	1.165	-3.23	82.7
Uu	0	0.403	0.014	1.213	-0.56	33.8
Uls	0	0.399	0.023	1.198	-2.04	40.2
Us	0	0.395	0.027	1.224	-2.73	35.5
Ut2	0.010	0.400	0.019	1.221	-1.38	29.3
Ut3	0.005	0.403	0.017	1.207	-1.20	27.7
Ut4	0.028	0.416	0.017	1.205	-0.77	24.6
Tt	0	0.524	0.066	1.052	0.00	154.7
Tl	0	0.493	0.073	1.063	0.00	172.5
Tu2	0	0.497	0.072	1.061	0.00	178.7
Tu3	0	0.459	0.055	1.082	0.00	123.8
Tu4	0.017	0.437	0.045	1.120	0.00	88.6
Ts2	0	0.484	0.084	1.077	0.00	249.9
Ts3	0.078	0.437	0.062	1.146	0.00	118.0
Ts4	0	0.436	0.209	1.114	-7.61	322.3
fS,fSms,fSgs	0	0.410	0.150	1.336	-0.33	285.1
mS,mSfs,mSgs	0	0.389	0.261	1.353	-0.58	507.5
gS	0	0.377	0.221	1.466	+1.38	872.6

A3 Estimation of bulk density from E-DIN 4220

Soil type	ρ_b for LD = 3
Ss	1.63
Sl2	1.60
Sl3	1.58
Sl4	1.55
Slu	1.54
St2	1.59
St3	1.54
Su2	1.62
Su3	1.60
Su4	1.59
Ls2	1.50
Ls3	1.51
Ls4	1.52
Lt2	1.46
Lt3	1.41
Lts	1.45
Lu	1.48
Uu	1.54
Uls	1.53
Us	1.57
Ut2	1.52
Ut3	1.50
Ut4	1.47
Tt	1.26
Tl	1.35
Tu2	1.35
Tu3	1.41
Tu4	1.44
Ts2	1.37
Ts3	1.44
Ts4	1.49

A4 Derivation of the diffusion coefficients

The diffusion coefficients determine the resulting distribution of humidity around a power cable during operation. Hence, special diligence must be paid in their computation, which is therefore illustrated in detail below.

A4.1 Diffusion coefficients of water

Using the pressure head as the state variable, the diffusion coefficient of liquid water due to the gradient of the latter equals the hydraulic conductivity

$$D_{l,h_{hy}} = k \quad (\text{A.37})$$

If, however, the water content shall act as the state variable, the expression of the diffusion coefficients is derived with the help of the chain rule. Starting from equation (4.36) and omitting the gravity term, we get

$$\vec{m}_l = -\rho_w D_{l,h_{hy}} \cdot \text{grad } h_{hy} \quad (\text{A.38})$$

Deriving equation (A.38) leads to

$$\text{grad } h_{hy} = \text{grad } h_{hy}(\theta_l, T) = \frac{\partial h_{hy}}{\partial \theta_l} \cdot \text{grad } \theta_l + \frac{\partial h_{hy}}{\partial T} \cdot \text{grad } T \quad (\text{A.39})$$

Inserting (A.39) into (A.38) yields

$$\vec{m}_l = -\rho_w D_{l,h_{hy}}(\vec{r}, t) \cdot \left(\frac{\partial h_{hy}}{\partial \theta_l} \cdot \text{grad } \theta_l + \frac{\partial h_{hy}}{\partial T} \cdot \text{grad } T \right) \quad (\text{A.40})$$

or

$$\vec{m}_l = -\rho_w (D_{l,\theta_l} \cdot \text{grad } \theta_l + D_{l,T} \cdot \text{grad } T) \quad (\text{A.41})$$

Comparing equation (A.41) with (A.40) leads to

$$o = \frac{\partial h_{hy}}{\partial \theta_l} \cdot D_{l,h_{hy}} \quad D_{l,h_{hy}} = \frac{\partial \theta_l}{\partial h_{hy}} \cdot D_{l,\theta_l} \quad (\text{A.42})$$

$$D_{l,T} = \frac{\partial h_{hy}}{\partial T} \cdot D_{l,h_{hy}} \quad (\text{A.43})$$

A4.2 Diffusion coefficients of vapour

The driving force of movements of water vapour are differences in the partial pressure of water vapour. Hence

$$\vec{m}_v(\vec{r}, t) = -D(T) \frac{p}{p - p_v} \cdot \frac{M}{R \cdot T} \text{grad } p_v \quad (\text{A.44})$$

Where:

$D(T)$: Diffusion coefficient of water vapour in air

p_v : Partial pressure of vapour

M : Molar mass of water

R : Universal gas constant

With respect to the diffusion coefficient of vapour, the relation in [VRI1967] is used to express the dependency of the temperature

$$D(T) = 21.1 \cdot 10^{-6} \cdot \left(\frac{T}{273.15 \text{ K}} \right)^{1.88} \quad (\text{A.45})$$

The partial pressure of water vapor can – as it is assumed to be saturated – be expressed as the product of the saturated water vapor pressure and a factor h_{rel} that represents the forces exerted by the advection forces. Hence

$$p_v = h_{\text{rel}} \cdot p_v^{\text{sat}} \quad (\text{A.46})$$

where

$$h_{\text{rel}} = e^{\frac{M \cdot g \cdot h_{\text{hy}}}{R \cdot T}} \quad (\text{A.47})$$

Regarding the saturation pressure, the Magnus formula can be used

$$p_v^{\text{sat}} = 611.2 \cdot e^{\frac{17.52 \cdot (T - 273.15 \text{K})}{T - 30.03 \text{K}}} \quad (\text{A.48})$$

Hence, partial pressure of water vapor is also a formula of the pressure head and temperature

$$p_v = f(h_{\text{hy}}, T) \quad (\text{A.49})$$

Therefore, the gradient in equation (A.44) can be written in terms of these state variables

$$\text{grad } p_v(h_{\text{hy}}, T) = \frac{\partial p_v}{\partial h_{\text{hy}}} \text{grad } h_{\text{hy}} + \frac{\partial p_v}{\partial T} \text{grad } T \quad (\text{A.50})$$

Inserting equation (A.50) into (A.44) leads to

$$\vec{m}_v = -D(T) \frac{p}{p-p_v} \cdot \frac{M}{R \cdot T} \left(\frac{\partial p_v}{\partial h_{\text{hy}}} \text{grad } h_{\text{hy}} + \frac{\partial p_v}{\partial T} \text{grad } T \right) \quad (\text{A.51})$$

so that

$$D'_{v,h_{\text{hy}}} = \frac{1}{\rho_l} \cdot D(T) \cdot \frac{p}{p-p_v} \cdot \frac{M}{R \cdot T} \cdot \frac{\partial p_v}{\partial h_{\text{hy}}} \quad (\text{A.52})$$

$$D'_{v,T} = \frac{1}{\rho_l} \cdot D(T) \cdot \frac{p}{p-p_v} \cdot \frac{M}{R \cdot T} \cdot \frac{\partial p_v}{\partial T} \quad (\text{A.53})$$

In analogy to the formulation of flow of liquid water, the volumetric water content can also be expressed in terms of the gradient of volumetric water content and temperature. Comparing the two expressions leads to

$$D^*_{v,\theta_l} = \frac{\partial h_{\text{hy}}}{\partial \theta_l} \cdot D'_{v,h_{\text{hy}}} \quad D'_{v,h_{\text{hy}}} = \frac{\partial \theta_l}{\partial h_{\text{hy}}} \cdot D^*_{v,\theta_l} \quad (\text{A.54})$$

$$D^*_{v,T} = \frac{\partial h_{\text{hy}}}{\partial T} \cdot D'_{v,h_{\text{hy}}} + D'_{v,T} \quad D'_{v,T}(\vec{r}, t) = \frac{\partial \theta_l}{\partial T} \cdot (D^*_{l,\theta_l} + D^*_{v,\theta_l}) + D^*_{l,T} + D^*_{v,T} \quad (\text{A.55})$$

With respect to the vapor transport, [KEM1981] proposed to acknowledge the effect of the porespace via two reduction factors: First of all, it must be taken into account that the presence of water inside the pores restricts the movement of vapor in comparison to the free diffusion that is described by (A.44). Or, in other words, if the pore space is completely full of water, there can be no diffusion of vapour. Hence, a factor F is introduced with

$$F(\theta_l) = \begin{cases} \varepsilon_{\text{soil}} & \text{for } \theta_l < \theta_{\text{crit}} \\ \varepsilon_{\text{soil}} - \theta_l + \theta_l \cdot \frac{\varepsilon_{\text{soil}} - \theta_l}{\varepsilon_{\text{soil}} - \theta_{\text{crit}}} & \text{for } \theta_l > \theta_{\text{crit}} \end{cases} \quad (\text{A.56})$$

Where

θ_{crit} : Critical water content

For the sake of simplicity, the porosity in equation (A.56) can be changed to the saturation water content θ_s . The mentioned critical water content is widely defined as the value of water content, where the water bridges between the soil particles break up and hydraulic conductivity diminishes abruptly. In order to quantify this value, two possibilities arise: It may be possible to define this value with the help of the relation between the thermal resistivity and the water content, as it is proposed by [CIG1992], stating that the critical saturation is reached when the thermal resistivity is at 110 % of the value at saturation. This, however, does not seem a very tangible criterion, taking into account the flat curves of loamy and silt soils. More tangible seems a definition that is orientated at the hydraulic conductivity, although the actual value is also open to a discussion. Referring to the curves in Figure A6, a value of $10^{-12} \text{ m}\cdot\text{s}^{-1}$ seems plausible and will be chosen in the following.

Secondly, as the gradient of temperature inside the air is generally higher than the gradient inside the solid grain structure due to the lower thermal conductivity, [KEM1981] proposes a factor G

$$G = 1.5 \dots 3 \quad (\text{A.57})$$

In theory, it may be possible to derive a plausible value of G by the connection between the vapor diffusion coefficient due to gradients of temperature and the thermal conductivity. However, as it is shown in Figure A6, the actual value is of little importance to the overall results. Hence, the computation should not be made deliberately complicated, and a value of $G = 2.25$ is chosen for all soils.

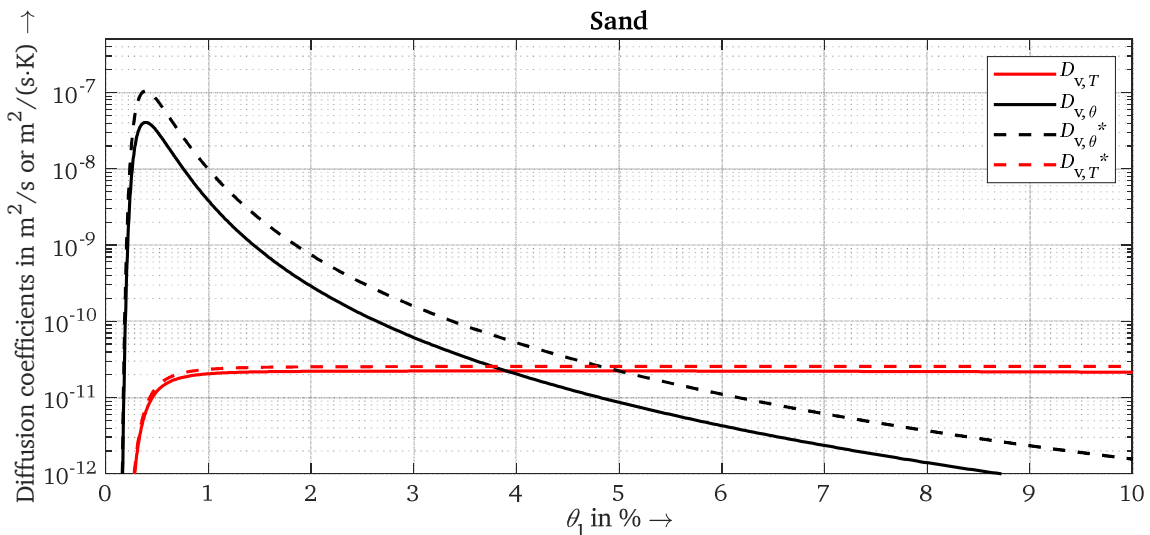


Figure A6: Illustration of the effect of the correction factors F and G from equations (A.56) and (A.57) on the diffusion coefficients of the sand "Ss" with the parameters specified by [E-DIN4220]

Hence, the final diffusion coefficients for the volumetric water content as state variable can be written as

$$D_{v,\theta_1}^{**} = F(\theta_1) \cdot D_{v,\theta_1}^*(\vec{r}, t) \quad (\text{A.58})$$

$$D_{v,T}^{**}(\vec{r}, t) = G \cdot F(\theta_1) \cdot D_{v,T}^*(\vec{r}, t) \quad (\text{A.59})$$

From the results of equations (A.58) and (A.59), the coefficients with the hydrostatic potential as state variable can be derived from the expressions in (A.54) and (A.55).

A5 On the temperature dependency of the retention curve and hydraulic conductivity

In contrast to many other studies, the temperature dependency of the soil characteristic is also implemented in the framework of the presented simulation. Regarding the water retention curve, differences of the surface tension of water have an effect on the retention capability of the soil. Therefore, with respect to the hydraulic potential at a given water content, one may write [DÖR1994]

$$h_{hy}(\theta_l, T) = \frac{\sigma(T)}{\sigma(T_{ref})} \cdot h_{hy,ref}(\theta_l) \quad (\text{A.60})$$

Where:

$\sigma(T)$: Surface tension of water

$$\sigma(T) = 0.0728 \cdot (1 - 0.002 \cdot [T - 293.15 \text{ K}]) \quad (\text{A.61})$$

As a consequence, the temperature dependency of the inverse function of equation (A.60), i.e. the water content as a function of the hydraulic potential, can be written as

$$\theta_l(h_{hy}, T) = \theta_{l,ref} \left(\frac{\sigma(T_{ref})}{\sigma(T)} \cdot h_{hy} \right) \quad (\text{A.62})$$

With respect to the hydraulic conductivity, the temperature dependency of the viscosity and density of water was included, following the proposition of [19]

$$k(\theta, T) = \frac{\eta(T_{ref})}{\eta(T)} \cdot k_{ref}(\theta) \quad (\text{A.63})$$

where

$$\eta(T) = 0.02414 \cdot 10^{247.8 \cdot (T - 140.15)^{-1}} \quad (\text{A.64})$$

As an example of the importance of temperature on the resulting diffusion coefficients, the latter are illustrated for the three monofractional soils in Figure A7 for two different temperatures.

A6 Diffusion coefficients as a function of the hydraulic height

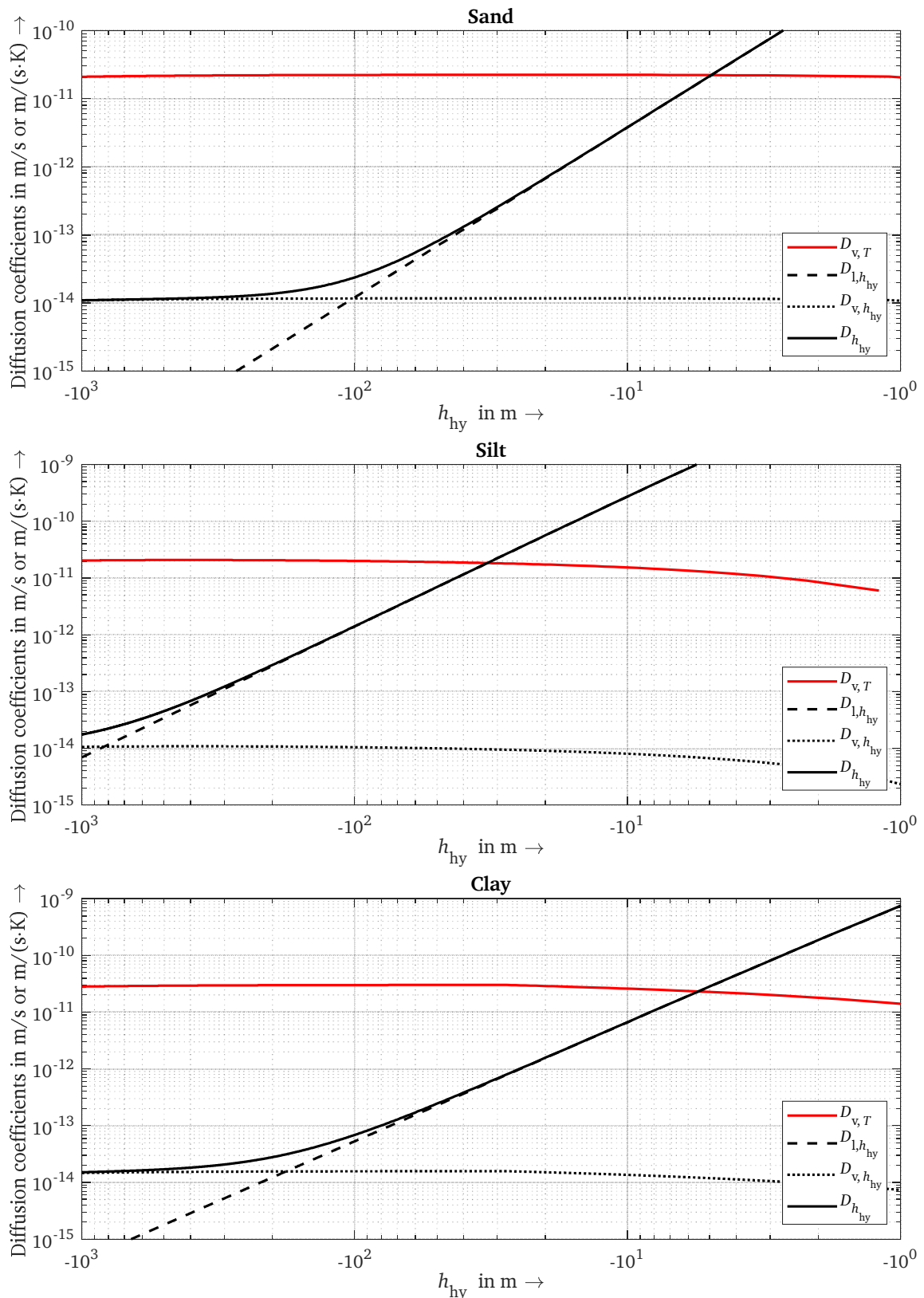


Figure A7: Diffusion coefficients as a function of the hydraulic height of the sand "Ss", silt "Uu" and clay "Tt" with the parameters specified by [E-DIN4220]

Bibliography

- [ALB2005] Abizu, I.; Mazón, A. J.; Zamora, I.: Methods for increasing the rating of overhead lines. IEEE Power Tech Conference, June 27th – 30th, St. Petersburg, 2005
- [AND1988] Anders, G. J.; Radhakrishna, H.S.: Power Cable Thermal Analysis with Consideration of Heat and Moisture Transfer in Soil
- [AND1997] Anders, G.J.: Rating of electric power cables – Ampacity Computations for Transmission, Distribution and Industrial Application. McGraw-Hill, New York and IEEE Press, New York, 1997
- [AND2003] Anders, G.J.; Napieralski, A., Zubert, M.; Orlikowski, M.: Advanced modeling techniques for dynamic feeder rating systems, IEEE Trans. on Industry Applications May-June 2003, Vol. 39, Issue 3, pp. 619-626
- [BAC1992] Bach, L. B.: Soil Water Movement in Response to Temperature Gradients: Experimental Measurements and Model Evaluation. Soil Science Society of America Journal, vol. 56, no. 1, 1992
- [BAL2009] Balzer, Gerd: Energieversorgung I, Vorlesungsskript TU Darmstadt. 2009
- [BAL2016] Balzer, Gerd; Neumann, Claus: Schalt- und Ausgleichsvorgänge in elektrischen Netzen, 1. Auflage, Springer Vieweg Verlag, Berlin, Heidelberg, 2016
- [BEY1985] Beyer, U.: Berechnung transienter Kabelerwärmungen unter Berücksichtigung möglicher Bodenaustrocknung. Dissertation, Technische Universität Darmstadt
- [BLU2011] Blume, H.-P.; Stahr, K.; Leinweber, P.: Bodenkundliches Praktikum. 3rd edition, Spektrum Verlag Heidelberg, 2010.
- [BRA1985] Brakelmann, H.: Belastbarkeiten der Energiekabel - Berechnungsmethoden und Parameteranalysen. VDE-Verlag GmbH, Berlin und Offenbach, 1985
- [BUL1951] Buller, F. H.: Thermal transients on buried cables, Trans. Amer. Inst. Elect. Eng., vol. 70, no. 1, pp. 45–55, July 1951
- [CAM1994] Campbell, G.; Jungbauer, Jr.; Bidlake, W.; Hungerford, R.: Predicting the effect of temperature on soil thermal conductivity. Soil Science, Vol. 158, Issue 5, pp. 307-313, 1994
- [CAR1959] Carslaw, H.S.; Jaeger, J.C.: Conduction of Heat in Solids, 2nd Edition, Oxford University Press, Oxford, 1959
- [CIG1992] Cigré Study Committee 21 (High Voltage Insulated Cables): Determination of a value of critical temperature rise for a cable backfill material, ÉLECTRA No. 145, Dezember 1992
- [CIN1965] Cinelli, G.: An extension of the finite hankel transformation and applications, Int. J. Engineering Science, Vol 3, pp. 539-559. Pergamon Press 1965
- [COL2011] Cole, K.D.; Haji-Sheikh, A.; Beck, J.V.; Litkouhi, B.: Heat Conduction using Green's Functions. 2nd Edition, CRC Press Taylor & Francis Group, Boca Raton, 2011
- [CRC2011] Haynes, W.M; Lide, D. R.: CRC Handbook of Chemistry and Physics, 92nd Edition, CRC Press, Taylor & Francis Group, Boca Raton, 2011

- [DIN18130-1] Baugrund - Untersuchung von Bodenproben; Bestimmung des Wasserdurchlässigkeitsbeiwerts - Teil 1: Laborversuche, 1998
- [DON1979] Donazzi, F.; Occhini, E.; Seppi, A.: Soil thermal and hydrological characteristics in designing underground cables. PROC. IEE, vol. 126, No 6, June 1979
- [DÖR1994] Dörfler, H. D.: Grenzflächen- und Kolloidchemie. VCH Verlagsgesellschaft mbH, Weinheim, 1994
- [DRE2016]: Drefke, C.; Schedel, M.; Balzer, C.; Hinrichsen, V.; Sass, I.: Experimentelle Bestimmung der Dynamik von Bodenaustrocknung und der Wiederherstellung der Bodenfeuchte um Energiekabel. VDE-Fachtagung Hochspannungstechnik 2016, ES.2. Berlin, November 14th-16th. Published in: ETG Fachbericht
- [DRE2017] Drefke, C.; Schedel, M.; Stegner, J.; Balzer, C.; Hinrichsen, V.; Sass, I.: Measurement Method of Thermal Properties of Cementitious Bedding Materials and Unsaturated Soils: Hydraulic Influence on Thermal Parameters. Geotechnical Testing Journal (ISSN 01496115), 40, (1), p. 160-170, Online-Edition: <http://dx.doi.org/10.1520/GTJ20160027>
- [EBE2019] Eberg, E., Espeland, K., Hellesø, S., Hvidsten, S., Solheim, K. T.: Development of a web-based user-friendly cable ampacity calculation tool. 25th International Conference on Electricity Distribution CIRED, Madrid, 2019
- [E-DIN4220]: DIN Deutsches Institut für Normung e.V.: Bodenkundliche Standortbeurteilung – Kennzeichnung, Klassifizierung und Ableitung von Bodenkennwerten (normative und nominale Skalierungen), Beuth Verlag GmbH, Berlin, 2008- Ab November 2020 zurückgezogen und ersetzt durch: DIN 4220:2020-11: Bodenkundliche Standortbeurteilung – Kennzeichnung, Klassifizierung und Ableitung von Bodenkennwerten (normative und nominale Skalierungen).
- [FAO1998]: Allen, R. G.; Pereira, L. S.; Raes, D.; Smith, M.: FAO Irrigation and Drainage Paper No. 56. Crop Evaporation (guidelines for computing crop water requirements). FAO, Rome, 1998
- [FER1996]: Ferkal, Kamel; Poloujadoff, Michel; Dorison, Eric: Proximity effect and eddy current losses in insulated cables. IEEE Transactions on Power Delivery, Vol 11, No. 3., July 1996
- [FGH2014] Forschungsgemeinschaft für Elektrische Anlagen und Stromwirtschaft e.V. (Ed.): Planungshandbuch zur Integration von Erzeugungsanlagen in Verteilungsnetze, FGH, Mannheim, 2014
- [FRE1996] Freitas, D. S.; Prata, A.T.; de Lima A.J.: Thermal performance of underground power cables with constant and cyclic currents in presence of moisture migration in the surrounding soil. IEEE Transactions on Power Delivery, Volume 11, Issue 3, S. 1159-1170. 1996.
- [GEN1980] Van Genuchten, M. T.: A closed-form equation for predicting the hydraulic conductivity of unsaturated soils. Soil science society of America journal, 44(5), 892-898, (1980)
- [GOL1958] Goldenberg, H.: The calculation of cyclic rating factors and emergency loading for one or more cables laid direct or in ducts. Proceedings of the IEE - Part C: Monographs, vol. 105, no. 7, pp. 46-54, March 1958.

- [GOL1969] Goldenberg, H: External thermal resistance of three buried cables in trefoil touching formation, restricted application of superposition. Proc. IEE, Vol 116, No 11. November 1969.
- [GRA1957] McGrath, M. H., Neher, J.H.: The calculation of the temperature rise and load capability of cable systems. *Transactions of the American Institute of Electrical Engineers. Part III: Power Apparatus and Systems*, vol. 76, no. 3, pp. 752-764, April 1957.
- [GRO1984] Groeneveld, G.J.; Snijders, A. L.; Koopmans, G.; Vermeer, J.: Improved method to calculate the critical conditions for drying out sandy soils around power cables. IEE Proceedings C – Generation, Transmission and Distribution, vol. 131, issue 2, 1984
- [HAH2012] Hahn, David W.; Özisik, M. Necati: Heat Conduction, 3rd Edition, John Wiley & Sons, Inc., Hoboken, New Jersey, 2012
- [HOL2015] Holyk, C., Anders, G. J.: Power Cable Rating Calculations - A Historical Perspective. IEEE Industry Applications Magazine, vol. 21, no. 4, p. 6-64, 2015
- [IEC60287-1] International Electrotechnical Commission: International Standard IEC 60287-1: Electric cables – Calculation of the current rating Part 1-1: Current rating equations and calculation of losses in general, Edition 2.0, Genf, Schweiz, 2006.
- [IEC60287-2] International Electrotechnical Commission: International Standard IEC 60287-2-1: Electric cables – Calculation of the current rating Part 2-1: Thermal resistance, Edition 1.2, Genf, Schweiz, 2006.
- [IEC60853-1] International Electrotechnical Commission: International Standard IEC 60853-1: Calculation of cyclic and emergency current rating of cables Part 1: Cyclic rating factor for cables up to and including 18/30 (36)kV, First Edition, Geneva, 1985.
- [IEC60853-2] International Electrotechnical Commission: International Standard IEC 60853-2: Calculation of cyclic and emergency current rating of cables Part 2: Cyclic rating factor for cables greater than 18/30 (36) kV and emergency ratings for cables of all voltages, First Edition, Geneva, 1989.
- [IEC60853-3] International Electrotechnical Commission: International Standard IEC 60853-3: Calculation of cyclic and emergency current rating of cables Part 3: Cyclic rating factor for cables of all voltages with partial drying of the soil, First Edition, Geneva, 2002.
- [KEM1981] Snijders, A. L., Groenveld G. J., Vermeer, J., Van de Wiel, G.M.L.M. (1981): Moisture migration and drying-out in sand around heat dissipating cables and ducts, A theoretical and experimental study, Kema/Heidemij report, Heidemij, Arnhem (NL).
- [KEN1893] Kennelly, A.E.: On the carrying capacity of electric cables submerged, buried or suspended in air. Proc. Minutes 9th Annu. Meeting Association Edison Illuminating Companies, p. 79-92, 1893
- [KOO1989]: Koopmans, G.; Van de Wiel, G.M.L.M.; Van Loon, L.J.M.; Palland, C.L.: Soil physical route survey and cable thermal design procedure, in: IEE Proceedings, vol. 163, Pt. C, no.6, 1989

- [KOS1978] Kosmann, F.-J.: Versuche zur Bodenaustrocknung bei erdverlegten Kabeln. Elektrizitätswirtschaft, Jg. 77, Heft 26, 1978.
- [KÜC2011] Küchler, A.: Hochspannungstechnik, Grundlagen – Technologie – Anwendung. 3., neu bearbeitete Auflage, Springer Verlag Heidelberg, 2011
- [KÜP2006] Küpfmüller, Karl; Mathis, Wolfgang; Reibiger, Albrecht: Theoretische Elektrotechnik, 17th edition, Springer, Verlag, Berlin, Heidelberg, New York 2006
- [KRE1967] Kretz, W.: Formelsammlung zur Vierpoltheorie. R. Oldenburg Verlag, München und Wien, 1967
- [LAN2003] Langguth, H.-R., Voigt, R.: Hydrogeologische Methoden. 2. Auflage, Springer Verlag Berlin Heidelberg New York, 2003
- [LAT1995] Latour, L.L.; Kleinberg, R.L.; Mitra, P.P.; Sotak, C.H.: Pore-size distribution and tortuosity in heterogeneous porous media. Journal of magnetic resonance, series A, vol. 112, issue 1, pp.83-91, 1995
- [LEH2010] Lehner, Günther: Electromagnetic Field Theory for Engineers and Physicists, Springer Verlag Berlin, Heidelberg, 2010
- [LOG2001] Logan, D.J.: Transport Modeling of Hydrogeochemical Systems. Springer Verlag, New York, 2001
- [LU2014] Lu, Y.; Lu, S.; Horton, R.; Ren, T.: An empirical model for estimating soil thermal conductivity from texture, water content, and bulk density. Soil Science Society of America Journal. Vol. 78, no. 6, pp. 1859-1868, 2014
- [LÜC1981] Lücking, H. W.: Energiekabeltechnik. Friedr. Vieweg &Sohn Verlag Braunschweig/Wiesbaden, 1981
- [MAI1971] Mainka, G.: Berechnung der Belastbarkeit von in Erde verlegten Starkstromkabeln unter Berücksichtigung von Belastungsfaktor und Bodenaustrocknung. ETZ-A vol 92, pp. 125 – 130, 1971
- [MAI1974-1] Mainka, G.: Dosierte Bodenaustrocknung bei erdverlegten Energiekabeln Energiekabel. ETZ-A vol 95, pp. 279 – 282, 1974
- [MAI1974-2] Mainka, G.: Häufung erdverlegter Energiekabel. ETZ-A vol. 95, pp. 517 – 519, 1974
- [MAI2000] Maillet, D., André, S., Batsale, J.C., Degiovanni, A., Moyne, C. : Thermal Quadrupoles – Solving the heat equation through integral transforms. John Wiley & Sons, West Sussex, 2000
- [MAR2017] Markert, A.; Bohne, K.; Facklam, M.; Wessolek, G.: Pedotransfer Functions of Soil Thermal Conductivity for the Textural Classes Sand, Silt, and Loam. Soil Science Society of America Journal, 2017
- [MAT1987] Mathis, W.: Theorie nichtlinearer Netzwerke. Springer Verlag Berlin, Heidelberg, New York, 1987
- [MOO1971] Moon, Parry; Spencer, Domina Eberle: Field Theory Handbook, 2nd Edition, Springer Verlag, Berlin, Heidelberg, New York, 1971
- [MUA1976] Mualem, Y.: A new model for predicting the hydraulic conductivity of unsaturated porous media, Water Resour. Re., vol. 12, no. 3, pp.513-522, 1976

- [NEH1953-1] Neher, J. H.: Procedures for calculating the temperature rise of pipe cable and buried cables for sinusoidal and rectangular loss cycles . *Transactions of the American Institute of Electrical Engineers. Part III: Power Apparatus and Systems*, vol. 72, no. 3, pp. 541-562, June 1953
- [NEH1953-2] Neher, J. H.: A simplified mathematical procedure for determining the transient temperature rise of cable systems. *Transactions of the American Institute of Electrical Engineers. Part III: Power Apparatus and Systems*, vol. 72, no. 4, pp. 712-718, Aug. 1953
- [NOL2013] Nolting, W.: Grundkurs theoretische Physik 3 – Elektrodynamik. 10. Auflage, Springer Spektrum Verlag Berlin, Heidelberg, 2013
- [OLS2012] Olsen, R.S., Gudmundsdóttir, U.S.: Dynamic Temperature Estimation and Real Time Emergency Rating of Transmission Cables. IEEE Power & Energy Society General Meeting, San Diego, 2012
- [OLS2013-1] Olsen, R.: Dynamic Loadability of Cable Based Transmission Grids, Dissertation, Technical University of Denmark, 2013
- [OLS2013-2] Olsen, R.; Anders, G.J.; Holboell, J.; Gudmundsdóttir, U.S.: Modelling of dynamic transmission cable temperature considering soil specific heat, thermal resistivity and precipitation. *IEEE Transactions on Power Delivery*, vol 28, no. 3, pp. 1909-1917, July 2013
- [OLS2015] Olsen, R., Rasmussen, C., Holboell, J., Gudmundsdottir, U. S.: Electrothermal coordination in cable based transmission grids, operated under market based conditions. 9th Internation Conference on Insulated Power Cables Jicable, Versailles, 2015
- [PHI1957] Philip, J.R.; DeVries, D.A.: Moisture movement in porous materials under temperature gradients, *Trans. Amerc. Geophy. Union*, 38, S. 222-232, 1957
- [PIR1999] Pirelli Kabel und Systeme GmbH, Ed.: Heinhold, S., Stubbe, R.: Kabel und Leitungen für Starkstrom. 5. Auflage, Publicis MCD Verlag, Erlangen, 1999
- [PUR2014] Purushothaman, Sujit; de León, Francisco; Terracciano, Matthew: Calculation of cable thermal rating considering non-isothermal earth surface, *IET Generation, Transmission & Distribution*, vol 8, Iss 7, Seiten 1354-1361, 2014.
- [RAD1984] Radhakrishna, H.S.; Lau, K.-C.; Crawford, M.: Coupled Heat and Moisture flow through soils. *Journal of Geotechnical Engineering*, vol. 110 is. 12, 1984
- [ROC2009] Roch, S.: Mathematik I-III für Eiti, WI(ET) SpoInf. Vorlesungsskript TU Darmstadt. 2009
- [SCH2010] Scheffer, F., Schachtschabel, P., Blume, H.-P., Brümmer, G. W., Horn, R., Kandeler, E., Kögel-Knabner, I., Kretzschmar, R., Stahr, K., Wilke, B. M.: Lehrbuch der Bodenkunde, vol. 16, Spektrum Akademischer Verlag, Heidelberg, 2010
- [SCH2014-1] Schaum's outlines, Ed.: Nahvi, M.; Edminster, J. A.: Electric circuits, Sixth Edition. McGraw Hill Education, New York, 2014
- [SCH2014-2] Schaum's outlines, Ed.: Potter, M.C., Somerton, C.W.: Thermodynamics for Engineers, Third Edition. McGraw Hill Education, New York, 2014

- [SIE1998] Siemens AG, Berlin, Ed.: Peschke, E. F., Olshausen, R.v.: Kabelanlagen der Hoch- und Höchstspannungstechnik. Publicis Verlag Erlangen und München, 1998
- [STE2000] Stephen, R. et al.: Description of state of the art methods to determine thermal rating of lines in real-time and their application in optimising power flow. Cigre 2000, Paper No. 22-304, Paris, 2000.
- [TAL2008] Taleb, N. N.: Der Schwarze Schwan 1. Auflage, Hanser Verlag München, 2008
- [TAY1954] Taylor, S. A., & Cavazza, L.: The movement of soil moisture in response to temperature gradients. Soil Science Society of America Journal, Vol. 18, No. 4, 351-358, 1954
- [VDE0276-1000] DIN Deutsches Institut für Normung e.V. und VDE Verband der Elektrotechniker e.V.: DIN VDE 0276-1000: Starkstromkabel – Teil 1000: Strombelastbarkeit, Allgemeines, Umrechnungsfaktoren, VDE VERLAG GMBH, Berlin, 2010.
- [VDE0276-620] DIN Deutsches Institut für Normung e.V. und VDE Verband der Elektrotechnik Elektronik Informationstechnik e.V.: DIN VDE 0276-620: Starkstromkabel – Energieverteilungskabel mit extrudierter Isolierung für Nennspannungen von 3,6/6 (7,2) kV bis einschließlich 20,8/36 (42) kV, VDE VERLAG GMBH, Berlin, 2010.
- [VDEW1997] Vereinigung Deutscher Elektrizitätswerke – VDEW e.V.: Kabelhandbuch. 5. Auflage, VWEW-Verlag, Frankfurt am Main, 1997
- [VRI1958] De Vries, D. A.: Simultaneous transfer of heat and moisture in porous media. Eos, Transactions American Geophysical Union, Vol. 39, No. 5, pp. 909-916, 1958
- [VRI1967] de Vries, D.A., Kruger, A.J.: "Phénomènes de transport avec changement de phase dans les milieux poreux ou colloïdaux", Proc. C.N.R.S. Symp No, 160, Paris, 1967
- [WEI2010] Weiland, Thomas: Grundlagen der Elektrodynamik. Vorlesungsskript TU Darmstadt. 2010
- [WIN1971] Winkler, F.: Der Einfluß des Bettungsmaterials auf die Belastbarkeit von Energiekabeln. ETZ-A vol.92, pp.131-137.
- [WIN1978] Winkler, F.: Strombelastbarkeit von Starkstromkabeln in Erde bei Berücksichtigung der Bodenaustrocknung und eines Tageslastspiels. ETZ-Report 13, VDE Verlag GmbH, Berlin, 1978
- [WOR1955] Van Wormer, F. C.: An improved approximate technique for calculating cable temperature transients. Power Apparatus Syst., Part III. Trans. Amer. Inst. Elect. Engineers, vol. 74, no. 3, pp. 277–280, 1955.
- [WUN1985] Wunsuch, G.: Geschichte der Systemtheorie – dynamische Systeme und Prozesse. Akademie-Verlag, Berlin und R. Oldenburg Verlag GmbH, München, 1985

Publications under contribution of the author

- [BAL2020]: Balzer, C.; Hallas, M.; Hinrichsen, V.; Neumann, C.; Koch, H.: Comparison of Current Carrying Capacities and Investment Costs of Directly Buried HVDC Cable and GIL Transmission Systems. VDE Hochspannungstechnik 2020, Berlin, November 9th-11th (accepted)
- [BAL2019-2]: Balzer, C.; Hinrichsen, V.; Tausend, W.: Efficient Lightning Protection of a Gas Insulated Substation Replacing an Air-Insulated Substation. 21st International Symposium on High Voltage Engineering (ISH) 2019, Budapest, Hungary, August 26th -30th.
- [BAL2019-1]: Balzer, C.; Drefke, C.; Stegner, J.; Hinrichsen, V.; Sass, I.; Hentschel, K.: Enhanced adoption of the two-zone model to implement the drying out of soil in ampacity calculations of directly buried cable systems for different types of soil. 10th International Conference on Insulated Power Cables - Jicable 2019, D6.3. Versailles, France, June 24th – 26th
- [BAL2018]: Rusek, B.; Steevens, S.; Kleinekorte, K.; Balzer, C.; Hannig, M.; Hinrichsen, V.; Neumann, C.: Dimensioning of Electrical Clearance of OHL Using Correlation between Weather Condition and Lightning Strike Probability. Cigré Session 2018, B2-106. Paris, France, August 26th -31st
- [BAL2017-1] Balzer, C.; Drefke, C.; Schedel, M.; Hinrichsen, V.; Sass, I.: Quantifizierung des Einflusses von Umweltbedingungen und bodenphysikalischen Eigenschaften der Bettung auf die thermische Stromtragfähigkeit von Mittelspannungs-Energiekabelsystemen. International ETG Congress 2017, E3.13. Bonn, November 28th – 29th. Published in: ETG Fachbericht 155; International ETG Congress 2017 (ISBN: 978-3-8007-4505-0), p. 410-415
- [BAL2017-2] Balzer, C.; Drefke, C.; Schedel, M.; Hinrichsen, V.; Sass, I.: Analytical calculation of the thermal impedance of soil under various boundary conditions to enhance current ratings of buried power transmission and distribution cable systems. 20th International Symposium on High Voltage Engineering ISH 2017, PF1, ID 317. Buenos Aires, Argentinia, August 28th – September 1st
- [DRE2017] Drefke, C.; Schedel, M.; Stegner, J.; Balzer, C.; Hinrichsen, V.; Sass, I.: Measurement Method of Thermal Properties of Cementitious Bedding Materials and Unsaturated Soils: Hydraulic Influence on Thermal Parameters. Geotechnical Testing Journal (ISSN 01496115), 40, (1), p. 160-170, Online-Edition: <http://dx.doi.org/10.1520/GTJ20160027>
- [BAL2016]: Balzer, C.; Hinrichsen, V.; Rusek, B.: Statistische Bestimmung von Überspannungen bei Einschaltvorgängen von Freileitungen zur Dimensionierung von Isolatorketten. VDE-Fachtagung Hochspannungstechnik 2016, EMV.3. Berlin, November 14th-16th. Published in: ETG Fachbericht 150; VDE Hochspannungstechnik (ISBN: 978-3-8007-4310-0), p. 166-171
- [DRE2016]: Drefke, C.; Schedel, M.; Balzer, C.; Hinrichsen, V.; Sass, I.: Experimentelle Bestimmung der Dynamik von Bodenaustrocknung und der Wiederherstellung der Bodenfeuchte um Energiekabel. VDE-Fachtagung Hochspannungstechnik 2016, ES.2. Berlin, November 14th-16th. Published in: ETG Fachbericht 150; VDE Hochspannungstechnik (ISBN: 978-3-8007-4310-0), p. 756-761

-
- [BAL2015-1]: Balzer, C.; Drefke, C.; Stegner, J.; Hinrichsen, V.; Sass, I.; Hentschel, K. ; Dietrich, J.: Improvement of Ampacity Ratings of Medium Voltage Cables in Protection Pipes by Comprehensive Consideration and Selective Improvement of the Heat Transfer Mechanisms within the Pipe. In: 9th International Conference on Insulated Power Cables - Jicable 2015, F2.19. Versailles, France, June 22nd – 24th
- [BAL2015-2]: Balzer, C.; Drefke, C.; Stegner, J.; Hinrichsen, V. ; Sass, I.; Hentschel, K. ; Dietrich, J.: Ampacity Rating of Directly Buried Distribution Cables under the Consideration of Soil Properties to Improve Efficiency of Distribution Networks. 23rd International Conference on Electricity Distribution - CIRED 2015, paper ID: 1498. Lyon, France, June 15th – 18th

Supervised student theses

- 2016: Kräuter, Alois: *Simulation des Wassergehaltes und der Wasserbewegungen in Böden mit Hilfe der Methode der finiten Elemente durch Analogien zur Elektrostatik und Konduktion.* Bachelorarbeit, Nr. 1981, TU Darmstadt, 2016
- Schneider, Martin: *Darstellung der Berechnungsmethoden der Wärmeübertragung durch die Methode der finite Elemente.* Bachelorarbeit, Nr. 1976, TU Darmstadt, 2016
- Bhandari, Diwash: *Thermal modelling of a medium voltage cable joint. Master Thesis.* Nr. 1971, TU Darmstadt, 2016
- Trabelsi, Hichem: *Verifizierung der Berechnung von Verlusten in Kabelsystemen nach IEC 60287 durch Vergleich mit analytischen Methoden und Modellierungen der finiten Elemente.* Bachelorarbeit, Nr. 1970, TU Darmstadt, 2016
- 2015: Tsoukala, Anni: *Entwicklung von thermischen Ersatzschaltbildern zur Ermittlung des Einflusses alternativer Lastkurven auf die Erwärmung von Kabelsystemen.* Studienarbeit, Nr. 1956, TU Darmstadt, 2015
- Haberzettl, Jens Klaus: *Modellierung von kombinierten Wärme- und Massentransportmechanismen in vollgesättigten Böden um erdverlegte Mittel- und Niederspannungskabel.* Bachelorarbeit, Nr. 1954, TU Darmstadt, 2015
- 2014: Thome, Lukas: *Untersuchung bestehender Monitoring Verfahren unter Berücksichtigung regulatorischer Rahmenbedingungen im Verteilnetz.* Bachelorarbeit, Nr. 1940, TU Darmstadt, 2014

Curriculum Vitae

Constantin Balzer

Born 19.04.1988 in Heppenheim (Hessen, Germany)

Eduction

- 2007: Abitur (German qualification for university entrance); Goethe Gymnasium Bensheim an der Bergstraße
- 2010: Bachelor degree in Electrical Engineering and Information Technology, TU Darmstadt
- 2012: Diplôme d'ingénieur, Institut polytechnique de Grenoble, École nationale supérieure de l'énergie, l'eau et l'environnement
- 2013: Master degree in Electrical Engineering and Information Technology, TU Darmstadt

Employment History

05/2015 – 11/2020: Scientific researcher at High Voltage Laboratories (HST), TU Darmstadt

09/2014 – 04/2015: Scientific researcher at Institute of high voltage (IFHT), RWTH Aachen

Internships

- 2012: Thesis internship of six months at ABB AG, Corporate Research, Västerås, Sweden: Development of an algorithm for the automatic generation of switching topologies regarding user-defined criteria
- 2011: Industrial internship of two months at Siemens AG, department „Transmission & Distribution“, Grenoble, France: Modelling of an HVDC connection and evaluation of its transient behaviour
- 2009: Voluntary Internship of one month at „EnBW Trading GmbH“ (Karlsruhe/Germany) in the field of energy market analysis: Development of an indicator model with respect to the dependency of power injection from wind power plants and day ahead energy prices

Erklärungen laut Promotionsordnung

§ 8 Abs. 1 lit. c PromO

Ich versichere hiermit, dass die elektronische Version meiner Dissertation mit der schriftlichen Version übereinstimmt.

§ 8 Abs. 1 lit. d PromO

Ich versichere hiermit, dass zu einem vorherigen Zeitpunkt noch keine Promotion versucht wurde.

§ 9 Abs. 1 PromO

Ich versichere hiermit, dass die vorliegende Dissertation selbstständig und nur unter Verwendung der angegebenen Quellen verfasst wurde.

§ 9 Abs. 2 PromO

Die Arbeit hat bisher noch nicht zu Prüfungszwecken gedient.

Datum und Unterschrift